DEVELOPMENT OF A LONG-TERM DURABILITY SPECIFICATION FOR POLYMER MODIFIED ASPHALT

A Dissertation

by

WON JUN WOO

Submitted to the Office of Graduate Studies of
Texas A&M University
in partial fulfillment of the requirements for the degree of

DOCTOR OF PHILOSOPHY

August 2007

Major Subject: Chemical Engineering

DEVELOPMENT OF A LONG-TERM DURABILITY SPECIFICATION FOR POLYMER MODIFIED ASPHALT

A Dissertation

by

WON JUN WOO

Submitted to the Office of Graduate Studies of
Texas A&M University
in partial fulfillment of the requirements for the degree of

DOCTOR OF PHILOSOPHY

Approved by:

Chair of Committee, Charles J. Glover
Committee Members, Richard R. Davison
Amy Epps Martin
Michael A. Bevan
Head of Department, N.K. Anand

August 2007

Major Subject: Chemical Engineering

ABSTRACT

Development of A Long-Term Durability Specification
for Polymer Modified Asphalt. (August 2007)
Won Jun Woo, B.S., Myongji University;
M.S., Myongji University
Chair of Advisory Committee: Dr. Charles J. Glover

In recent years an increased use of polymers has occurred to modify asphalt binders, mainly to decrease pavement rutting but also to improve binder failure strain in direct tension. Whereas all of these effects positively impact the durability of polymer-modified pavements, a need exists to quantify these improvements and the duration in the presence of oxidative aging.

This research evaluated the durability of polymer modified asphalt (PMA) through a number of determinations that included the characterization of the original binder property and pavement-aged binder for modified and unmodified binders.

Changes in styrene-butadiene-styrene (SBS) polymer modified binder properties from oxidation were analyzed using dynamic shear rheometry, ductility, and force ductility. Previous literature reports using size exclusion chromatography showed that degradation of the molecular weight profile of SBS accompanied the loss of PMA ductility. Yet base binder embrittlement also occurred, as evidenced by ductility and force ductility. Testing aged PMA binders at higher temperatures to soften the base binder restored the polymer modulus to the force ductility measurements as did blending with a softer deasphalted oil. These measurements indicate that the more significant cause of PMA degradation with aging is base binder embrittlement rather than polymer degradation.

Sixteen pavements in 11 Texas Districts, plus four MnRoad pavements were evaluated in order to obtain a more detailed profile of binder oxidation in pavements. Slices of each core provided detail on binder oxidation and air voids. The data confirm

that binders can oxidize at least several inches into the pavement. However, oxidation also can be significantly slowed, apparently by very low accessible air voids. Interestingly, the data indicate that the air voids that are relevant to the binder at a specific depth of the pavement are those in the immediate vicinity of the binder; low air voids above or below the binder do not seem to significantly affect the binder oxidation rate. Furthermore, that binders oxidize inches below the surface shows that temperature conducts well into the pavement, consistent with a heat conduction model that is used to calculate ground temperatures as a function of depth.

DEDICATION

I dedicate this dissertation to my parents, Jong-Hwan and Gi-Ja, other family, Won-Suck, Seung-Min and Je-In, my wife, Jung-Min, and my son, Je-Hyun, for their love, encouragement and support.

ACKNOWLEDGMENTS

I would like to thank my advisor, Dr. Charles J. Glover, for his support and guidance through my graduate studies. I appreciate Dr. Richard R. Davison, Dr. Amy Epps Martin, and Dr. Michael A. Bevan for serving on my committee and for their encouragement. I also would like to thank Dr. Victor Ugaz for his support.

I would also like to express appreciation for my research group members: Sung Hoon Jung, Nikornpon Prapaitrakul, Zachry Kraus, Tyner Devine, Ericka Rios, Arif Chowdhury, Allex Alvarez Lugo, and Edward Ofori-Abebresse.

Finally, I really appreciate my lovely wife, Jung-Min, who has always supported my efforts. Without her help and support I would never have achieved my goals.

NOMENCLATURE

G'(ω)	Elastic (storage) Dynamic Shear Modulus
G"(ω)	Viscous (loss) Dynamic Shear Modulus
G*(ω)	Complex Dynamic Shear Modulus
G'/(η'/G')	DSR Function
r_{η}	Binder Hardening Rate
r_{CA}	Binder Oxidation Rate (Rate of Carbonyl Area Formation)
η'(ω)	Dynamic Shear Viscosity
ω	Angular Frequency

TABLE OF CONTENTS

CHAPTER

CHAPTER

Page

LIST OF FIGURES

Page

Page

Page

Page

LIST OF TABLES

Page

CHAPTER I
INTRODUCTION

Polymer modification has been increasingly employed in asphalt concrete, primarily for control of short-term permanent deformation (rutting) (Bouldin and Collins, 1992; Lu and Isacsson, 1999). By adding polymer to a conventional asphalt, the Superpave performance grade span (low temperature grade plus high temperature grade, e.g., PG 64-22 span is 86) can be increased by increasing the upper grade without harming the lower grade significantly. Some state Department of Transportations (DOTs) require that if a binder is to have a grade span of 92 or above, then it must be a modified material.

At the same time, polymer modification typically improves binder ductility, thereby providing a binder that is more durable to pavement stress and deformation, due, e.g., to low-temperature thermal contraction or traffic loads, including the effects of fatigue (Glover et al., 2005).

Finally, there is evidence that polymer modifiers may improve the aging characteristics of a binder so that the deleterious impact of oxidative aging is delayed, leading to a more durable pavement (Glover et al., 2005).

While all of these effects positively impact the durability of polymer-modified pavements, there is a need to quantify these improvements and their duration in the presence of oxidative aging. Such an improved understanding will lead to better modified binder selection and to a better cost-benefit analysis, thereby leading to more efficient use of Texas highway construction dollars.

This research was designed to develop a better quantitative understanding of the relation between laboratory accelerated binder aging and field aging, a test procedure to measure a property of an aged binder that correlates to failure on the road, and a proposed specification for estimating the relative durability of binders.

The dissertation follows the style of the *AIChE Journal*.

Objectives

With the increasing use of modified asphalt binders there is a great need for methods that can evaluate the effectiveness of modifiers, including variables such as modifier content and composition of the base asphalt, and for specifications that are applicable to these materials.

This research was conducted to provide needed information for evaluating the ability of polymer modifiers to extend the service life of a pavement binder and thus for determining a polymer's cost effectiveness. The results also are useful for evaluating in-service pavements that contain either unmodified or polymer modified binders to estimate their remaining life. Such estimates will be valuable to the scheduling of maintenance and rehabilitation dollars and resources.

The specific objectives of this research were as follows:

1. Understand how to determine which modified binders provide maximum initial durability benefit with minimum degradation due to aging and to improve understanding of the polymer asphalt interactions that lead to good durability
2. Determine whether and to what extent polymers stay active in the face of oxidative aging
3. Learn to relate the laboratory aging tests and the resulting state of the aged binder to actual in-service field aging
4. Propose a specification for testing an aged binder as an indication of ultimate failure of the binder after aging

The discussion that follows presents more details concerning fundamentals of binder oxidation and its impact on binder properties, conventional and modified asphalt binder durability, and a summary of durability issues addressed by this research.

A Brief Review of Binder Oxidation and Hardening Kinetics

The issue of developing an accelerated binder aging test that ranks asphalts the same as pavement aging is challenging at best and fundamentally impossible at worst because of the different effects of time, temperature, and pressure on different materials. Equation I-1 shows the mechanisms by which hardening occurs in the absence of diffusion resistance:

$$\ln \eta_t = \ln \eta_o + \Delta(\ln \eta_{ot}) + \Delta(\ln \eta_j) + r_\eta(\text{time}) \qquad \text{(I-1)}$$

where η_o is the original viscosity, η_t is the viscosity at any time, $\Delta(\ln \eta_{ot})$ is the hardening in the hot-mix plant simulated by an oven test, $\Delta(\ln \eta_j)$ is the hardening that occurs in an early rapid "initial jump" stage, and r_η is the subsequent constant rate of hardening.

Figure I-1 shows the sequence in which η_{ot} is the viscosity after the oven test and η_j is the viscosity after the initial jump defined by the intercept of the constant-rate line. Region A will be defined as the time for the initial jump, and region B is a constant-rate region. If there is diffusional resistance, this rate will decline as the asphalt hardens. Equation I-1 and Figure I-1 are expressed in terms of zero-shear viscosity η_o* but hardening in terms of other properties (such as the dynamic shear rheometer, [DSR] function G'/(η'/G'), discussed in the next section, follow the same hardening kinetics).

This asphalt oxidative hardening is almost entirely caused by asphaltene formation (Lin et al., 1995, 1996, and 1998), and the rate can be expressed as follows:

$$r_\eta = \frac{\partial \ln \eta}{\partial t} = \frac{\partial \ln \eta}{\partial \text{AS}} \cdot \frac{\partial \text{AS}}{\partial \text{CA}} \cdot \frac{\partial \text{CA}}{\partial t} \qquad \text{(I-2)}$$

where ∂ln η/∂AS is the impact of asphaltene (AS) increase on increasing viscosity and is affected by asphaltene size, which in turn is affected by maltene solvent power. ∂AS/∂CA is the extent to which increases in carbonyl area (CA) produce asphaltenes, and ∂CA/∂t is the rate of CA formation. The increase of CA correlates linearly with oxidation (Liu et al., 1998a).

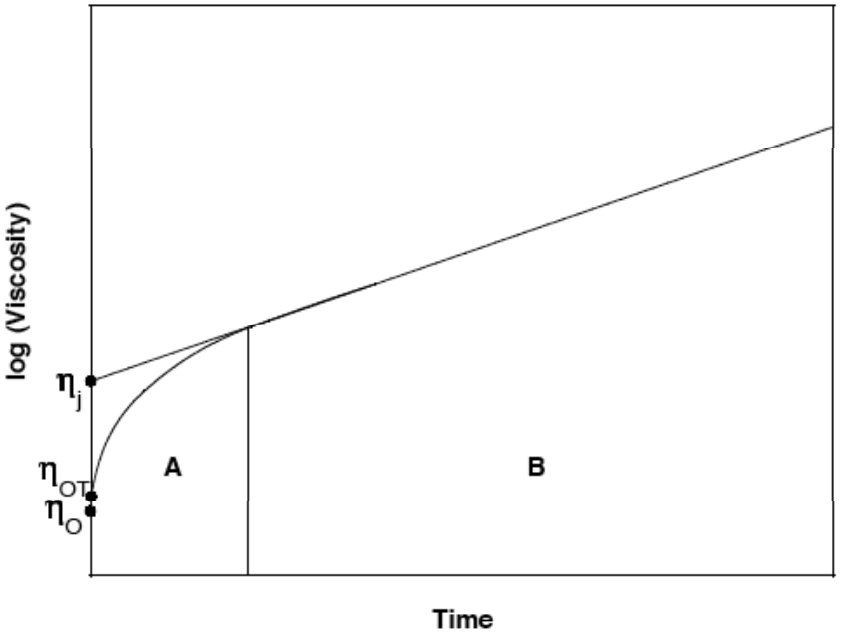

Figure I-1. Typical Hardening Response of an Unmodified Asphalt Binder to Oxidation

Equation 1-2 can be simplified as:

$$r_\eta = \mathrm{HS} \cdot r_{CA} \tag{I-3}$$

where HS is the combination of the first two terms in Equation I-2. This combination is remarkably constant as oxidation proceeds and is independent of oxidation temperature below about 100 - 110 °C. It has a characteristic value for each asphalt except that it is

pressure dependent. This term is called the hardening susceptibility (Lau et al., 1992; Domke et al., 1999).

The rate of carbonyl formation is (Lin et al., 1996; Lin et al., 1998; Liu et al., 1997):

$$r_{\mathrm{CA}} = \frac{\partial \mathrm{CA}}{\partial t} = AP^{\alpha} e^{-E/RT} \tag{I-4}$$

where A is the frequency (pre-exponential) factor, P is the pressure, α is the reaction order with respect to oxygen pressure, E is the activation energy, R is the gas constant, and T is the absolute temperature. Values of A, E, and α are very asphalt dependent, though A and E are generally correlated (Liu et al., 1996). Recent studies (Domke et al., 2000) show that the activation energy, E, is also pressure dependent for many asphalts, and this dependence is a function of asphaltenes. The following equation summarizes these results where [P] or [T,P] or [P] indicates that the property is a function of temperature or temperature and pressure, or just pressure:

$$\ln \eta_t = \ln \eta_{ot} + \Delta(\ln \eta_j)[P] + r_{\mathrm{CA}}[T,P] \cdot \mathrm{HS}[P](\mathrm{time}) \tag{I-5}$$

As only one term is multiplied by time, this means that the relative rankings of asphalts from any accelerated aging procedure will change with the length of the test as well as with the temperature and pressure. In previous research (Glover et al., 2005), a long-term simulation was done in an environmental room held at 60 °C (140 °F), and other conditions were then compared as to relative rankings with the results from the environmental room. It is noted that particularly relevant hardening rate parameters are the hot-mix binder hardening ($\ln \eta_{ot} - \ln \eta_o$), the initial jump ($\eta_j$), the hardening susceptibility (HS), and the oxidation rate, r_{CA}.

Binder Oxidation and Embrittlement – Unmodified Binders

In accordance with the oxidative hardening discussed above, asphaltic binders experience hardening and embrittlement over time that reduces the performance of flexible pavements. The process is relentless and thus, over enough time, can destroy the pavement. The constancy of the hardening rate over time and the depth to which oxidation occurs, based on recent pavement data, are surprising and at the same time critical to understanding pavement durability for both unmodified and modified binders.

As binders oxidize, carbonyl (–C=O) groups are formed that increase the polarity of their host compounds and make them much more likely to associate with other polar compounds. As they form these associations, they create less soluble asphaltene materials, which behave like solid particles. This composition change, taken far enough, results in orders-of-magnitude increases in both the asphalt's viscous and elastic properties. The kinetics of this process were described in the previous section. The end result is a material that increases its stress greatly with deformation (high elastic stiffness) and simultaneously cannot relieve the stress by flow (high viscosity) leading to a pavement that is very brittle and susceptible to fatigue and thermal cracking.

This embrittlement of binders has been captured with the discovery of a correlation between binder ductility (measured at 15 °C, 1 cm/min) and binder DSR properties (dynamic elastic shear modulus, G' and dynamic viscosity, η', equal to G"/ω), shown in Figure I-2. A very good correlation exists between binder ductility and G'/(η'/G') (or, equivalently G'/[G"/ωG']), demonstrating the interplay between elastic stiffness and the ability to flow in determining binder brittleness.

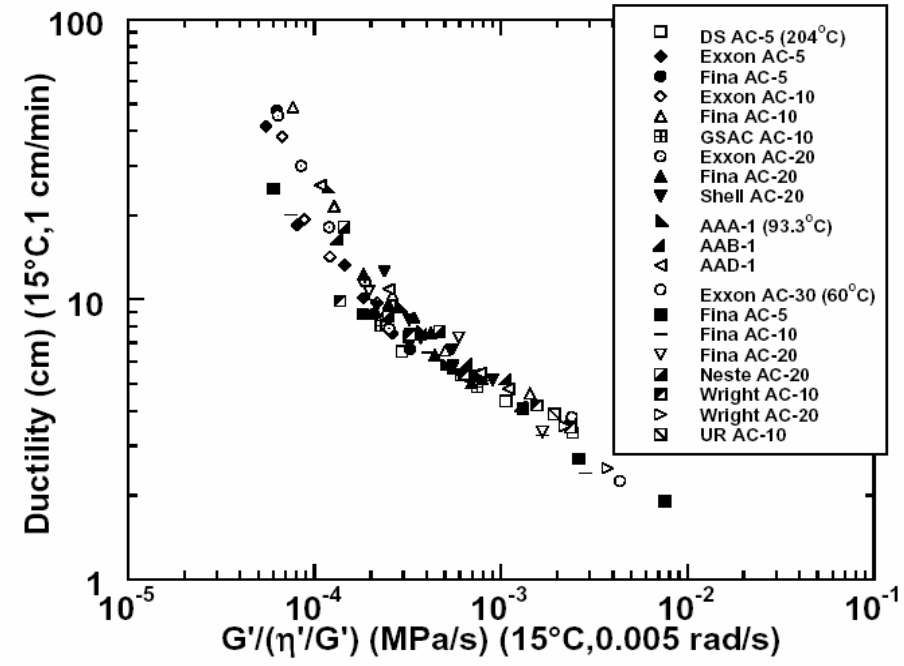

Figure I-2. Correlation of Aged-Binder Ductility with the DSR Function G'/(η'/G') for Unmodified Binders (Ruan et al., 2003a)

This correlation is depicted on a "map" of G' versus η'/G' (Figure I-3), which tracks a pavement binder as it ages in service (Ruan et al., 2003a). This particular binder is from SH-21 between Bryan and Caldwell in Texas, but represents the trends for all conventional binders. On this type of plot, with increased aging a binder moves over time, from the lower right toward the upper left as the result of increases in both the elastic stiffness and viscosity (but note that G' increases more than viscosity, i.e., G''/ω, because movement is toward the left, i.e., smaller values of η'/G'). Note also the dashed lines that represent lines of constant ductility, calculated from the correlation of Figure I-2 below 10 cm.

Recent evidence suggests that pavement binders age at surprisingly constant rates and to surprising depths. Figure I-3 illustrates this conclusion. This highway was constructed from July 1986 to July1988 in three, 2-inch lifts. The solid symbols (with the exception of the solid diamond) are binder measurements from cores taken from the

third lift down from the surface of the pavement, as originally constructed. With each lift being 2 inches thick, this bottom lift had 4 inches of pavement on top of it. (Note: In 2000, this pavement had a chip seal and overlay placed on top of it, burying the original lifts even more.) Yet, even buried this deeply, we see its binder moving across the DSR "map" in a relentless fashion and at about the same pace as the top lift (open symbols). Binder from the 1989 bottom lift has an estimated ductility of 20 cm at 15 °C. By 1996, it is reduced by aging to 5.6 cm, and by 2002, it is less than 5 cm. Meanwhile, the top lift binder's ductility was estimated to be 16 cm in 1989, 4.5 cm in 1996, and about 4 cm in 2002. The march across the DSR map was not that different for the top lift, compared to the bottom lift. Binder from the middle lift, taken in 1989 and 1992, is also shown and tracks well with the other lifts. Note that the rolling thin-film oven test (RTFOT) plus pressure aging vessel (PAV) laboratory-aged binder matches the 1992 pavement-aged binder, suggesting that for this pavement, RTFOT plus PAV is approximately equivalent to hot-mix and construction aging, plus four years of pavement aging.

These results are rather remarkable and strongly suggest, as noted above, that oxidative aging rates are remarkably constant over time and, beyond the very top portion of the pavement, proceed at remarkably uniform rates, at least to several inches below the surface of the pavement.

It should be noted that the literature reports that ductility values in the range of 2 to 3 cm for 15 °C at 1 cm/min appear to correspond to a critical level for age-related cracking. Thus, the top-left corner of the pavement aging figure is a suspect region for pavement performance. While this region has not yet been verified conclusively to be a critical zone, recent pavement data (Glover et al., 2005) are consistent with this early conclusion.

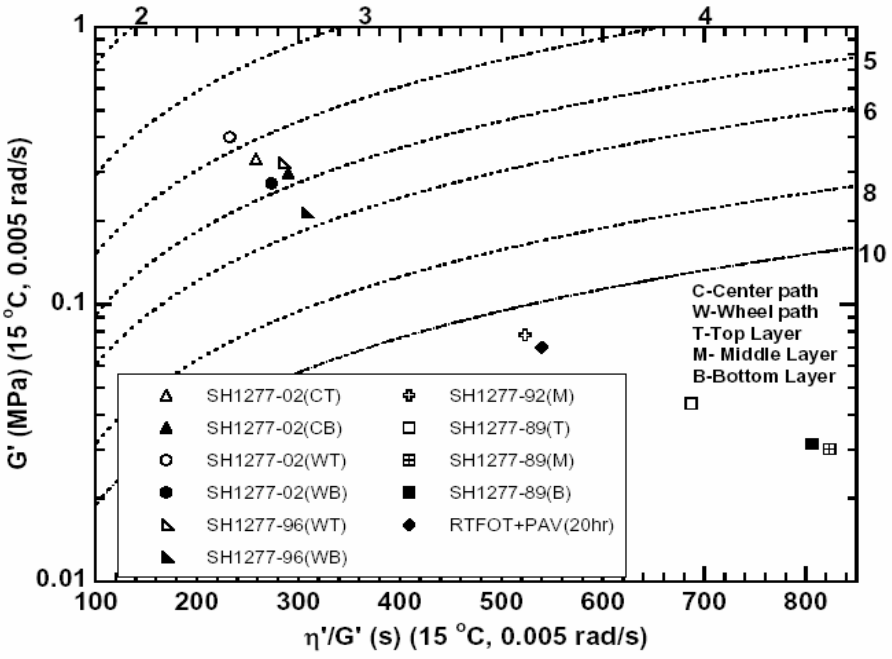

Figure I-3. Binder Aging Path on a G' versus η'/G' Map (Pavement-aged Binders) (Glover et al., 2005)

Binder Oxidation and Embrittlement – Polymer-Modified Binders

While polymer-modified binders behave qualitatively the same as unmodified binders with respect to durability loss due to oxidative aging, there are some important quantitative differences. These differences are highlighted below.

Improved Rate of Durability Loss

Figure I-4 shows comparisons of the zero-shear viscosity (ZSV) hardening rates for a number of base asphalts and their modified materials. The specific base materials and their modifiers are not the point so much as the fact that in each case the ZSV hardening rate is significantly greater for the unmodified binders (top bars), in some

cases by a factor of two. Hardening is a bottom-line issue in terms of durability, so a lower hardening rate translates directly into a longer life span.

Figure I-5 shows carbonyl area oxidation rates, $\partial CA/\partial t$. For these materials, and this property, the differences are not so stark, although generally, the oxidation rate is less for the modified materials.

Figure I-6 shows another piece of the puzzle, the hardening susceptibility. This property is the extent to which oxidation (CA) causes hardening of the binder (Equation I-3). Again, the effects are not as dramatic as for the hardening rates but it is generally true that the modified materials are less affected by the oxidation than the unmodified binder. The net effect of the oxidation rates and hardening susceptibilities gives the more obvious improvements to the hardening rates.

The bottom-line result is that polymer modification can retard the hardening rate of a binder significantly.

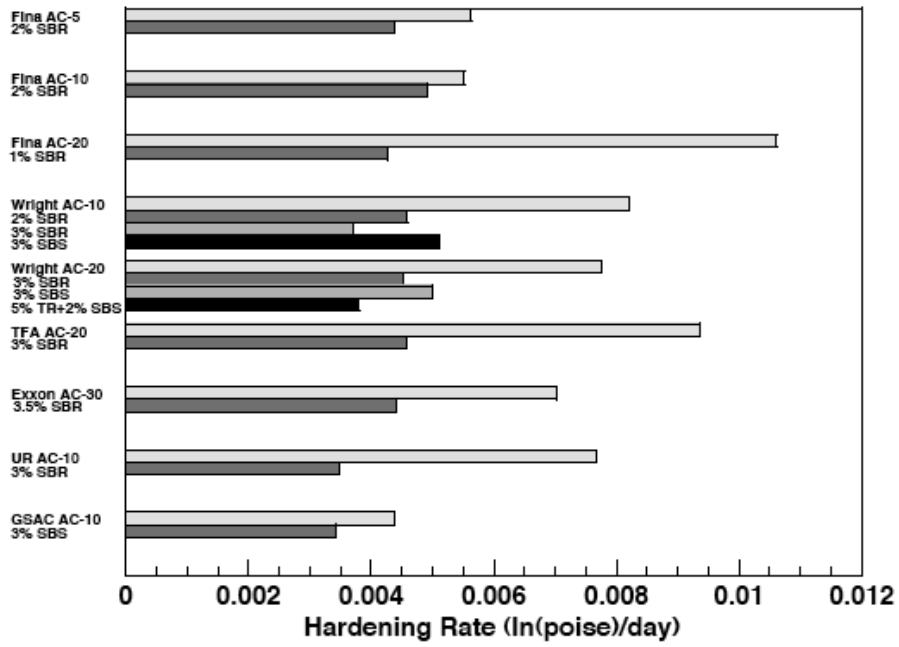

Figure I-4. The Effect of Modifiers on Binder Hardening Rates

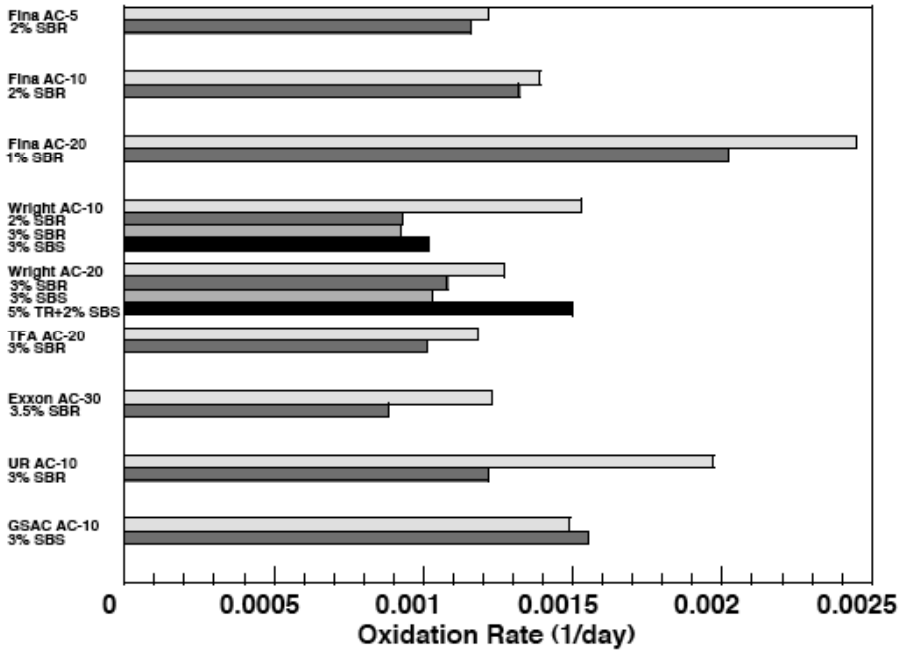

Figure I-5. The Effect of Modifiers on Binder Oxidation Rates

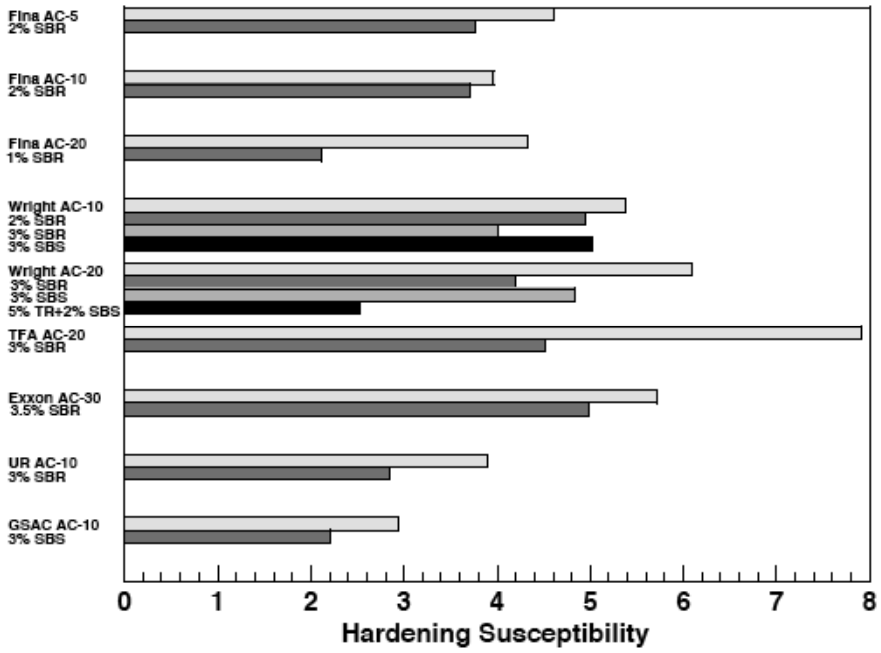

Figure I-6. The Effect of Modifiers on Binder Hardening Susceptibility

Improved Durability

One measure of a binder's durability is its ductility. Several studies report that a value of the 15 °C ductility at 1 cm/min in the range of 2 to 3 cm corresponds to a critical level for age-related cracking in pavements (Clark, 1958; Doyle, 1958; Halstead, 1963 and 1984; Kandhal, 1977; Kandhal and Wenger, 1975; Kandhal and Koehler, 1984; Welborn, 1984).

Figure I-7 shows force-ductility (FD) data at 4 °C for a base asphalt and two polymer modified blends. As elongation increases, the unmodified binder draws out into a thin thread, and the stress declines. The modified binders in this region, however, show a second elastic modulus, due to the stretching of polymer chains, and this leads to an extended and stable elongation.

Figure I-8 shows the dramatic decline in ductility with oxidative aging, to the point that there is essentially no difference in this test between the unmodified and modified binders. The reason for this loss of ductility is not well understood. There is clear evidence from size exclusion chromatography measurements (SEC, also known as gel permeation chromatography, GPC) that there is some degradation of the polymer with respect to its molecular weight distribution due to oxidative aging (Lu et al and Isacsson, 1999; Glover et al., 2005). An alternate explanation may be that as the asphalt stiffens with oxidation, the polymer can no longer provide a benefit to the binder; with deformation the stress builds in the asphalt to the point of failure during the first asphalt modulus phase of the stress-elongation curve (Figure I-7) in which case the polymer may as well not be in the binder. The extent to which each of these mechanisms plays a role in the loss of a polymer modified binder's durability is an important question that was addressed by this research.

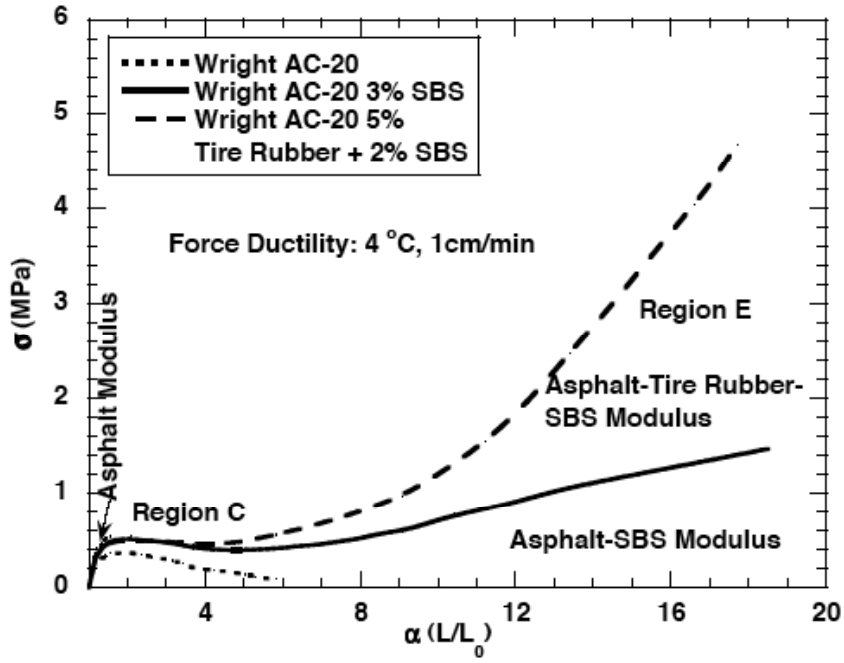

Figure I-7. Stress versus Elongation, 4 °C: Unaged

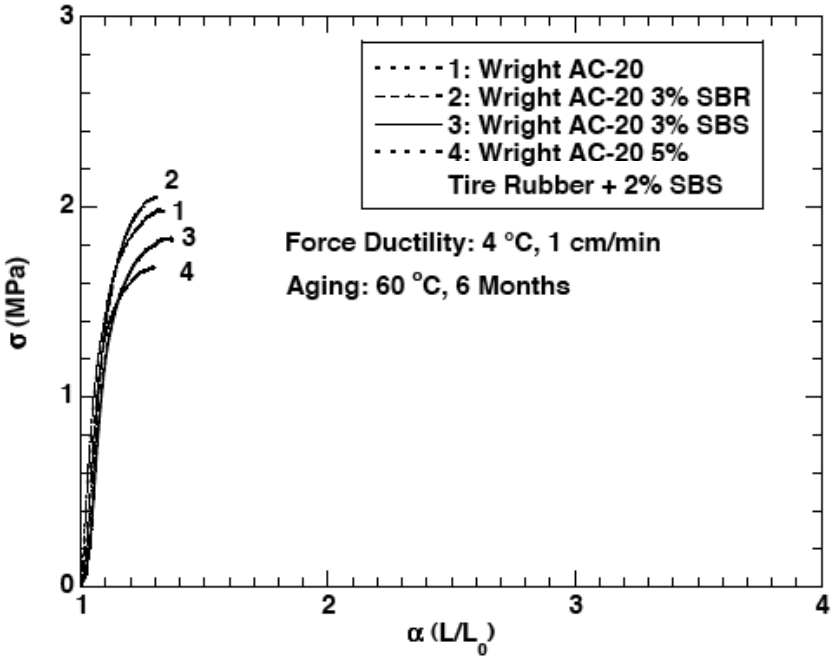

Figure I-8. The Effect of Modifiers on Binder

Nevertheless, it seems likely that a stiffening asphalt base plays a significant role in this oxidative aging loss of ductility. This assumption leads to the hypothesis that effective polymer modifiers enhance the durability of the binder, and the most benefit will be realized if the polymer enables a lower low-temperature Superpave performance grade base binder to be used, thereby lengthening the time required for oxidation to excessively stiffen the underlying base asphalt.

A second view of polymer improvements to ductility is shown in Figure I-9 (Glover et al., 2005). This figure shows the correlation of Figure I-2 (without the data points) as a solid line. Lying above it are data points for polymer-modified binders. Several important points are evident. First, for each modified-binder data point, the ductility, for a given value of the DSR function (G'/[η'/G']), lies above the unmodified binder line; the ductility is improved. Second, the data fall in groups that depend upon the base binder, showing the distinct differences that may be seen between binders. Third, with each group of base binders, as aging progresses the ductility benefit declines until finally the modified lines converge to the unmodified correlation. At this point, the modifier appears to have lost its durability benefit.

Another point should be made about Figure I-9. Because the polymer modified data show such significant scatter above the unmodified line (compared to the unmodified data of Figure I-2), the DSR function may not be as useful for modified materials as it seems to be for unmodified, at least before the polymer benefit is reduced and the modified lines in Figure I-9 converge on the unmodified correlation.

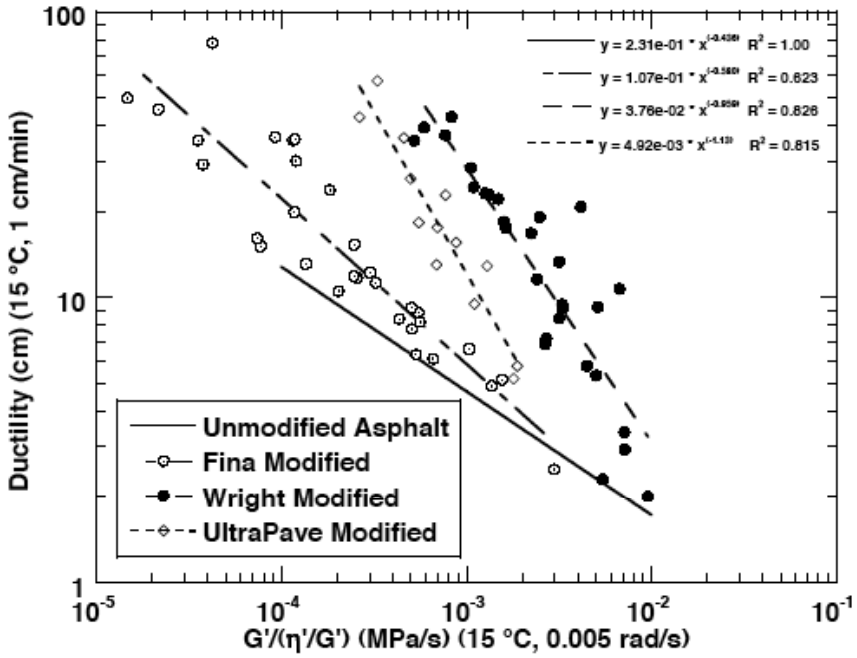

Figure I-9. Ductility versus G'/(η'/G') for Modified Asphalt Groupings

Summary of Durability Issues

From the above discussions the following polymer-modified binder durability issues have been identified:

- hardening improvement by modifiers, including hardening rate (both zero shear viscosity [ZSV] and DSR function);
- the benefits of using a lower low-temperature performance grade asphalt;
- the ability of a modifier to improve the binder failure stress (higher failure stress means a higher failure strain);
- the role of the base binder composition in achieving improved durability;
- the extent to which durability loss with oxidative aging is due to polymer degradation versus base binder stiffening;
- the life extension of a binder provided by the polymer durability enhancement; and

- relation between laboratory and field aging rates.

Outline of the Dissertation

Chapter II presents measurements of characteristics of polymer-modified asphalts (PMA) that are believed to impact binder durability, including the initial characteristics of binders, and how oxidative aging impacts binder characteristics. This chapter is an essential element to developing a durability test and specification. Actual commercial modified products and their base asphalts were studied.

Chapter III presents studies of the specific issue of the extent to which polymer effectiveness is lost due to binder oxidation and whether this loss is due to base binder stiffening or polymer degradation.

Chapter IV is an extensive study of modified and unmodified binder oxidation and hardening in pavements. Included are measurements of binder hardening over time, and at various pavement depths, as a function of accessible (or interconnected) air voids. From the data, a pavement aging model is proposed that includes daily and annual temperature variations. Data from 16 Texas pavements in 11 districts, plus the MnRoad test site in Minnesota are included.

Chapter V presents the proposed polymer modified binder durability aging protocol, binder test and comparison procedures, and durability specification.

Finally, Chapter VI provides an executive summary of the dissertation.

CHAPTER II
DURABILITY EFFECTIVENESS OF SELECTED POLYMER-ASPHALT SYSTEMS

Key to understanding the durability of PMA in pavements is to understand their fundamental properties and the changes that occur to these properties due to oxidative aging in service. In particular, the physical properties of the binder (i.e., its rheological stiffness), the role of the polymer in establishing these properties, and the manner and rate at which these properties change due to oxidation all are critically important. Furthermore, these properties are specific to each polymer-modified system and thus vary according to the base binder, the modifier, and the relative amounts of the two.

Thus the role of this chapter is to study the rheological properties and aging characteristics of a number of polymer-modified asphalt systems used in Texas. As such, this research includes determining the characteristics of the base binders in these systems together with a number of modified systems created from these base binders. The base binders are primarily PG 64-22 asphalts, but also include one PG 58-28. The modified binders include materials up to a PG 76-22 and incorporate styrene-butadiene styrene (SBS), styrene-butadiene rubber (SBR), and tire rubber (TR) as modifiers.

These properties lay the foundation for understanding the oxidative aging and performance of PMA in pavements in Texas that is documented in Chapter IV and finally the PMA assessment procedure that is proposed in Chapter V.

Research Objectives

The objectives of the work presented in this chapter were to determine the principal characteristics of polymer-modified asphalts and their base asphalts that are typically used in Texas. The characteristics evaluated in this chapter include binder DSR properties (master curves and the DSR function as it is defined below), infrared measurements to determine carbonyl area (which indicates binder oxidation), and size

exclusion chromatography to assess the level and nature of the polymer modification. Changes to all of these properties that result from oxidation (carried out by a number of means including 60 °C environmental room aging, high pressure and temperature accelerated aging, the standard PAV aging method, and a surrogate for RTFOT aging, the SAFT method) were investigated. Other rheological data included the measurement of binder ductility and force ductility values. Compositional measurements included the Corbett analysis of saturates, naphthene aromatics, polar aromatics, and asphaltenes at different levels of aging.

Methodology

Materials

The materials studied are shown in Table II-1. These materials were provided by seven suppliers and include seven distinct base binders (although the base binders do not correspond directly to the refinery suppliers). Note that for the seven base binders, a number of polymer-modified systems were provided that include modification to different levels of PG grade and by different polymers that include SBS, SBR, and TR.

These materials also include samples obtained from the MnRoad test site as an opportunity to compare the materials used in Texas versus Minnesota and are also shown in Chapter IV that compare pavement aging rates in Texas to pavement aging rates in Minnesota. The Minnesota binders were said to have used a base binder that was a PG 58-28 and when modified with the polymer, provided PG 58-34 and 58-40. One of the MnRoad sites was placed in the early 1990s and at that time was classified as an AC 120/150 grade asphalt under the old penetration viscosity classification method. Note also that while most of the binders are generic binders and not associated with any particular pavements that were studied in this research, there is one exception; the Valero Oklahoma SBR binder was the binder used in a US 281 pavement that is also studied in Chapter IV. While this is a short list of binders that are used within Texas, it

does provide a reasonable set of suppliers to TxDOT and shows a representative sample of these suppliers.

Table II-1. Collected PMAs and Base Materials from Suppliers

Supplier	PG Binder	Comment	Modifier Content
Wright	64-22 B	Base Binder Except 76-22 SA	-
	70-22 S	SBS Modified	2 – 5 % SBS
	76-22 TRS	SBS & Tire Rubber Modified	2 – 5 % SBS & 5 % TR
	76-22 SA	Atlanta Core Binder	2 – 5 % SBS
	76-22 SB	Lab Mixture Binder	2 – 5 % SBS
Alon	58-28 B	Base Binder for PG *-28	-
	70-28 S	SBS Modified	3.4 – 3.6 % SBS
	64-22 B	Base Binder for PG *-22	-
	70-22 S	SBS Modified	2.3 – 2.5 % SBS
	76-22 TRS	SBS & Tire Rubber Modified	2.3 – 2.5 % SBS & 5 % TR
Koch	64-22 B	Base Binder for PG *-22	-
	70-22 S	SBS Modified	-
	76-22 S	SBS Modified	-
	70-28 S	SBS Modified	-
	76-28 S	SBS Modified	-
MnRoad	58-28 B	Base Binder for PG 58-*	-
	58-34 S	SBS Modified	-
	58-40 S	SBS Modified	-
	AC 120/150	Unmodified	-
Lion Oil	64-22 B	Base Binder	-
	70-22 S	SBS Modified	1.5 % SBS
	76-22 S	SBS Modified	3 % SBS
Valero-Houston / **O**klahoma / **C**orpus	64-22 B	Base Binder	-
	70-22 S	SBS Modified	-
	76-22 S	SBS Modified	-
US281 (Valero-O)	64-22 BSR	Base Binder for PG 76-22 SR	-
	76-22 SR	SBR Modified	3 – 3.5 % SBR

Aging Methods

Stirred Air-Flow Test (SAFT)

This aging method (Vassiliev et al., 2002) simulates changes in the properties of asphalt during conventional hot-mixing processes in lieu of the rolling thin-film oven test (RTFOT). Preheated materials weighing 250 g were placed in an air-flow vessel which was equipped with an impeller, temperature control sensor and air-cooled condenser. Air was blown through materials that were heated in a vessel for 35 min at 163 °C. The mixing of air and materials was performed by the air flow at a rate of 2000 mL/min and the impeller speed at a rate of 700 RPM.

Pressure Aging Vessel (PAV*)*

The purpose of this test is to simulate long-term asphalt aging after hot-mix aging such as SAFT and RTFOT. This method was modified from the standard PAV procedure. Materials with 1 mm film thickness were placed in a PAV pan and aged for 16 hr and 32 hr at 90 °C. The pressure and temperature controller were set to 2.2 MPa and 90 °C.

.

Environmental Room (ER)

An approximate simulation of road-aging is achieved using an environmental room controlled to 60 °C and 1 atm air with 25 percent relative humidity. Samples for examining hardening susceptibility were placed in trays measuring 4 cm by 7 cm, and trays measuring 14 cm by 14 cm were used for ductility measurement of samples, resulting in an approximately 1 mm thick film.

Analytical Measurements

Dynamic Shear Rheometer (DSR)

Complex viscosity (η*) at 60 °C and 0.1 rad/s, storage modulus (G') and dynamic viscosity (η') at 44.7 °C and 10 rad/s of asphalt materials were measured using a Carri-Med CSL 500 Controlled Stress Rheometer operated in an oscillatory mode. A 2.5 cm composite parallel plate geometry was used with a 500 μm gap. The operating ranges of temperature, angular frequency and torque were -10 to 99.9 °C, 0.1 to 100 rad/s and 10 to 499,990 dyne-cm, respectively.

Fourier Transform Infrared (FT-IR) Spectroscopy

A Mattson Galaxy series 5000 FT-IR Spectrometer, using the attenuated total reflectance (ATR) method with a zinc-selenide prism, was used to measure infrared spectra. The integrated carbonyl area under the carbonyl absorbance band wavenumber from 1820 to 1650 cm^{-1} was used to represent the extent of oxidation in asphalt materials (Liu et al., 1998b).

Gel Permeation Chromatograph (GPC)

The molecular size distribution of asphalt materials was measured using a Waters GPC HPLC system with both refractive index and intrinsic viscosity detectors. Asphalt binder (0.2 g) was dissolved in 10 mL of Tetrahydrofuran (THF), and this solution was passed through the GPC columns at a flow rate of 1.0 mL/min after filtering through a 0.4 μm PTFE syringe filter. GPC is also referred to as size exclusion chromatography (SEC).

Ductility and Force Ductility (FD)

Ductility measurements were performed at 15 °C and at an extensional speed of 1 cm/min until binder failure. The initial gauge length of the sample was 3 cm. Force ductility (FD) was measured at 4 ^{o}C on a specimen of uniform cross-section 1 cm by 0.5 cm. Stress as a function of extension ratio was determined from the force measurement assuming a uniform cross-section throughout elongation.

Corbett Analysis (CA)

Conventional asphalt binders were separated by means of the Corbett precipitation and alumina column chromatographic procedure (ASTM D4124) into four fractions: saturates, naphthene aromatics, polar aromatics, and asphaltenes. Some modifications of the Corbett procedure were implemented to reduce sample size and increase efficiency as suggested by Thenoux et al. (1988). According to Corbett (1979), asphalt can be viewed as an associated system of asphaltenes dissolved in the maltene (non-asphaltene) phase. Asphaltenes contribute to a good viscosity temperature susceptibility, and they are important viscosity builders. Polar aromatics greatly contribute to ductility and the dispersion of asphaltenes. Both saturates and naphthene aromatics work against good ductility.

Results and Discussion

Asphalt Composition and Changes in Composition with Oxidative Aging

Figures II-1 and II-2 show the base binder Corbett compositions as unaged asphalts and also at their various levels of aging including SAFT and PAV* 16 hr and PAV* 32 hr aging. The same data are tabulated in Appendix A.

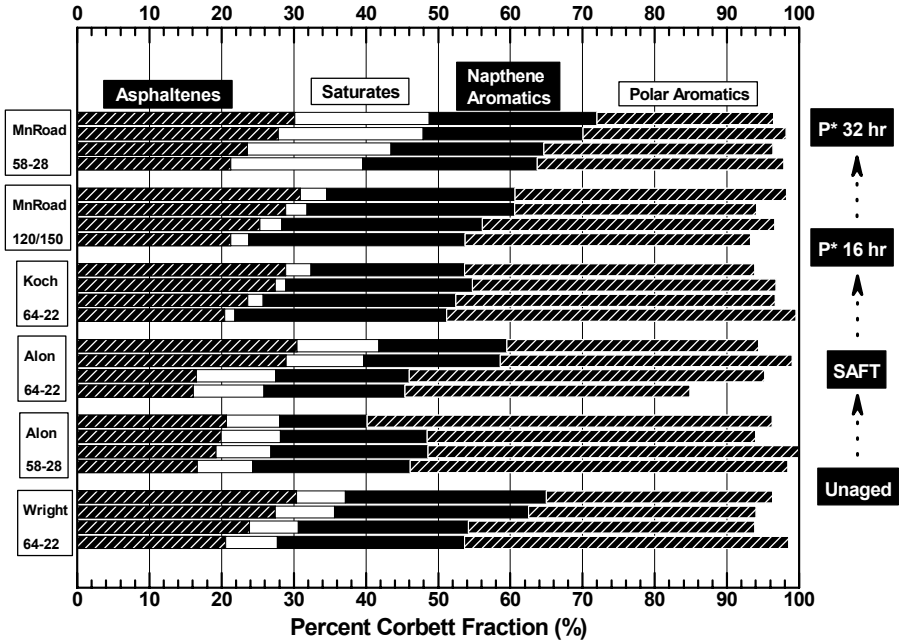

Figure II-1. Corbett Analysis for Unaged and PAV* Aged PMAs and Base Binders (Wright through MnRoad)

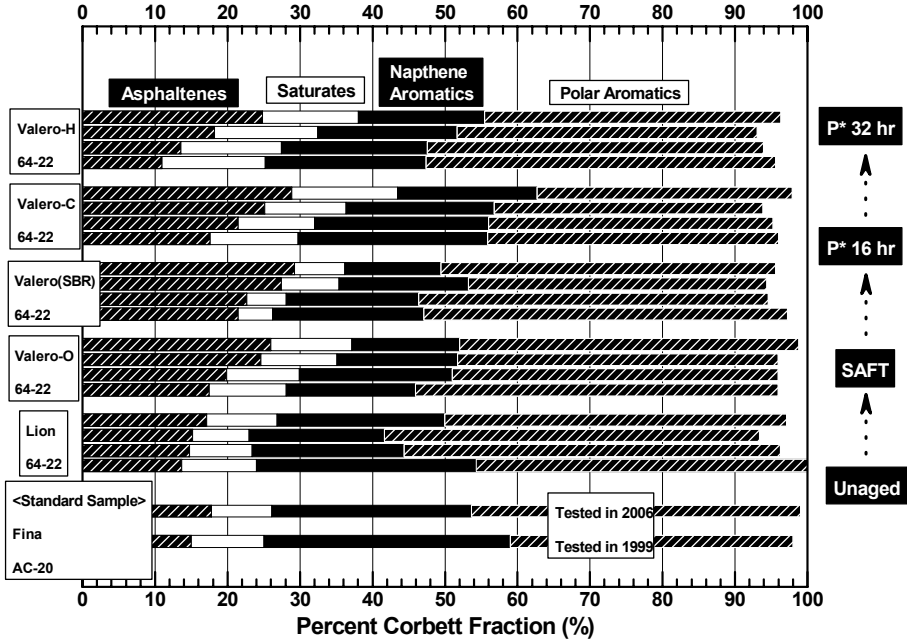

Figure II-2. Corbett Analysis for Unaged and PAV* Aged PMAs and Base Binders (Lion through Valero)

From these graphs, distinct differences between some of the base binders were seen. For example, the Koch PG 64-22 binder is very low in saturates and correspondingly high in polar aromatics. The MnRoad AC 120/150 binder is also very low in saturates and the Valero Oklahoma PG 64-22 base binder that was blended with SBR is low also although not to the same extreme as the Koch and MnRoad; the Valero binder has saturates in the range of 5-7 percent, whereas, the other two are less than 3 percent. These low saturates are notable because previous work has shown that in order for binders to have a good temperature susceptibility as unmodified binders, the saturates and asphaltenes tend to be in rough balance in the range of 15-20 or even 25 percent. The Wright asphalt base binder also has saturates under 10 percent, and the Valero Oklahoma and Lion are about 10 percent. The unaged asphaltenes level of these binders typically is 15-20 percent. Although the Valero-Houston and the Lion binders have asphaltenes below that level, it should be noted that the asphaltenes composition increases with aging and at the expense primarily of polar aromatics. With progressively more oxidation, the level of asphaltenes increases, and the increase comes at the expense of polar aromatics. As the heaviest, or near-asphaltene, polar aromatics are oxidized, they convert to asphaltenes. In a similar fashion, the heaviest naphthene aromatics that are near-polar aromatics may be converted to polar aromatics upon oxidation. Saturates, however, maintain a stable composition.

Concerning the asphaltene's composition, it is noted that for most of the binders, there is a regular progressive increase in asphaltenes for each level of oxidation. Two exceptions are the Alon and the Lion materials. For the Alon, there is relatively little increase in asphaltenes due to SAFT oxidation but significantly more due to the PAV* 16 hr oxidation. Then the PAV* 32 hr oxidation provides relatively little additional asphaltenes. Whether this is a true representation of the actual change in composition or whether it is an experimental anomaly for this particular experiment is not known. There is no reason to believe the data are in error. The Lion base asphalt, on the other hand, has a relatively low increase in asphaltenes with each additional step of aging, although, the increase occurs evenly at each level. Ultimately, the objective of these data

would be to correlate the asphalt polymer compatibility to Corbett composition. If achieved, this would be a very simple way to characterize compatibility. However, because the composition is only crudely measured by the Corbett fractions (each fraction from one asphalt to the next can be widely different due to its sub-composition), the ability to make a compatibility assessment based on only Corbett composition is probably unlikely.

Effect of Aging on Ductility and Rheological Properties

Plots of ductility (measured at 15 °C and 1 cm/min) versus the DSR function for all the modified binders and their base materials are shown in Figures II-3 and II-4. Also shown is a dashed line based upon the work of Ruan et al. (2003a), which is representative of the correlation he developed for a wide range of unmodified binders. This relationship was linear between log ductility and log DSR function below ductility of about 10 cm. While it is noted that in large part the polymer modified data fall close to the unmodified binder correlation, some significant exceptions were also noted in both modified binders and one of the Texas base binders, as well as the MnRoad materials. For each material, there are four data points: the unaged binder, the SAFT aged binder, the PAV* 16 hr aged binder, and the PAV* 32 hr aged binder. These latter two aging levels provide significant aging of the binders and therefore typically move them down into the ductility region near or below (and in some cases well below) 10 cm. Note that the unaged binders, and in some cases even the SAFT aged binders, are quite ductile materials and have ductilities that exceed the maximum measurable ductility of this apparatus. These points are all plotted at the ductility maximum of 100 cm even though they exceed that ductility.

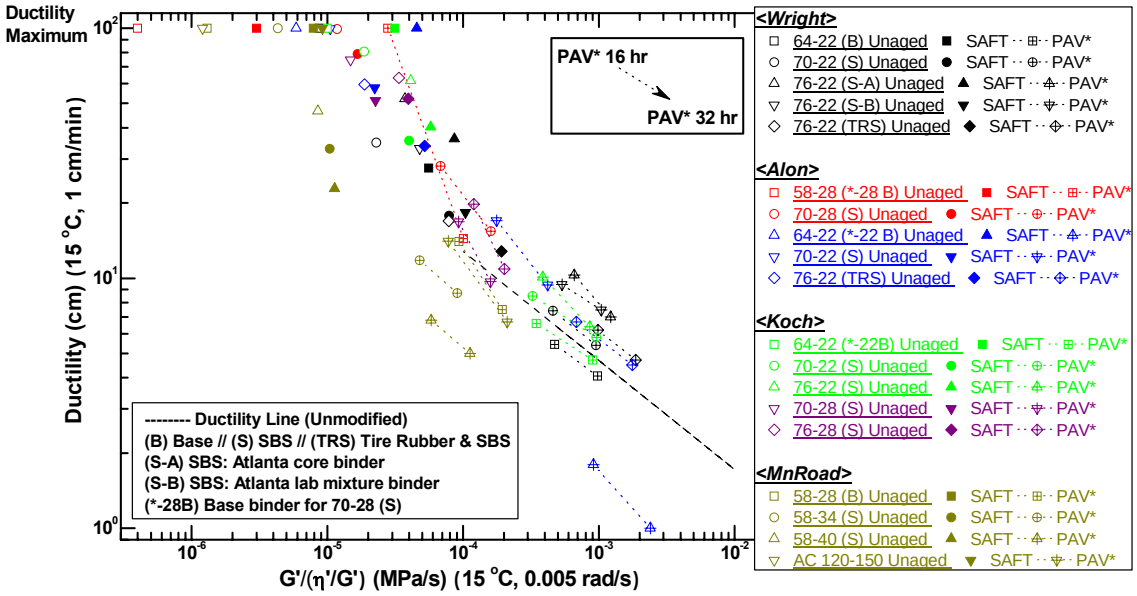

Figure II-3. Ductility versus DSR Function [G′/(η′/G′)] for Unaged and PAV* Aged PMAs and Base Binders (Wright through MnRoad)

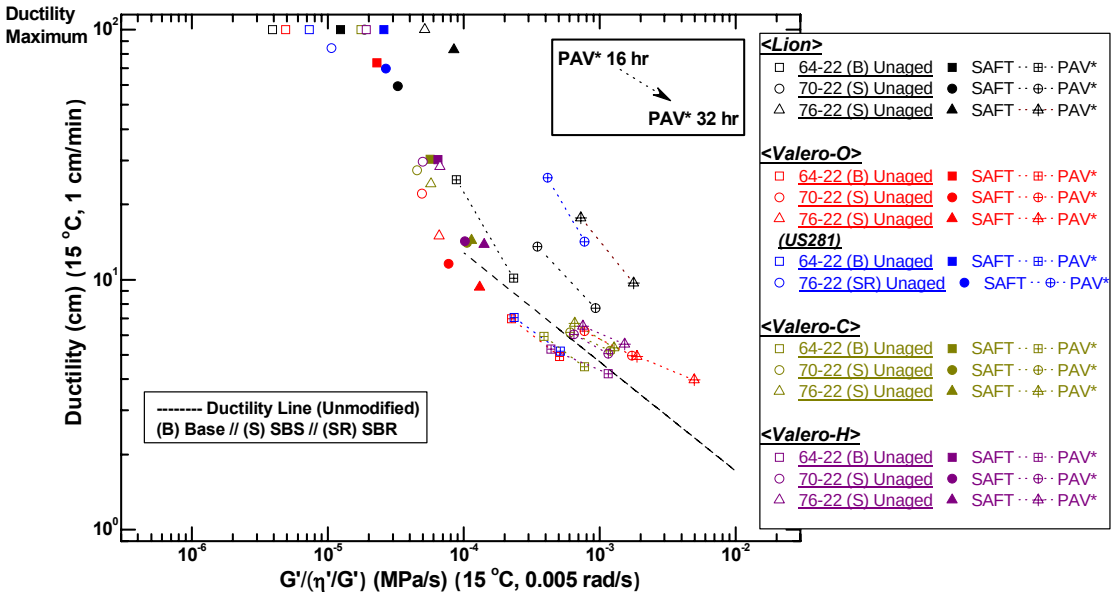

Figure II-4. Ductility versus DSR Function [G′/(η′/G′)] for Unaged and PAV* Aged PMAs and Base Binders (Lion through Valero)

There are a good many data sets on each of these two graphs and in order to assess the results, one must consider each set in turn and in particular compare the base binders to their respective modified binders. For example, perhaps the most interesting pair is the Alon PG 64-22 base binder (Figure II-3) compared to its PG 70-22 SBS modified binder. In this case, it is noted that the base binder (especially looking at the PAV* 16 hr and 32 hr aged binders) underperforms significantly the typical unmodified binder relationship established by Ruan et al. (2003a), falling significantly below the dashed line correlation. In contrast, however, is its PG 70-22 SBS modified binder. For this material, the PAV* 16 hr and 32 hr binders have moved above the unmodified binder correlation and there has also been a significant decrease in a DSR function comparing the unmodified PAV* 16 hr aged binder to the modified PAV* 16 hr aged binder. Thus, in this case, it appears that the unmodified binder, at least by the criterion of ductility, is really quite poor, whereas the modified binder has been improved very significantly by the SBS polymer, to the point of its ductility exceeding significantly the unmodified binder correlation. This result suggests some unique compatibility or effectiveness of the polymer modification for this particular binder.

Other binders show some similar shifts between the base binder and the modified binder but not to this degree in either ductility improvement or in reducing the DSR function value. For example, the Wright asphalt material shows an improvement in ductility with respect to the unmodified base binder, but the DSR function value is left largely unchanged. A similar observation is true of the Koch material for both the PG 70-22 and PG 76-22 modified binders (the base binder for the Koch PG 70-28 and PG 76-28 modified binders were not available for testing so such observations about these modified binders are not possible). In Figure II-4, the biggest differences in ductility between the base binder and the modified binder are observed with the Valero Oklahoma SBR binder that was used in US 281. However, for this binder there is again, as for some of the others noted above, relatively little change in the DSR function with modification. The Lion material also shows a movement toward higher ductility away from the unmodified binder correlation. However, there is a significant increase in a DSR

function with modification that may work against the binder in service by providing a stiffer binder from the beginning, thereby making the binder less tolerant than the base binder of aging in service. The significance of these discussions is elaborated on in Chapter IV where binder aging in pavements is considered.

Figures II-5 through II-8 present the same data as in Figures II-3 and II-4 but plotted as the DSR function map (log G′ versus η′/G′). On this map, the ductility-DSR function correlation of Ruan et al. (2003a) converts from a line to a family of ductility curves, and these curves are shown as dashed lines in the two figures. The numbers on the dashed lines correspond to the ductilities, and the curves are shown for ductility values 10 cm or less. As a binder oxidizes, it generally moves from the lower right on this map toward the upper left corner. The exact path taken is determined by the specific rheological properties of the individual binders. Figure II-6 is an expansion of the top left corner of Figure II-5 and shows those data points in more detail. In these graphs, the actual binder ductilities are not shown, and the relative position on the map corresponds to the DSR function value for the binder. Thus, a smaller DSR function corresponds to a less aged binder having a higher calculated ductility and appears to the lower right on the map, whereas a higher DSR function corresponds to a more aged binder having a lower calculated ductility and appears more toward the top left portion of the map. Thus, comparing the Alon PG 64-22 base binder to its PG 70-22 modified binder, it was seen that the modified binder is shifted significantly so that the 16 hr PAV* aging level for the unmodified binder is at a calculated ductility value of 5 cm whereas for the modified binder, the corresponding level of aging places it at a calculated ductility of 10 cm. Again, this shift reflects only the change in the DSR function and not the actual increase in ductility afforded by the modification, which is plotted only in Figures II-3 and II-4. In these DSR maps, we also observe the shift in path as a result of the polymer modification.

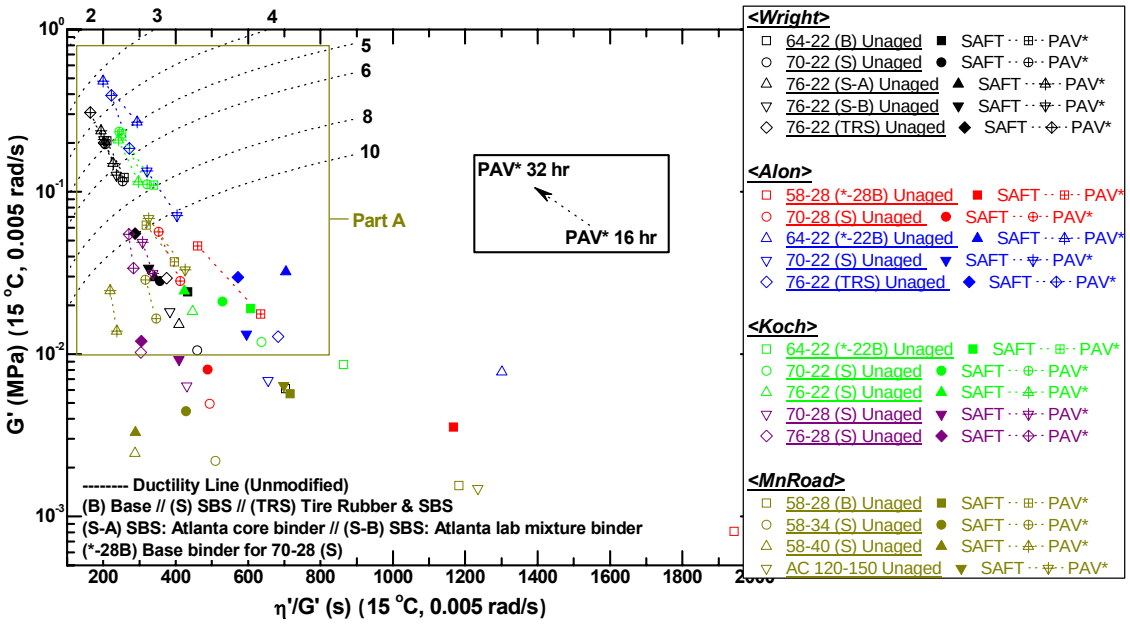

Figure II-5. G′ versus η′/G′ for Unaged and PAV* Aged PMAs and Base Binders (Wright through MnRoad)

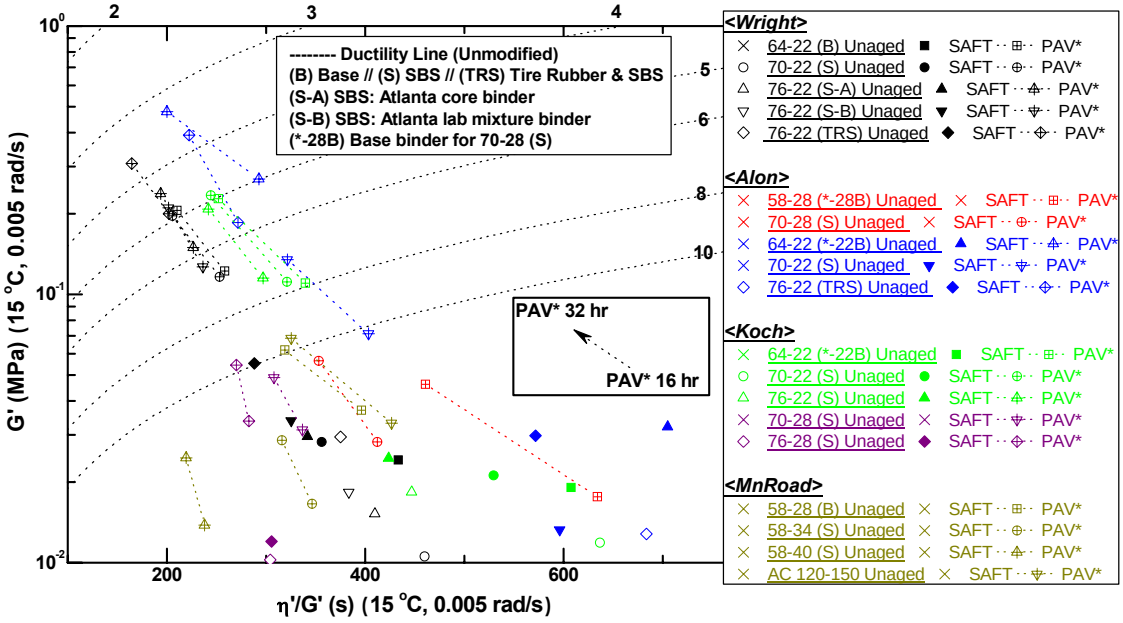

Figure II-6. Part A: G′ versus η′/G′ for Unaged and PAV* Aged PMAs and Base Binders (Wright through MnRoad)

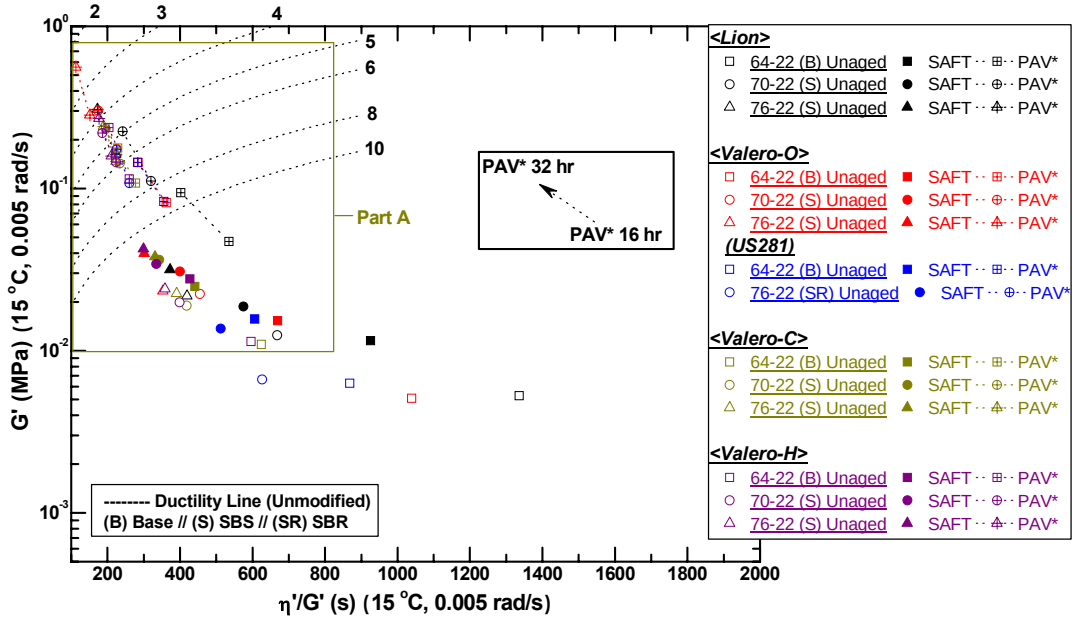

Figure II-7. G′ versus η′/G′ for Unaged and PAV* Aged PMAs and Base Binders (Lion through Valero)

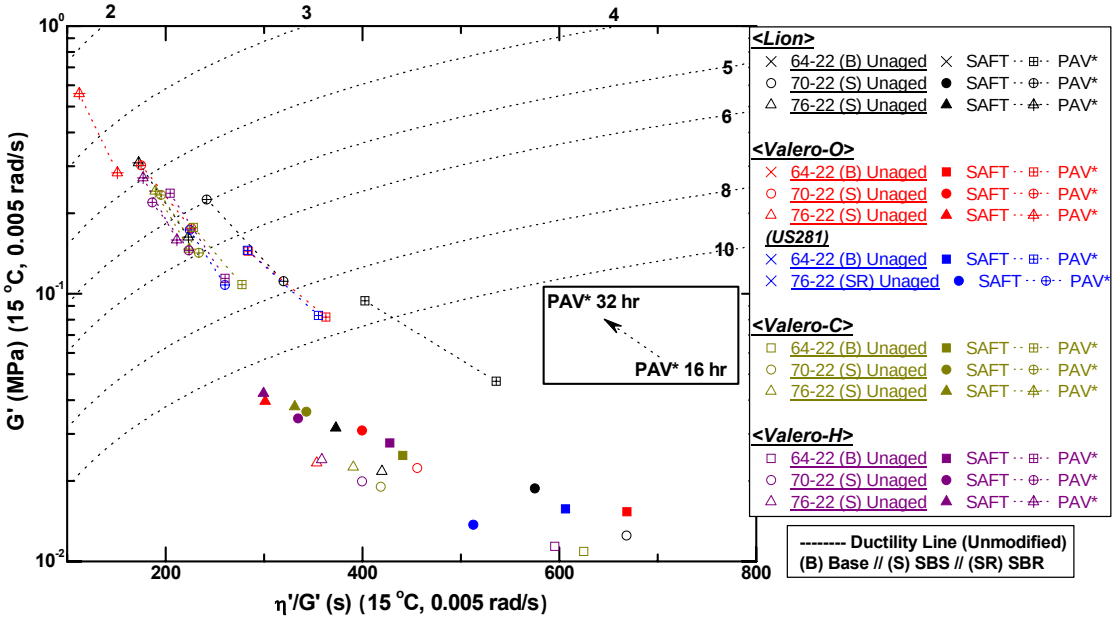

Figure II-8. Part A: G′ versus η′/G′ for Unaged and PAV* Aged PMAs and Base Binders (Lion through Valero)

Additional insight to the aging of polymer-modified binders and its impact on their DSR properties is provided through Figures II-9 and II-10. These two graphs build on Figures II-3 and II-4 by adding data for the environmental room aging of the neat film binders for 3, 6, 9, and 12 months beyond SAFT aging.

Again, a very interesting binder system is the Alon base binder and its PG 70-22 SBS modified binder shown in Figure II-9. As noted above, the base binder falls well below the ductility-DSR function correlation whereas the polymer-modified binder falls above the correlation and shifted to a lower DSR function value. The 3 months environmental room thin film aging data point virtually coincides with the PAV* 32 hr point. The 6, 9, and 12 month aging points fall at regularly higher values of the DSR function and at 6 months, the data point lies on the correlation whereas for the 9 and 12 month points, the data fall below.

Likewise, the PG 76-22 tire rubber/SBS modified binder starts out above the line at 3 months but the 6, 9, and 12 months data points fall well in line with the unmodified binder. This trend will be mentioned again in discussions of the force ductility curves but is stated here with the conclusion that after enough aging, the benefit of the polymer modifier toward improving the ductility of the binder is lost, probably largely because of the hardening of the underlying asphalt binder, but also because of degradation of the modifier, as is noted in Chapter III.

This observation has an important impact on methods used to evaluate the durability of modified binders because it suggests that in addition to knowing the basic properties of the modified binder itself, testing should be used to evaluate the base binder properties, independent of the modified binder. After all, it appears to be the underlying base binder properties that ultimately determine the modified binder properties after a sufficient amount of oxidative aging. Thus, it is important to know where the modified binder ultimately is headed. This observation of the merging of the modified binder ductility-DSR function aging path to the unmodified base binder path is also seen clearly in Figure II-10 with the Valero Houston base binder and its two modified SBS binders.

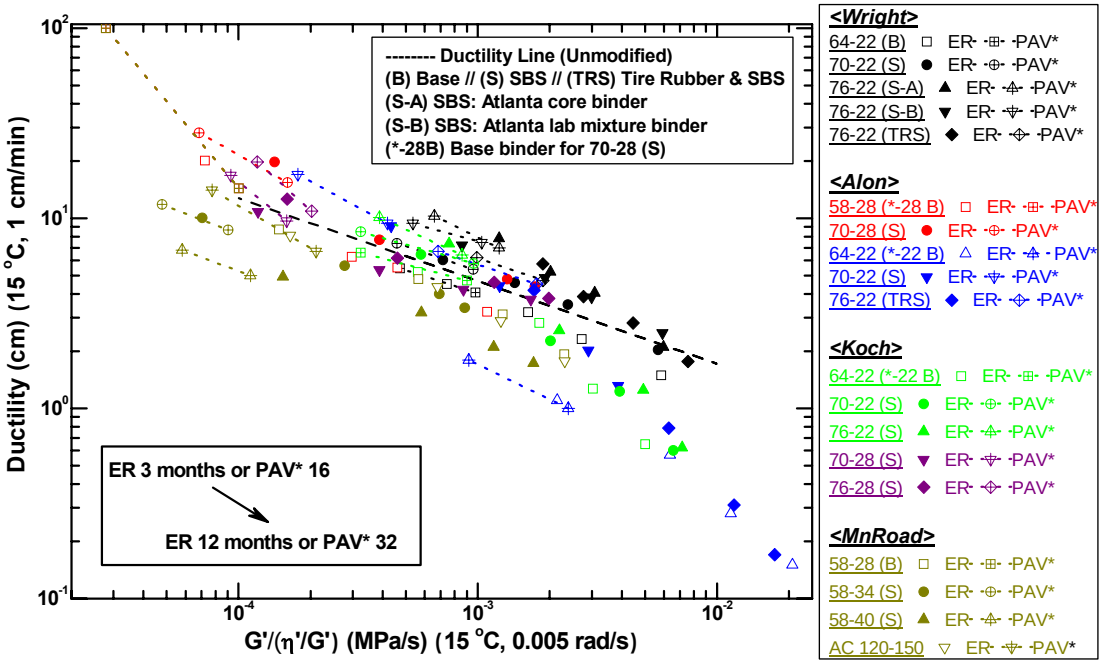

Figure II-9. Ductility versus DSR Function [G′/(η′/G′)] for PAV* and ER Aged PMAs and Base Binders (Wright through MnRoad)

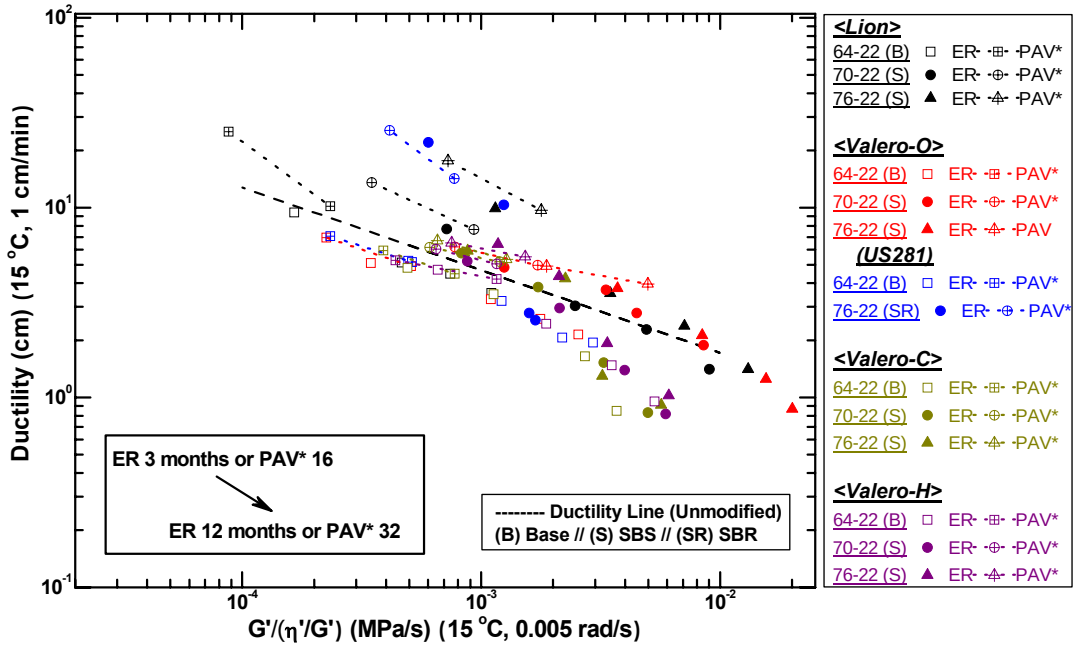

Figure II-10. Ductility versus DSR Function [G′/(η′/G′)] for PAV* and ER Aged PMAs and Base Binders (Lion through Valero)

Another interesting comparison is seen in Figures II-11 and II-12. In these graphs, the data for all the base and modified binders are shown but not identified with respect to the binder suppliers. Instead, they are identified simply as to performance grade so that both PG 58-28 base binders are shown with the same symbol, all the PG 64-22 are shown with another symbol, all the PG 70-22 as another symbol, and so on.

In Figure II-11, all of the data are shown for both environmental room thin film binder aging out to 12 months and for the PAV* 16 and 32 hr PAV apparatus aging conditions. Generally, it is observed that with a performance grade shift to higher temperatures, there is a shift of the data from below the ductility-DSR function correlation to above the correlation. This point is made more clearly in Figure II-12 where only the data points for which ductility values between 3 and 10 cm are shown. Additionally, there are correlating lines shown for each of the performance grades. Clearly, the PG 58-40 performance grade lies well below the correlation of Ruan et al. (2003a), followed by the PG 58-34 and then the two base binders, PG 64-22 and PG 58-28, all of which lie below the correlation but with the base binders closer than the modified binders. Lying above the correlation are the PG 70-22 and the PG 76-22 modified binders, and with each PG shift, there is an approximate corresponding shift of the line toward or away from the Ruan et al. (2003a) correlation.

This result suggests that in general, polymer modification shifts the base binder performance in the direction of increased ductility. Note that the Alon base binder does not appear in Figure II-12 because the PAV* 16 and 32 hr condition binders fall below a ductility of 3 cm.

Another conclusion that might be proposed based upon Figure II-12 is that suppliers in the course of the developing modified binder systems have gravitated to using base binders that fall below the average of most base binders (at least compared to those reported by Ruan et al., 2003a) as well as the ones measured in this project that fall below his correlation. Now this may not be a generalizable observation because of the small number of binders studied. However, it is something that might be considered in future studies when evaluating the optimization of polymer-modified binder systems and

whether this might in fact be something that manufacturers have learned to do as a good practice.

It should be noted also that typically polymer modification more likely raises the high temperature end (changes 64 to 70 or 76) rather than change the low temperature end. Thus, the modified binders made from the PG 64-22 binders become PG 70-22 or PG 76-22. It is noted that the MnRoad binders appear to be anomalous in that the PG 58-28 binder is modified by the addition of polymer, and in this case the high temperature grade is maintained at 58 while the low temperature number is decreased from -28 to -34 to -40. This fact is likely the reason for the shift of the lines of those binders away from the ductility correlation to the direction of lower ductility for a given DSR function (or smaller DSR function for a given ductility). This observation is mentioned again in the discussion of the GPC chromatograms of these materials. As a preview to that discussion and recognizing that the -34 and -40 binders have also employed, according to the manufacture, sulfur cross linking during the hot-mix process, it is hypothesized that apart from polymer modification, there has been some additional modification of the base binder perhaps with a lighter asphaltic material that serves to reduce the low temperature grade.

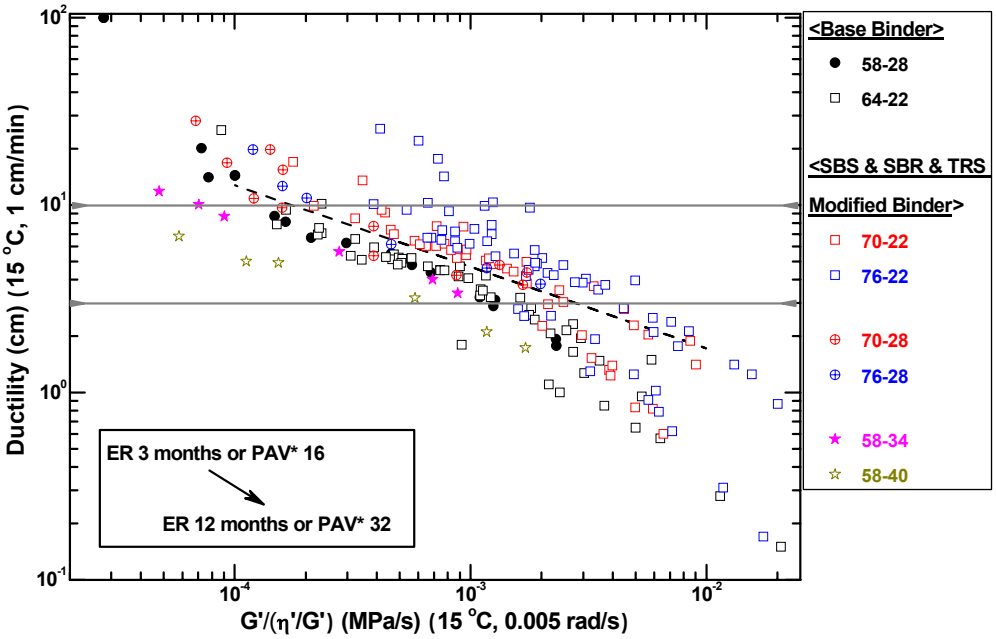

Figure II-11. Ductility versus DSR Function [G′/(η′/G′)] for PAV* and ER Aged PMAs and Base Binders

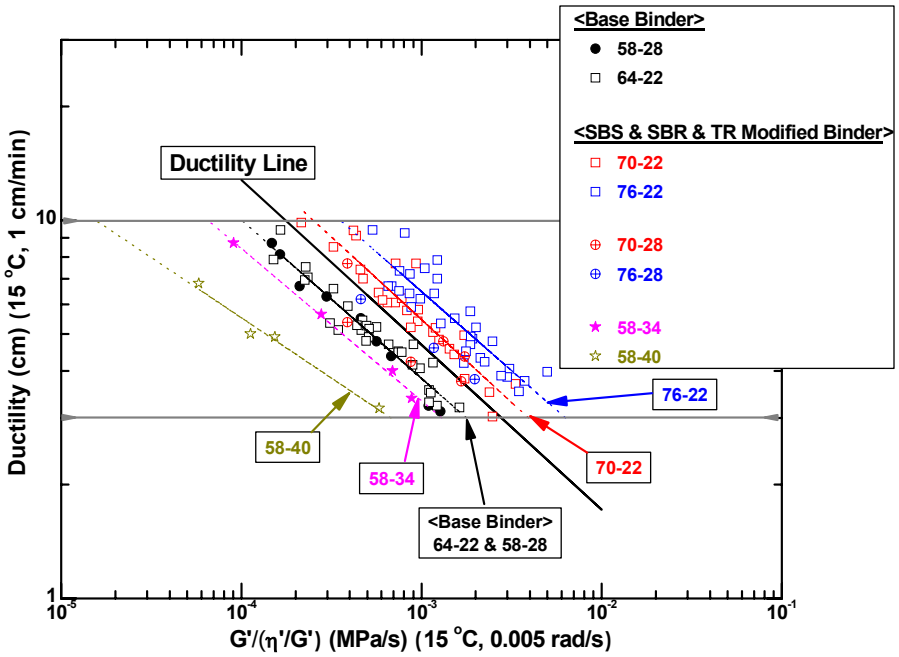

Figure II-12. Ductility versus DSR Function [G′/(η′/G′)] for PAV* and ER Aged PMAs and Base Binders (Ductility from 3 to 10 cm)

The same data that were shown in Figures II-9 and II-10 are repeated in Figures II-13 and II-14 in the form of DSR function maps. Again, these data include not just the PAV* 16 and 32 hr aging conditions but also the environmental room thin film binder aging experiments at 3, 6, and 9 months. In these graphs, we compare the aging path followed by the PAV* conditions to the aging path followed by the atmospheric air pressure 60 °C aging conditions. Again, the different binders follow different paths across the map. From these graphs, we observe that very nearly, probably within experimental errors, the environmental room aging and the PAV apparatus aging paths are the same for all the binders. This fact suggests (but does not prove) that the changes in the materials that occur as a result of oxidation are the same changes, or nearly so, whether conducted at the more severe 20 atm, 90 °C aging as at the 1 atm, 60 °C aging. We know that such cannot be said of the chemical reaction kinetics. However, it may well be that the products of the reaction ultimately turn out to be essentially the same at least as far as the rheology and changes in the rheology of the materials is concerned. This result suggests that even though we might not be able to reproduce the hardening rates with accelerated conditions, we may well be able to reproduce the aging state with accelerated conditions and all that needs to be done is to calibrate the aging state after a given length of time at the PAV* conditions to the aging state achieved by the environmental room or the aging state achieved in the pavement. This could be a significant fact to be taken into account when developing an accelerated aging protocol that would allow one to predict binder durability in pavements. This issue will be discussed further in Chapter V.

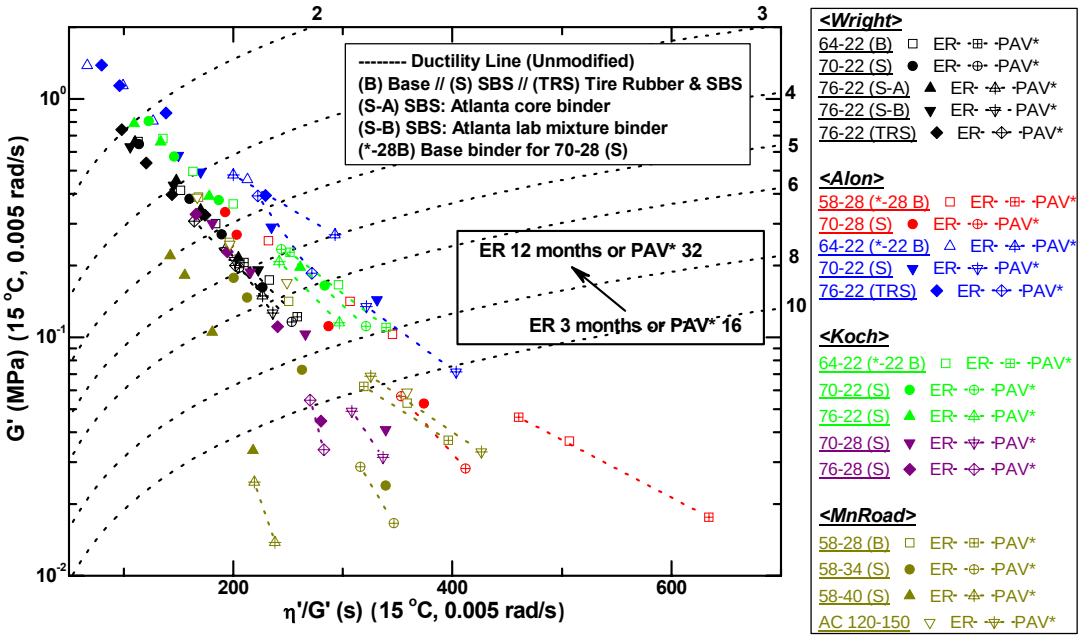

Figure II-13. G′ versus η′/G′ for PAV* and ER Aged PMAs and Base Binders (Wright through MnRoad)

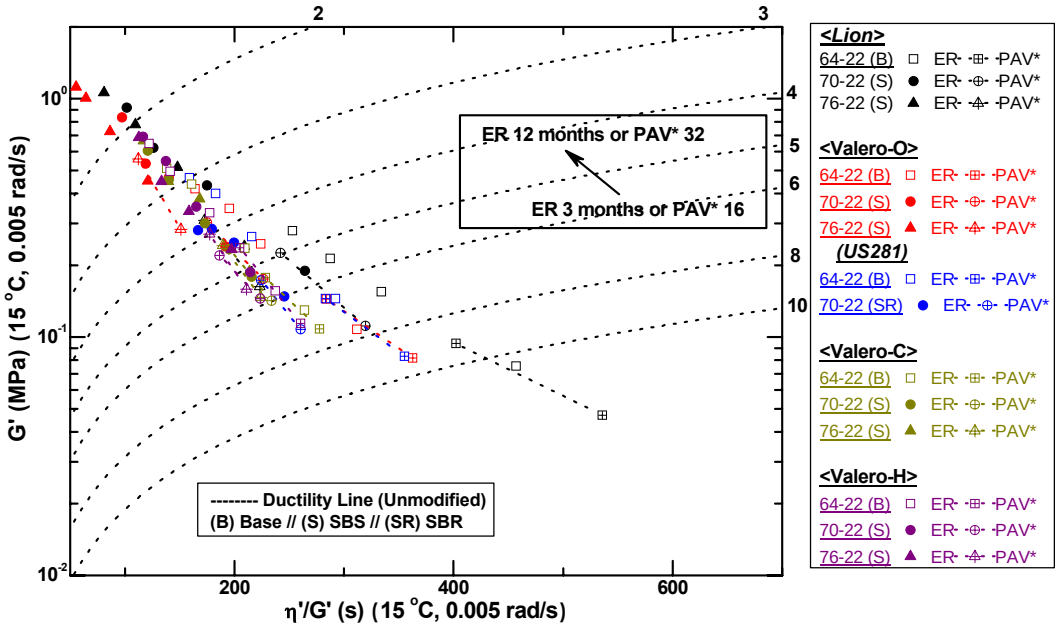

Figure II-14. G′ versus η′/G′ for PAV* and ER Aged PMAs and Base Binders (Lion through Valero)

Oxidative Hardening Rates

A potentially important issue in establishing binder hardening in pavements and the rate at which it occurs is the oxidation kinetics and resulting hardening response that is intrinsic to each binder. Figures II-15 and II-16 provide the DSR function hardening rates at 60 °C from the environmental room aging for various binders studied in this chapter. These data are insufficient to establish complete reaction kinetic expressions for the binders (thus to allow calculations of reaction rates and hardening rates as a function of temperature history) because they are measured at only one temperature. However, 60 °C is a meaningful temperature because it is the approximate maximum pavement temperature that the binders experience and as such, it is the temperature near which a good fraction of the oxidation probably occurs. Nevertheless, the oxidation data are measurements at only a single temperature.

Included in the information of the legend for each base and modified binder is the slope of the line, expressed as [log (MPa/s)]/mo. For the materials presented in this chapter, the rates vary from about 0.1 to about 0.3. This factor of three is likely significant when it is reflected into pavement aging rates. The lowest value of this DSR function hardening rate is 0.11 for the PG 76-22 SBR modified binder that was used in US 281. The highest rate of 0.29 was measured for the Alon PG 70-28 and the Koch PG 70-28 binders, although a value close to 0.3 is not unusual and is approached by a number of the other asphalts.

Note that the SAFT level of aging (equivalent to RTFOT aging) appears at zero months and was the starting point of these binders when placed in the environmental room. Note also that the aging at 3, 6, 9, and 12 months form essentially a straight line that intercepts 0 months well above the SAFT level of aging as has been documented in the literature (Lau et al., 1992; Liu et al., 1996). This offset is typical of binder oxidation and hardening kinetics and complicates assessing binder aging in pavements. The intercept of the long term hardening rates compared to the SAFT values has been called an initial jump and represents the fact that between 0 and 3 months (at 60 °C), there is a

higher aging rate period which eventually declines and transitions into a steady rate after a period of time. The reaction chemistry responsible for this early high rate is not well understood, but very likely is a result of free radicals that exist in the binder and that are ready to oxidize as soon as they come in contact with oxygen. Once these are depleted, the oxidation proceeds at a slower but steady rate.

Also, it has been noted previously that the hardening of a binder is a process that involves two separate phenomena. On one hand, the oxidation reaction kinetics is a function of temperature and oxygen pressure in the binder. The reaction kinetics for a large number of binders has been well documented in the literature (Lau et al., 1992; Liu et al., 1996; Glover et al., 2005). The second issue is the result of structuring in the binder that leads to physical changes. The oxidation of the binder forms carbonyl compounds, and these carbonyl compounds result in the formation of more polar materials that associate and behave like asphaltenes. These asphaltenes in turn act like solid particles in the binder, which serve to structure the material significantly and thereby result in a large amount of stiffening of the binders (Lin et al., 1996; Liu et al., 1998a and 1998b). This two-step process, oxidation followed by molecular associations that result in binder stiffening, is reflected in Figures II-15 and II-16 as a single process.

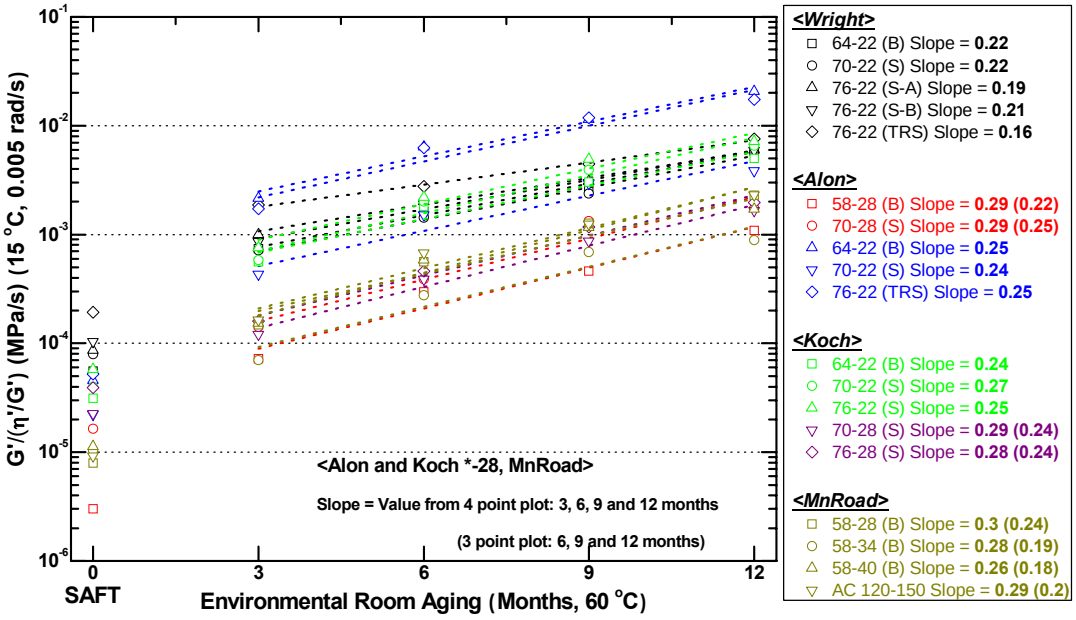

Figure II-15. DSR Function [G′/(η′/G′)] Hardening Rate for ER Aged Binders (Wright through MnRoad)

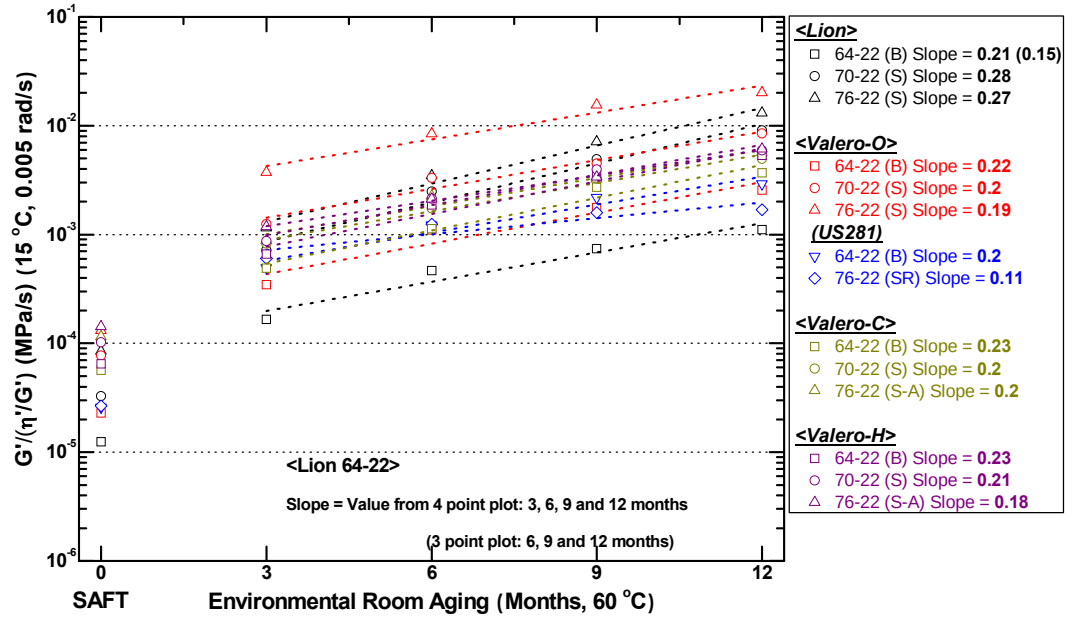

Figure II-16. DSR Function [G′/(η′/G′)] Hardening Rate for ER Aged Binders (Lion through Valero)

Within the context of this two-step process, it is noted that a high hardening rate could be the result of a high oxidation rate accompanied by a moderate amount of associations, and consequent stiffening the binder, or it could be the result of a moderate oxidation rate accompanied by an exceptionally high stiffening in response to the oxidation, or both the oxidation rate and the stiffening in response to oxidation could be high which could result in a very high hardening rate. It was noted in the discussion of the Corbett compositions that the Lion asphalt did not seem to grow asphaltenes very much as a result of the oxidation. Yet, in Figure II-16, it is noted that its hardening rate for both the PG 70-22 and the PG 76-22 binders is virtually as high as any of the others. This may well be the result of a high oxidation rate in spite of a moderate tendency to produce asphaltenes in response to the oxidation.

Figures II-17 and II-18 show similar hardening rates but in terms of a different rheological property, the low shear rate dynamic viscosity at 60 °C. These hardening rates are quite similar to the DSR function hardening rates although generally, they are lower. The range in these two figures is a low of 0.13 (again, for the US 281 PG 76-22 SBR modified binder) to a high value of about 0.25 for the Lion PG 70-22, for the Wright base binder and for two of the MnRoad binders.

Although both the DSR function and low shear rate limiting viscosity hardening rates have been presented in these figures, the DSR function is used instead of viscosity because we believe it relates better to pavement performance; it correlates to ductility over an important range where failure likely occurs and ductility has been previously observed in the literature to relate well to pavement performance (Clark, 1958; Doyle, 1958; Kandahl, 1977; Goodrich, 1988). Appendix A tabulates the DSR function data.

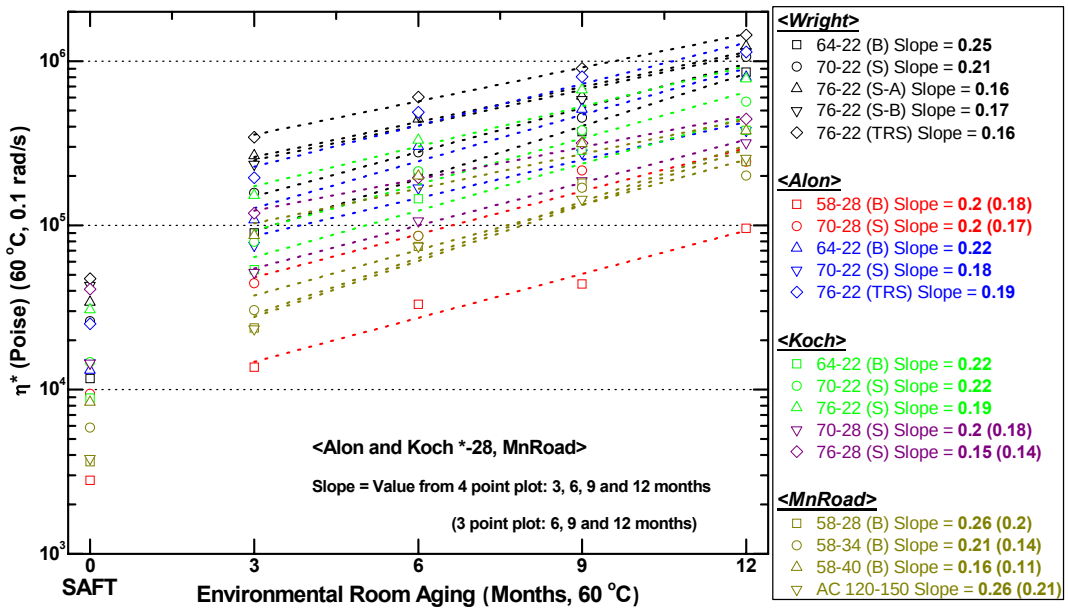

Figure II-17. η* Hardening Rate for ER Aged Binders (Wright through MnRoad)

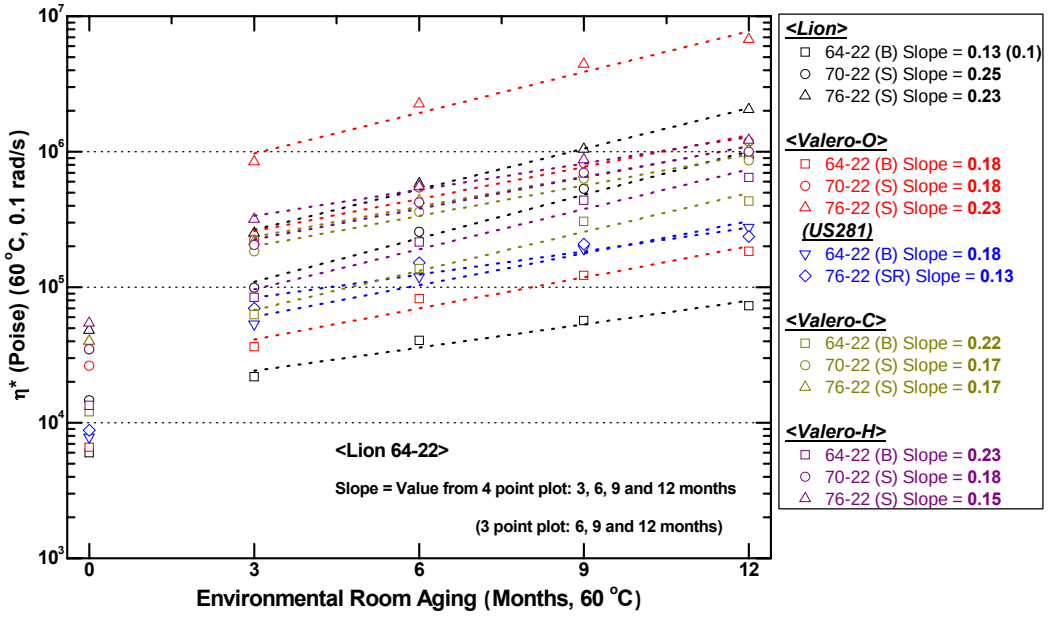

Figure II-18. η* Hardening Rate for ER Aged Binders (Lion through Valero)

GPC Spectra

Size exclusion chromatograms provide definitive evidence of the extent of polymer modification of the various binders. Figures II-19 through II-21 show GPC chromatograms for the Koch base binder (PG 64-22) and for the two levels of modification (PG 70-22 and PG 76-22). In each figure, there are two sets of chromatograms. One set was measured using the refractive index detector (left axis) and the other using the specific viscosity detector (right axis). The specific viscosity detector is much more sensitive to the presence of polymer so that the polymer peak that occurs at about 19 minutes is much more evident with this detector. However, the refractive index detector is a much better detector of the smaller molecular weight components, and thus we present both sets of chromatograms.

Figure II-19 shows the unmodified base binder. In this figure, we note the typical presence of the asphaltene peak that elutes from the column at about 23 minutes and the presence of the maltenes peak, at about 29 minutes. It is also noted that the asphaltenes peak grows significantly as a result of oxidation so that the SAFT, PAV* 16 hr and PAV* 32 hr asphaltenes peaks lie significantly above the unaged asphaltenes peak in the refractive index detector response.

Figure II-20 shows the corresponding chromatograms for the PG 70-22 modified binder. In this case, we see from the specific viscosity detector a very prominent polymer peak at about 19 minutes. Furthermore, it is noted that with increased aging, the size of this polymer peak decreases rather noticeably, and that this decrease is accompanied by an increase in the material that elutes between the polymer peak and the asphaltenes peak. Evidently, with oxidation, the polymer modifier is broken down by reaction to smaller molecular weight components. By the time the modifier has been subjected to PAV* conditions for 32 hr, the polymer peak has been reduced to well under half its height in the unaged state.

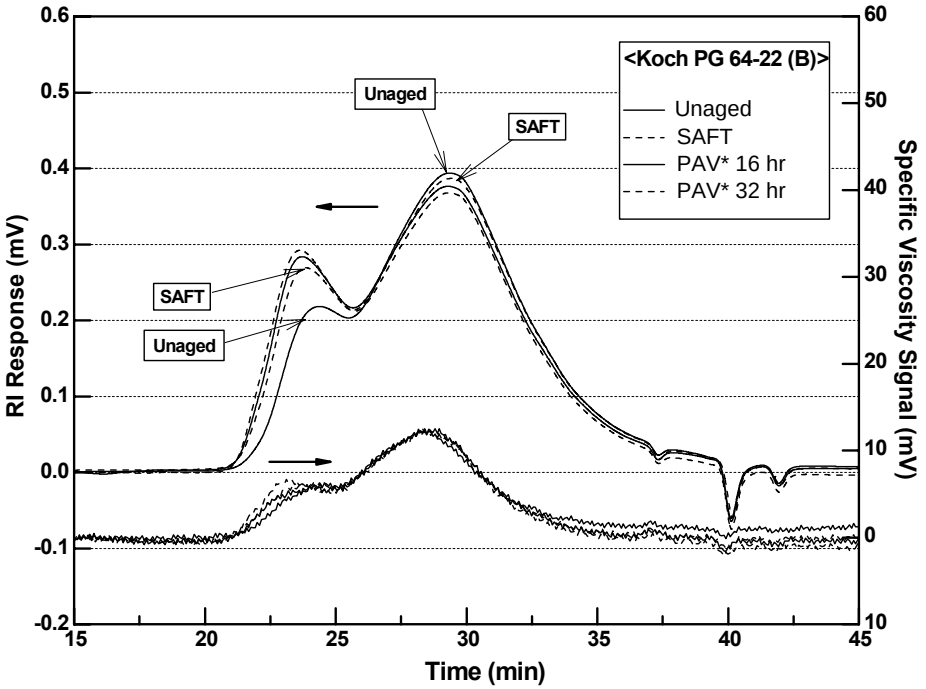

Figure II-19. GPC Chromatograms for Koch PG 64-22

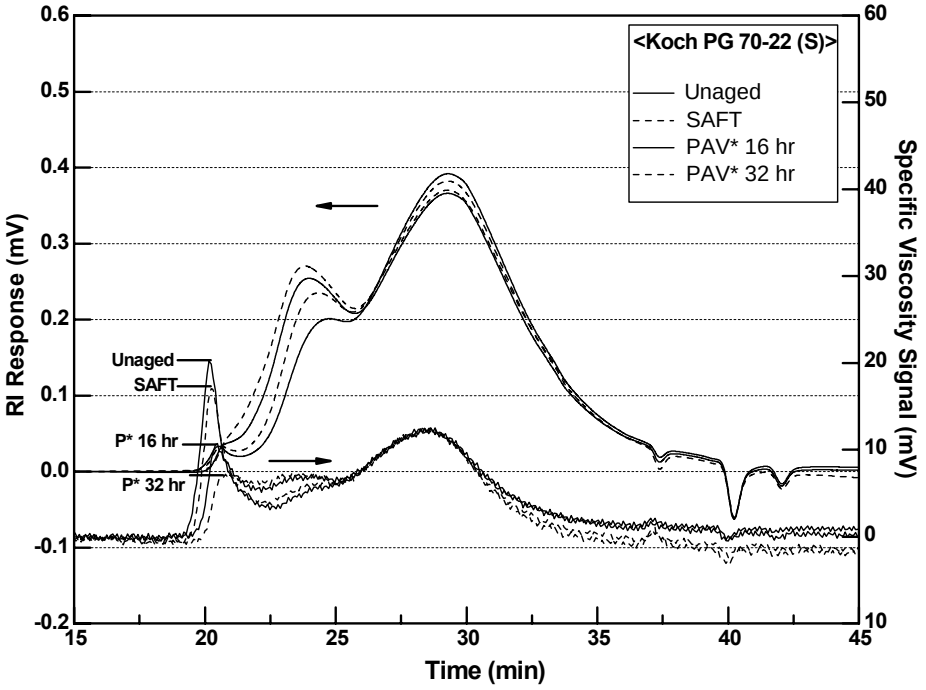

Figure II-20. GPC Chromatograms for Koch PG 70-22

Figure II-21 shows the corresponding graphs for the Koch PG 76-22 binder. Again, the same trends are evident except that now the amount of modifier is much greater than it was for the PG 70-22 binder. Nevertheless, it is again noted that after PAV* 32 hr oxidative aging, the size of the polymer peak has been reduced to well under half its unaged height. At the same time, of course, the asphaltenes peak is growing significantly (as observed with refractive index chromatograms) so that there are two effects that occur simultaneously during oxidation of the binder: production of asphaltenes which results in stiffening the base binder, and reaction of the polymer to reduce its average molecular weight and most certainly thereby reducing its effectiveness. The net effect of both of these phenomena is to convert the modified binder to a binder that becomes closer and closer in character to the unmodified base binder.

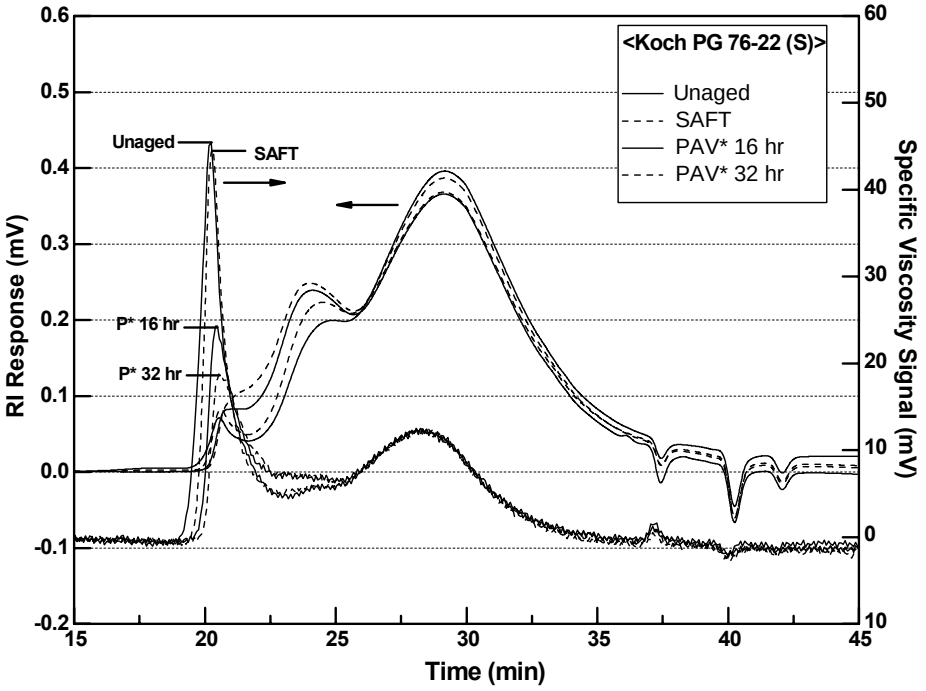

Figure II-21. GPC Chromatograms for Koch PG 76-22

Figures II-22 through II-24 are chromatograms of the PG 58-28 base binder for the MnRoad site and the modified binders for Cells 34 and 35 which are the PG 58-34 and PG 58-40 binders. In this case, in addition to the same trends that were observed for the Koch binder, it is seen that there is a difference in the character of the maltenes peak between the modified and unmodified chromatograms. For the modified binders, the maltene's peak is significantly sharper, even triangular in shape, than it is for the unmodified binder. This different shape is very unusual and suggests, that in addition to the polymer modification, there may have been adjustments to the base binder maltenes. Such changes would explain the reduction in the low temperature performance grade from -28 to -34 to -40, even as polymer is added to the binder. Increasing the concentration of polymer normally increases the high temperature grade without greatly affecting the low temperature grade. So it appears that in this case the maltenes have been blended so as to maintain the high temperature grade constant while reducing the low temperature grade in an effort to achieve improved resistance to thermal cracking without adversely affecting pavement performance with respect to rutting**.**

Again, with MnRoad modified binders as was the case to the Koch modified binders, there is a significant reduction in the height of the polymer peak as a result of oxidation, and this reduction likely results in a decrease of the performance of the modified binder. Note that in Figure II-24, for the specific viscosity detector, the scale has been increased so that the amount of polymer relative to that in Figure II-23 is even greater than a visual comparison of the figures would suggest.

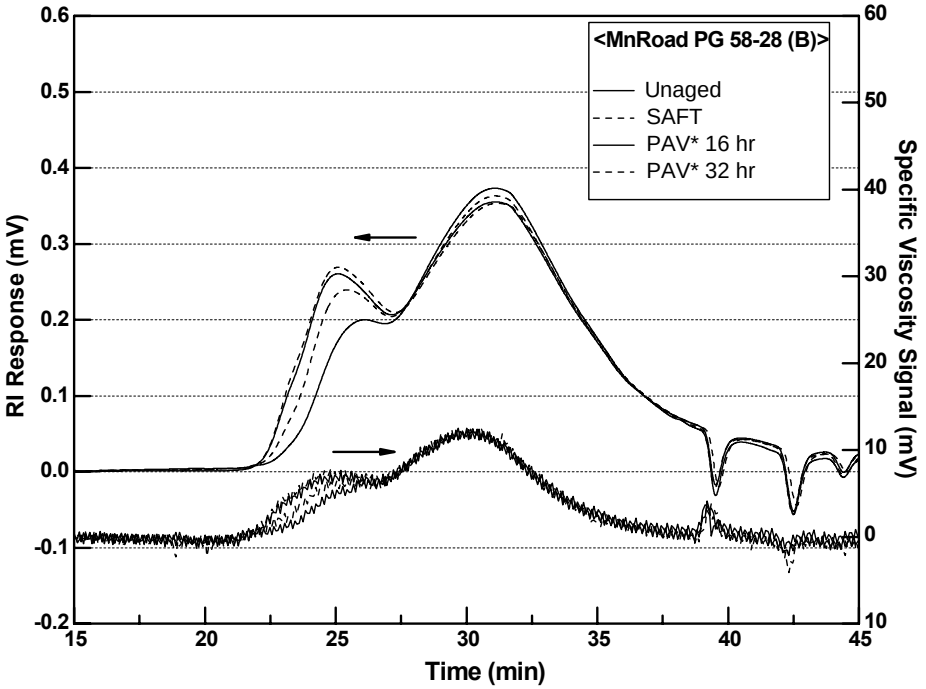

Figure II-22. GPC Chromatograms for MnRoad PG 58-28

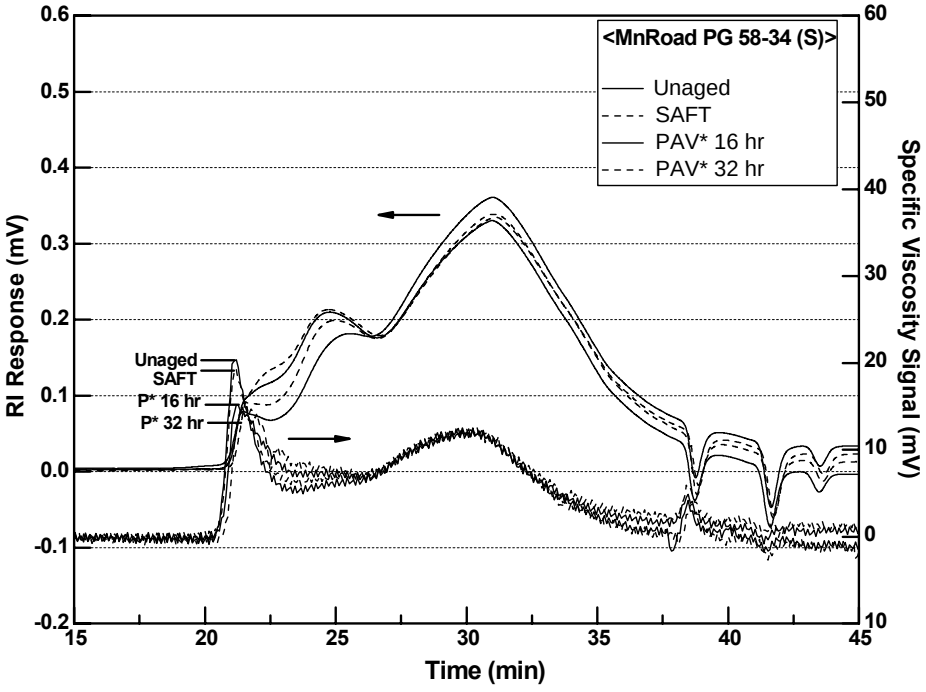

Figure II-23. GPC Chromatograms for MnRoad PG 58-34

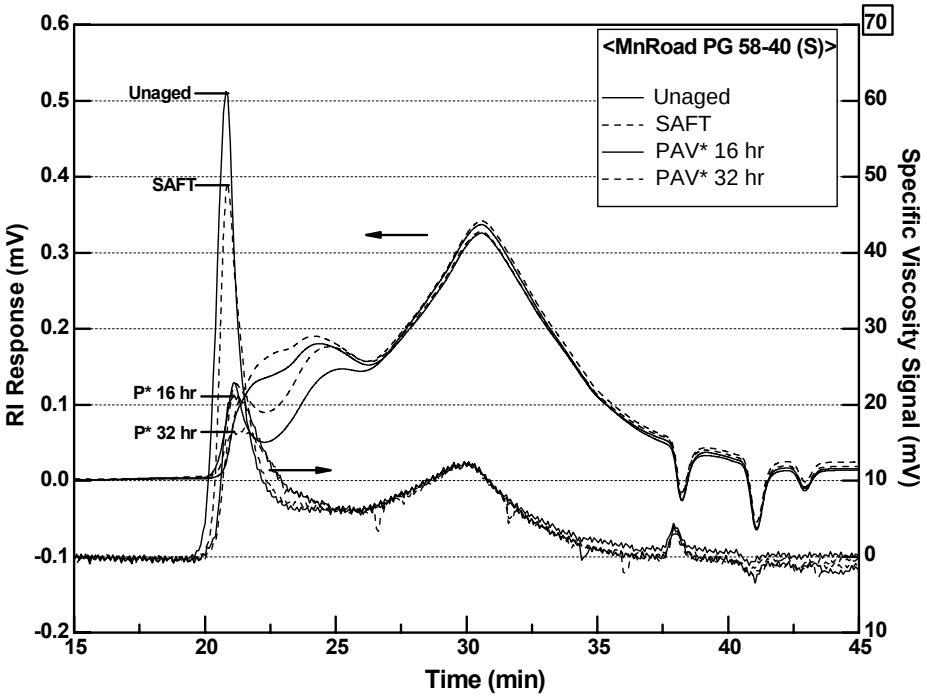

Figure II-24. GPC Chromatograms for MnRoad PG 58-40

Effect of Polymer Modifier on Elongational Properties

An additional dimension of the performance of the modified binders is obtained using the force ductility apparatus. In this work, force ductility values were measured at 4 °C for binders aged to different levels. Figures II-25 through II-27 show results for the Wright asphalts.

Figure II-25 shows the results for the SAFT aged binders. Here, it is seen that as the base binder of the sample is drawn out, the stress increases to a maximum value of 1 MPa and then declines without fracture as the relatively soft binder flows with elongation. This is typical of a viscoelastic material where at short elongation ratios (short times) the material behaves elastically so that an elastic stress elongation path is followed. However, at longer times, the viscous flow dominates and as the material flows, the stress declines with increasing elongation just as it would for a purely viscous material.

For the PG 70-22 and PG 76-22 SBS modified binders, however, there is a decidedly different behavior. For these two materials, at short times, the stress increases just as it did for the unmodified binder. However, once it reaches a maximum, and elongation continues, the presence of the polymer modifier keeps the binder from transitioning to viscous flow so that the maximum stress is held and even increased depending upon the amount of polymer present in the binder. This allows significantly longer elongation ratios to be achieved with binder remaining intact than was the case for the unmodified binder. For the PG 70-22 modified binder, an elongation ratio in excess of 9 is achieved; for the PG 76-22 SBS binder, an elongation ratio of about 7 is obtained and up to that point, the stress in the material has continued to increase, reaching a maximum at about 2 MPa.

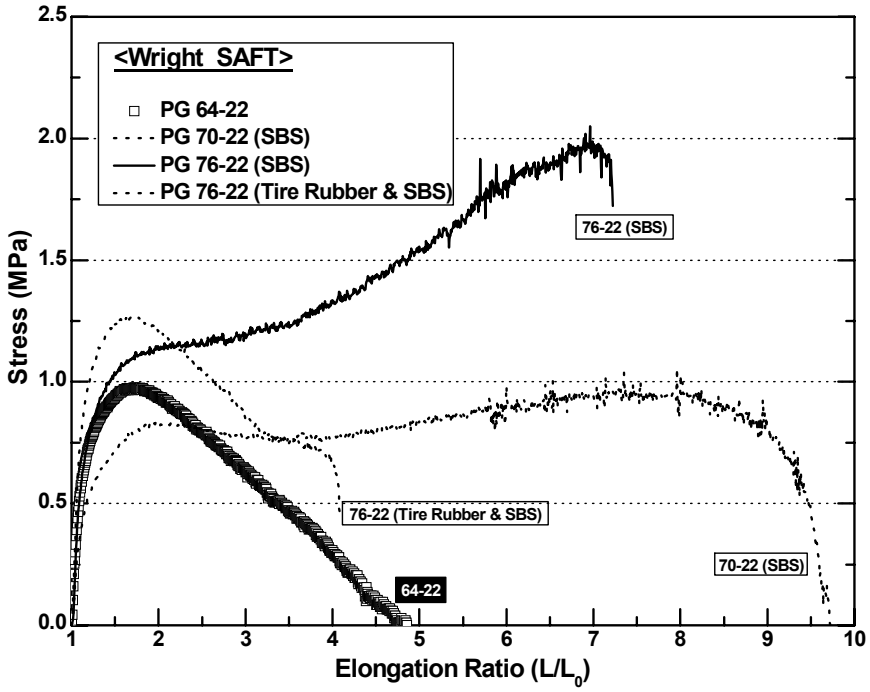

Figure II-25. Force Ductility at 4 ^{o}C for SAFT Aged Wright Asphalts

The fourth material shown in this graph is the PG 76-22 binder that was modified with both tire rubber and SBS, and it shows very little of the polymer character that is evident in the other two modified binders. However, the binder is clearly a different material from the base binder.

Figure II-26 shows the same binders aged at the PAV* 16 hr condition. In this case, it is seen that the force ductility performance of the modified binders is greatly degraded probably partly due to the degradation of the polymer noted in the GPC chromatograms but also due to the stiffening of the asphalt base binder due to the oxidation and consequent formation of asphaltenes. This process results in a stiffer binder and it is seen that the maximum stress level is increased significantly for all four of the binders. It is known that there is still some residual effect of the polymer in the two SBS modified binders in that the elongation ratios are significantly greater than they are for the unmodified binder. However, it is also clear that the elongation ratios are significantly reduced compared to the SAFT aged binders.

Figure II-27 shows the force ductility curves for the PAV* 32 hr aged Wright binders, and now we see that the elongation ratio is further degraded so that for both SBS modified binders, the ratio is reduced to about 1.6. In these force ductility curves, we see confirmed the earlier observation that with oxidation, the modified binders perform more and more like their unmodified base binders.

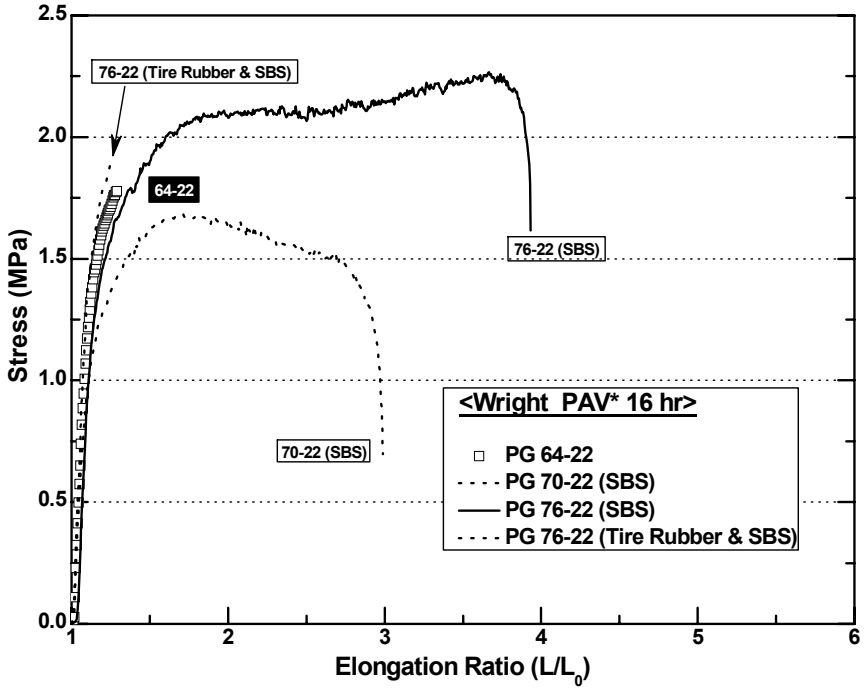

Figure II-26. Force Ductility at 4 °C for PAV* 16 hr Aged Wright Asphalts

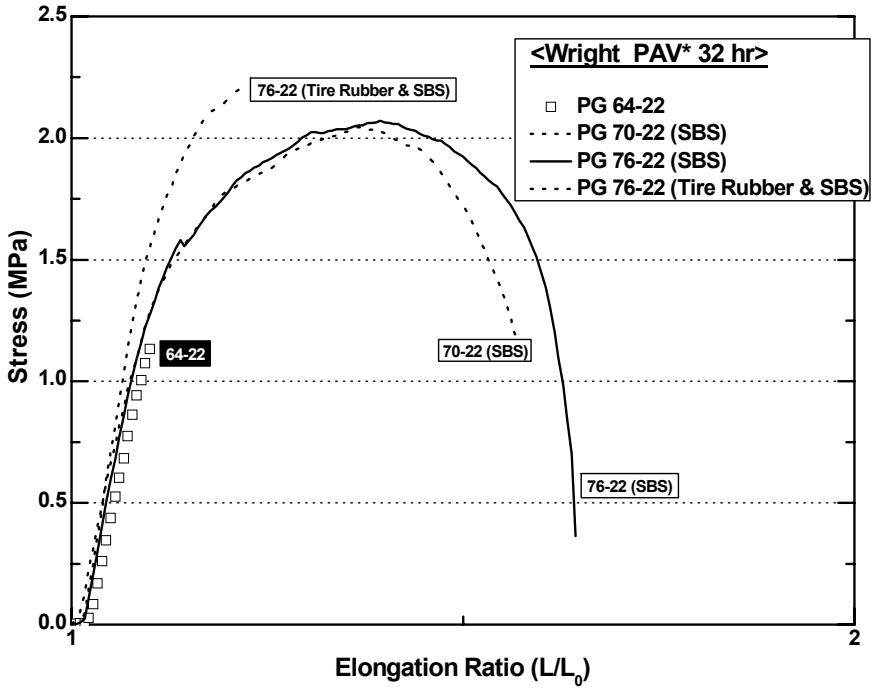

Figure II-27. Force Ductility at 4 °C for PAV* 32 hr Aged Wright Asphalts

Figures II-28 through II-30 contain the corresponding data for the Alon asphalts. In Figure II-28, we see a typical unmodified binder response that looks like a viscoelastic material. For the PG 58-28 unmodified binder and for the PG 64-22 binder, we see comparable qualitative responses (elastic stiffening followed by viscous flow) except that the PG 64-22 base binder is stiff enough that it never reaches a point where it can flow before the binder breaks at about 2 MPa. The modified binders, however, all show a very nice response where there is an asphalt peak followed by a second rise in stress with increasing elongation that is the consequence of the polymer modifier. For this polymer, it is seen that the 70-28 binder looks significantly softer than the 70-22 (as you might expect because it has the same high temperature PG grade but a lower low temperature PG grade), and we see that the PG 76-22 binder looks stiffer because it has a higher stress upon initial elongation due to the apparently higher grade base asphalt and this is followed by a continued rise to a stress level of 4.5 MPa in response to the presence of the polymer. These comparison graphs show the varied responses of the different materials.

Figure II-29 shows the same binders after the PAV* 16 hr aging process. Now we see that the elongation ratio of all the binders, except for the PG 70-28, have decreased very significantly. Even the PG 70-22 has an elongation ratio of only about 1.5. The PG 70-28, because of its design for a lower low-temperature PG grade, still can sustain significant elongation without breaking and reaches a maximum elongation ratio of about 10 at which point the maximum stress is 2.5 MPa.

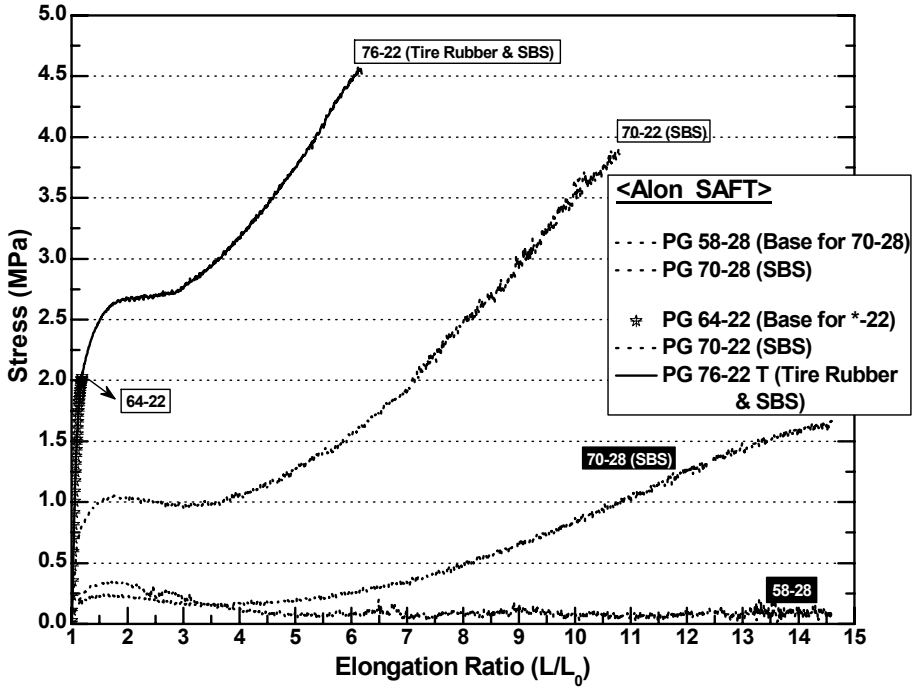

Figure II-28. Force Ductility at 4 °C for SAFT Aged Alon Asphalts

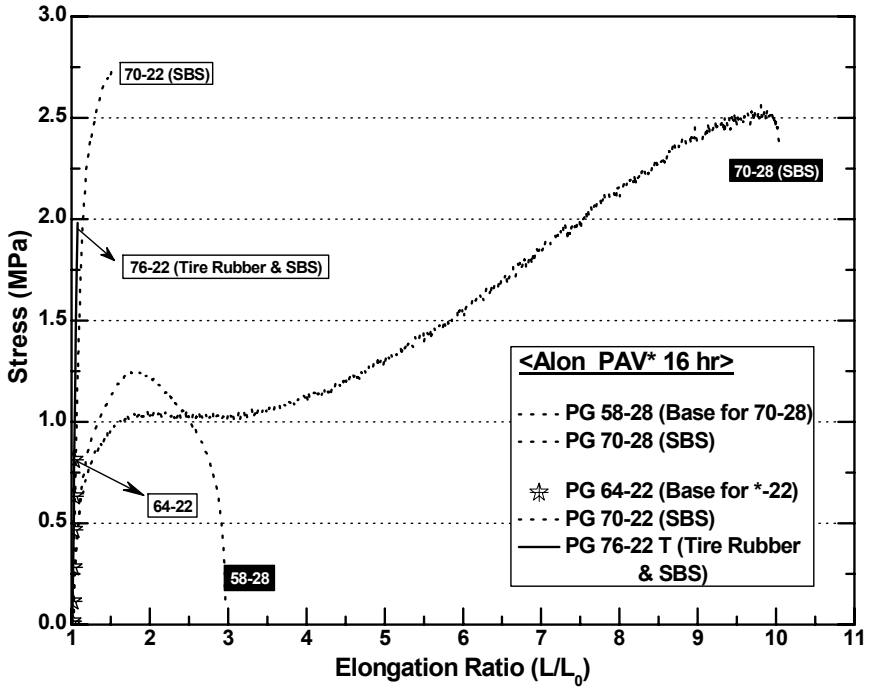

Figure II-29. Force Ductility at 4 °C for PAV* 16 hr Aged Alon Asphalts

In Figure II-30, we see that these effects are exaggerated even more, although the PG 70-28, perhaps surprisingly, still is able to support considerable elongation, out to a value of about six. In spite of this rather severe level of laboratory aging, this excellent force ductility performance was reflected in Figure II-3 for this material where we see that the PAV* 16 hr and 32 hr aging produces a binder with a ductility significantly above the Ruan correlation and has only stiffened the binder to a level of 10^{-4} MPa/s for the DSR function.

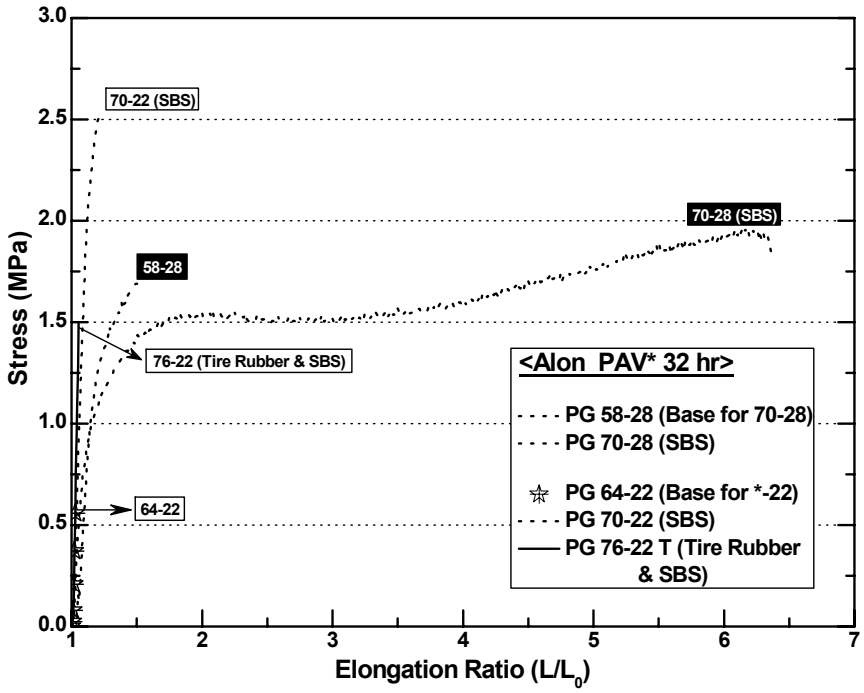

Figure II-30. Force Ductility at 4 ^{o}C for PAV* 32 hr Aged Alon Asphalts

Figure II-31 shows force ductility data for the aged Alon asphalts at 9 months in the environmental room. Note that even the PG 70-28 binder no longer has an elongation ratio that is significantly greater than the base binder.

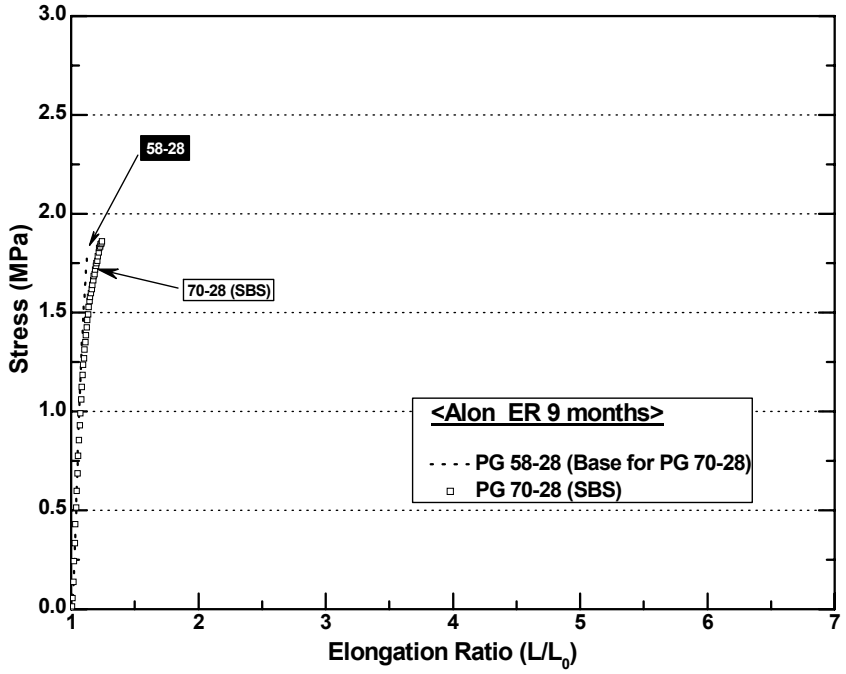

Figure II-31. Force Ductility at 4 ^{o}C for ER 9 Month Aged Alon Asphalts

Figure II-32 shows the SAFT aged Valero Oklahoma asphalts, and here it is seen that even at this fairly mild level of aging, for these binders the polymer modification shows very poor (from the point of view of force ductility) characteristics. This poor performance is reflected in Figure II-4 in which the binder, upon modification, shows an increase in the DSR function compared to the base binder. Although the ductility for the PAV* 32 hr aged PG 76-22 binder is greater than it would be for an unmodified binder at that same level of DSR function, it is still not a very great ductility because the DSR function has increased rather significantly compared to that of the base binder.

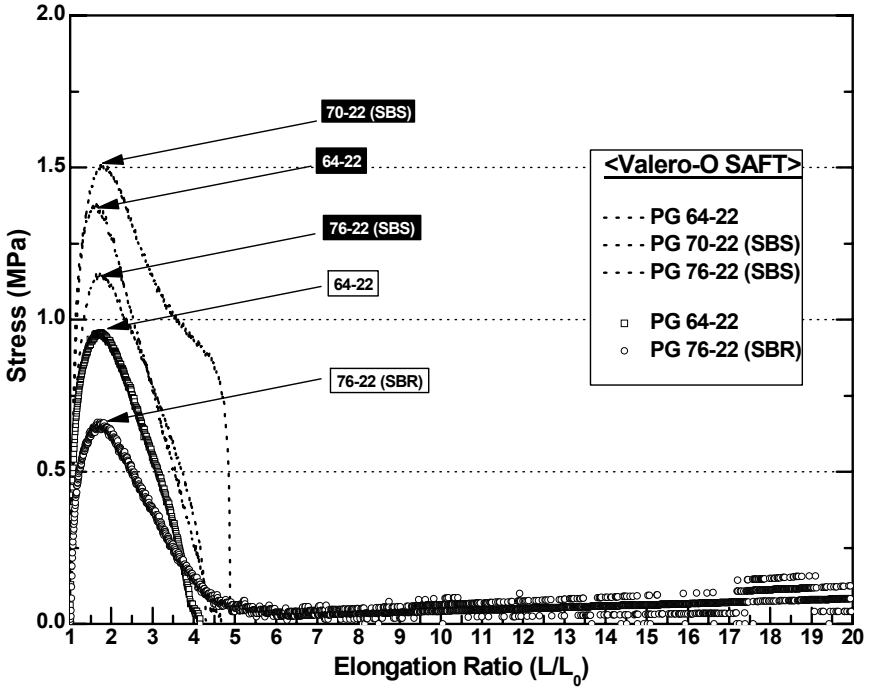

Figure II-32. Force Ductility at 4 ^{o}C for SAFT Aged Valero-Oklahoma Asphalts

Some Important Binder Measures Related to Durability

Reviewing the previous discussion, it is noted that there are a number of binder characteristics that may be of some importance with respect to base binders and their modified binder hardening. On one hand, it is expected that ductility enhancement (or degradation) compared to Ruan's correlation could be important. If it is observed that a modified asphalt is above Ruan's correlation on the ductility versus DSR function graph, then presumably that should be good, and if the base binder is below the correlation, then as a benchmark, it is expected that is not as good.

Figure II-33 shows this comparison of the ratio of a binder's actual ductility to its calculated ductility based on the Ruan correlation for its measured DSR function. So for example, if a modified binder has a ratio greater than one, then the modified binder ductility is greater than would be expected according to Ruan's correlation. If the base binder ratio is less than one, then this means that it falls below Ruan's correlation. It is

noted especially the Alon PG 64-22 base binder which has a ratio of about 0.4 and this is the base binder that at the PAV* 16 and 32 hr levels of aging was so significantly below the Ruan correlation. At the same time, the Valero Oklahoma PG 76-22 SBR modified binder has a ratio of about 3.6 reflecting a very significant ductility improvement due to the modification. It is also noted the Alon PG 58-28 which, because of its low PG grade, has a very high ratio for the PAV* 16 hr level of aging while its modified binder, the PG 70-28 SBS modified binder has a ratio of 1.8. So, the polymer modification has, in effect, reduced to some significant degree the enhancement that already was present in the base binder at least by this measure.

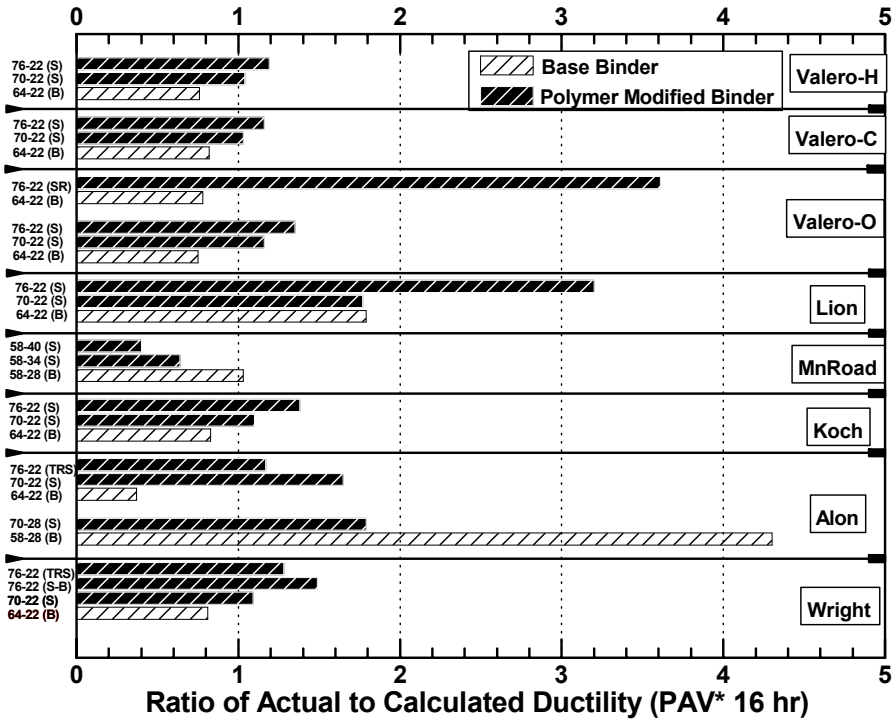

Figure II-33. Ratio of Actual Ductility to Calculated Ductility (PAV* 16 hr)

A second indicator that might be important in assessing the performance of polymer modification is a comparison of the PAV* 16 hr DSR function for the modified binder compared to the base binder (Figure II-34). If this DSR function increases as a result of the polymer modification, then it may be that the binder has shifted in the direction that would mimic increased aging, thereby giving it a shorter lifespan on the pavement. Thus, a ratio of the modified binder DSR function to the base binder DSR function (both after PAV* 16 hr aging) that is greater than 1.0 might be considered to be counter-productive whereas a ratio that is less than 1.0, meaning that the modified binder has moved in the direction of smaller DSR function and therefore likely giving it added life, would be good. By this measure, the Valero Oklahoma PG 76-22 SBS modified binder at a ratio of over eight and the Lion PG 76-22 SBS binder, also over eight, bear considerable further evaluation to assess whether they would be good performing modified binders. The Alon PG 70-22 SBS binder had a very low value, less than 0.4, and by this measure would seem to be very good. Note, however, that by the ductility criteria mentioned above, this same binder has a problem in that the base binder ductility places it well below the Ruan correlation; with enough aging, the modified binder eventually transitions to the poor ductility of the aged unmodified binder.

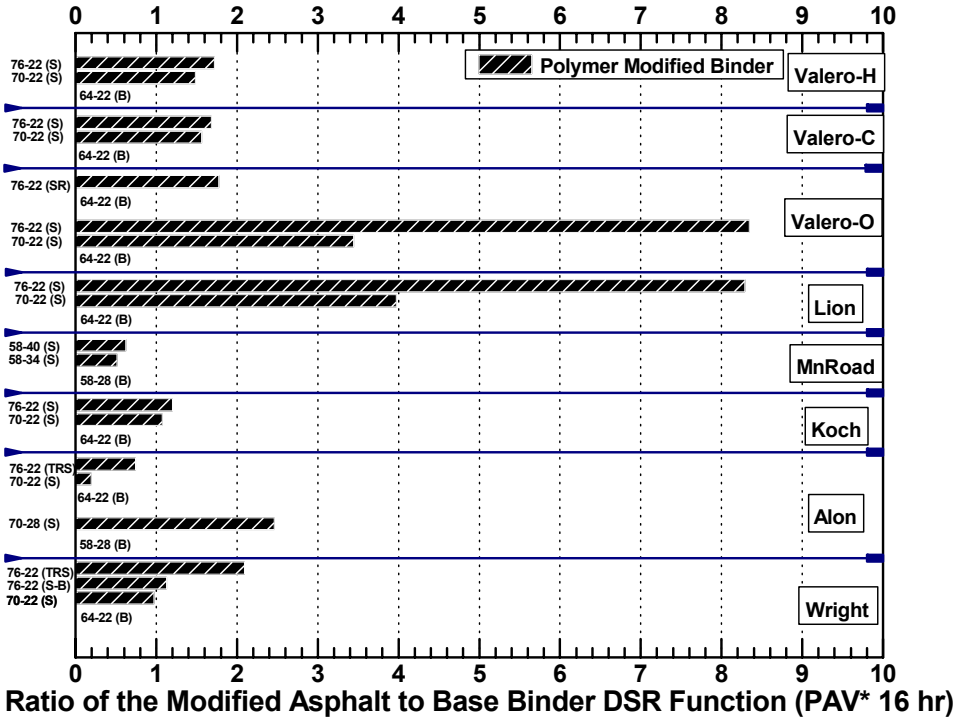

Figure II-34. Ratio of the Modified Asphalt to Base Binder DSR Function (PAV* 16 hr)

A third measure of the effect of modification that is considered is the hardening rate of the modified binder compared to the base binder hardening rate, using the PAV* 32 and 16 hr aging levels. Any comparison using hardening rates, however, is extremely suspect because it is known that accelerated rate measurements are inherently and fundamentally wrong because accelerating by temperature and pressure accelerates the various reactions to different degrees. Nevertheless, we present such a comparison in Figure II-35. A significantly increased hardening rate of the modified binder, compared to the base binder, potentially would not be good. In this case, for all the modified binders, no warning signs emerge in terms of hardening rates; virtually all ratios are at, or close to, unity.

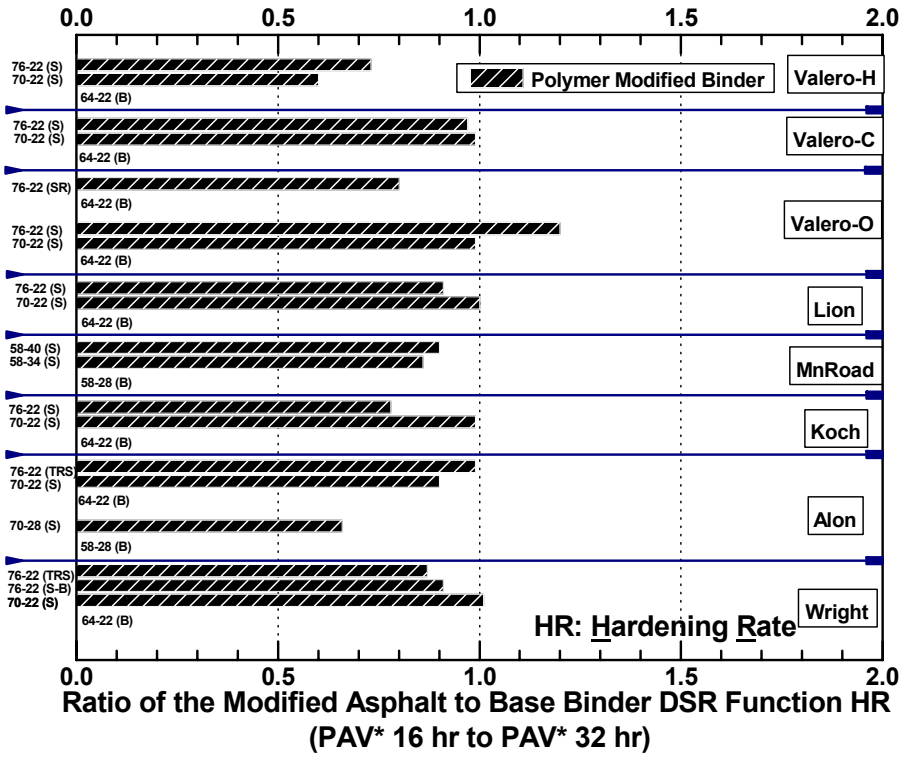

Figure II-35. Ratio of the Modified Asphalt to Base Binder DSR Function Hardening Rate (PAV* 16 hr to PAV* 32 hr)

As a fourth possible measure of polymer modified durability and effectiveness, consider the absolute level of the DSR function for the modified binders (and for the base binders) after PAV* 16 hr aging. In Figure II-36, the DSR function is divided by a value of 10^{-4} as an arbitrary value that would indicate a good value to achieve if it could be done without sacrificing performance grade. By this measure, in Figure II-36, it is seen that very few of the binders are less than or equal to this value of 10^{-4} (i.e., have a ratio less than 1.0). One exception is the Alon PG 70-28 SBS binder (achieved because the base binder was a soft binder to begin with) and another is the MnRoad binder (but of course, it was soft because it was designed for a cold climate). A notable binder on the high side is the Valero Oklahoma PG 76-22 SBS modified binder, which is well over an order of magnitude higher than the arbitrary criterion of 10^{-4} which places it well out

along the DSR function toward what might normally be thought of as the end of a binder's viable life. It is also noted that the Wright asphalt, tire rubber – SBS modified PG 76-22, also has a DSR function an order of magnitude greater than our arbitrary target.

These are four criteria that might be used to compare and assess binder modification. These criteria will be discussed in the context of pavement performance and designing a modified binder test protocol in Chapter V.

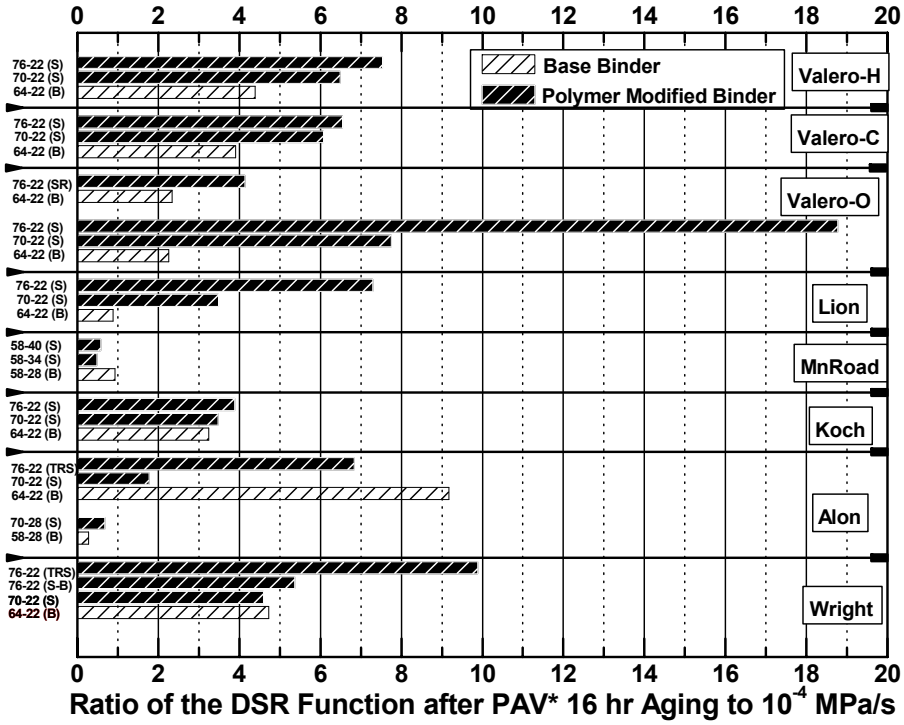

Figure II-36. Ratio of the DSR Function after PAV*16 hr aging to 10^{-4} MPa/s

Summary

Corbett compositions of both modified and unmodified binders change with aging, as has been observed previously and reported in the literature.

There is a clear trend that polymer modification leads to an improvement in binder ductility, relative to the base binder, at low levels of oxidation. However, with increased oxidation, the ductility improvement dissipates.

Size exclusion chromatography of polymer-modified binders clearly shows a decrease in the size of the polymer peak maximum accompanied by an increase in polymeric material at smaller molecular weights due to oxidation.

The DSR function G'/(η'/G'), which relates to binder ductility for oxidatively aged unmodified binders, may either decrease or increase with polymer modification. Oxidative aging causes an increase in the DSR function so that modification, if it serves to start binder pavement service at a higher value of the DSR function, may work against its long-term durability.

Most of the modified binders show a DSR function hardening rate that is less than that for the unmodified binder, by as much as 40 percent. This result suggests that the polymer degradation that occurs due to oxidation may serve to moderate the hardening that occurs due to asphaltene formation and other composition changes that occur due to oxidation.

CHAPTER III
EFFECTIVENESS OF POLYMER MODIFIER AFTER AGING*

It is well known that early failure of asphalt pavement, such as rutting (permanent deformation) usually results from inadequate initial mixture properties, while later-term failure can be the result of significant changes to the pavement due to fatigue and oxidative aging of the asphalt binder. In order to reduce the deterioration and cracking of pavements that result in huge maintenance expenditures, efforts have been made to improve the properties of asphalt binders with regard to increased resistance to high-temperature rutting, fatigue, and low-temperature thermal cracking.

Polymer modified asphalt (PMA), which is the blending and interaction of polymers in a base asphalt binder, has been used with increasing frequency for the construction of pavements, primarily due to its ability to stiffen the binder at high temperature but without stiffening it at low temperatures, resulting in reduced permanent deformation without harming thermal cracking. In addition, it was found that polymer modifiers in some cases were able to decrease the deleterious impact of binder oxidative aging and thereby result in more durable pavements (Ruan et al., 2003b, 2003c; Leicht et al., 2001; Lu et al., 1997a, 2000, and 2001).

The properties of PMA depend upon the characteristics and content of the polymer, the nature of the base asphalt binder, and the preparation process. For the modification of asphalt binder, two kinds of polymeric additives, elastomers and plastomers, typically are used. The styrenic block copolymer, which is termed thermoplastic rubber or elastomer, has proved to have the greatest potential when blended with asphalt binder. Therefore, the modification of asphalt binder using styrene-butadiene-styrene (SBS) has been widely studied (Lu et al., 1997b).

---

* Presented at the 86th Annual Meeting of the Transportation Research Board, January 24, 2007, Washington, D.C., and accepted for publication in the 2007 series of the Transportation Research Record: Journal of the Transportation Research Board (forthcoming). Reprinted with permission of TRB.

Several reported studies indicated that oxidation of SBS modified asphalt resulted in an increase of asphaltenes in base binders, and SEC chromatography indicated that polymer modifiers degraded to a lower molecular size (Ruan et al., 2003b; Lu et al., 1997a). In addition, researchers found that oxidative aging could either increase or decrease the temperature susceptibility of SBS modified asphalt due to competing effects. Increased asphaltenes decrease temperature susceptibility while degradation of the polymer modifier increases temperature susceptibility (Lu et al., 1997a, 2000, and 2001). The net change in temperature susceptibility depends upon which effect is greater.

While SBS modified asphalt may positively improve the durability of pavements, there is a need to quantify the effectiveness of polymer modification and its interaction with the base binder as oxidative aging progresses, in light of the accompanying base binder stiffening and polymer degradation (Ruan et al., 2003b and 2003c; Lu et al., 2001). Such detailed data and understanding will lead to better PMA preparation and to better durability and life-cycle cost.

Research Objectives

It is clear that with binder oxidation, two parallel mechanisms in PMA may occur: degradation of the polymer modifier and embrittlement of the base binder. The primary purpose of this work was to determine the extent to which each mechanism plays a significant role in the durability loss of SBS modified asphalt due to oxidative aging and how much oxidative aging affects the ability of the polymer to stay active. These issues are important to help understand the difference between durability loss in unmodified versus modified binders. A second purpose of this work was to provide a better understanding of PMA design and rejuvenation of SBS modified asphalt.

Methodology

Material Preparation

Table III-1 shows the properties of all materials used in this work. Two commercial SBS modified asphalts and their base binders were tested for oxidative aging properties and for their rejuvenated properties after blending with a deasphalted oil (Murphy oil). Both the PG 70-22 and the PG 76-22 used the same base asphalt, the PG 64-22, and contained 3 percent SBS, plus other modification (for the PG 76-22). The deasphalted oil's Corbett composition was 0.1 percent asphaltenes, 20.3 percent saturates, 53.4 percent naphthene aromatics, and 26.2 percent polar aromatics. The method used for blending was that specified in ASTM D4887. The amount of Murphy oil used in the blending was calculated using viscosity mixing rules by Chaffin et al. (1995). Each material needed between 12 and 20 weight percent Murphy oil to reach the target viscosity. Researchers used several methods of oxidative aging, as outlined below.

Test Methods

Complex viscosity (η^*) at 60 °C and 0.1 rad/s, storage modulus (G') and dynamic viscosity (η') at 44.7 °C and 10 rad/s of asphalt materials were measured using a Carri-Med CSL 500 Controlled Stress Rheometer. Ductility and Force Ductility measurements on unaged and aged asphalt materials were performed at 15 ^{o}C and 4 ^{o}C respectively, and an extensional speed of 1 cm/min.

Table III-1. Representative Viscosities of Each Material

Materials		60 °C Viscosity (0.1 rad/s, Poise)	Comments
PG 64-22	Unaged	2,589	Base Binder
	SAFT	5,470	
	PAV* 16 hr	28,259	
	ER 2 months	17,957	
	ER 4 months	30,647	
	ER 8 months	72,555	
PG 70-22	Unaged	4,346	SBS Modified Binder
	SAFT	10,306	
	PAV* 16 hr	53,614	
	ER 2 months	37,935	
	ER 4 months	61,105	
	ER 8 months	122,710	
PG 76-22	Unaged	11,523	SBS Modified Binder
	SAFT	31,484	
	PAV* 16 hr	119,830	
	ER 2 months	83,365	
	ER 4 months	159,030	
	ER 8 months	330,960	
Murphy Oil		46	Deasphalted Oil

Results and Discussion

Effect of Aging on Ductility and Rheological Properties

According to field data, the ductility of an asphalt binder correlates with aged pavement cracking. In literature reports, it was found that the ductility measured near 15 ^{o}C, and 1 cm/min was a good indicator of pavement cracking (Vellerga and Halstead, 1971; Kandahl et al., 1975). Researchers observed that if the ductility was above 10 cm, then the pavement condition generally was good. However, if the ductility was less than between 3 and 5 cm then generally cracking was found. Ruan et al. (2003c) developed G'/(η'/G'), a rheological function, and concluded that G'/(η'/G') (DSR Function) correlated well with the ductility of unmodified asphalt when ductility was below 10 cm. More specifically, his research showed that the logarithm of the DSR function correlated linearly with log ductility, and that all unmodified asphalts followed essentially the same

correlation. In the case of modified asphalts, the ductility correlated with the DSR function reasonably well for modified asphalts having the same base binder.

Ductility versus DSR function and the map of G' vs. (η'/ G') are shown in Figures III-1 and III-2, respectively. In Figure III-1, with oxidative aging, a binder moves from the top left toward the lower right. Unmodified binders below 10 cm ductility generally follow the solid line, established by Ruan; modified binders may follow a similar line but shift relative to their base binder. For the materials shown in this figure, the shift due to the modifier is significant and about the same for both the PG 70-22 and the PG 76-22 PMA binders. Typically, the PMA binders have improved ductility for a given DSR function value. It was observed that the aging method does not greatly impact the path followed with increased oxidation by either the unmodified or modified binders.

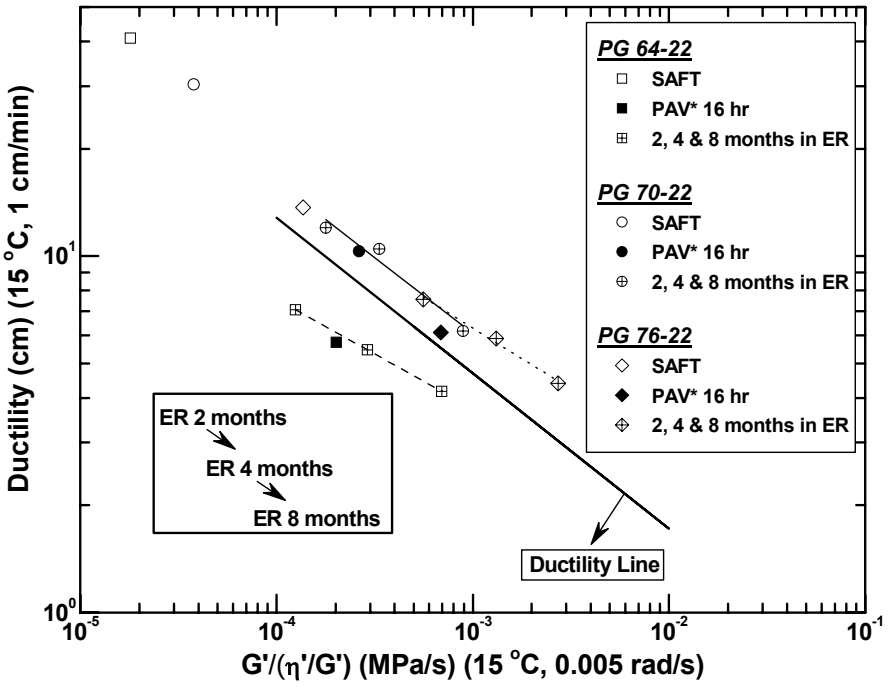

Figure III-1. Ductility versus DSR Function [G′/(η′/G′)] for PMAs and Base Binder

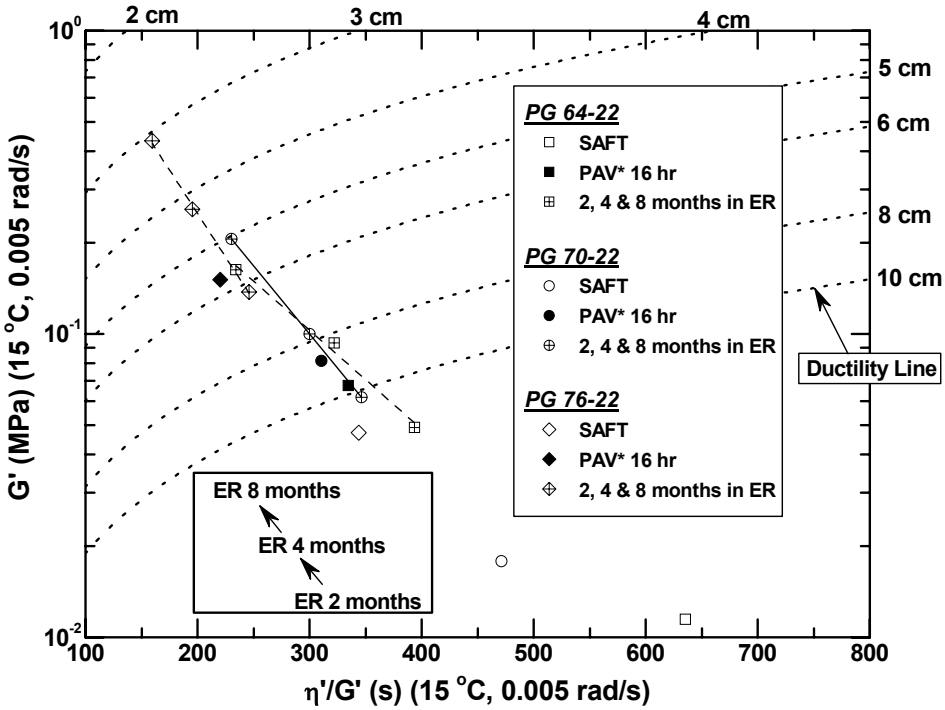

Figure III-2. G′ versus (η′/G′) for PMAs and Base Binder

Figure III-2 shows the same data as Figure III-1 but with G' and (η'/G') separated and plotted against each other. The dashed lines are lines of constant ductility (for unmodified binders) where each point on the (unmodified binder) solid line of Figure III-1 plots as a line of constant ductility in Figure III-2. In this graph, with increased oxidative aging, a binder moves from the lower right to the upper left and ductility decreases along this path. With this type of graph, different base binders can follow starkly different paths (Ruan et al., 2003a) but a base binder and its SBS modified binders tend to follow essentially the same path, in spite of the fact that modification may increase measured ductility values. It is worth reiterating that in this graph, the lines of constant ductility are not the measured ductility values of the modified binders.

Comparing the three binders in Figure III-1, we see that the PG 70-22 binder has significant ductility enhancements at a given aging state, compared to the unmodified binder whereas the PG 76-22 has little or no such increase, again relative to the base

binder. For example, for the PAV*, 16 hr aged materials (solid symbols in Figures III-1 and III-2), the base (unmodified) PG 64-22, PG-70-22, and PG 76-22 ductilities are approximately 5.8 cm, 10 cm, and 6 cm, respectively. In Figure III-2, the actual modified binder ductilities are not shown so that in this plot, the differences between the PG 64-22 base binder and the PG 70-22 PMA seem relatively small, reflecting a small shift in the DSR function values (see Figure III-1), whereas the PG 76-22 PMA is shifted significantly more toward the upper-left corner, relative to the base binder, reflecting the significant increase in the DSR function values that resulted from the additional modification (see Figure III-2).

Effect of Polymer Modifier on Elongational Properties

The force ductility test compares different binders in their elongational elastic and viscous flow properties at 4 ^{o}C and at a constant elongation rate of 1 cm/min. Figure III-3 shows the stress versus elongation ratio for unaged and SAFT-aged asphalts. For the unmodified PG 64-22, unaged asphalt, the stress initially increases with elongation, builds to a maximum, and then flows to relieve the stress. The SAFT-aged binder shows similar qualitative behavior except that the higher viscosity prevents it from flowing as quickly and as a result the binder builds to a higher maximum stress (and more quickly because of its stiffer elastic modulus due to the aging), and ultimately (when sufficiently aged) breaks to relieve the stress.

However, the modified materials exhibit qualitatively different behavior by having a second wave of stress increase that leads to a second (relative) maximum stress. Additionally, the stress level of this second maximum is greater than that provided by the asphalt alone. Shuler et al. (1987) termed the slope of first stress-elongation region the “asphalt modulus” and the second region the “asphalt-polymer modulus,” suggesting that it is the result of elongation of an asphalt-polymer network. Also for the modified materials (as was the case for the unmodified base binder), the maximum stress level reached during the asphalt modulus portion of the elongation, increased with oxidation,

the result of the base binder stiffening with respect to both elastic modulus and viscosity. However, unlike the unmodified material, the presence of the polymer strengthened the SAFT-aged asphalt and allowed it to be drawn to a much greater elongation ratio (and at a higher stress level) before failure occurred after the second peak provided by the asphalt-polymer modulus.

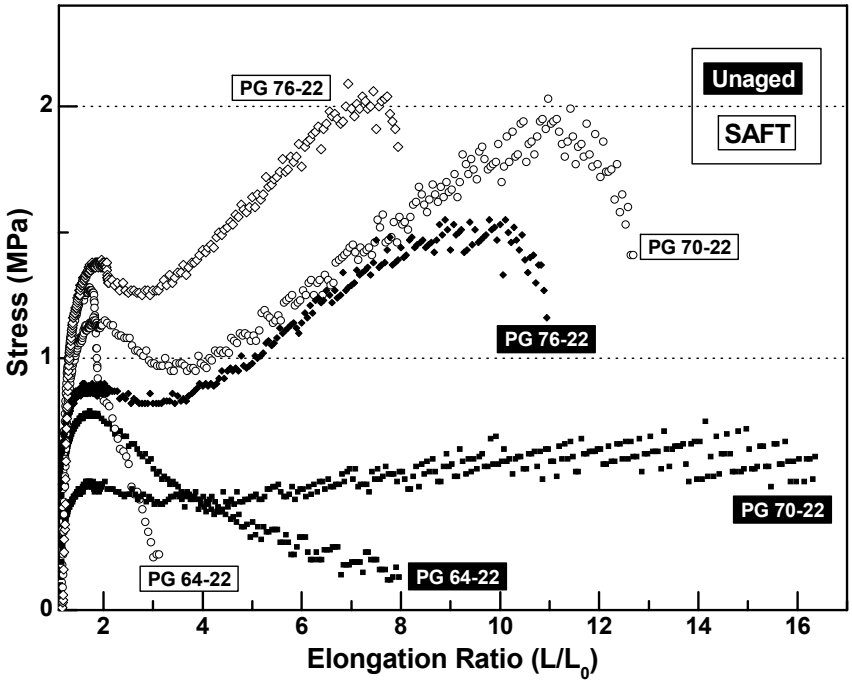

Figure III-3. Stress versus Elongation at 4 ^{o}C for PMAs and Base Binder

Figure III-4 shows force ductility curves after aging to the PAV* 16 hr condition and at two temperatures. Testing at 4 ^{o}C provides little information to distinguish the modified binders from the unmodified. Two questions arise. "Has the polymer been degraded by oxidative aging to the point that it is no longer effective and therefore unable to provide a benefit to the base binder?" Alternatively, "Has the base binder oxidized, and therefore stiffened, to the point that the polymer can no longer be effective?" In other words, because the base binder is stiffer, stress builds more rapidly as the result of a greater elastic modulus and then cannot relax because of a higher

viscosity, ultimately leading to an excessive stress level and failure before elongation is enough to "engage" the asphalt-polymer modulus.

To answer these questions, Figure III-4 also shows force ductility results at 10 ^{o}C. At this higher temperature, the base binder is softened so that the stress cannot build to as high a level and the characteristic asphalt-polymer modulus again is clearly seen in the modified binders. Evidently, even though the polymer has degraded to some degree from the oxidation, it is still capable of providing benefit to the ductility performance of the binder, provided the base binder is soft enough to prevent an excessive stress level being reached during the asphalt modulus portion of the elongation test. It should be noted also that at the higher temperature, the polymer modulus is reduced and together with some polymer degradation from the oxidation, results in a softer asphalt-polymer modulus.

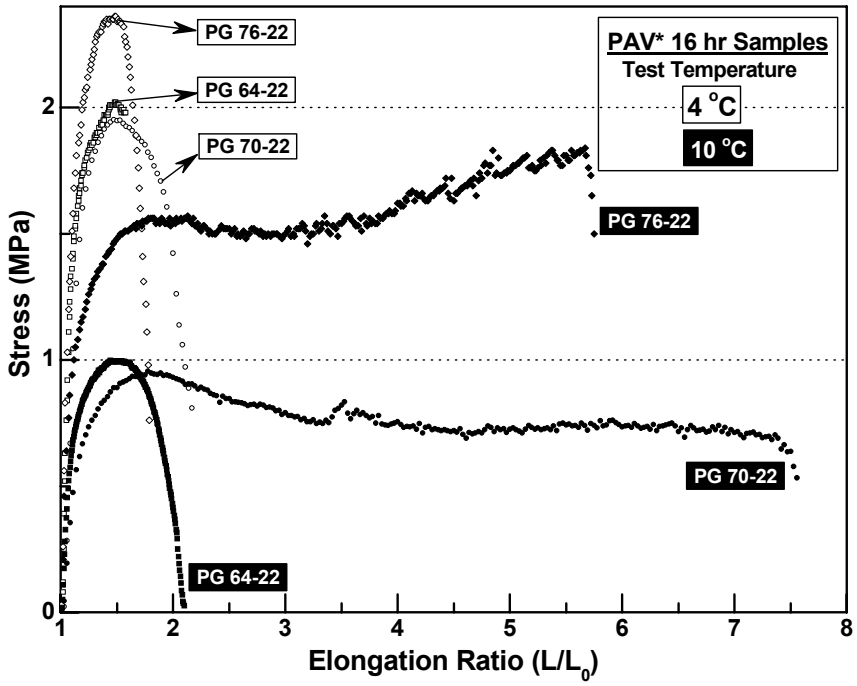

Figure III-4. Force Ductility Measurements at 4 ^{o}C versus 10 ^{o}C for PMAs and Base Binder

Figure III-5 shows additional comparisons, all for the same PG 70-22 PMA and aged at the more moderate ER temperature. Again, the heavily aged material (2, 4, and 8 months in the ER) does not exhibit the polymer modified elongation character when tested at 4 ^{o}C. However, when tested at 10 ^{o}C, the presence of the polymer is revealed, along with the trend toward a higher asphalt modulus stress maximum with increased aging and towards a reduced failure elongation ratio with increased aging. In other words, the typical unaged or lightly aged polymer modified binder FD behavior is recovered in heavily aged binders by testing at a higher temperature.

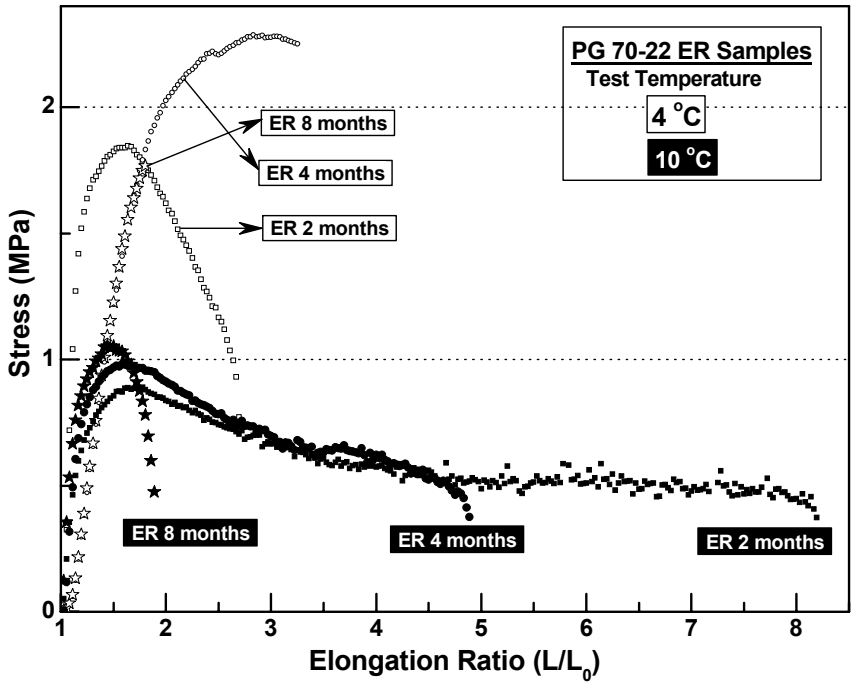

Figure III-5. Force Ductility Measurements at 4 ^{o}C versus 10 ^{o}C, PG 70-22 PMA

Rheological and Elongational Properties of Rejuvenated Heavily Aged PMA

As an additional means of assessing the relative impact of binder hardening versus polymer degradation, researchers conducted a number of aging and blending experiments. The 2-, 4-, and 8-months aged PMA materials shown in Figure III-5, together with the PAV* aged material, were blended with the Murphy deasphalted oil with the objective of creating blended materials that would have the same base binder stiffness as the PG 70-22 SAFT material; the aged starting materials, the PG 70-22 SAFT material, and the blended materials are shown in the DSR map of Figure III-6. The blended materials did not perfectly overlay the SAFT material, but the results were quite acceptable. As additional verification of the blending results, Figure III-7 shows the 60 ºC viscosity master curves for the aged and blended materials, and for the target SAFT-aged binder.

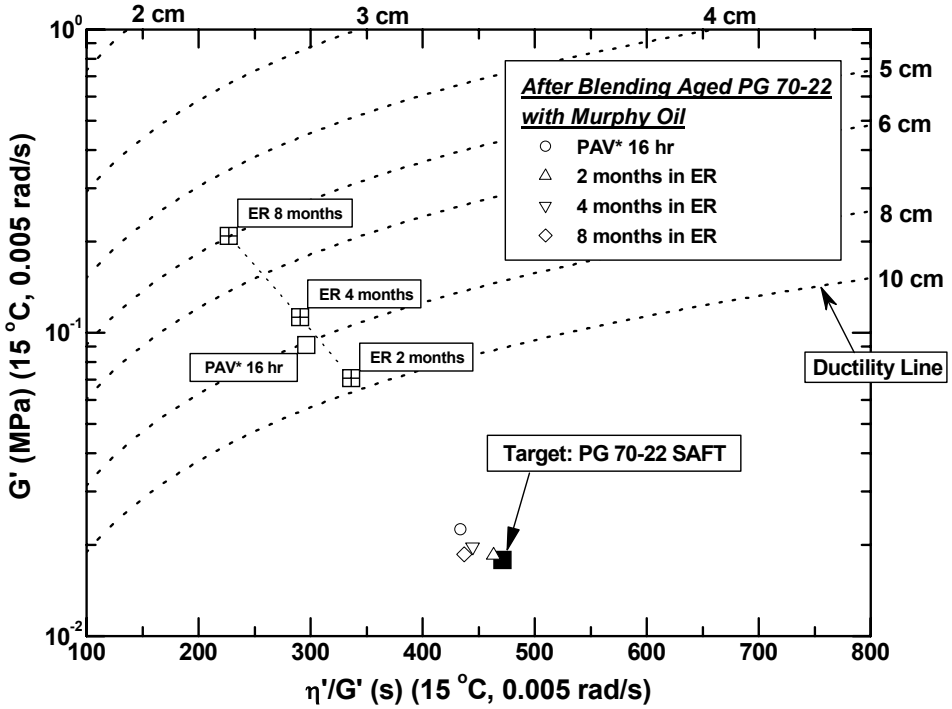

Figure III-6. DSR Map for Blending Aged PG 70-22 with Murphy Oil

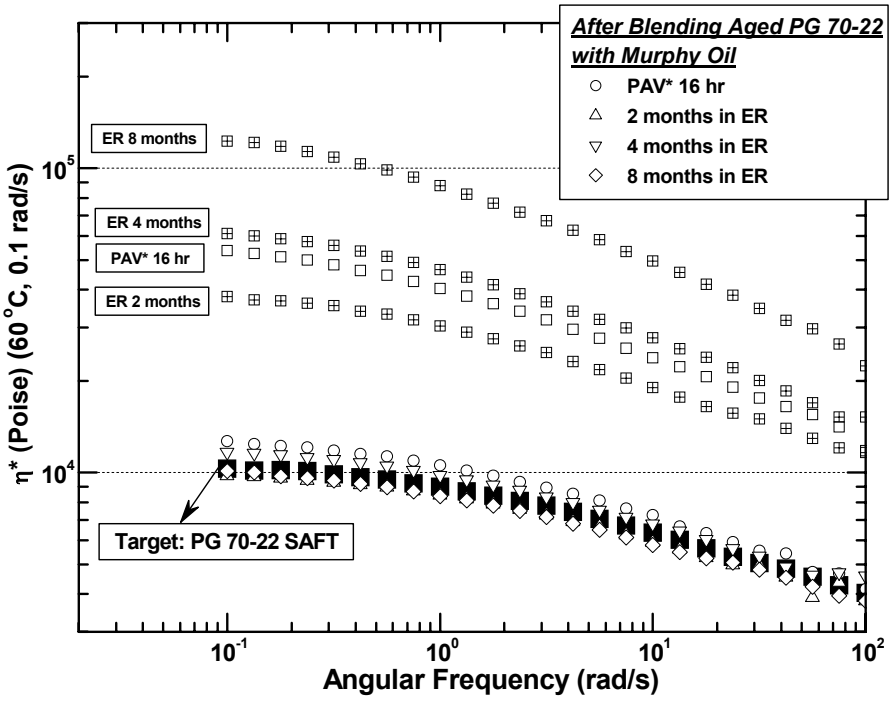

Figure III-7. Master Curves for Blending Aged PG 70-22 with Murphy Oil

FD measurements of the blends are shown in Figure III-8. The results are very good in the region of the asphalt modulus maximum stress, indicating that the rheology of the base asphalt itself in each case was reproduced quite well, even though the materials had all been aged to different levels and then blended with different amounts of the Murphy oil. The region of the asphalt-polymer modulus is not as good, however, probably due primarily to the different concentrations of polymer. Certainly, the trends are consistent with this hypothesis as the strength of the asphalt-polymer modulus decreases as the aging level of the unblended material increases (and thus as the polymer concentration decreases with greater dilution).

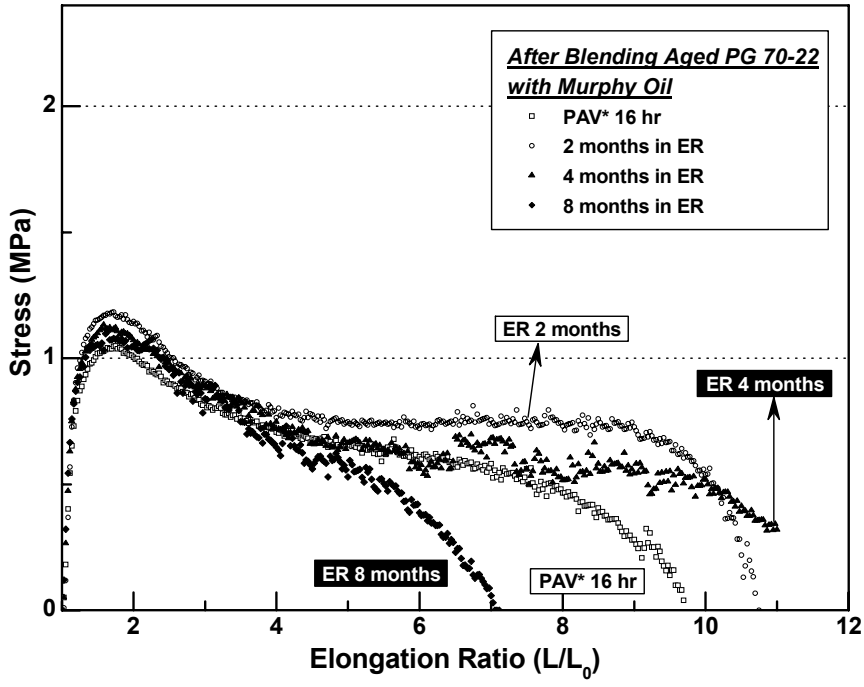

Figure III-8. Stress versus Elongation for Blending Aged PG 70-22 with Murphy Oil

However, another possibility exists: the more heavily aged material also has more extensively degraded polymer, and this hypothesis too would lead to a decrease in the asphalt-polymer modulus with aging that is observed in Figure III-8. To test this hypothesis, the PG 70-22 SAFT-aged material was blended with base binder that had been aged to the appropriate level such that, when blended with the SAFT-aged PMA, it would give a blended binder with the same base binder characteristics as the PAV* 16 hr blended material (shown as the open circle in Figure III-6), and give the same polymer dilution as the PAV* blended material. This blending is depicted in Figure III-9 and was devised following the viscosity mixing rules developed by Chaffin et al (1995). Thus, FD comparisons of the blended SAFT-aged PMA and the blended PAV* 16 hr blended material to the undiluted SAFT-aged PMA would give an indication of the relative effects of dilution versus polymer degradation.

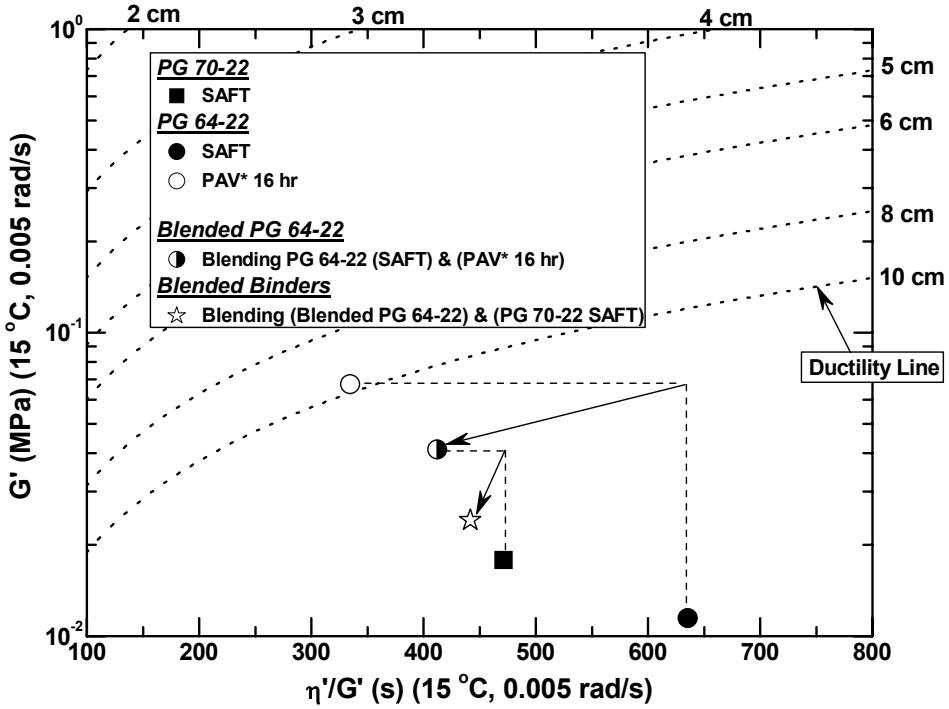

Figure III-9. DSR Map for Blending Modified with Unmodified Binders

The FD result of this diluted SAFT-aged PMA, together with the undiluted SAFT-aged PMA from Figure III-3 and the blended (diluted) PAV* 16 hr material are shown in Figure III-10. The blended materials should both have essentially the same concentration of polymer and essentially the same asphalt rheology for the base binder while the SAFT-aged PMA has a higher polymer concentration. Clearly, the largest differences in the FD data are the result of the concentration difference, but there also are clear differences between the blended SAFT and PAV* 16 hr aged binders that presumably are the result of polymer degradation.

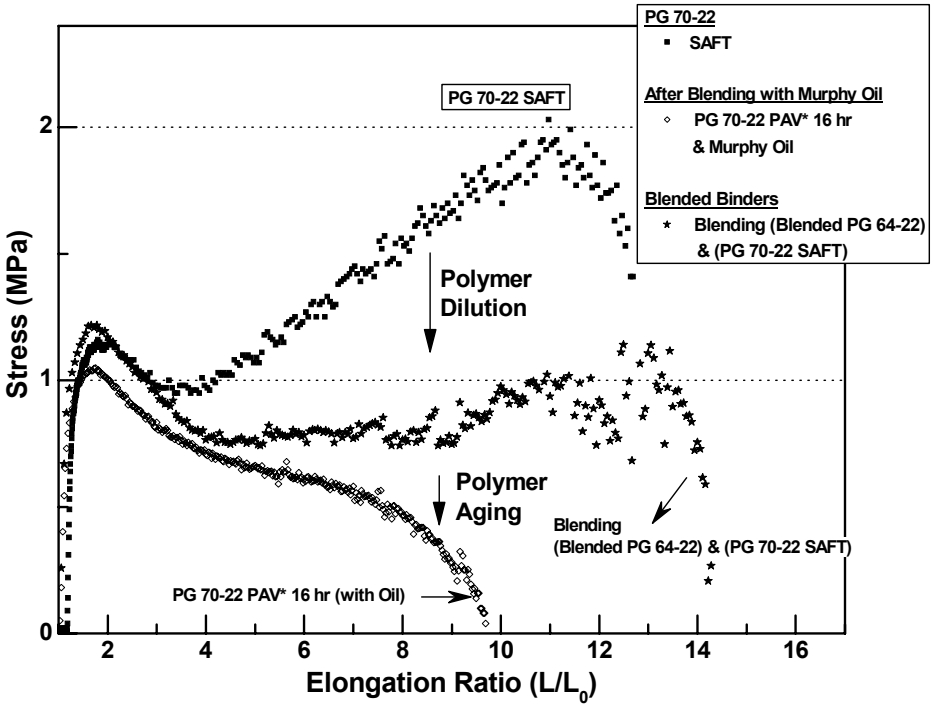

Figure III-10. Stress versus Elongation for Blending Modified with Unmodified Binders

Summary

Oxidative aging of asphalt materials causes an embrittlement, and thus a loss of ductility, of both unmodified and modified binders. SBS polymer modification typically results in ductility improvements to the base binder, but oxidative aging degrades this improvement significantly over the life of the pavement. Dynamic shear rheometer, ductility, and force-ductility measurements show that the primary cause of this degradation is base binder stiffening due to the oxidation. A secondary cause is polymer degradation (molecular size reduction), also from oxidation. Softening a modified binder, either by raising the temperature or by blending with a softer asphaltic material, recovers the enhanced ductility performance of the modifier to a significant degree, but

not fully. However, polymer degradation that may have occurred due to oxidation remains a factor contributing to reduced performance.

CHAPTER IV
TOWARDS AN OXYGEN AND THERMAL TRANSPORT MODEL OF BINDER OXIDATION IN PAVEMENTS

The oxidation of binders in asphalt pavements has been a subject of interest for a significant number of years, even decades. This ongoing effort has several important facets that are separate, but related.

Perhaps the most fundamental issue is the basic oxidation chemistry. This issue has been explored rather extensively in reports by Petersen et al (1993). Significant reports are by Lee and Wang (1973), Lau et al. (1992), and Petersen et al. (1993). A general observation of these reports is that carbonyl compounds form as a result of oxidation and that, while the exact nature of the carbonyl compounds and the formation rates may vary from asphalt to asphalt, the common factor is that for each asphalt the carbonyl content can be used as a surrogate for total oxidative changes; qualitatively the carbonyl growth varies linearly with total oxygen increase, even though the quantitative dependence varies from asphalt to asphalt (Liu et al., 1998b).

A second aspect of binder oxidation is the oxidation kinetics of an asphalt, studied and reported by Petersen et al. (1993), Liu et al. (1996), and others. The basic carbonyl reaction rate can generally be described using an Arrhenius expression for temperature variation and pressure dependence:

$$\frac{d\mathrm{CA}}{dt} = r_{\mathrm{CA}} = AP^{\alpha}e^{-E/RT} \qquad \text{(IV-1)}$$

Lau et al. (1992) reported results for 10 asphalts in which they determined values for the activation energy E, the oxygen pressure reaction order, and the constant A. It was also noted that in general, the reaction rates of asphalt binders undergo an initial rapid rate period that declines over time until a constant rate period is reached and the reaction rate given in the equation above describes this constant rate period. The early

time faster rate period has been variously described as the “initial jump” (Lau et al., 1992) or the “initial spurt” by Petersen (1993). The point is that while the parameters of the oxidation rates vary from one asphalt to another, the basic form of the reaction rates are essentially the same. Kinetic parameters have been determined for a number of different asphalts including the SHRP core asphalts and others. Many of these results are reported by Glover et al. (2005).

A third facet of binder oxidation is the impact that the oxidation has on the binder’s physical properties. Fundamentally, the oxidation of the binder creates carbonyl compounds, primarily by oxidizing aromatic compounds in the naphthene aromatic, polar aromatic, and asphaltene fractions. These more polar carbonyl groups result in stronger associations between asphalt components, which increase the asphaltene fraction, and in turn lead to a stiffening of the binder in both its elastic modulus and its viscosity. Results have been reported in terms of the low shear rate limiting viscosity, and it has been observed that this viscosity increases in direct proportion to the carbonyl band infrared carbonyl growth (Martin et al., 1990). The proportionality factor has been termed the hardening susceptibility (Lau et al., 1992; Domke et al., 1999). More recently, a DSR function has been defined that includes both elastic and viscous properties and at more mid-range test conditions (frequency and/or temperature) than are represented by the low shear rate limiting viscosity which, by definition, is at very low frequency or equivalently at high temperatures. This DSR function also increases linearly with carbonyl content, and the slope of this relationship is termed the DSR function hardening susceptibility. This parameter, also measured for a number of asphalts, has been reported as well (Glover et al. 2005). For either of these hardening functions, one can develop kinetic equations, just as can be done for carbonyl formation kinetics, in that the hardening rate can be expressed in an Arrhenius rate form, thereby by passing explicit representation of the carbonyl reaction kinetics. Equivalently, the hardening susceptibility can be multiplied by the oxidation reaction rate to obtain the hardening rate, again, after the initial jump period has been passed, with the reaction rate constant at a fixed temperature.

A fourth issue regarding binder oxidation is "So what?" Assuming binders oxidize in pavements, what is the importance of this oxidation to pavement performance? For example, to what extent is the fatigue life of a pavement impacted by binder oxidation? This is a question that has recently been addressed by Walubita et al. (2005, 2006). Recent literature reports also address this issue (Walubita et al., 2006). These results indicate that binder oxidation in pavements can have a very significant negative impact on pavement fatigue life. While the mechanism of this fatigue life decline with oxidation is not yet well understood, it is believed to be a very important phenomenon, and early data indicate that there may be significant differences between different mixture designs.

The final issue of binder oxidation in pavements is the question of whether, in fact, binders oxidize in pavements at all, in the face of presumed reduced temperatures and restricted oxygen transport to the binder below the surface. The work discussed above showed that binders harden as a result of oxidation, that the kinetics of oxidation and the hardening that results from oxidation are quite well known (or can be measured) and can be described quantitatively in terms of oxidation temperature and pressure. The work discussed above also indicates that if binders oxidize in pavements, the impact on pavement fatigue performance can be profound.

All of these factors, however, will be moot points if binder oxidization doesn't occur in pavements, and the question of whether this oxidation occurs has no clear answer in the literature. In fact, a very well cited and accepted literature report concludes that binder oxidation occurs only in the top inch of the pavement and that below the top inch, the binder is left virtually unaffected by years of use and years of environmental exposure (Coons and Wright, 1968). And their conclusion is formalized in a recently developed mechanistic empirical pavement design guide (MEPDG, AASHTO (2002)) that assumes in its calculation that binders oxidize only in the top inch. Parenthetically, calculations performed using the MEPDG suggest that binder oxidation and the consequent increase in pavement stiffness (and the presumed decrease in deformation under load as a result of this stiffness) actually have a positive impact on pavement

fatigue life. Contradicting the work of Coons and Wright and the assumptions of the pavement design guide are the extensive data reported in Glover et al. (2005) in which a large number of Texas pavements were cored, the binder extracted and recovered, and tested to determine binder stiffness as a function of age in the pavement. The results of this work indicate rather strongly that in fact binders can age in pavements well below the surface and that the hardening of binder in the pavement is virtually unabated over time. These data also are reported in a recent paper by Al Azri et al. (2006).

Research Objectives

While this recent study of binder aging in Texas pavements provides strong evidence that binder oxidation occurs well below the surface of a pavement, the data are not detailed enough to be the basis for a quantitative deterministic model of binder oxidation in pavements, a model that is needed in order to incorporate binder oxidation into pavement design. Thus, one of the objectives of the work reported in this chapter was to measure the oxidation and hardening of binders in pavements as a function of depth below the surface.

A second research objective was to begin the effort to rationally predict binder oxidation in pavements through a quantitative deterministic model. Ideally, such a model would estimate binder oxidation and hardening in pavements as a function of time, daily and annual temperature variations, depth in the pavement, and a parameter that indicates the accessibility of the binder to oxygen (e.g., accessible air voids).

Meeting the above objectives will provide a direct approach based on fundamentals to meeting the primary objective of this work, which is to be able to predict the durability of polymer modified asphalt binders.

Work toward achieving these objectives is reported in this chapter.

Methodology

The work of this chapter rests upon measurements of binder oxidation that has occurred by a number of different methods. First and foremost, of course, is binder aging in pavements. Binder properties determined after extraction and recovery were measured and included the DSR properties, oxidation (reported as infrared carbonyl area, CA), and size exclusion chromatograms (SEC). The DSR properties are rheological master curves from which are determined low shear rate viscosities and the DSR function measured at 10 rad/s and 44.5 °C but time temperature superposition shifted to 0.005 rad/s and 15 °C. Other data measured on pavement core samples include both total and accessible air voids, together with bulk specific gravity and binder content. Additionally, neat binder aging is conducted by methods including environmental room aging at 60 °C, pressure aging vessel aging at 90 °C (modified by carrying out the aging in nominally 1 mm thick films) and also by the stirred air flow (SAFT) method which is designed to be equivalent to the rolling thin film oven test (RTFOT) procedure (Vassiliev et al., 2002). Binder properties (DSR, SEC, CA, etc.) were measured to characterize the binders and their oxidative hardening rates. The methods and materials used are explained in more detail in the following sections.

Materials

Table IV-1 lists the pavement test sites and the binders used in the pavements. The location of the Texas site locations are shown in Figure IV-1. The Texas sites range from the Northern Panhandle to the Southern Rio Grande Valley and from Odessa in the West to the Luftkin and Atlanta districts in the East. Furthermore, most of the Texas pavements used polymer modified binders, and mostly SBS modifier, but also SBR (Fort Worth). Additionally, the San Antonio, Bryan, and Paris district pavements contained unmodified binders. The thicknesses of the various pavement layers ranged up to 3.5 inches but down to as little as 1 inch. In some cases, two layers in the same pavement

were tested; for both the San Antonio and Paris districts, an original surface layer placed in the mid-80s was overlaid in the 1998-2000 timeframe and sampling both the 20-yr old original surface layers, and the fairly new overlays, provided an interesting comparison. In some cases, the original binder was available for the Texas pavements including the Atlanta RG binder and the Fort Worth 281 binder.

Cores also were included in the study from the MnRoad test site in Minnesota. The Cells that were studied are depicted in Figure IV-2, which shows the thickness of the asphalt layer as well as the underlying base layer. The original binders for the MnRoad Cells were available, which provided the ability to independently measure oxidation reaction kinetics data of the binders. Two of the MnRoad Cells (Cells 1 and 3) contained unmodified binder, the other three Cells (33, 34 and 35) were constructed from the same base binder with Cell 33 containing the unmodified base binder and Cells 34 and 35 SBS modified binder in different amounts to provide a PG 58-34 in Cell 34 and PG 58-40 in Cell 35. Each of these three Cells had a nominal pavement thickness of 4 inches. Cores were obtained from the MnRoad site early in the project in November of 2004 and at the end of the project in July of 2006. Coring at two times allowed a calculation of the actual field aging rates (although the short duration of the project, compared to the slow aging rates of binders in the field and experimental uncertainty, does not provide a very reliable measure of hardening rates).

This collection of pavement cores provided data that could be used to assess the effects of temperature extremes (Texas versus Minnesota), modified versus unmodified binders, and the type of modifier (SBS versus SBR). As usual, however, field data, because of the limited number of cores that can be obtained (due to the expense and time in obtaining them) and the uncontrolled variables that occur from site to site are far from definitive indicators of the effects of these various variables. Nevertheless, this project includes more measurements of binder aging in pavements over time (including the effects of depth) than any previous study.

Table IV-1. Collected Cores from TxDOT and MnRoad District

No.	TxDOT District	Highway	Thickness: Inch	PG (Modifier)	Binder Supplier	Cons.	1st Coring	2nd Coring
1	**Atlanta**	IH-20 (RG) IH-20 (SS) IH-20 (Q)	2 2.75 2.25	76-22 (SBS)	Wright	2001	11/2004	11/2005
2	**Odessa**	FM1936	3	70-22 (SBS)	Alon	2002	12/2004	04/2006
3	**Waco**	IH-35	(OSL) 3.4	70-22 (SBS)	Alon	(OSL) 2002	10/2005	N/A
4	**Yoakum**	FM457	2.5	70-22 (SBS)	Koch	2001	01/2005	05/2006
5	**Amarillo**	US54	1.75	70-28 (SBS)	Alon	2000	12/2004	06/2006
6	**Pharr**	FM2994	3.4	70-22 (SBS)	Eagle	2002	02/2005	04/2006
7	**Lufkin**	US69	2.2	70-22 (SBS)	Marlin	2003	02/2005	06/2006
8	**Fort Worth**	SH183	1.75	AC-10 (SBR)	-	1985	04/2005	05/2006
		FM51	2	AC-10 (SBR)	-	1994		
		US281	1	76-22 (SBR)	Valero-O	2003		
9	**San Antonio**	FM1560	(OL) 1.9 (OSL) 1.2	- (Un)	-	(OL) 1998 (OSL) 1986	07/2002	10/2005
10	**Bryan**	US290	(OSL) 1.7	64-22 (Un)	Fina	(OSL) 2002	10/2005	07/2006
		SH-6	(OL) 1.8 (OSL) 1.7	- (Un)	-	(OL) 2000 (OSL) 1991	07/2002	10/2005
11	**Paris**	SH19/24	(OL) 2.2 (OSL) 3.1	- (Un)	-	(OL) 2000 (OSL) 1985	07/2002	10/2005
Cell No.	**MnRoad District**	**Highway**	**Thickness (Inch)**	**PG (Modifier)**	**Binder Supplier**	**Cons.**	**1st Coring**	**2nd Coring**
1	**Metro Area**	I-94 (Mainline Test Road)	5.9	AC 120 (Un)	-	1992	11/2004	07/2006
3			6.3	AC 120 (Un)	-			
33		I-94 (Low Volume Test Road)	4.04	58-28 (Un)				
34			3.92	58-34 (SBS)	Koch	1999		
35			3.96	58-40 (SBS)				

RG: River Gravel // SS: Sandstone // Q: Quartzite
(Un) : Unmodified // (OL) Overlay // (OSL) Original Surface Layer

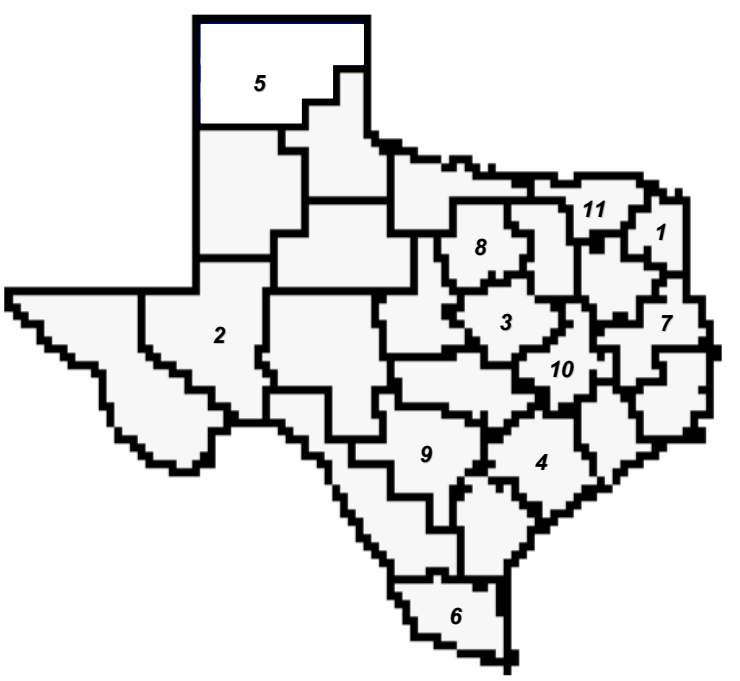

Figure IV-1. Selected TxDOT Districts for Collecting Cores

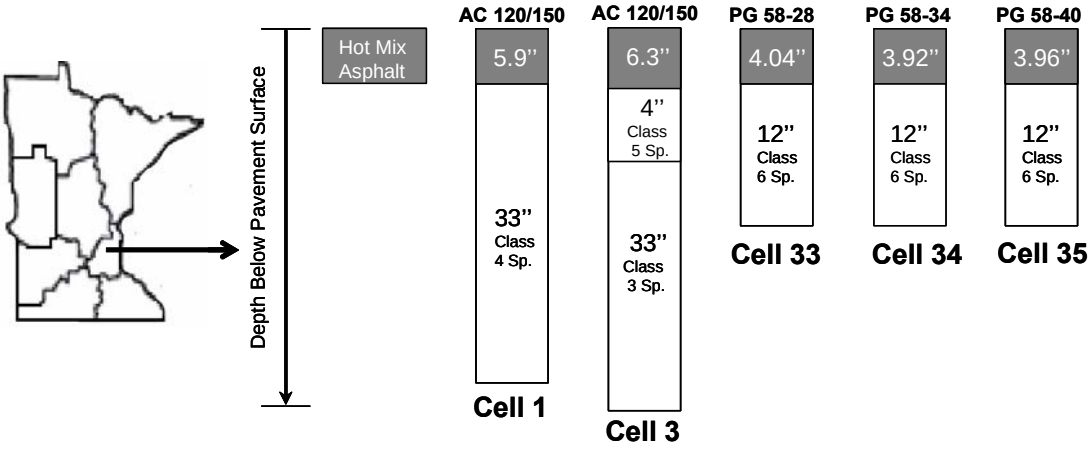

Figure IV-2. Pavement Layer Details for the MnRoad Cores

Pavement Core Properties

A number of properties of intact pavement cores are of interest. These include the bulk and maximum specific gravities and the total and accessible air voids content. These properties are determined by a number of weight measurements including the weight of the dry core in air, the weight of the saturated core underwater, and the weight of the dry core underwater. Two methods were used to determine these weights, a saturated surface dry method (SSD) and the core lock method. The SSD method uses measurements of the unsealed core while the core lock method uses underwater measurements of the evacuated core sealed in a plastic bag.

The measurements and the calculations for the two methods are given by the following equations and notation:

$$\text{Bulk Specific Gravity} = \frac{DA}{SaA - SaW} \quad \text{(SSD method)} \tag{IV-2}$$

$$\text{Accessible Air Void} = \frac{SaA - DA}{SaA - SaW} \quad \text{(SSD method)} \tag{IV-3}$$

$$\text{Bulk Specific Gravity} = \frac{DA}{SeA - SeW - \frac{BA}{B_{sg}}} \quad \text{(Core lock method)} \tag{IV-4}$$

$$\text{Accessible Air Void} = \frac{SeA - SeW - \frac{BA}{B_{sg}} - (DA - SaW)}{SeA - SeW - \frac{BA}{B_{sg}}} \quad \text{(Core lock method)} \tag{IV-5}$$

$$\text{Maximum Specific Gravity} = \frac{DA}{SeA_{broken} - (SaW_{broken} + BW) - \frac{BA}{B_{sg}}} \tag{IV-6}$$

$$\text{Total Air Void} = 1 - \frac{\text{Bulk Specific Gravity}}{\text{Maximum Specific Gravity}} \qquad \text{(IV-7)}$$

where, DA = Dry sample weight in Air

BA = Bag weight in Air

BW = Bag weight in Water

B_{sg} = Bag Specific Gravity

SaA = Saturated (intact) sample weight in Air (surface dry)

SaW = Saturated (intact) sample weight in Water

(Core lock method: SaW does not include bag weight)

SaW_{broken} = Saturated broken sample weight in Water

SeA = Sealed (intact) sample weight in Air

SeA_{broken} = Sealed broken sample weight in Air

SeW = Sealed (intact) sample weight in Water

In method ASTM D 6857-03 the mixture is well broken so that trapped air pockets are opened. Then this broken mixture is vacuum sealed in a bag to determine SeA_{broken}, Then the bag and sample are immersed in water, the bag opened, and the saturated sample and bag weighed together underwater to obtain (SaW_{broken}+BW) as a single measurement.

Each of these methods of determining air voids has inherent measurement errors, and taken together, the two provide a useful check on the one hand, and their comparisons provide an indication of the types of errors, on the other. For example, the SSD method is subject to greater error for more open, porous mixtures. This is because the SSD method relies on being able to obtain a weight of the saturated core that still contains all of the water inside the pores of the core. However, if the mixture is open enough, the water will tend to drain out, giving a lower saturated weight and also, higher air voids. On the other hand, the core lock method will give higher air voids if the surface of the core has a lot of texture to it because the bag cannot collapse around this texture completely and therefore, this texture appears as air voids in the pavement.

These methods are based on the standard methods for determining bulk specific gravity of compacted specimens, ASTM D 6752-03 (Vacuum Sealing Method) and AASHTO T166-00 (SSD), and on ASTM D 6857-03 for determining maximum specific gravity.

Binder Extraction and Recovery

Extraction and recovery of the binder in the cores is conducted based on the procedures outlined by Burr et al. (1993). These procedures provide for a thorough wash and therefore extraction of the binder from the aggregate but with minimal hardening or softening of the binder in the solvent and with care taken to assure complete solvent removal during the recovery process (Burr et al., 1990, 1993). The extraction process uses washes in toluene followed by a 15 percent ethanol in toluene solvent mixture and size exclusion chromatography to assure removal of the solvent from the recovered binder. It should be noted that the more aged binder requires a more extended recovery time in order to remove the solvent from the stiffer, more heavily aged binder.

Binder Content

The binder from the extraction recovery process is quantitatively recovered and weighed and provides a determination of binder content as a percent of the initial core weight.

Binder Analytical Measurements

The recovered binder was analyzed for a number of properties and also aged to determine binder hardening rates at 60 °C. Additionally, original binders where available were also characterized by these methods. FTIR samples were analyzed using a Mattson Galaxy 5000 FTIR and the attenuated total reflectance method described by Jemison et

al. (1992). The carbonyl area was determined by finding the area under the absorbance peaks from 1650 to 1820 cm^{-1}. The CA was used to monitor the progress of the asphalt oxidation.

Size Exclusion Chromatography

After the binder was extracted and recovered, the SEC analysis assessed complete solvent removal using previously reported methodology (Burr et al., 1993). Tests samples were prepared by dissolving 0.2 plus or minus 0.005 g of binder in 10 mL of carrier. The sample of interest was then sonicated to ensure complete dissolution. The sonicated sample was then filtered through a 0.45 μm PTFE syringe filter. Samples of 100 μL were injected into 1000, 500, and 50 Å columns in series with tetrahydrofuran carrier solvent flowing at 1.0 mL per minute. The chromatograms of binder obtained from replicate extractions should overlay each other. Incomplete solvent removal results in a peak located at 38 minutes on the chromatogram.

Dynamic Shear Rheometer

The rheological properties of the binder were determined using a Carimed CSL 500 controlled-stress rheometer. The rheological properties of interest were the complex viscosity η_o* measured at 60 °C and 0.1 rad/s (approximately equal to the low shear rate limiting viscosity) and the storage modulus (G´) and the dynamic viscosity (η´), both at 44.7 °C and 10 rad/s, in the time-sweep mode. A 2.5 cm composite parallel plate geometry was used with a 500 μm gap between the plates.

DSR measurement was also important for deciding whether the binder was changed in some way by the extraction and recovery process (Burr et al., 1990, 1991, 1994; Cipione et al., 1991). If two extraction and recovery replicates yielded binders with matching SEC chromatograms but significantly different complex viscosities, then

at least one of the binders was suspected of having undergone solvent hardening or softening.

Aging Methods

In this study, binders were aged by a variety of methods including aging in service in the pavement, an uncontrolled process which occurred over a wide range of temperatures and subject to variabilities in other parameters such as accessibility to oxygen and binder film thicknesses. In addition, a number of controlled laboratory aging methods were used on both recovered binders that had been previously aged in pavement and original binders obtained for a small number of the pavement sites, including MnRoad. These methods include environmental room aging at 60 °C, SAFT aging (approximately equivalent to RTFOT aging), and PAV* aging.

A stirred air flow test which simulates the hot mix process was used for short-term aging (Vassiliev et al., 2002). The standard pressure aging vessel procedure, was modified and is referred to as the PAV* procedure. This PAV* method was conducted at 90 °C and in 1 mm thick films (one third the thickness of the standard PAV test) and conducted for two test periods: 16 hr and 32 hr of aging, both at 20 atmospheres of air (the standard PAV pressure). The thin film provides increased access of the binder to oxygen and thus enhancement to the binder aging rate, even at 20 atmospheres air pressure.

Results and Discussion

Texas and Minnesota Aging Rates

In a previous project, results were obtained from Texas Highway 21 between Bryan and Caldwell (Glover et al., 2005). These results provided an early, albeit very approximate, indication of binder aging in Texas pavements and suggested strongly that

binders age even inches down into the pavement. These results were used to obtain a quantitative estimate of binder aging rates and, using these data, a value of 0.028 Δ (ln MPa/s) per month (or equivalently 0.028/month) was reported in Table 9-8 of that report. It was noted, however, that this rate may have been a bit high because it included cores from 1989, only two years after the pavement was placed. These cores likely were not yet out of the initial jump reaction kinetics period, and therefore were probably aging at a higher rate than the longer term post initial jump aging rate. Nevertheless, it gave an approximate value for an aging rate for this binder in this pavement in this part of Texas.

Data were also shown of binder properties at different pavement depths in the same pavement over an extended period of time. Figure 9-14 of that report is repeated here in Figure IV-3. Note that binder properties were measured in the top 2 inches of the pavement (designated by T, top), and in the next 2 inches (designated by M, middle) and the next 2 inches below that (designated by B, bottom). Thus, the B layer had four inches of pavement on top of it and had an average depth of 5 inches below the surface.

Figure IV-3 shows that all of these pavement layers aged at close to the same rate although it does seem clear that the top layer ages somewhat faster than the middle or bottom layers, as in each case the binder from the top layer is more aged than that from the bottom or middle layer. Nevertheless, the striking feature of these data is that all of those binder samples progressed across this DSR function map from the bottom right corner toward the top left corner with oxidation over the years, and the progression across this map was far greater than any differences in aging between the various layers.

From these results, the tentative conclusion was that environmental conditions in the pavement, temperature and oxygen availability, controlled the binder aging rate and that these conditions don't change as much with depth as conventional wisdom assumes. Another way of stating this is that even though one might expect that inches into the pavement both temperature and oxygen availability would be reduced enough that binder oxidation would be significantly lower than at the surface, these assumptions do not seem to be supported by the experimental evidence.

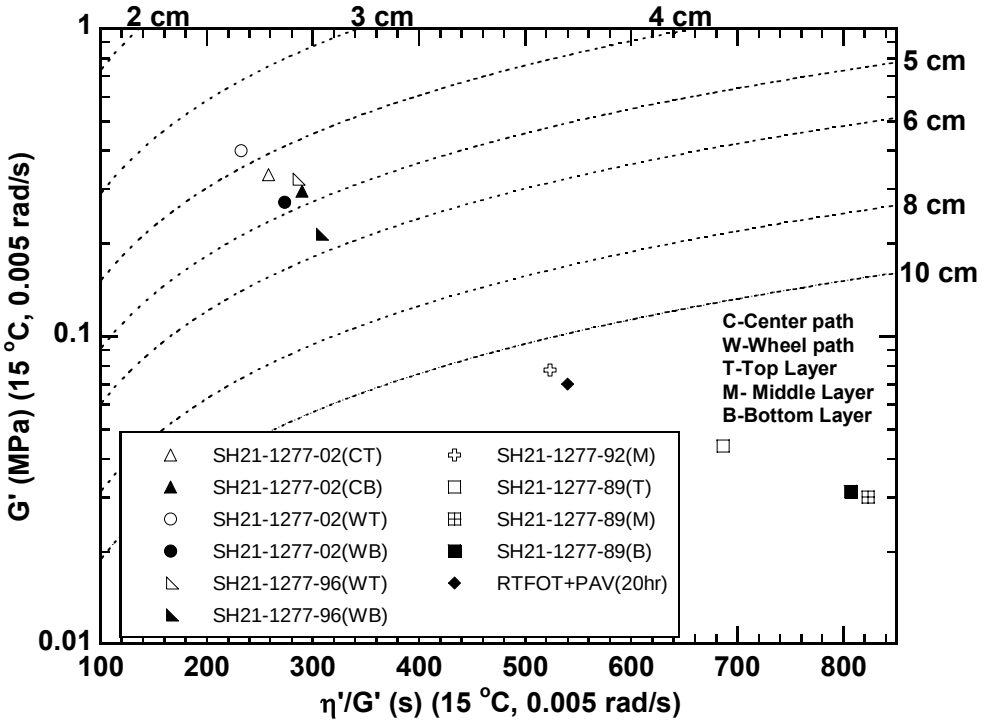

Figure IV-3. Movement of Binder across the DSR Map, Station 1277, SH 21

As a further study of binder aging in pavements as a function of pavement temperature and depth below the surface, the MnRoad test site was brought into this new project. The MnRoad site is located in Minnesota near Minneapolis-St. Paul and is a well-crafted site for the scientific study of road pavements and their performance, including the performance of binder properties. The test pavements at this site are very carefully designed and constructed to specific design parameters and thus make an ideal site for study within the objectives of this TxDOT project (MnDOT, 2002). The MnRoad test site consists of a portion of I 94 in Minnesota with part of it being of the main line interstate highway and part of it a test loop just off of the interstate highway. The presence of the test loop allows controlled test traffic over the pavement so that the traffic loading and frequency becomes a controlled variable.

Cells 1 and 3 from the main line test road and Cells 33, 34, and 35 from the low volume test loop were incorporated within this project. Cells 1 and 3 used an unmodified AC 120-150 penetration grade binder, and Cells 33, 34, and 35 contain an unmodified base binder (Cell 33) and two levels of SBS modification to produce a PG 58-34 binder (Cell 34) and a PG 58-40 binder (Cell 35). Cells 1 and 3 were constructed in 1992 whereas Cells 33 through 35 were constructed in 1999. Coring of all of these cells occurred in November of 2004 and again in July of 2006 thus giving 12 years of service for the first coring in Cells 1 and 3, and five years of service for the first coring of Cells 33 through 35. As mentioned above, details on the pavement thicknesses are given in Table IV-1. Data on the pavement cores and their binders follow.

Figures IV-4 through IV-6 show the binder content for Cells 1, and 33 through 35, as well as the total air voids (Figure IV-5) and the accessible (or interconnected) air voids (Figure IV-6). In Figure IV-4, we see that the binder content of each of these four cores is quite consistent, with all of them being 5 percent (more or less), with the exception of Cell 35, which while still having a consistent binder content within itself, this content is lower, at approximately 4 percent. Incidentally, the design binder content for the two modified pavements, Cells 34 and 35, were both 5.8 percent, so the actual binder content, while consistent with each core, appears to be significantly below the target design percentage.

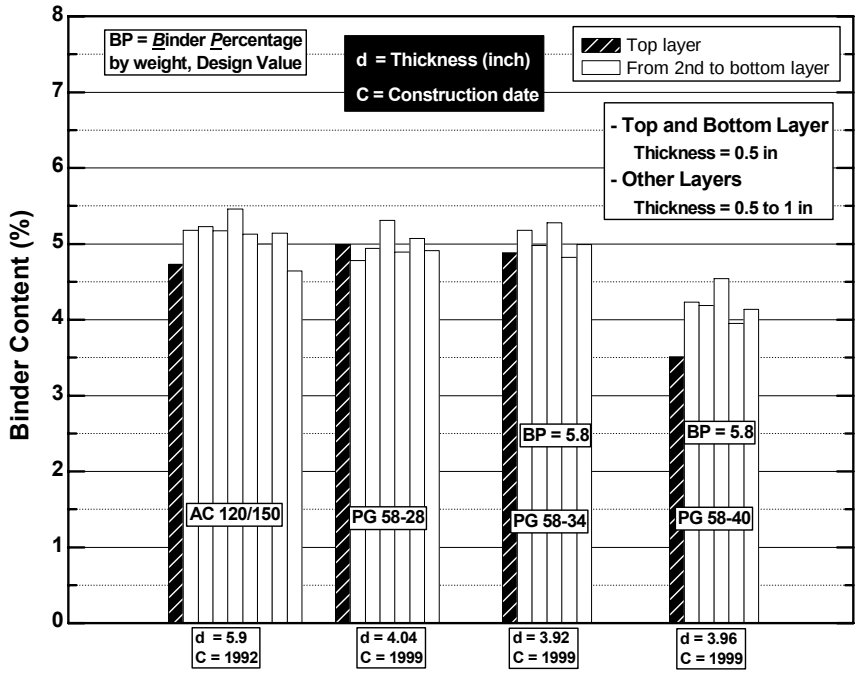

Figure IV-4. MnRoad Binder Content

Figure IV-5 shows the total air voids in each of the pavements as determined by both the saturated surface dry and the core lock methods. Note that there is very reasonable agreement between the two methods and also that the total air voids in each of the pavement cores is about 7 percent. There is a variability so that the range is from about 5 to 9 percent. It should also be noted that in Cell 1, in particular, the total air voids increases with depth into the pavement. This observation is also true for Cells 33, and to a lesser extent, 34. Also in 33, there does appear to be variability from layer to layer so the progression is not uniform. In Cell 35, the total air voids content even appears to progress in an opposite direction so that there is a decrease in total air voids with depth into the pavement. However, this decrease is quite minimal given the variability in the air voids measurement from layer to layer.

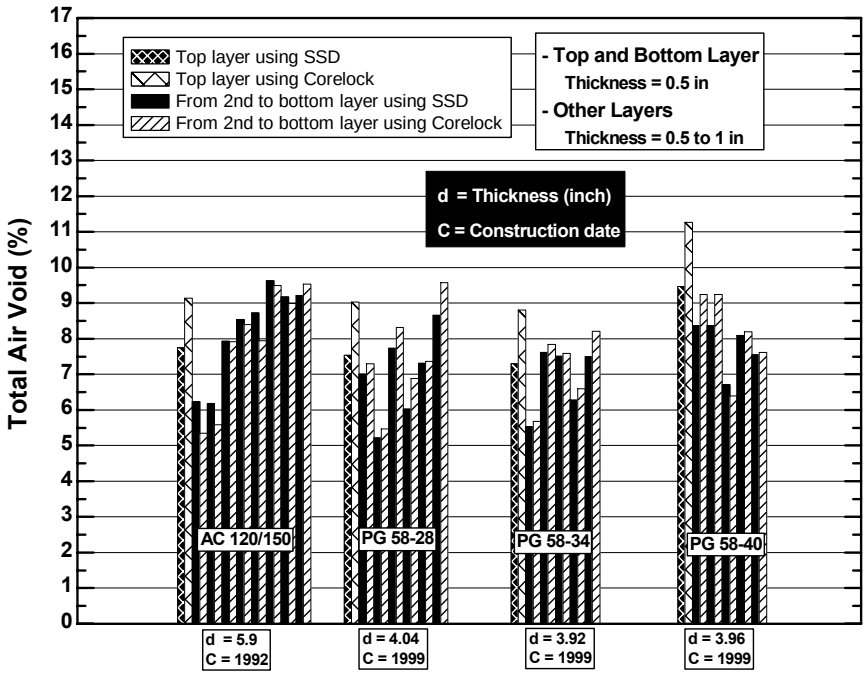

Figure IV-5. MnRoad Total Air Voids

The accessible or interconnected air voids, shown in Figure IV-6, are particularly interesting and appear to bear on the binder oxidation, as will be discussed below. Cells 33, 34, and 35 all have a fairly uniform interconnected air void content of from 3 to 5 percent. Cell 35 seems to have a significantly higher percentage in the surface layer, but this may be due to a surface roughness and therefore distortion of the actual interconnected air voids measurement. The interesting core with respect to interconnected or accessible air voids comes from Cell 1. In this core, the interconnected air voids level is quite low, even below 1 percent for the layers in the top half of the core (top 3 inches), and then as the layers progress down deeper into the core, they increase to the 4 to 5 percent range of the other cores. The reason for this cell having such low interconnected air voids is not known but could be the result of binder content coupled with the mix design and compaction during construction. At any rate, this particular core does appear to be definitively different from the others with respect to accessible air voids.

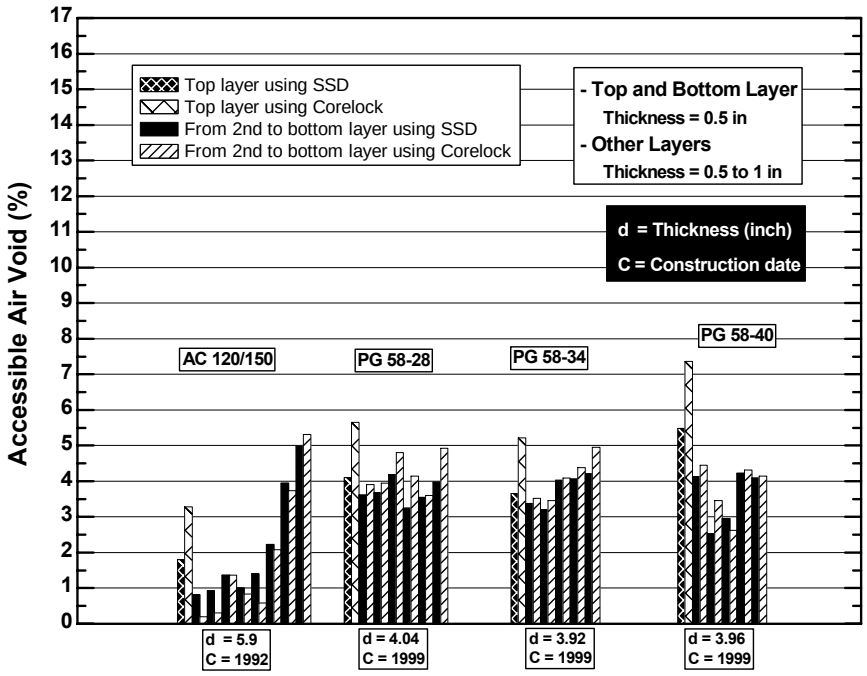

Figure IV-6. MnRoad Accessible Air Void

Figures IV-7 through IV-9 show the condition of extracted and recovered binder from the Cell 1 core that was obtained in 2004. This core was sliced into layers of a nominal 1/2 inch thickness and then the binder was extracted, recovered and tested for its DSR properties, as well as carbonyl content, to assess its level of oxidation. The DSR function properties are plotted in Figures IV-7 through IV-9 on the DSR map, which is a plot of G' versus the ratio of η' to G'. This plot of a binder's elastic modulus versus the ratio of its viscosity to elastic modulus shows the progression of a binder as it oxidatively hardens. As this hardening occurs, a binder moves from the vicinity of the lower right corner in the direction of the top left corner. This was noted previously in Figure IV-3 of the Texas Highway 21 recovered binder data.

Note that in addition to the recovered binder properties on these three figures, the original binder properties aged to different levels are also shown. These levels include the equivalent of a rolling thin film oven test aging procedure (designated SAFT) and two aging states that were obtained in a SHRP pressure aging vessel apparatus. These

two aging states are designated as PAV* 16 hr and PAV* 32 hr and were described previously in the research methodology section. Note that the SAFT aging is at the lower right corner, and the PAV* 32 hr aging is moved toward the top left corner near the dashed line that indicates a ductility of 10 cm. These dashed ductility lines are obtained from the correlation by Ruan et al. (2003a) and come from his correlation for unmodified binders between the DSR function and ductility measured at 15 °C, 1 cm/min.

The binder DSR data for the top four layers of the Cell 1 core are also shown in Figure IV-7. Note that for these four layers, the binder that is deeper in the pavement is less aged. Again, these are for the top 2.5 inches of the pavement. In fact, we note a rather regular progression from layer to layer in a direction of the binder being less aged with depth into the pavement. The order of this progression would be expected if the temperature in the pavement with depth into the pavement is lower and if the access of oxygen to the binder at greater depths in the pavement is reduced.

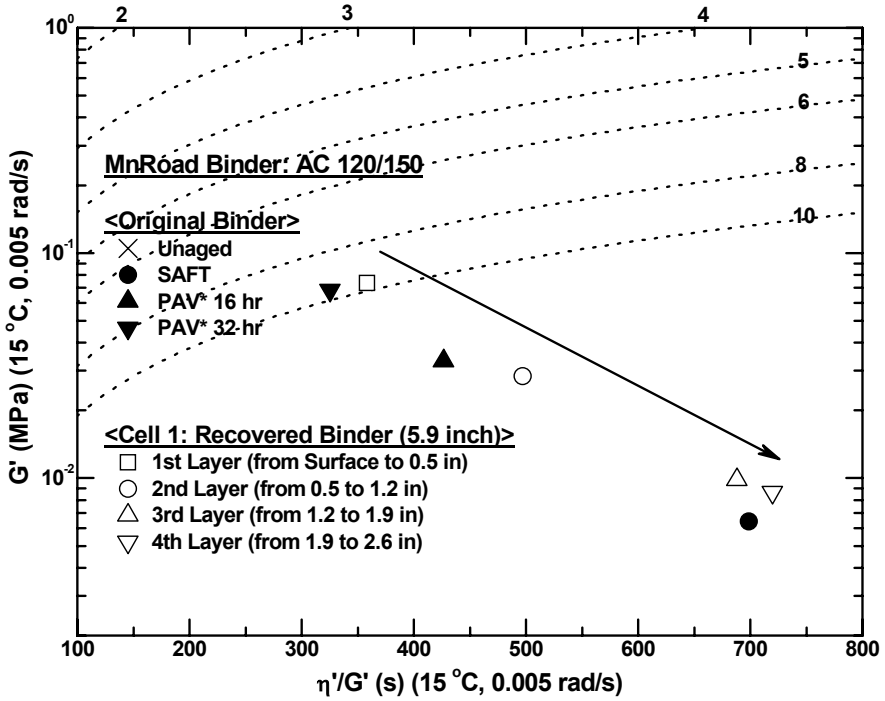

Figure IV-7. MnRoad Aging Comparison of the Surface to the Middle Layers

Figure IV-8 tells a different story, however. These data from the Cell 1 core move in the opposite direction. That is, as binder is recovered from progressively greater depths into the pavement (from 2.6 to 6 inches deep into the pavement), the binder is progressively more aged, even to the extent that the binder that is recovered from the layer that is nearly 6 inches deep into the pavement is as aged as the binder at the surface of the pavement. One might attribute this range of binder DSR data that is covered in Figures IV-7 to IV-8 to experimental variation except that the progression is so orderly, first decreasing monotonically in stiffness with increasing depth from the surface to the middle of the core, and then increasing monotonically with increasing depth from the middle to the bottom of the core.

The data for all of the nine layers are shown in Figure IV-9. Note that all the recovered binders fall along the same path which we would expect to be true of the same binder when it is recovered from the pavement. The difference in levels of aging, however, in working from the top of the pavement to its center and then to the bottom is remarkable and quite surprising. We also note that the lab aged binders, that is the SAFT and the two PAV* laboratory aged binders, follow a path in the same direction as the binders recovered from the core. But their path appears to be shifted slightly relative to the recovered binders. While the reason for this shift is unclear, it should be noted that the two PAV* binder aging processes are conducted at 20 atm air, 90 °C, conditions that vary significantly from the condition of the pavement aging. The SAFT binder aging conditions are also different in that the temperature is 325 °F (163 °C), which is significantly different again from road aging even though the pressure is atmospheric air.

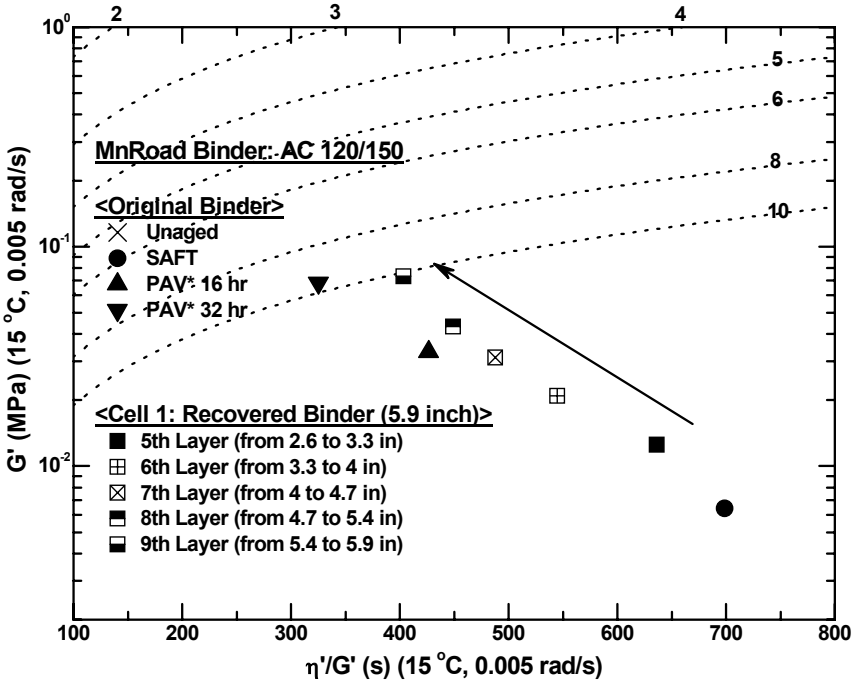

Figure IV-8. MnRoad Aging Comparison of the Middle to Bottom Layers

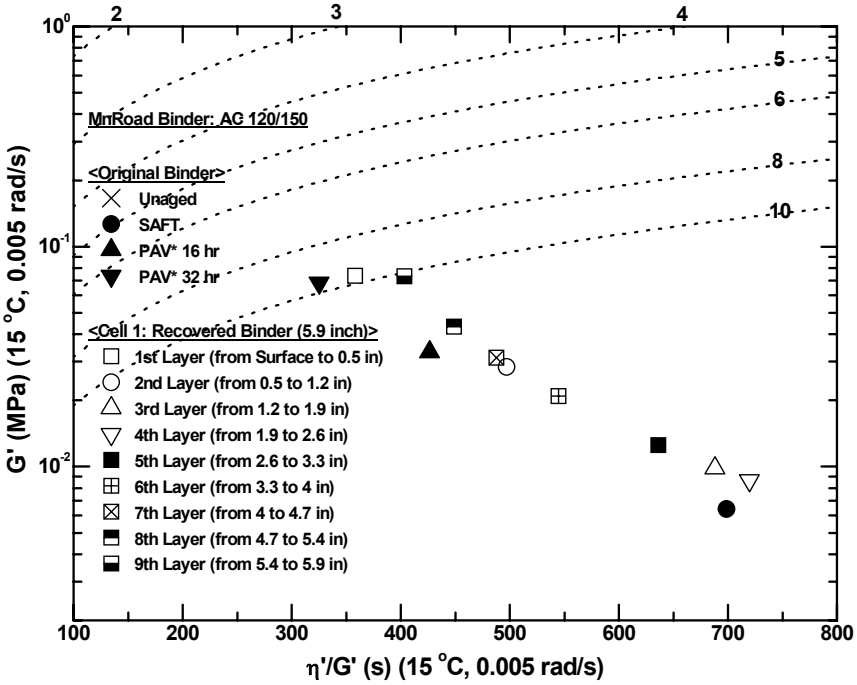

Figure IV-9. MnRoad Aging Comparison of the Surface to Bottom Layers

To summarize the results of these figures, we note three things. First, we note that twelve years of aging in pavements of Minnesota, at least in this pavement, is not very severe compared to Texas aging. The most severely aged binder from the Minnesota core, which is at the 10 cm ductility line is near the point of about four to five years from the Texas Highway 21 pavement. Of course, the Minnesota binder started out as a softer binder in order to sustain the colder, winter climates than the binder in Texas. But, nevertheless, it is a fair observation that the oxidative hardening rate in Minnesota is significantly less than that in Texas. The second observation is the significant difference we see in different layers. In the Texas pavement, such differences were not measured, and these differences receive further discussion below. The third observation is that this increased aging with increased depth is a surprise. As noted in the introduction, many literature papers and technical reports assume that the conclusion of Coons and Wright (1968) is approximately correct. This conclusion states that binders below the top inch of the pavement do not oxidize. These MnRoad data as well, as Texas Highway 21 data, definitively contradict that conclusion.

Figure IV-10 is a repeat of Figure IV-9 except that it also includes binders that have been aged in the 60 °C environmental room. These binders include both the original MnRoad AC 120-150 binder and also the binder recovered from the Cell 1 core taken as a mixture of all of the layers. Still shown are the SAFT and PAV* laboratory-aged data points. Finally, there is another data point that represents the blended binder from a second core taken 20 months after the first core from this cell. Note again that the binders recovered from the core and measured without additional aging all fall on the same path on this DSR function map, whereas the laboratory aged binder, even when it was aging of the recovered binder from the core, followed a path that was somewhat shifted. The recovered binder aged in the environmental room was aged at conditions that were much closer to those in the pavement i.e. they were aged at 60 °C and 1 atm of air pressure and yet they too, track along the shifted path away from the aging in the core. This fairly small shift may indicate some effect of the aggregate or perhaps some other effect. The SAFT (RTFOT equivalent) aging plus an additional three months in the

environmental room at 60 °C places the binder at about the same level of aging as the most severely aged binder recovered from the pavement after 12 years of pavement service.

From the environmental room aged binders, environmental room hardening rates at 60 °C were obtained and compared, for the binder recovered from the field and for the original binder samples, in Figure IV-11. Note that there is very good agreement of the PG 58-28 unmodified binder between the recovered binder and the original binder that was sampled at the time of pavement placement, 0.22 versus 0.23 ln (MPa/s)/month (equivalent to units of month^{-1}). For the AC 120-150 binder, however, the agreement is not as good with the original binder showing a 60 °C hardening rate of 0.20/month while the recovered binder shows a hardening rate of 0.27/month. The reasons for this difference are unknown.

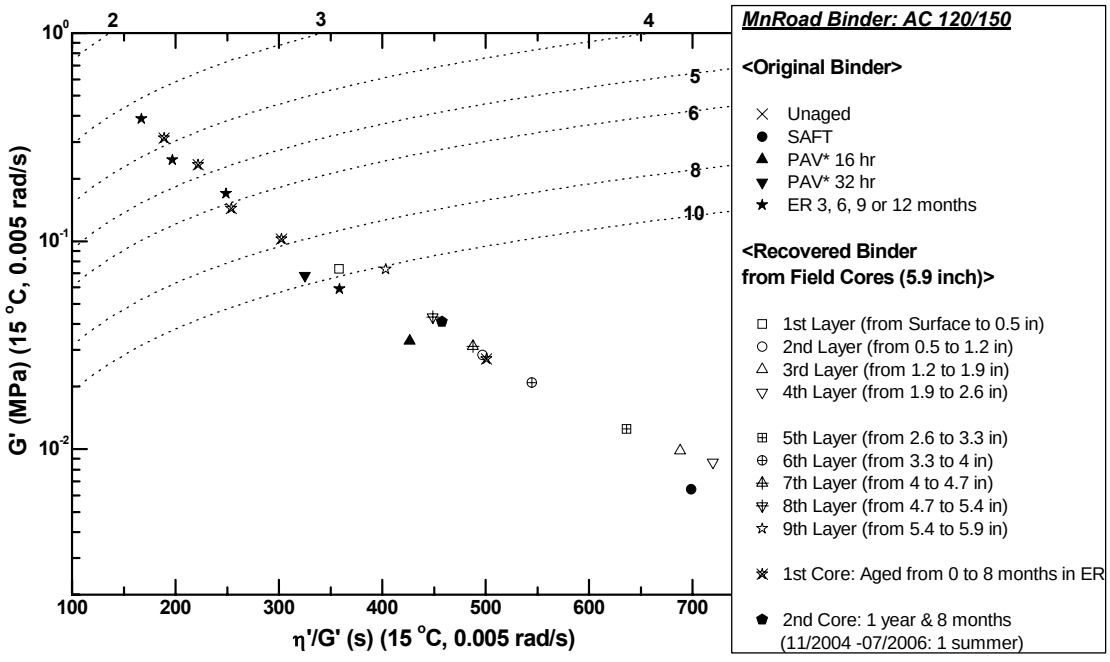

Figure IV-10. MnRoad Aging Path from 1st Core to 2nd Core, Plus Recovered Binder Thin Film Aging

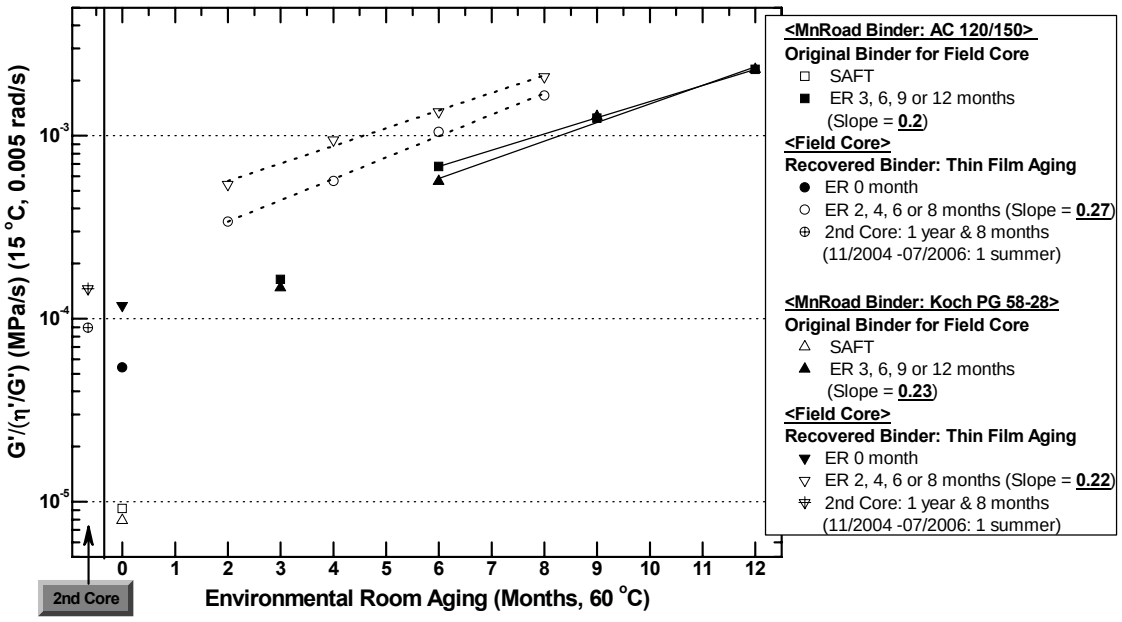

Figure IV-11. MnRoad DSR Function Hardening Rate for Unmodified Binders

Figure IV-12 shows laboratory and recovered binders for the other MnRoad pavements, as well as the unmodified AC 120-150 binder. The recovered binder data are all shown layer by layer, and the laboratory aged binders include the original unaged binder, the SAFT aged binder, and the two PAV* aged binders. In this figure, considering the binder recovered from the pavement layers, it is noted that, none of the other pavement cores provide the extreme range of aging of the binder layer by layer through the pavement as did Cell 1. The MnRoad PG 58-28 (unmodified) binder shows some significant variation from top to the bottom of the layer, but yet it is only about half of the differences exhibited by the AC 120-150 binder.

The two modified pavement binders, PG 58-34 and PG 58-40, show more aging at the surface but the rest of the layers binder properties cluster together on the DSR map. It should be noted, however, that Cells 33, 34, and 35 were all placed in 1999 and thus have seven years less pavement aging than the AC 120-150. It is expected therefore to be less aged than the Cell 1 binder. However, the differences are not so great, and the

surface binder for Cells 33, 34, and 35 are close to the same level of aging as the surface binder of Cell 1. It should also be noted that for these modified binders, there is a much larger shift between the laboratory aged binder and the field aged binder. While these shifts could be a result of modified versus unmodified binders, there is likely another factor that plays a significant role. These modified binders were treated with sulfur prior to being placed in the pavement for the purposes of cross-linking the binder in the pavement. We suspect that the binder that was tested as the original binder did not undergo any of this cross-linking, and therefore is a different product from the binder that was recovered from the pavement.

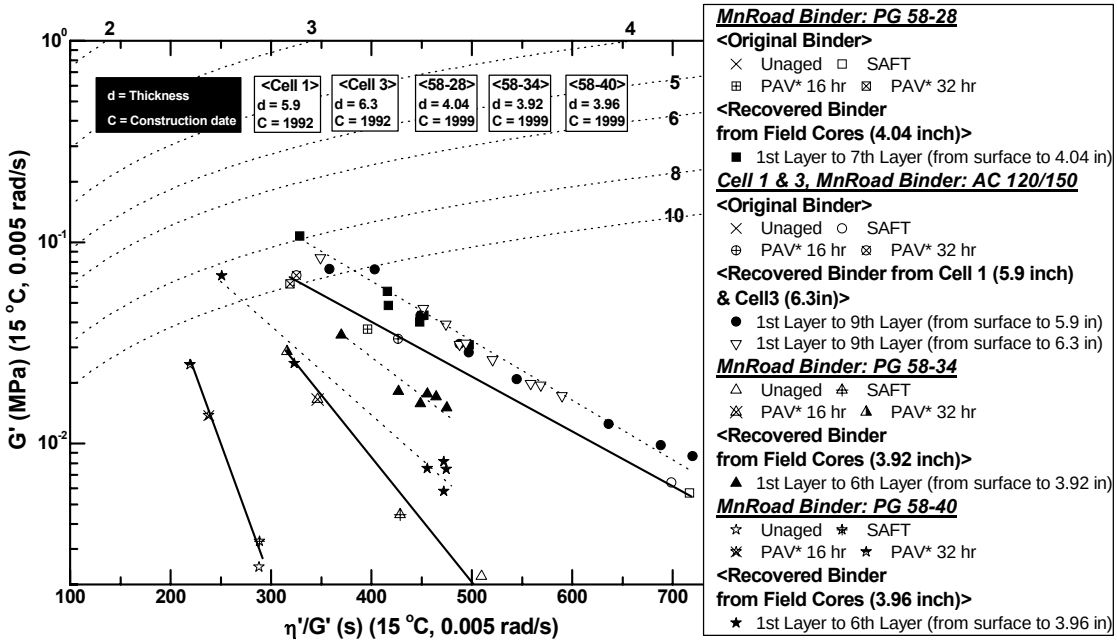

Figure IV-12. MnRoad (PMA and Base Binders) Aging Comparison of the Surface to Bottom Layers

Some final observations about these MnRoad pavements are appropriate. Previously, it was noted that the Cell 1 core had a significantly lower level of interconnected air voids than any of the others, and these lower levels were evident in the top layers of the pavement while the bottom layers were in the range of 2 to 5

percent interconnected air voids. A possible conclusion is that the variation in aging levels of that core with depth in the pavement is the result of these very low interconnected air voids. Looking at Figure IV-6, it can be seen that the air voids are less than 2 percent for the top five layers and then the sixth, seventh, eighth, and ninth layers increase progressively from 2 to 5 percent interconnected air voids. These data suggest that the progressively lower amount of aging deeper into the pavement could be due to this very low level of interconnected air voids and then that the increased aging towards the bottom of the pavement layer is a result of the increasing air voids with depth in that part of the pavement.

It is also noted that the interconnected or accessible air voids in the other Cells are all in the range of 3 to 5 percent and in fact, the data did not appear to show aging variations in those cores that might be attributed to differences in air voids. Thus, it is tentatively hypothesized that aging of the binder in a pavement is reduced by a deficiency of air if the accessible air voids are low enough, locally in the pavement, to affect binder oxidation. In other words, it is hypothesized that the oxidation of a binder in a pavement is affected by the air voids near that binder and not as much by the air voids some distance away from the binder. The according to this hypothesis, oxygen generally is available to the binder in the pavement (to the extent that the pavement has accessible air voids) but only locally in a pavement if the air voids are sufficiently high; if the local air voids are low enough, then there can be a significantly reduced binder oxidation rate. This hypothesis is in progress and more data are required to establish its correctness.

So, to summarize binder oxidation in these MnRoad cores, it is observed:

- Binder aging in Minnesota occurs at a generally lower rate than in Texas because of the lower temperatures.
- Aging rates may be different in different layers of the pavement, and it is hypothesized that these differences are a result of the accessibility of oxygen to the binder locally.

- Generally, there is a shift between the aging path followed on the DSR map by binders aged in pavement versus binders aged in the laboratory in neat binder films. This shift occurs even in binders recovered from the pavement and subsequently aged in a laboratory in thin films.
- This shift between binders aged in cores and binders aged in the laboratory is very significant for the two modified binders of the MnRoad cores, and this accentuated shift may be the result of cross-linking of the binder in the field as a result of added sulfur.

Additional data on the MnRoad binders are shown in the Appendix C and include size exclusion chromatograms of the modified and unmodified binders, layer by layer.

Model Development of Binder Aging in Pavements

In the previous sections, data were considered that were obtained from pavements in Texas and Minnesota and the rates and extent to which binders aged in those pavements. In this section, the effort was begun of developing a quantitative model to describe this binder aging.

Consider that the pavement might behave as a semi-infinite slab with an imposed periodic temperature at the pavement surface. The periodicity occurs daily because of daytime and nighttime temperature swings, and yearly due to seasonal variations of temperature. It is noted that such a model is used extensively in geology to estimate the temperature of the earth's crust as a function of time and depth, and it is now considered whether such a model is applicable for hot mix asphalt pavements (U.S. Geological Survey, 2006). Such a model of temperature in the pavement as a function of time and depth below the surface follows the well-known thermal diffusion model given by Equation IV-8 in which $\Theta(x,t) = (T(x,t) - T_{avg})$ is the temperature deviation from (i.e. oscillation about) an average temperature, t is time, and x is depth below the surface into the pavement.

$$\frac{\partial \Theta}{\partial t} = \kappa \frac{\partial^2 \Theta}{\partial x^2} \tag{IV-8}$$

In this equation, κ is the thermal diffusivity, which is equal to k/(ρC), where k is the thermal conductivity, ρ is density, and C is the heat capacity of the solid material. This model assumes no temperature variation parallel to a pavement's surface. So, it is an unsteady-state, one-dimensional model.

It is assumed the pavement is initially at uniform temperature (T_{avg}) and that at the surface there is imposed a temperature oscillation (of amplitude A, frequency ω and phase shift ε). These conditions provide initial and boundary conditions according to Equations IV-9.

$$\begin{aligned} &\text{I.C.: } \Theta(x,0) = 0 \\ &\text{B.C.: for } x = 0 \text{ and } t > 0,\ \Theta(0,t) = A\cos(\omega t - \varepsilon) \end{aligned} \tag{IV-9}$$

The solution to this problem is given by Equation IV-10 (Carslaw and Jaeger, 1959).

$$\Theta = Ae^{-x(\omega/2\kappa)^{1/2}} \cos\left[\omega t - x\left(\frac{\omega}{2\kappa}\right)^{1/2} - \varepsilon\right] - \frac{2A}{\pi^{1/2}} \int_0^{x/(2\sqrt{\kappa t})} \cos\left[\omega\left(t - \frac{x^2}{4\kappa\mu^2}\right) - \varepsilon\right] e^{-\mu} d\mu \tag{IV-10}$$

Note that this solution consists of the first term, a sinusoidal oscillation that perpetuates indefinitely plus the second transient term that decays over time to zero. The second term is due to the uniform temperature initial condition, which as time goes on becomes less and less important compared to the periodic surface boundary condition.

Thus, it is seen that according to this model, the temperature, after a sufficiently long period of time persists as a periodic temperature profile that is attenuated in amplitude according to the depth below the surface, and also shifted in phase according to the depth below the surface. The solution for amplitude as a function of dimensionless time and depth are shown in Figure IV-13. Again, note that with increasing depth, the peak-to-peak amplitude decreases, and also, the time of the maximum temperature at depth *x* is shifted relative to the time of the maximum temperature at the surface.

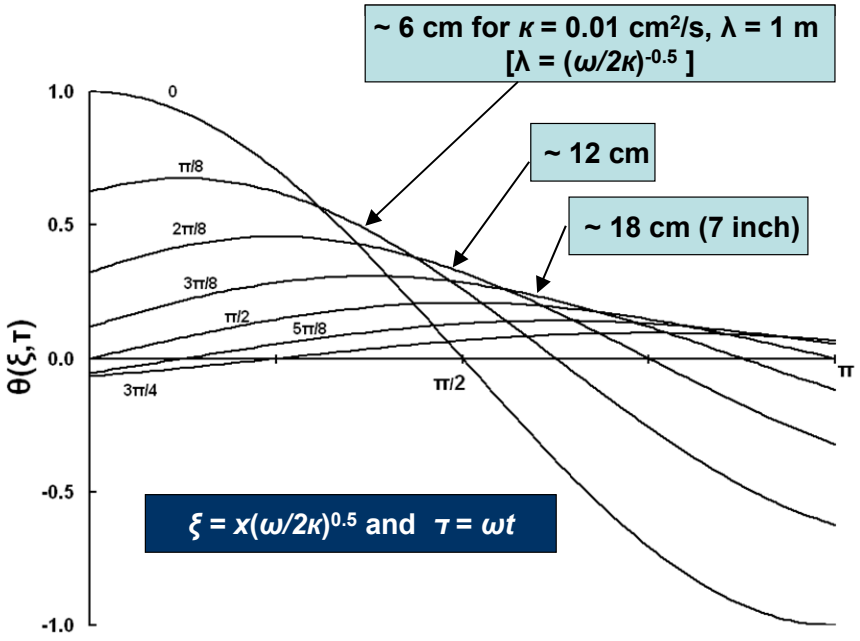

Figure IV-13. Calculated Temperature versus Time and Depth

Measured temperature profiles are available from the SHRP program long-term pavement performance (LTPP) site measurements and are shown in Figure IV-14. These data are for LTPP section 48-1060 in Refugio, Texas for different times during the summer, in June, July, August, and September, and also at different depths below the surface ranging from 1 to 7 inches. Note that these actual pavement temperature measurements also confirm a periodic temperature profile that attenuates in amplitude

with pavement depth and shifts in phase with pavement depth, in agreement with the above model. Using these data, values were estimated of the thermal diffusivity independently from both the amplitude attenuation and from the phase shift. Figures IV-15 and 5-16 show these comparisons for the Refugio data. Note that the amplitude data provide an estimate of thermal diffusivity of 0.0084 cm^2/s, and the phase shift data provide an estimate of 0.010 cm^2/s. This is very good agreement between these two estimates. (Incidentally, Carslaw and Jaeger report that the thermal diffusivity for rock material is 0.01 cm^2/s.) Note also that the model says that the temperatures at various depths should oscillate about the same average temperature. The data of Figure IV-14, while not exactly reproducing deviations about the same average temperature, appear to do so quite well.

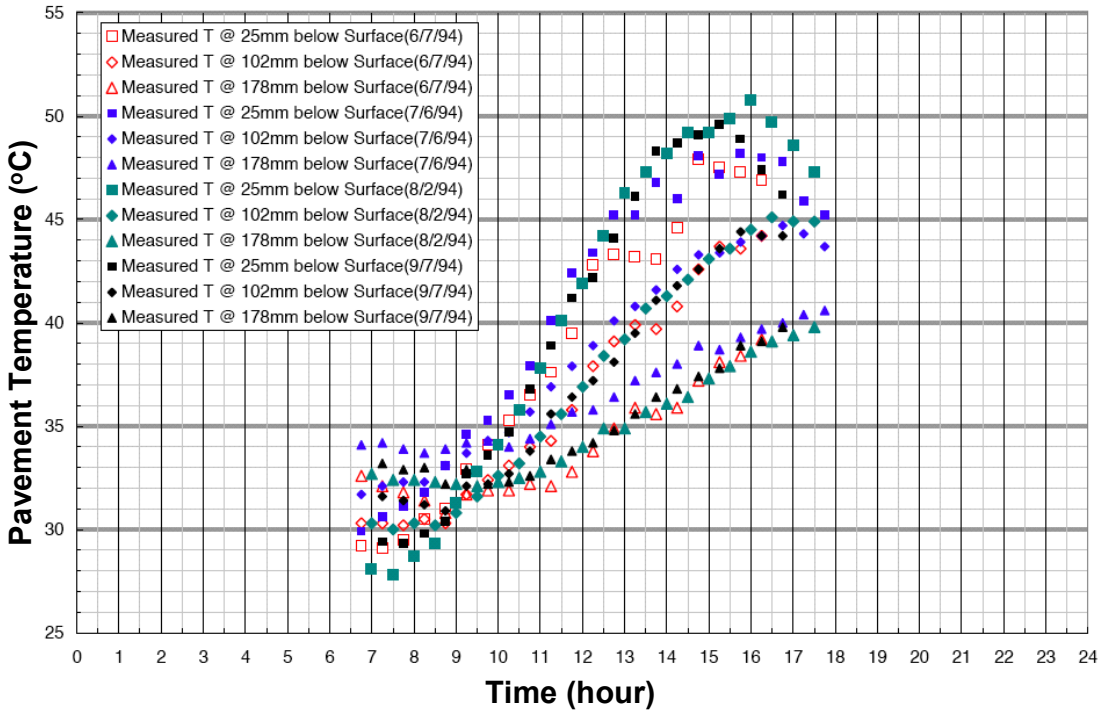

Figure IV-14. Refugio, TX, Measured Temperature with Depth in Summer 1994

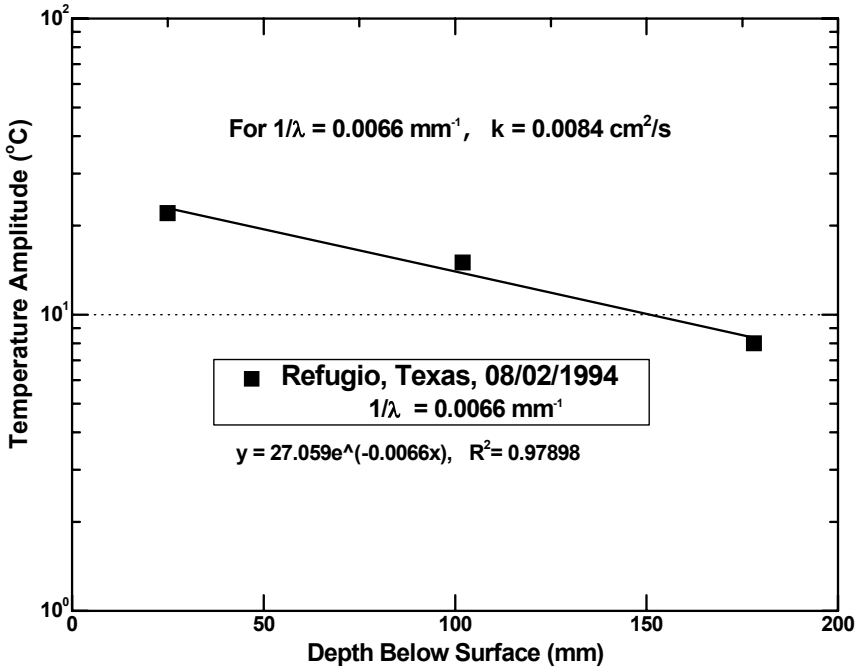

Figure IV-15. Refugio, TX, Temperature Amplitude versus Depth below Surface

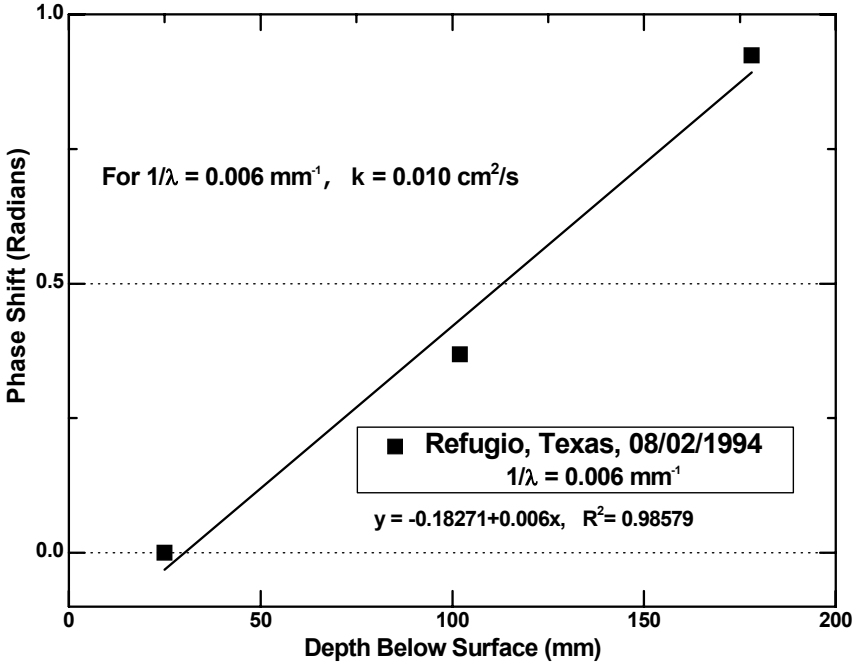

Figure IV-16. Refugio, TX, Phase Shift versus Depth below Surface

So, with the assumption that the semi-infinite slab model is a reasonable characterization of the temperature variation in a pavement over time and with depth, and using an average value of thermal diffusivity for the Refugio site obtained from the amplitude and phase measurements of 0.0092 cm^2/s, calculations of temperature over time were made and are reported in Figures IV-17 and IV-18. Figure IV-17 is over a 50-day time frame showing day-to-day temperature variations during the summer months, and Figure IV-18 shows a yearly time span with the seasonal variations together with the much more frequent daily variations. Note that the temperature profiles at two depths, 0 and 178 mm are shown. The difference in amplitude with depth is evident; the difference in phase is not so evident because of the time scales of the plots.

Using this model for pavement temperature as a function of time and depth, estimates were calculated of binder oxidation in pavements knowing the asphalt binder oxidation kinetic parameters and assuming that the transport rate of oxygen to the binder is high compared to the kinetics oxidation rate. This last assumption is not necessarily true (in light of the apparent effect of very low air voids in the MnRoad core) but by proceeding with the calculations, an idea can begin of the extent to which it might be true, and this calculation gives a limiting case estimate of binder oxidation rates.

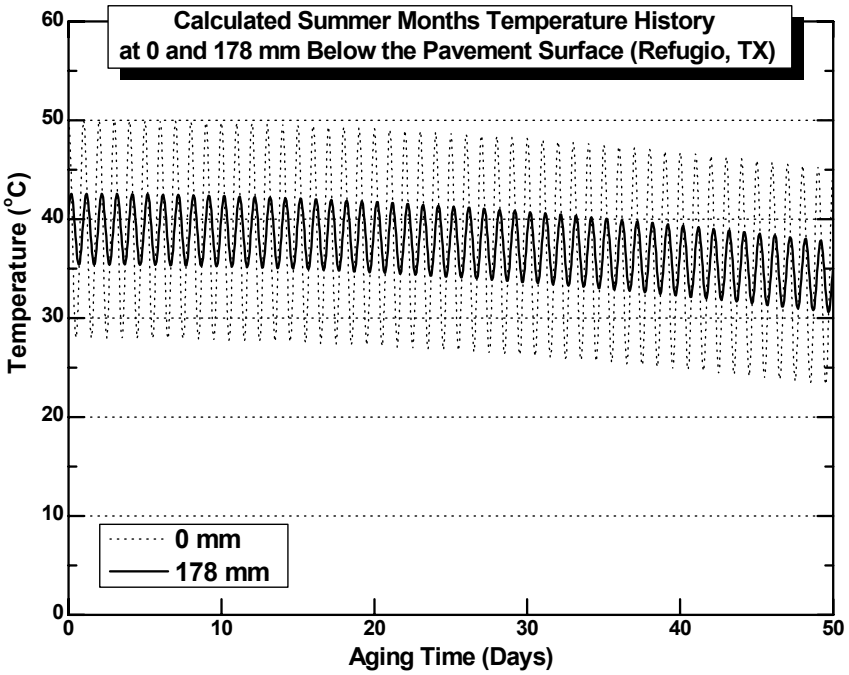

Figure IV-17. Refugio, TX, Calculated Summer Months Temperature History over 50 Days

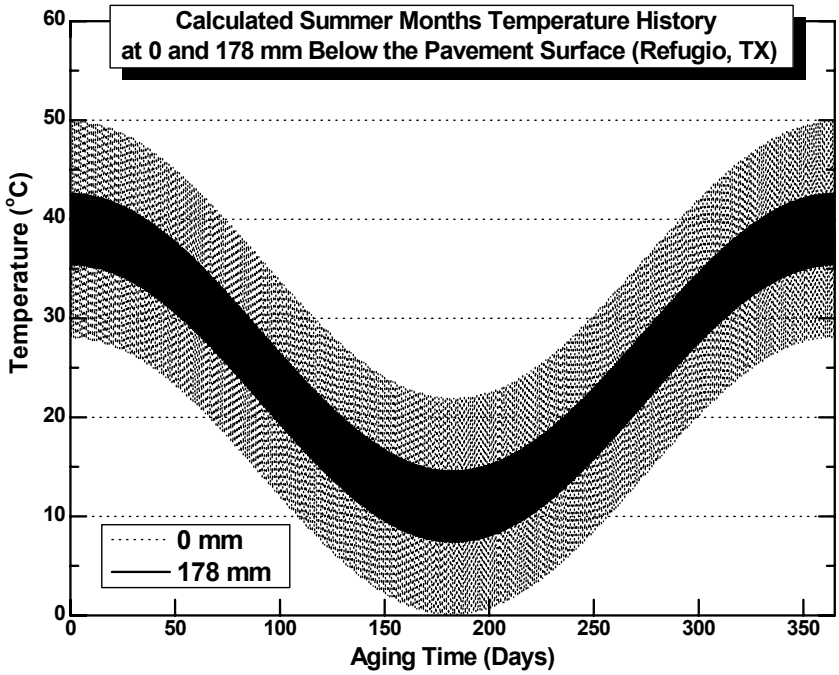

Figure IV-18. Refugio, TX, Calculated Temperature History over 360 Days

So, using this model, with the thermal diffusivity estimated from the Refugio pavement temperature data and the oxidation kinetic parameters for the binder used in the Highway 21 pavement between Bryan and Caldwell, estimates were calculated of binder oxidation and hardening over time (for the period after the initial jump oxidation period had passed). Both sites are in Texas and the temperature profiles are not terribly different. Probably the oxidation rates will be measurably different between the two sites, but for a first estimate and in the absence of actual Highway 21 pavement temperature data, the Refugio data was used.

Figure IV-19 shows calculated binder carbonyl area growth rate over time in the pavement out to 4000 days, and Figure IV-20 shows the binder hardening over time expressed in terms of the DSR function. Note that calculations are made for the surface and 178 mm (7 inches) below the surface. According to the model, while greater depths provide different rates, they do not provide grossly different rates, compared to zero. Also shown in Figure IV-20 is a line that represents the actual measured hardening rate of the binder in the pavement after about the first four years of pavement life. This time period is chosen so that the pavement is most likely past the much higher initial jump aging rate period. The agreement between the actual pavement hardening rate and the calculated hardening rate based upon the temperature model and the binder oxidation kinetics is quite remarkable and suggests that for this pavement, the assumption of good oxygen availability to the binder is acceptable. The Highway 21 data were reported in previous research (Glover et al. 2005) and are approximately the same rates for binders near the surface as for binders recovered from 5 inches below the surface. In the calculated carbonyl and DSR function oxidation curves, the practically zero hardening rate during the winter months versus the much higher hardening rate during the summer months is evident in the stair-step calculations.

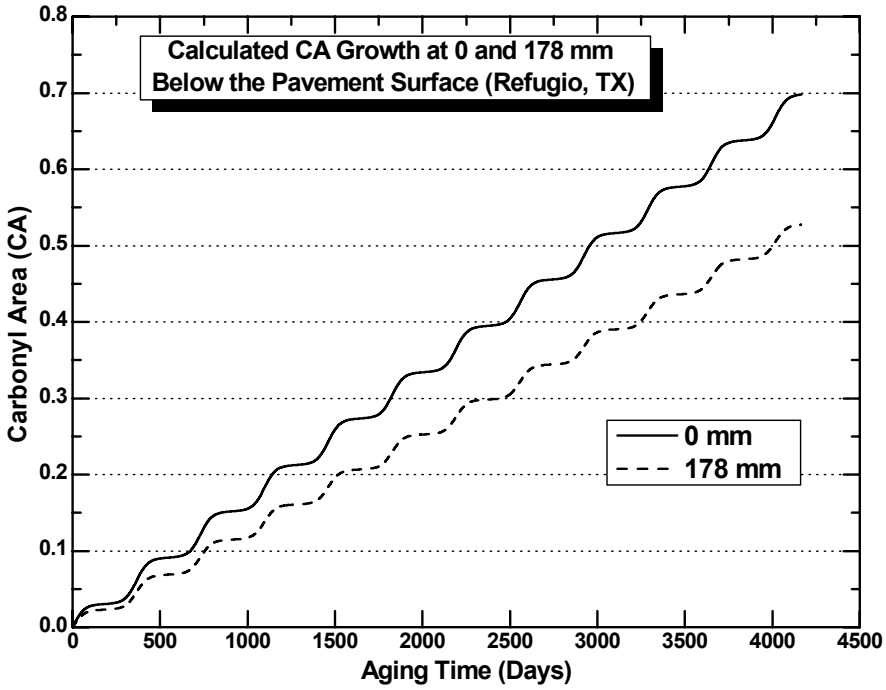

Figure IV-19. Refugio, TX, Calculated Carbonyl Area Growth

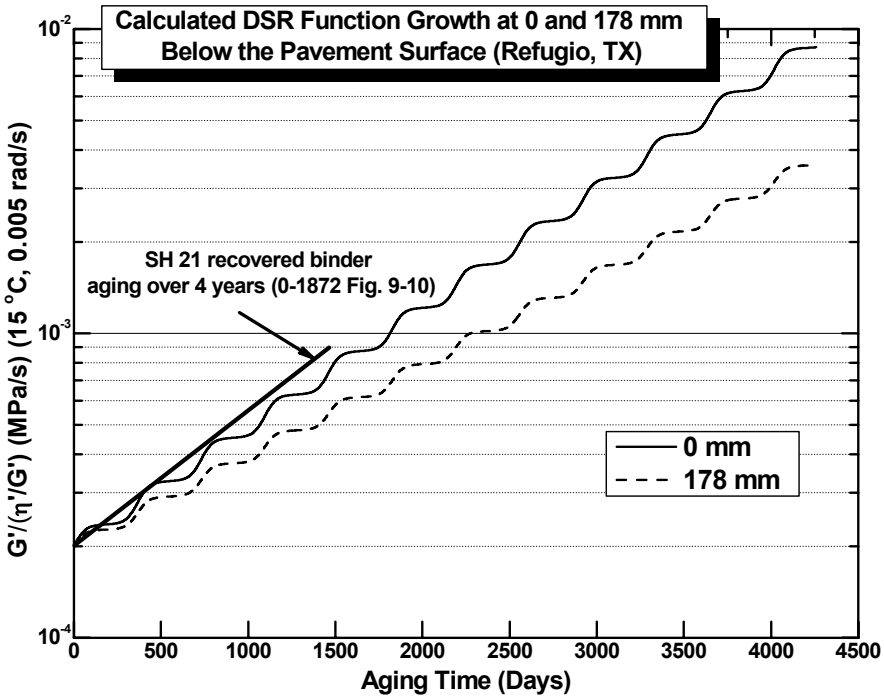

Figure IV-20. Refugio, TX, Calculated DSR Function Growth

Using these calculations, Figure IV-21 shows a calculated DSR function as a function of pavement depth at aging times out to 10 years. Here it is noted that below about 7 inches, there is very little difference between aging rate of the binder whereas in the top 3 inches or so, there are some significant differences in rates. However, the binder oxidizes at depth at a significant rate so that, comparing the absolute DSR function at 10 years and 20 inches below the surface to the DSR function at 10 years at the pavement surface, the differences are not so great (their ratio in DSR function is only a factor of 2.5 to 3 harder at the surface) compared to the difference between 10 year aging (at any depth) and no aging. A similar graph of binder variation with depth is shown in Coons and Wright (1968). Their conclusion is that below the top 1.5 inches of pavement, binders don't oxidize. According to the calculations and assumptions of this model, it's not that the binders don't oxidize, but rather that below the top few inches, differences in oxidization and hardening rates are minimal. The binder is harder at the surface than it is several inches into the pavement, but the difference is not nearly as great as it would be if, in fact, there were zero oxidization beyond 1.5 inches deep into the pavement as they concluded.

From the perspective of this model, the reason the binder at the surface oxidizes at a higher rate than below the surface is not because the average temperature varies with depth (it doesn't), but rather because of two interactive effects. First, the amplitude of the oscillations about the mean temperature is greatest at the surface and attenuates with depth into the pavement. Second, the reaction rate is not linear with temperature; rather it is exponential. Thus, the higher temperatures above the mean provide higher reaction rates that are not cancelled by the lower rates at temperatures below the mean. At enough depth, the rates are controlled entirely by the average temperature as the oscillation amplitude about that mean becomes very small.

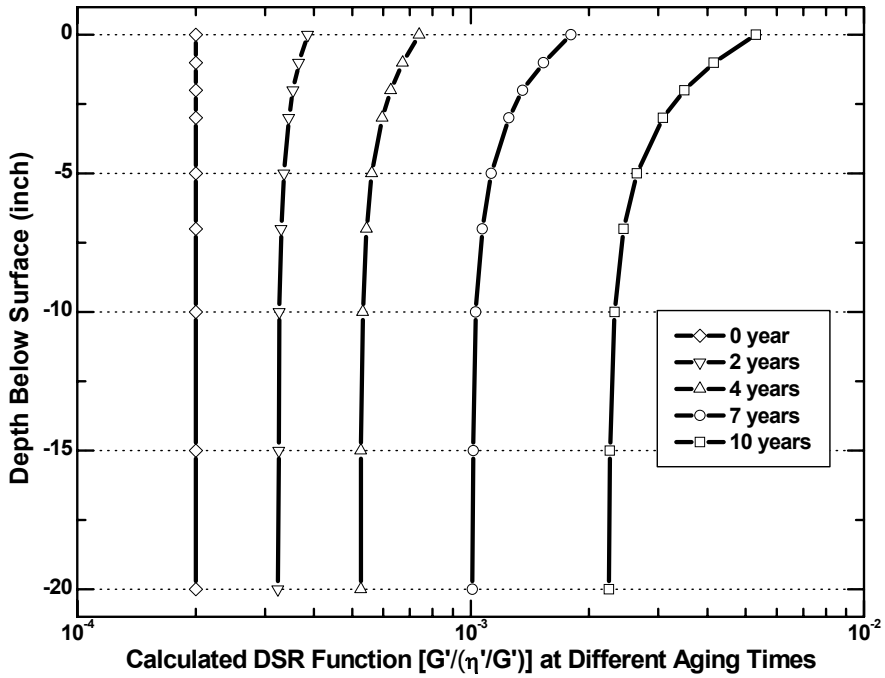

Figure IV-21. Depth versus DSR Function at Different Aging Times

MnRoad Pavements

The same procedure was followed that was outlined above for a pavement that was aged in service in Minnesota as part of the MnRoad performance study. Temperature data over time were obtained from Cell 1 at depths up to 131 mm (5 inches). Data are shown in Figure IV-22 for Cell 3. Using these data and again estimating thermal diffusivity from the attenuation of the temperature amplitude and the phase shift, it was estimated the thermal diffusivity of the compacted mix of the pavement to be approximately 0.015 cm^2/s.

Using these values, temperature profiles over time were calculated, and Figure IV-23 shows the variation at 0 and 5 inches below the surface for 50 days during the summer months. The daily oscillation is about an average temperature of 35 °C, which is significantly lower than the average temperature of 39 °C in Refugio. Temperature

variations over an annual span of time are shown in Figure IV-24. The minimum average temperature is approximately -10 °C.

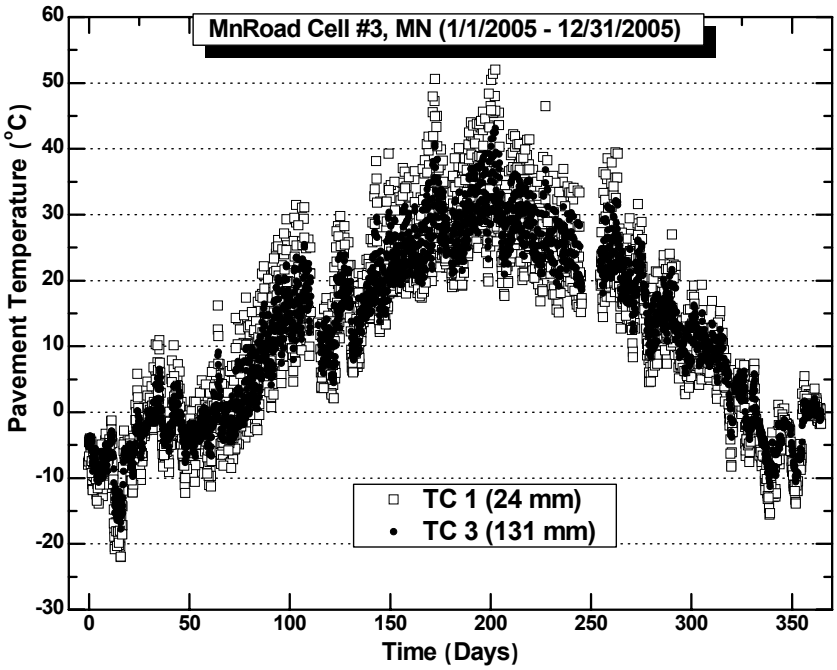

Figure IV-22. MnRoad Cell 3 Measured Temperature with Depth, 2005

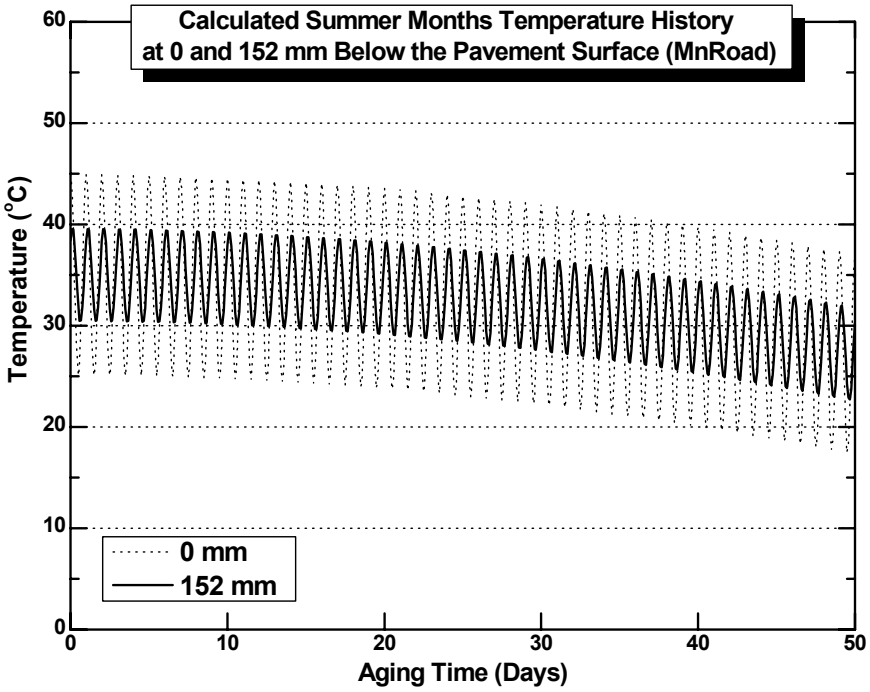

Figure IV-23. MnRoad Calculated Summer Months Temperature over 50 Days

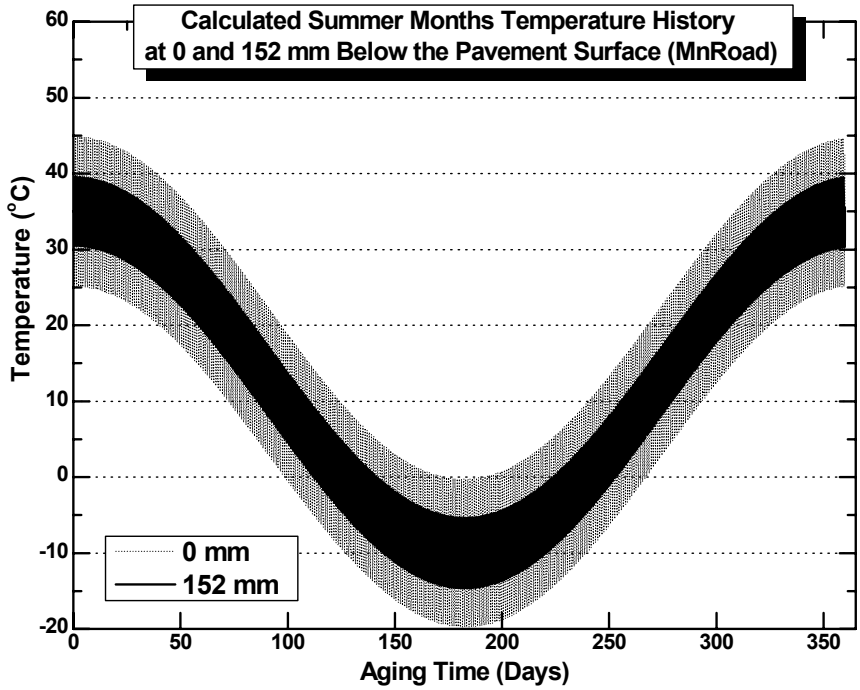

Figure IV-24. MnRoad Calculated Temperature over 360 Days

Original binder was not available for Cell 1 so binder oxidation kinetic parameters were determined experimentally by aging binder that was recovered from a Cell 1 core in the laboratory in 1 mm thick films and at 60 °C, 75 °C, and 95 °C. DSR function hardening at all three temperatures is shown in Figure IV-25, and an activation energy plot is shown in Figure IV-26. From these data, a ln DSR Function activation energy of 85.3 kJ/mol and a value for the constant A of 2.64 x 10^{11} ln(MPa/s)/day were determined for the constant-rate period kinetics equation:

$$\frac{\ln(\mathrm{DSRfn}_2)-\ln(\mathrm{DSRfn}_1)}{t_2-t_1}=\frac{\ln(\frac{\mathrm{DSRfn}_2}{\mathrm{DSRfn}_1})}{t_2-t_1}=Ae^{-E/RT} \qquad \text{(IV-11)}$$

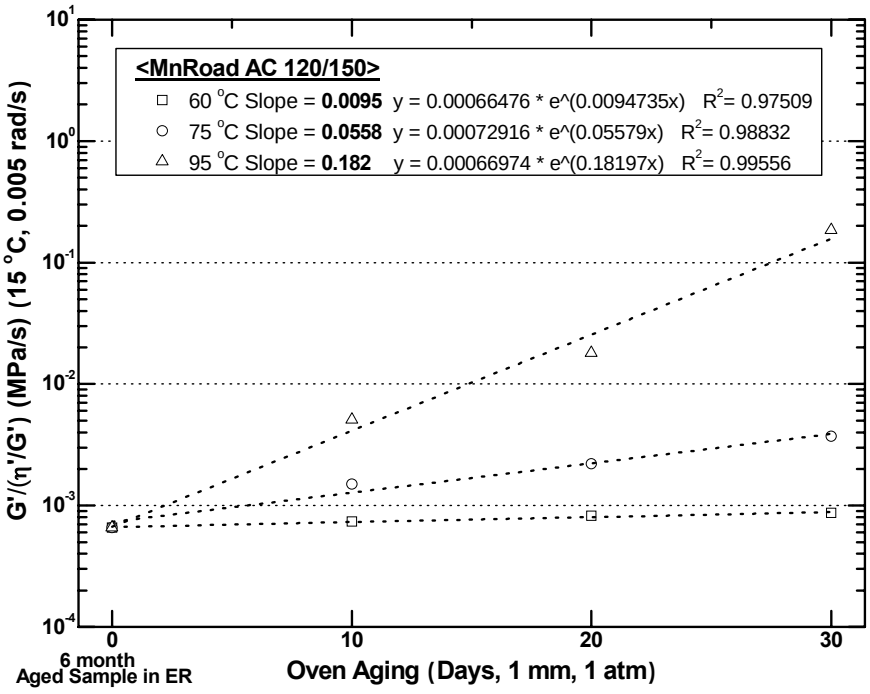

Figure IV-25. Effect of Temperature on MnRoad AC 120-150 Hardening Rate

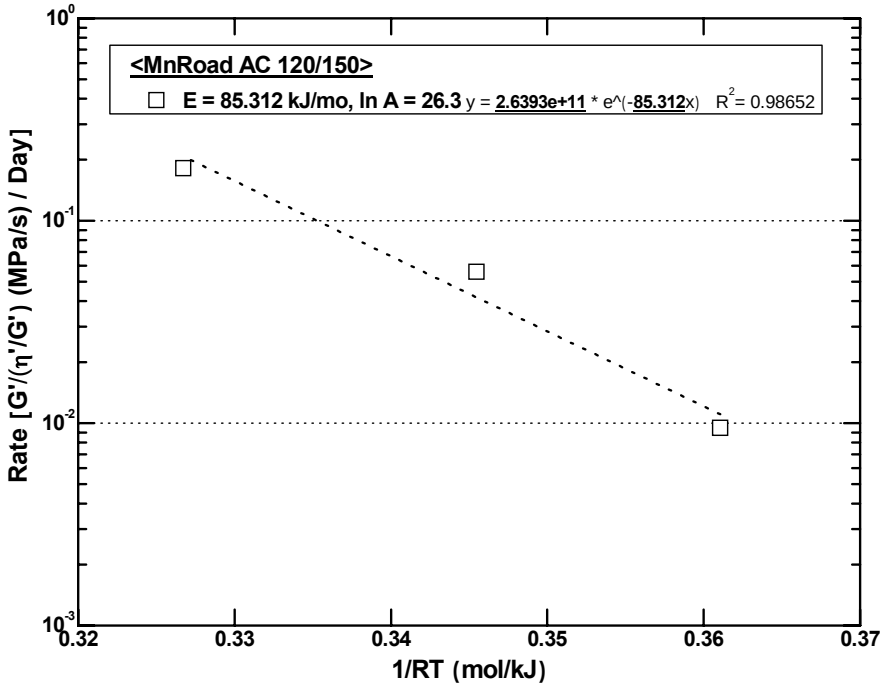

Figure IV-26. Estimation of MnRoad DSR Function Hardening Kinetic Parameters at 1 atm Air

Using the temperature model together with the pavement thermal diffusivity estimated from the measured pavement temperature data and the binder hardening kinetic parameters, binder oxidation and hardening over time in the MnRoad pavement was calculated. Figure IV-27 shows the carbonyl area growth over time, and Figure IV-28 shows the growth of the DSR function, i.e., the hardening of the binder in the pavement over time.

Note that in Figure IV-28, the hardening of the binder in Minnesota occurs at a significantly lower rate than the hardening of the binder in Texas Highway 21, shown again by the solid black line. In Figure IV-29, both the Highway 21 and the MnRoad data are shown, and aligned with the MnRoad calculations are approximate average hardening rates for the MnRoad pavement based on the 1st and 9th layers of the Cell 1 core. Remember that in this cell, there were significant differences in the hardening rate

of the binder at different depths below the surface, probably due to the variation in accessible air voids in the pavement. The 1st and 9th layers both appear to have ample access to oxygen and aged at essentially the same rate. Thus, it is those rates that are depicted by the slopes of the two lines together with the calculations.

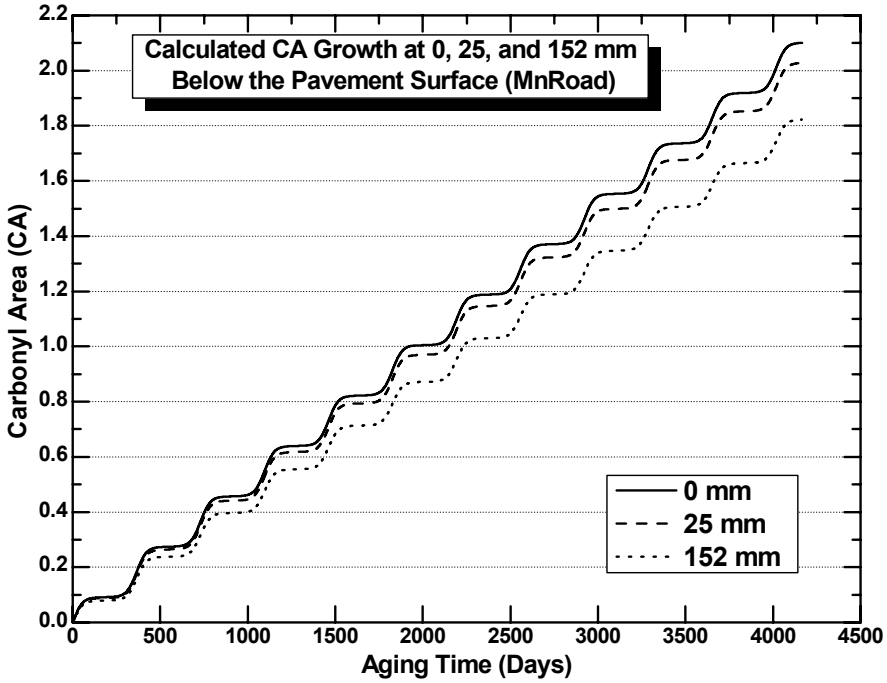

Figure IV-27. MnRoad Calculated Pavement Carbonyl Area Growth at 1 atm Air

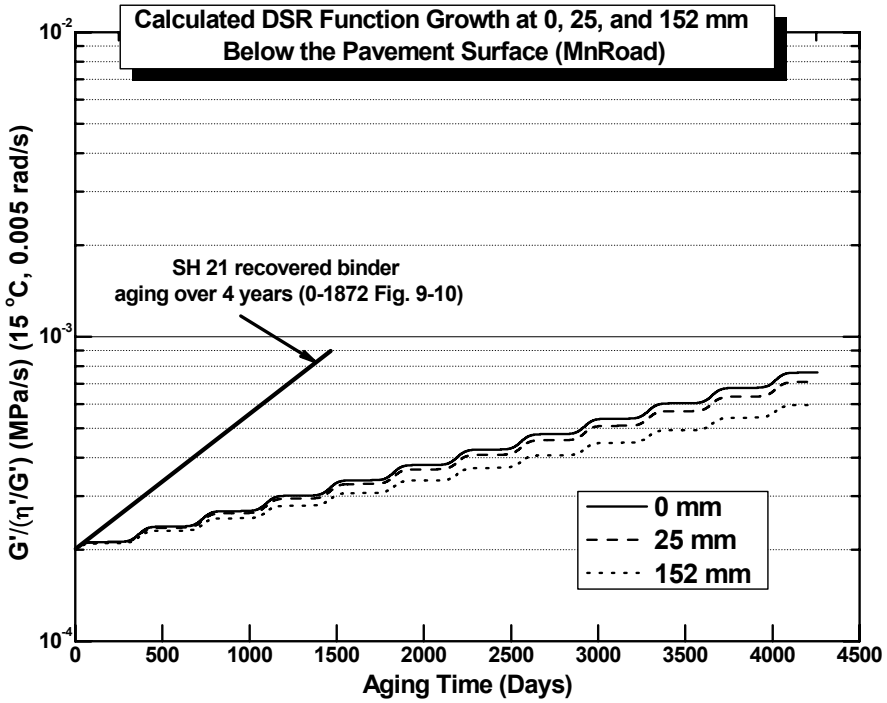

Figure IV-28. MnRoad Calculated Pavement DSR Function Growth

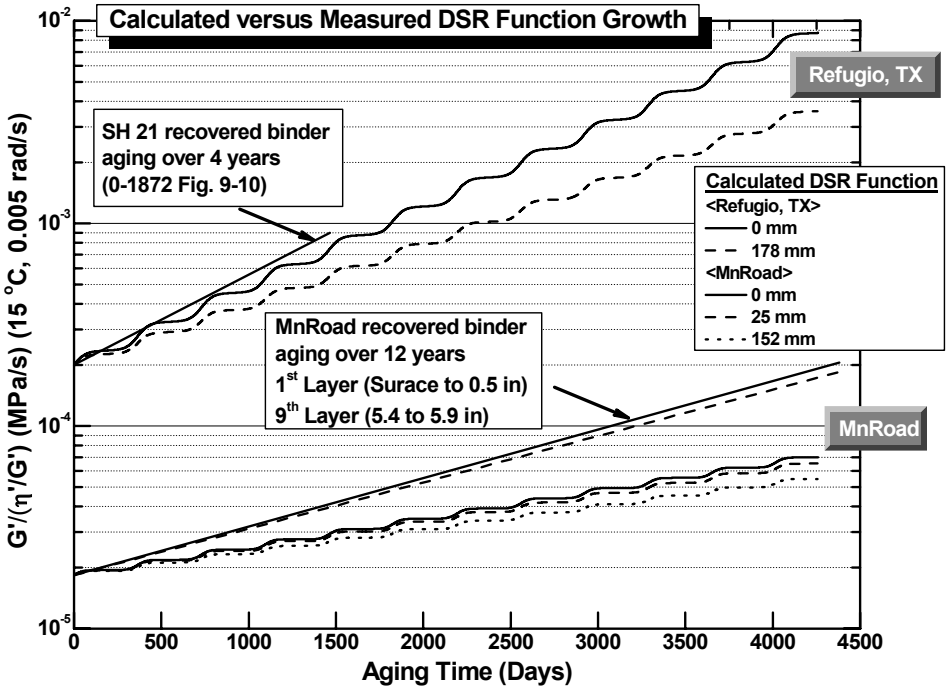

Figure IV-29. Calculated and Measured Pavement DSR Function Growth

Again, it is seen what is actually a good comparison between the actual binder aging rates and the calculated rates based upon measured temperatures in the pavement, measured binder reaction kinetic and hardening parameters, and based upon the semi-infinite slab temperature heat conduction model for temperature in the pavement as a function of time and position. For the MnRoad recovered binder hardening, an initial pavement value was not measured so that an estimate had to be made. Furthermore, for the recovered binder, the aging over most of the service life of the pavement, based upon previous work with binder aging, may well have occurred during the initial jump portion of binder aging and therefore at a higher aging rate than would be described by the kinetic parameters that were for the aging after the initial jump period.

Taking these factors into consideration, it is not surprising that a higher aging rate estimated for the recovered binder is seen than was calculated based upon a temperature model and the binder oxidation and hardening kinetic parameters. The slope of the pavement binder is approximately 0.016 [ln (MPa/s)]/mo whereas the calculation at the surface gives a slope of 0.010 [ln (MPa/s)]/mo. For comparison, the data from Highway 21 for the recovered binder is 0.031 [ln (MPa/s)]/mo whereas for the calculation, the result is 0.028 [ln (MPa/s)]/mo at the surface of the pavement.

The point is that the Highway 21 pavement aged in Texas occurred at a significantly higher rate than the binder in the pavement in Minnesota and the differences can be largely attributed to the lower temperature and appear to follow quite well the very simple model of the heating of a semi-infinite slab with a periodic boundary condition. Again, the middle layers of the MnRoad pavement that have significantly lower accessible air voids appear to be notable deviations from the model.

Further observations on the pavement hardening rates in both the Texas and Minnesota pavements are appropriate. The results for both pavements are summarized in Table IV-2 where data are shown for the approximate pavement aging rates that were calculated based upon recovered-binder DSR function values, and both the surface aging rate and the hardening rate 7 inches below the surface based upon the temperature model calculations and the pavement binder oxidation and hardening kinetic parameters.

Table IV-2 Comparison of Measured and Calculated Pavement Hardening Rates

Pavement	DSR Function Hardening Rates (ln (MPa/s)/mo)			
		Model Calculated Rate		
	Measured Pavement Rate	0 mm (surface)	178 mm (7 in)	Ratio (Rate at 178)/(rate at 0)
TX 21	0.031	0.028	0.021	0.75
MnRoad Cell 1	0.016	0.010	0.008	0.76

From these data calculations, several observations are significant. First, hardening rates in both Texas and Minnesota determined from the recovered binders are higher than the calculated rates for binders at the surface of the pavement. These differences could be due to the already mentioned possibility that part of the pavement aging is spent in the initial jump period which has a higher average hardening rate than the constant rate period which occurs later, but also because the actual binder aging at the surface almost certainly is higher than that which would be calculated because of the especially high aging rates that occur due to solar radiation. However, this latter effect probably is fairly minor because such aging occurs over a very thin layer of the pavement surface and the binder at the very surface, once it's oxidized to a sufficiently high level, becomes quite water soluble and is likely removed over time by the effects of rain.

While there is a span of hardening rates with depth, calculated using the model in both the Texas and MnRoad pavements, the span is smaller than the total spread between the two locations. The rate calculated at the surface of the MnRoad pavement is still nearly half of that calculated in the Texas 21 pavement seven inches below the surface. This calculation shows the significant effect of the different temperatures in the two climates, which is mainly a reflection of the differences in the temperature in the summertime. The oxidation rate is an activation energy phenomenon and therefore, the rates increase exponentially with temperature. Thus, the hardening rate increases more than proportionately with temperature.

As a further example of this effect, the fact that there is a difference between the hardening rates at the surface and the rates 7 inches below the surface is due entirely to this nonlinear effect because according to the model, the temperatures in both parts of the pavement, while periodic, oscillate around identical average temperatures. Thus, the average hardening rates at the surface, according to the model, are higher than the average rate below the surface simply because 1) the hardening rate increase, per degree above the average temperature at the surface is more than the hardening rate decrease, per degree below the average surface temperature, due to the non-linear Arrhenius activation energy relationship, and 2) combined with the smaller temperature swings below the surface.

As a final observation, the ratio of the hardening rates 7 inches below the surface for these two examples is roughly 75 percent of that at the surface. Whether this is a good rule of thumb or not remains to be seen pending calculations in more climate zones coupled with recovered binder experimental data. But, it is a plausible approximate ratio as an engineering approximation for the moment.

Summary of the Pavement Aging Model

To summarize the pavement aging model, the following observations are made. First, a model that assumes that oxygen is readily available to the binder in the pavement appears to give reasonable calculations of temperature over time that compare well to measured temperatures in pavements and also, that provide binder hardening rates that compare quite well to measured hardening rates in pavements in Texas and Minnesota. The agreement, of course, is not perfect, but considering that the diffusion of oxygen is ignored, it appears to be surprisingly good. One component of this aging model is that while there is a 25 percent drop in binder hardening rate from the surface to 7 inches below the surface, beyond that there is very little further decline in binder hardening rate at greater depths into the pavement. This conclusion obtained from the model refutes

assumptions reported in the literature and embodied in the mechanistic empirical pavement design guide that binders oxidize in the top inch of a pavement, but beyond one inch they do not oxidize at all. The difference between these two conclusions on binder oxidation at depths into the pavement are profound and have significant impact on the considerations of binder performance in pavements and indeed of pavement performance itself in both fatigue and thermal cracking and therefore, on the long-term serviceability of highways. Further specific conclusions of the model and the data upon which it is based are discussed below;

- The temperature in the pavement varies periodically with daily temperature cycles and annually with seasonal temperature cycles.
- These temperature variations decrease in amplitude with increasing depth below the surface of the pavement; however, the average temperature about which the variations occur is constant with pavement depth, again according to the heat conduction model, and is supported quite well by the data.
- Data obtained from pavements of temperature variations over time and with depth were used to obtain values for the thermal diffusivity in the pavements in both Texas and Minnesota. These values of thermal diffusivity were quite close to the reported value of 0.01 cm^2/s for geological materials in the earth's crust. Therefore, if no other data were available, one could probably use a value of 0.01 cm^2/s for the thermal diffusivity and obtain reasonable calculations for temperature profiles in pavements.
- To calculate binder hardening rates in pavements, the kinetic oxidation and/or hardening values for the actual binder in question are required. While these values are tedious to measure, they do vary from material to material in both their initial jump and constant rate period hardening rate parameters and in their oxidation activation energies. These values need to be measured in order to have an accurate calculation of binder hardening rates in pavements.
- For pavements where the original binders are not available, and for which one would like to calculate the pavement hardening rates over time, it is possible, in

principal, to extract and recover the binder, age the binder at different temperatures over a period of months, and measure the hardening rate kinetic data and activation energies that are required.These data would provide the constant rate period kinetic data but would not provide the initial jump data.

- The calculations applied to the Texas and MnRoad sites provide significantly different hardening rates in the two pavements, and these different rates are quite consistent with the measured rates calculated from the recovered binders.
- Interestingly, at both sites, the model that assumes free oxygen access to the binder performs quite well at reproducing the actual pavement hardening rates. This conclusion appears to be valid at least as long as the accessible air voids in the pavement local to the binder are of the order of several percent. When these air voids are below 2 percent, the hardening rates are significantly reduced.
- Based on these data, it is recommended that a complete revision of the binder oxidation and hardening model in the mechanistic empirical pavement design guide (MEPDG) and elsewhere in design calculations be implemented.

Oxidative Aging in Texas Pavements

During the course of this project, 16 pavements in 11 TxDOT districts were evaluated. Most of these pavements used different binders that were both modified and unmodified. Furthermore for almost all of the pavements, cores were obtained twice during the project with 12-18 months between the two cores. For each pavement, the binders were extracted and recovered and measurements made on the recovered binders. These data included DSR rheological parameters, size-exclusion chromatograms, and infrared measurements of carbonyl area. In many cases, samples of the recovered binders were aged in a 60 °C environmental room to obtain DSR function hardening susceptibility characteristics of the binders and to obtain 60 °C hardening rate information at one atmosphere of air pressure. The detailed results are reported in the various appendices of this chapter with the DSR function values of the recovered binders

and subsequently aged recovered binders are reported in Appendix C. The data are extensive and represent a tremendous amount of work, almost certainly the most work reported in a single document on binders recovered from aged pavements. These data, together with comparable data for the MnRoad pavements, provide a database of very interesting results. The age of the pavement cores ranges from two to over 20 years.

Hardening of the various binders in the pavements in the form of the DSR function is summarized in Figure IV-30. This figure shows the DSR function values for the recovered binders for all of the cores that were studied in this project versus the corresponding service age for the cores. Both Texas pavements and the MnRoad pavements are summarized, and the Texas Highway 21 pavement between Bryan and Caldwell are included for reference. Both unmodified and modified binders appear in the data set and in the figure. The bulk of the binders reported are modified.

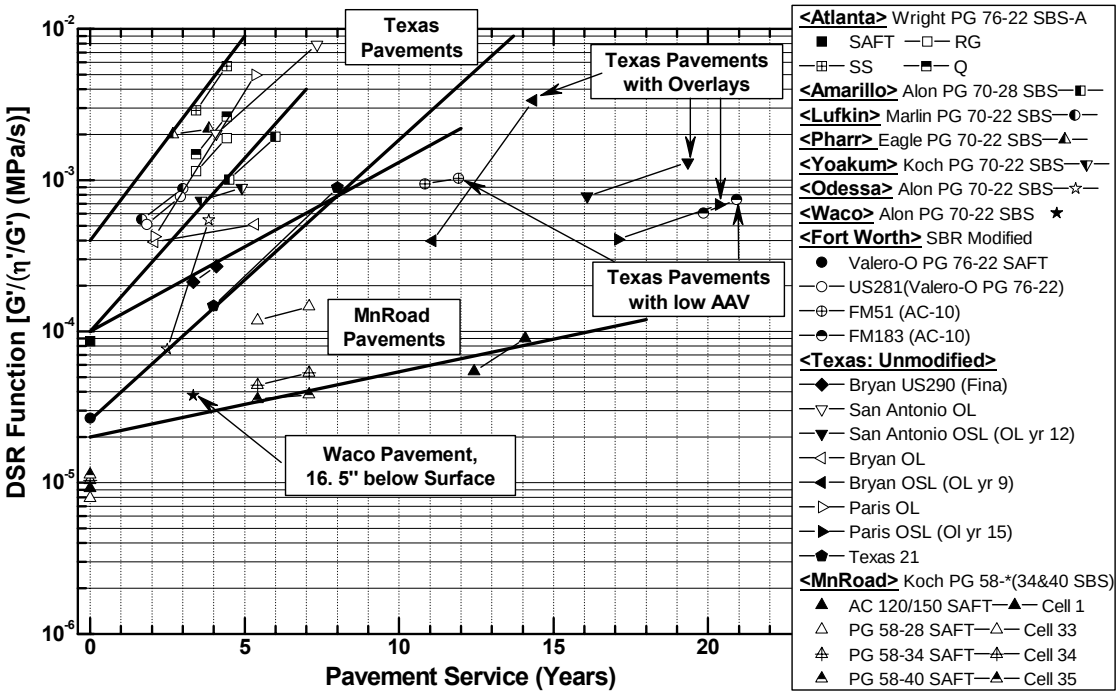

Figure IV-30. DSR Function Hardening with Pavement Service Time in Texas and MnRoad Pavements, Unmodified and Modified Binders

At first glance there appears to be a great deal of scatter and disorganization of the data. However, when considered in detail and evaluated from the perspective of the temperature aging model from the previous section, the results are, in fact, quite consistent. Most of the Texas pavements fall in the top left corner of the graph. At zero pavement service years a binder starts at an aging level that is probably beyond the RTFOT equivalent level by a factor of three or four which puts it at about the level of a 4-hour PP2 (now R30) aging protocol (Walubita et al., 2006). From there, binders age in the pavement, increasing over time. According to the aging model of the previous section the aging rate of a binder in the pavement eventually reaches an essentially constant rate (averaged over the year) and therefore in principle can increase indefinitely throughout the pavement life. Most of the Texas pavements fall between the two straight lines in the top left corner, and none of the pavements are aged beyond a DSR function value of 0.01 MPa/s. There are exceptions, however, and a number of Texas pavements are shown on the graph that lie outside this band. These exceptions will be discussed shortly.

A second pair of lines encompasses the Mnroad pavements. These lines fall below and to the right of the lines for the Texas pavements because of the lower hardening rate in the colder climates of Minnesota. The Cell 1 pavements (an unmodified binder) define the lower band, and the Cell 33 pavement (which is also an unmodified binder) defines the upper line. The two modified cells lie much closer to the unmodified Cell 1 line but inside the area between the two Minnesota lines.

There are six Texas pavements that fall outside the boundary lines for the other Texas pavements. One of these outliers is the Waco pavement that falls inside the MnRoad pavement lines at about three years. This binder appears to fall outside the Texas band for two reasons. First, it is a modified binder that appears to have an exceptionally good interaction between the polymer and base asphalt, thereby producing a very low initial DSR function, for this binder at the beginning of the pavement service life. Secondly, this binder is in a 3 inch layer of an interstate highway that after placement was immediately covered by about 18 inches of additional pavement.

Therefore, its aging rate, according to the temperature aging model of the previous section, is about 60-70 percent less than a comparable binder would be near the pavement surface. Keep in mind that the binder still ages at this depth (according to the model) but the rate is reduced below that of the surface. This reduced rate by itself is probably not enough to put the binder outside of the Texas boundaries. However, that reduced rate, coupled with the very low initial DSR function for this binder, probably is enough to move it to an outlier position.

Of the other five Texas pavements with binders that are outliers, three of them had recent overlays from one to three years prior to the first coring. It may well be that this overlay, together with the seal coat that is typically placed between layers at the time of placement of an overlay, could have penetrated into the original layer thereby softening the binder (either in situ or at least once it is recovered and blended with the original binder). While definitive data have not yet been obtained to verify this hypothesis, it is true that the number of observations of pavements that appear to have been softened due to an overlay or a seal coat is great enough and the effect is consistent enough that the conclusion seems more and more likely to be correct. This phenomenon was reported first by Glover et al. (2005).

The other two outlier binders, however, have no overlay or seal coat and yet have aged at significantly lower rates than the other Texas pavements. In these two pavements we believe that the lower average hardening rate is reduced by factors that are not observed in the other pavements. Both of these two pavements are AC10 binders modified with an SBR polymer and were placed in the Fort Worth district. Both pavements also have an exceptionally low accessible air voids in the range of 1 to 2 percent. Furthermore the pavement on SH 183 has been in service for 10 years and has a binder with an exceptionally low 60 °C hardening rate. Thus we believe that that binder is aging at an exceptionally low rate because of the combined effect of a low hardening rate binder coupled with a very low accessible air voids that hinders oxygen transport to the binder. Based on these data we anticipate that these pavement service lives will be

much longer than the other pavements. And in fact the SH 183 service life at 20 years already significantly exceeds normal performance.

One other observation is in order for all of these pavements. Except for the Waco Interstate 35 pavement, cores were obtained twice during the project period. In each case it was observed that the second coring provides a binder that is noticeably more aged than does the first coring, even though the time between corings was relatively short from the perspective of binder hardening rates in pavements. Nevertheless in each case it was observed that the binder is continuing to harden in the pavement and at rates that are comparable to the rates that would be indicated by their position in the graph given that all of the binders start in the pavements somewhere between $2x10^{-5}$ and $2x10^{-4}$ MPa/s for the DSR function. This result appears to confirm the aging model, which says that binders continue to oxidize virtually indefinitely, as far as the pavement lifetime is concerned. Stated differently these results appear to refute the assumptions of Coons and Wright (1968) and the assumptions of the MEPDG which are that after about 10 years of service, binder oxidation ceases. These data contradict that conclusion even for service lives between 15 and 20 years.

Granted this is a fairly qualitative way of assessing these data, but given the errors that are inherent in measuring pavement properties and also the variabilities of climate and binder properties, the fact that these kinds of consistencies exist within both the Texas and MnRoad pavements and that the outliers can be explained rationally with the data is rather remarkable. Again the full details and numbers are reported in the Appendix C.

For most of these Texas pavements the original binders were not available, and therefore it is really not known where these binders began at zero years of service. On the other hand, it is known from the data that the unmodified binders, as well as most of the modified binders, are in the neighborhood of 10^{-4} MPa/s for the DSR function and whether it is $2x10^{-4}$ or $3x10^{-4}$ or even something less such as $5x10^{-5}$ MPa/s, the exact value does not impact the above conclusions in a very significant way.

Figures IV-31 and IV-32 show the layer-by-layer accessible air voids of the 16 Texas pavements sites that were studied. Figure IV-31 shows the accessible air voids for all the polymer modified asphalt sites, and Figure IV-32 shows the accessible air voids for the unmodified asphalt sites and for both cores that were obtained during the study. The latter figure thus also shows the reproducibility from one year to the next with respect to accessible air voids measurements.

In Figure IV-31, it is noted that the Amarillo, Atlanta, Fort Worth, US-281, Lufkin, Pharr, and Yoakum sites all had accessible air voids that were fairly high, that is 4 percent or greater, and actually the Waco site had accessible air voids nearly that high, between 3 and 4 percent. However, the Fort Worth FM 51 and SH 183 sites, plus the Odessa site, all had accessible air voids below the first layer of the pavement that were 2 percent or less. These were exceptionally low air voids. And the Odessa even showed less than 1 percent. Air voids this low are believed sufficient to significantly retard the oxidation rate of the binder.

Figure IV-32 shows the accessible air voids for the unmodified sites, and in most cases they are 4 percent or greater, although at the Bryan LTPP site the original surface layer had the top surfaces quite low in air voids, 1 to 2 percent. Also the San Antonio original surface layer (OSL) that was cored in 2002 had one of the layers between 1 and 2 percent. So while most of these sites appear to have sufficient accessible air voids to allow unhindered oxidation of the binder, a couple of them may have somewhat retarded aging rates in some of the layers.

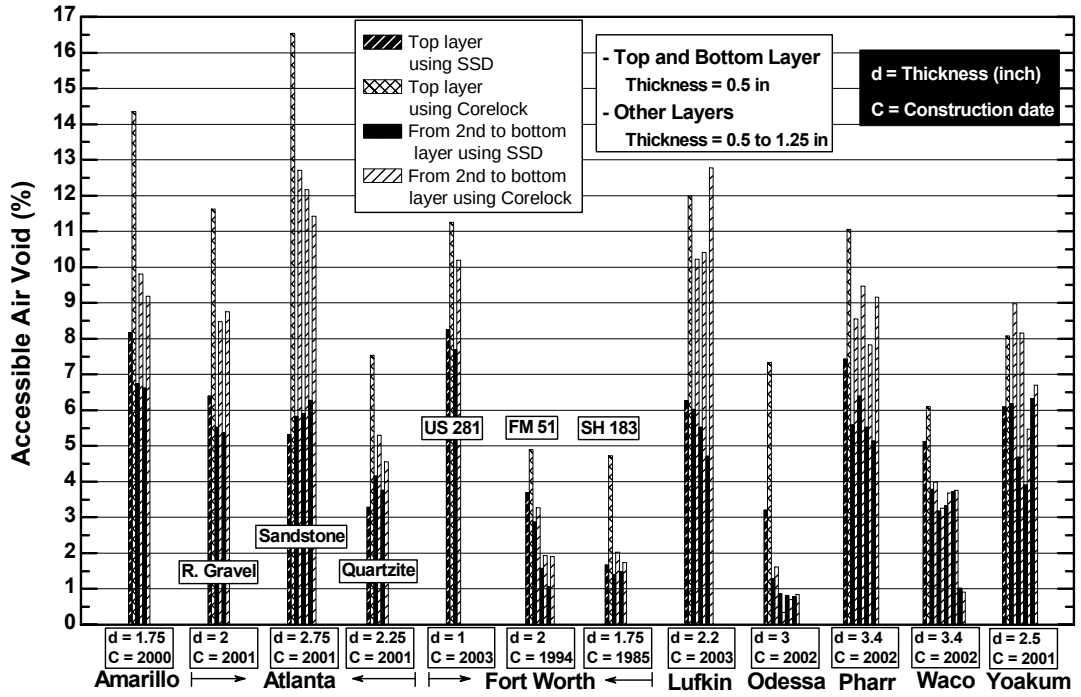

Figure IV-31. TxDOT (Polymer Modified Asphalt) Accessible Air Voids

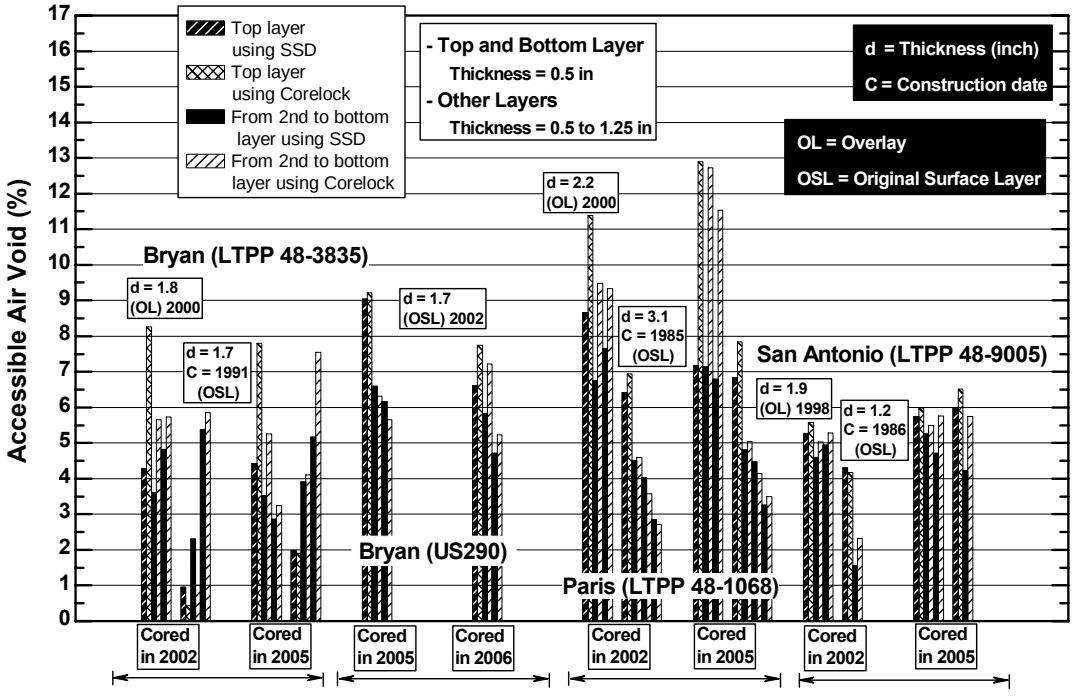

Figure IV-32. TxDOT (Unmodified Asphalt) Accessible (Interconnected) Air Voids

Figure IV-33 shows the DSR map locations for the various polymer modified binders, layer by layer. Looking at the Waco and Odessa layers and remembering that the Odessa accessible air voids was mostly less than 1 percent and the Waco accessible air voids in the bottom layer was less than 1 percent and the others in the 3 to 4 percent range, it is seen that locations of these binders on the DSR function map are consistent with these low air voids. Of course the Waco layer also had 16.5 inches of various kinds of asphalt pavement on top of it from the very beginning of its service and the fact that this Waco lift was so deep in the pavement probably put its aging rate at about 60-70 percent of a normal surface aging rate. On the DSR function map it is noted that all of the Waco layers are closely clustered at a very low level of aging, and this low level of aging was noted previously in Figure IV-30. The Odessa layers also cluster together quite closely at a low level of aging except for the layer which is at the very surface. The binder in that layer shows a calculated ductility of close to 7 cm, well away from the other layers of that core. Referring back to Figure IV-31, it is seen that the top layer has an accessible air void that is significantly higher than that of the others, 3 percent by the SSD method and 7.5 percent by the core lock method. The other layers in that core are 1 to 1.5 percent accessible air voids, which are very low values of air voids. Of course both Waco and the Odessa pavements were constructed in 2002 and therefore they only have two to three years of service before the first coring. At this fairly young age it is not necessarily expected for them to have a great deal of aging, anyway, although by comparison with some of the other pavements aging levels really are quite low.

The FM 51 pavement was constructed in 1994, and the SH 183 pavement was constructed in 1985. Both of these sites had very significant pavement service times when they were cored.

Looking at the SH 183 data points on the DSR function map in Figure IV-33, we see that the very top layer is located near the calculated ductility line of 5 cm and the second layer 8 cm and the third layer 10 cm. The second and third layers are fairly close together and not so heavily aged for a pavement that is 20 years old. The top layer, however, is considerably more aged although admittedly not so aged for a binder that is

20 years old. Again all of these layers in this SH 183 Fort Worth section have accessible air voids between 1 and 2 percent as measured by the SSD method.

Looking at the FM 51 data there are four data points on the map. The most heavily aged point, representing the surface, has a calculated ductility of 3 cm; and the second, third, and fourth points are close to the 6, 8, and (greater than) 10 cm lines. None of these points is very heavily aged considering the pavement itself was 10 years old at the time of coring. However, the differences between the top layer and the bottom layer are quite significant. The top layer, which has accessible air voids of around 4 percent, is quite heavily aged and likely near the end of its service life. The bottom two layers had accessible air voids between one and 2 percent and they are the least heavily aged and probably still have a good number of years left in their service life, based upon their measured rheology.

The other pavements in this figure were all constructed in the year 2000 or later, yet they all are at least as aged as the FM 51 binder. The recovered Pharr binder ranges from a calculated ductility of about 3 to 4.5 cm. The recovered Atlanta binders, considering all three types of aggregate, range from a calculated ductility of about 2.5 up to about 5.5 cm. The Amarillo binder from the pavement constructed in 2000 ranges from about 2.5 to 6 cm calculated ductility, and the Lufkin binder placed in 2003 ranges from about 5 to 7 cm calculated ductility. Again for binders that have only been exposed to a few years of service, these are all fairly heavily aged. Of course they are near the top of the pavement layers, the top 1 to 2 inches, but nevertheless, compared to the Odessa pavement for example, they are much closer to the end of their service life.

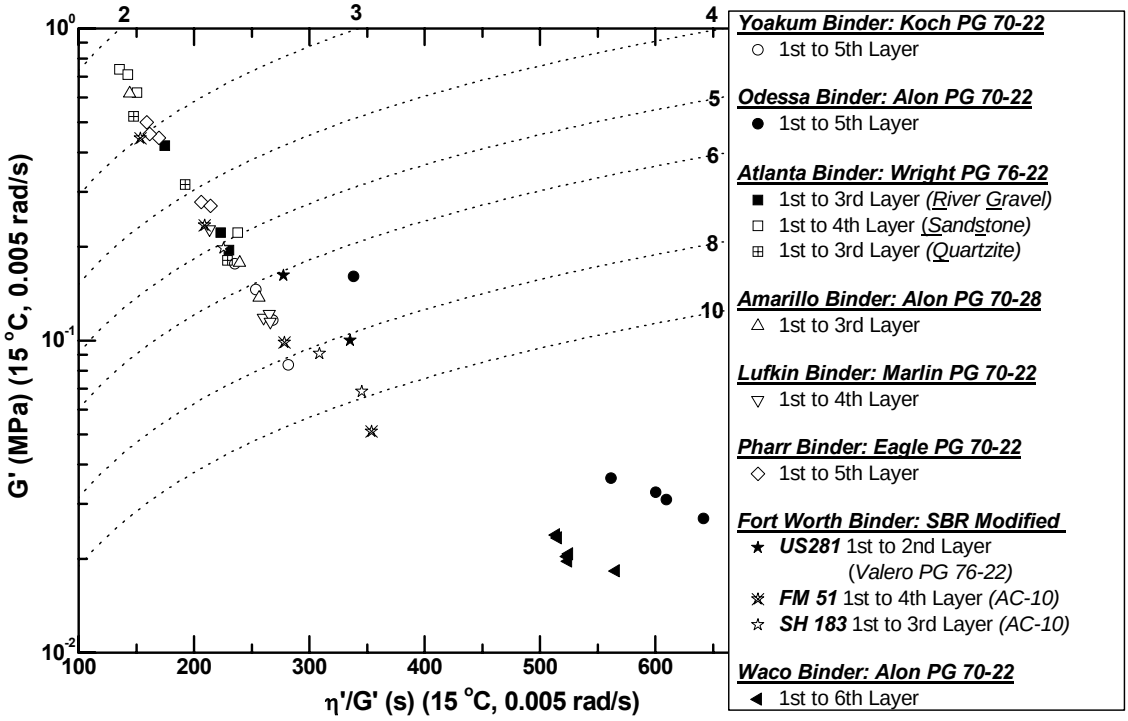

Figure IV-33. TxDOT (Polymer Modified Asphalt) Aging Comparison of the Surface to Bottom Layers

In an effort to further quantify the relationship between accessible air voids and binder aging, Figure IV-34 shows data for four pavements, where low accessible air voids appear to affect binder aging rates. While these specific data are from the MnRoad sites (used because of the 6 inch core thicknesses), the results appear to reflect aging in Texas pavements also, consistent with the discussion of Figures IV-31 through IV-33. In Figure IV-34, the binder DSR function is shown layer-by-layer versus the accessible air voids of that layer. Generally it is observed that the lower the accessible air voids, the lower the level of binder hardening, as represented by the DSR function. Each of these comparisons is for a specific pavement so that the aging time and condition in the layer-by-layer comparison are approximately the same with the exception of the accessible air voids. Of course it still holds that the deeper layers have a lower effective temperature and therefore a lower aging rate. As noted above, this temperature effect is not a major

effect, but can be significant to the point of accounting for a reduction in aging rate of about 30 percent. The general trend that is observed shows the lower accessible air voids, below about 3 percent, the lower the aging rate, whereas for accessible air voids at 4 percent or greater there appears to be a much reduced effect of accessible air voids on binder hardening.

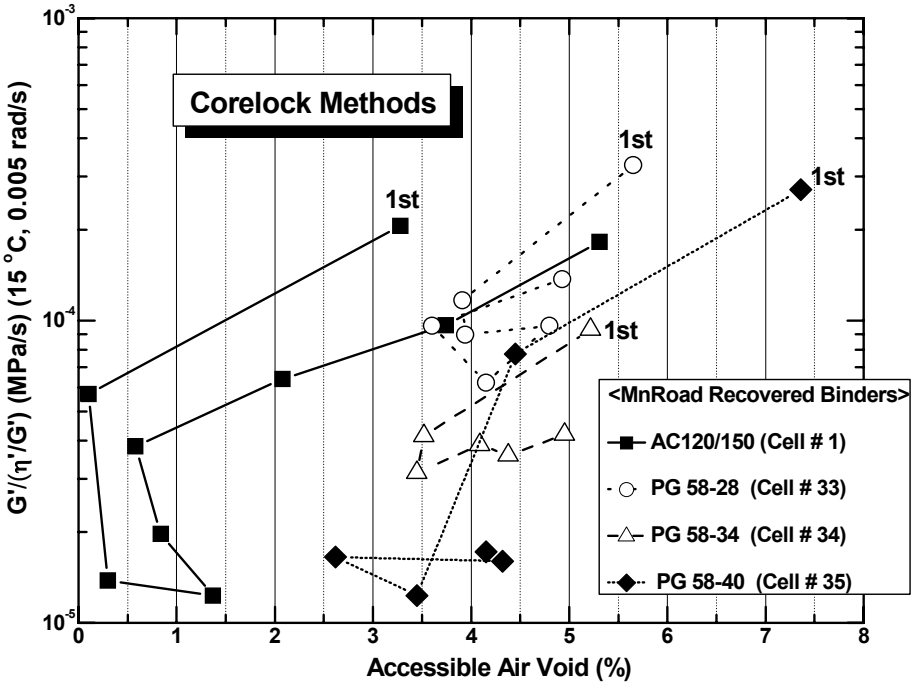

Figure IV-34. Binder Hardening Related to Local Pavement Accessible Air Voids

The oxidative aging model developed in this chapter can be used to provide additional insight to binder hardening in pavements. Table IV-3 uses the model, together with temperature calculations for Refugio, Texas, and DSR function hardening kinetic parameters (Glover et al., 2005) to estimate average binder hardening rates for a number of specific binders at the pavement surface. The kinetic data were for seven SHRP binders plus the binder used in the SH 21 pavement between Bryan and Caldwell and a high-cure tire rubber modified binder. The range of these rates is from 0.23 to 0.50 ln(MPa/s)/yr (equivalent to yr^{-1}). These binders are all unmodified binders with the

exception of the high cure tire rubber material. The value of 0.5 converts to an order of magnitude increase in the DSR function in the pavement over 4.6 years (two orders of magnitude over 9.2 years); the value of 0.23 would be an order of magnitude increase in the DSR function over 10 years (two orders of magnitude over 20 years). This range of hardening rates, which assume no diffusion resistance of oxygen (compared to the oxidation rate), agrees quite well (to the extent we can judge rates from the recovered binder data) with the binders recovered from pavement cores (Figure IV-30). These calculated rates are constant-rate period rates, after the initial jump reaction period has passed.

Table IV-3. Calculated Binder Pavement Hardening Rates for Refugio Temperatures

Binder	DSR Function Kinetic Parameters[a]			Calculated DSR Fn Pavement Hardening Rate (ln (MPa/s)/yr)
	E (kJ/mol)	ln A	α	
AAA-1	77.8	25.1	0.62	0.50
AAB-1	81.6	26.2	0.50	0.32
AAD-1	80.3	25.8	0.57	0.43
AAF-1	83.7	26.6	0.37	0.35
ABM-1	75.9	23.9	0.40	0.46
AAM-1	80.8	25.7	0.48	0.36
AAS-1	83.9	26.6	0.50	0.26
Lau4	84.6	27.0	0.44	0.32
TS2K	87.3	27.7	0.45	0.23

[a]Glover et al., 2005, Table 7-4.

As a second comparison, Table IV-4 shows the same calculations as Table IV-3 but for the MnRoad temperature history, and compares these hardening rates to those in Texas. From these calculations, we see that hardening rates in Texas (Refugio) are about twice those in Minnesota (MnRoad). Thus, an order of magnitude increase in the DSR function takes about twice as long in Minnesota as in Texas, according to this model and these data.

Table IV-4. Comparison of Calculated Binder Pavement Hardening Rates: Refugio, TX, versus MnRoad

Binder	Calculated DSR Fn Refugio Pavement Hardening Rate (ln(MPa/s)/yr)	Calculated DSR Fn MnRoad Pavement Hardening Rate (ln(MPa/s)/yr)	Ratio of Rates (Refugio/MnRoad)
AAA-1	0.50	0.24	2.1
AAB-1	0.32	0.20	1.6
AAD-1	0.43	0.20	2.2
AAF-1	0.35	0.16	2.2
ABM-1	0.46	0.22	2.1
AAM-1	0.36	0.17	2.1
AAS-1	0.26	0.12	2.2
Lau4	0.32	0.16	2.2
TS2K	0.23	0.10	2.2
Average			2.1

As a final comparison, for these same binders, the pavement hardening rate is compared to the constant temperature 60 °C rate in Table IV-5. The issue is whether the environmental room hardening rate might be a reasonable (in terms of accuracy, although very time consuming) surrogate for the binder hardening rate in pavements. The results show that the ER hardening rate is from 13 to 19 times higher than the pavement hardening rate (at the pavement surface). Interestingly, the ratio of 16 for the Lau4 asphalt corresponds very well to the number first reported by Glover et al. (2005), which was 15 and determined only from binder recovered from pavement cores over a number of years.

Besides the values of the HR ratios, the ranking of the rates is of interest. Because pavement aging occurs over a range of temperatures whereas the ER aging occurs at a single temperature, the nonlinear effect of temperature on reaction rates through the Arrhenius equation, in principle, can result in reversals of order in the rankings. In fact, some reversals are seen in these calculations. Specifically, AAB-1 is ranked with the second highest rate at 60 °C but is tied for sixth by the pavement calculation. Also, ABM-1 is fourth at 60 °C but second in the pavement. So, the

conclusion is that the only correct method for estimating (average) reaction rates in pavements is to measure binder rates at several temperatures and from these measurements calculate activation energies and then estimate pavement rates using a pavement oxidation model.

Table IV-5. Comparison of 60 °C Hardening Rates to Estimated Pavement Rates Using Refugio Temperatures

Binder	Calculated DSR Fn Pavement Hardening Rate	DSR Fn 60 °C Hardening Rate[a]	Ratio of HRs
	(ln (MPa/s)/yr)	(ln (MPa/s)/yr)	(60°C HR/Pavement HR)
AAA-1	0.504	6.78	14
AAB-1	0.324	6.26	19
AAD-1	0.432	6.00	14
AAF-1	0.348	5.40	16
ABM-1	0.456	5.78	13
AAM-1	0.360	5.24	15
AAS-1	0.264	4.08	16
Lau4	0.324	5.20	16
TS2K	0.228	3.89	17

[a]Based on the kinetic parameters in Table 5-3.

Summary of Binder Aging in Texas Pavements

Based upon the above data and discussion as well as the additional data in the appendices we arrive at a number of conclusions concerning modified and unmodified binder aging in pavements in Texas;

- Texas pavements, constructed from both modified and unmodified binders, age and harden at comparable rates given sufficiently high accessible air voids. The rate is largely determined by the temperature as a function of time and position (depth) in the pavement, provided the accessible air voids are sufficiently high (4 percent or greater). This temperature function is established solely by the climate conditions.

- This significant impact of temperature notwithstanding, there is significant evidence that when the accessible air voids in pavements are sufficiently low (2 percent or less) the hardening rate of binders in Texas pavements can be significantly reduced, thereby prolonging the service life of the pavements to 15 or 20 years or more.
- Some of the Texas pavements appear to be under aged relative to the other binders, perhaps due to the application of a chip seal and/or overlay one to three years before coring the pavement. This phenomenon has been observed before, and these data may be an indication again that the right kind of treatment during a pavement's service might well serve to soften the binder and rehabilitate it, thus providing an extended pavement life.
- The Texas pavements that were constructed from modified binders for the most part, (with the exception of the SBR modifier) appear to begin their service as stiffer binders than their corresponding unmodified binder. This observation is almost certainly the result of a desire to provide, through polymer modification, binders that have a greater resistance to rutting at higher pavement temperatures. But a side effect seems to be that by starting as stiffer binders (i.e., at a higher level of the DSR function) the binders may be hardening sooner to a level that renders them unserviceable. Perhaps the objective with a polymer-modified binder is to achieve a binder that is softer initially (or at least as soft as the unmodified binders) in the context of the DSR function and still provides the desired rut resistance. If a binder can begin service at a lower stiffness, then it may reach failure later. An example of a modified binder that began service at a low stiffness level is the Alon PG 70-22 SBS modified binder that was used in the Waco pavement and also the Odessa pavement. Note that the Amarillo PG 70-28 appears to not have such an advantage.
- If a binder with an inherently low hardening rate (slow oxidation kinetics and minimal physical response to the oxidation) is used in a pavement, and perhaps more practically, if a low enough level of accessible air voids can be achieved (in

the range of two percent or less), then the pavement has a real chance of providing service over a very extended period of time.

- Binder DSR function hardening rates in Texas are about twice the rate for the corresponding binder in Minnesota, and at comparable air void conditions.
- In order to estimate pavement binder hardening rates, values of the binder reaction kinetics parameters are required. Approximating the rate with measurements at 60 °C may give a rate from which a rough estimate can be calculated, but the nonlinear activation energy effect can cause significant error.
- Calculations from the pavement oxidation model and known binder reaction kinetics parameters indicate that 60 °C hardening rates range from 13 to 19 times the calculated pavement binder aging rates at Refugio temperatures.

CHAPTER V
A PROTOCOL FOR ASSESSING POLYMER MODIFIED ASPHALT DURABILITY IN PAVEMENT

Binders in pavements oxidize over time and, as a result, become brittle and more susceptible to thermal and fatigue cracking failure. While it is desirable to determine a critical binder condition at which failure will occur, such a condition, as a matter of fundamentals, cannot exist. Fatigue cracking, for example, is a function not just of binder properties, but also of traffic loading (frequency and amount of load), pavement system stiffness, and mixture design (probably including variables such as binder content, aggregate gradation, and air voids).

Nevertheless, binder properties play a critical role; after all, it is the binder that ultimately cracks in a pavement under normal usage and the passage of time, and binders in old pavements suffer fatigue cracking while binders in new pavements do not.

Within the context of these observations, this protocol is based on the properties of neat and pavement-aged binders; an improved understanding of the fundamentals that govern binder aging rates in pavements and its impact on fatigue cracking; and methods for predicting pavement life from the perspective of binder fatigue cracking.

This protocol consists of two steps: 1) determine measures of modified binder properties and performance, and 2) estimate pavement fatigue life based upon these and other measures. The first step may be used in a method of classifying the various binders as to expected durability in pavements while the second step provides a rationale for estimating that durability in terms of pavement life. The second step is based on the measured binder properties.

It is recognized that this second step requires non-conventional information on pavement mixtures that is not currently available and not easily obtained, and thus, likely cannot yet be implemented; a far better fundamental understanding of the impact of binder oxidative aging on fatigue life decline, and as it relates to mixture parameters, is required. However, it is anticipated that by putting forth this protocol, pavement design

engineers and researchers will begin the effort to obtain this required understanding and of working toward design and maintenance planning that will incorporate binder aging in a more fundamental and correct approach than is now used. This protocol of course is preliminary and will require revision and correction as more and better data are obtained and a better fundamental understanding is achieved.

Determine Measures of Modified Binder Performance

These binder conditioning steps and measurements are designed to estimate the impact of (change due to) polymer modifier on three base binder properties: 1) hardening rate (in terms of the DSR function) in 1 mm films at 90 °C and 20 atm air; 2) level of binder stiffness (in terms of the DSR function), and 3) elongation at break (either in terms of direct tension or ductility). A fourth measure addresses the absolute level of the modified binder stiffness (in terms of the DSR function): 4) DSR function stiffness relative to an arbitrary value of 0.0001 MPa/s.

The rationale for these measures is as follows.

1. It is desirable that polymer modification slow a binder's rate of stiffening due to oxidation relative to that of the base binder. While it is desired that such a measurement be made at conditions close to actual pavement oxidation (60 °C, 1 atm air, say), the length of time required for such measurements is prohibitive. Therefore the 90 °C measurement at 20 atm air pressure is used. Aging in a 1 mm film (instead of the conventional PAV 3 mm film) is used to reduce oxygen diffusion resistance to the binder and therefore to accelerate the oxidation rate, relative to standard PAV conditions. Aging for 16 hours at the PAV* conditions brings binders to being close to (or beyond) the initial jump region of oxidation kinetics. (The most desired oxidation reaction kinetics data would be measurements of oxidative reaction and hardening rates over a range of temperatures so as to provide reaction activation energies that can then be used to calculate accurate pavement oxidation rates. However, such measurements are

very time consuming. Even so, there is no substitute for correct data, and such measurements should be considered.)

2. It is desired that polymer modification should not unduly stiffen the binder to elongational flow, relative to the base binder. Excessive stiffening is believed to act counter to a prolonged pavement fatigue service life.
3. It is desired that polymer modification serve to improve a binder's elongational flow characteristics. A direct tension or ductility measurement is a direct indication of this property.
4. While measure 2 (above) is a measure of a binder's ability to undergo elongational flow, relative to that of the base binder, an absolute measure also is desired, and that is provided by this fourth measurement.

The binder conditioning and measurement procedures, and calculations of the screening parameters, are outlined below.

Age Both the Base and Modified Binders

- Age unmodified and modified base binders to (RTFOT or SAFT plus) PAV* 16 hr and PAV* 32 hr aging levels. The 16 hr level of aging corresponds quite well to PP2 4-hr aging and, according to measured pavement binders, approximates the initial state of a binder early in the pavement life. PAV* aging uses the standard Superpave PAV apparatus, but the binder is aged in 1 mm thick films, one-third the standard PAV thickness, and the temperature is fixed at 90 °C. The pressure is 20 atm air, standard for the PAV apparatus.

Measure Aged Binder Properties

- Measure the DSR function (DSRfn) after PAV* 16 hr aging for both the modified and base binder.
- Measure the DSRfn after PAV* 32 hr aging for both the modified and base binder.
- Measure the direct tension (DT) failure strain at -12 °C after PAV* 16 hr aging for both the modified and base binder, (or measure the ductility at 15 °C, 1 cm/min)

The DSRfn is defined as G'/(η'/G') = ωG'/tan δ, where the DSR properties are measured at 44.7 °C, 10 rad/s but converted to 15 °C , 0.005 rad/s by a time-temperature superposition (TTSP) frequency conversion ratio of 2000:

$$\text{DSRfn} \equiv \left[\frac{G'}{(\eta'/G')}\right]_{15\ ^\circ\text{C},\ 0.005\ \text{rad/s}} \approx \frac{1}{2000}\left[\frac{G'}{(\eta'/G')}\right]_{44.7\ ^\circ\text{C},\ 10\ \text{rad/s}} \qquad \text{(V-1)}$$

The TTSP calculation is approximate, based on the observation that binders all have approximately (but not exactly) the same TTSP shift factors, but the convenience of the measurement, using standard DSR equipment, warrants the approximation.

Calculate Screening Measures of Binder Performance

- Calculate PAV* 16 hr to PAV* 32 hr hardening in the DSRfn for the modified binder:

$$\begin{aligned}\text{PMA Binder}: \text{Hardening} &= \ln(\text{DSRfn}_{32\ \text{hr}}) - \ln(\text{DSRfn}_{16\ \text{hr}}) \\ &= \ln(\text{DSRfn}_{32\ \text{hr}}/\ \text{DSRfn}_{16\ \text{hr}})\end{aligned} \qquad \text{(V-2)}$$

- Calculate PAV* 16 hr to PAV* 32 hr hardening in DSRfn for the base binder:

$$\text{Base Binder : Hardening} = \ln(\text{DSRfn}_{32\text{ hr}}) - \ln(\text{DSRfn}_{16\text{ hr}}) = \ln(\text{DSRfn}_{32\text{ hr}} / \text{DSRfn}_{16\text{ hr}}) \quad \text{(V-3)}$$

- Estimate a measured ductility from Ductility-DT correlation:

$$\text{Ductility} = 4.2(\text{DT})^{2.60} \quad \text{(V-4)}$$

where the ductility is at 15 °C, 1 cm/min, and DT is measured at -12 °C, 1 mm/min. If the measured value of ductility is obtained, use this value.

- Calculate ductility based on the Ductility-DSRfn correlation:

$$\text{Calculated Ductility} = 0.23(\text{DSRfn})^{-0.44} \quad \text{(V-5)}$$

where the Calculated Ductility is at 15 °C, 1 cm/min, and the DSRfn is measured at 44.7 °C, 10 rad/s.

Based upon the above measurements, calculate the four screening measures of modified binders:

1) Calculate ratio of modified binder to the base binder hardening for PAV* aging.

Desired ratio < 1

2) Calculate the ratio: DSRfn_{mod}/ DSRfn_{base} after PAV* 16 hr aging.

Desired ratio <1

3) Calculate (ductility)/(calculated ductility) ratio at PAV* 16 hr conditions for both the base and modified binders.

Desired modified binder ratio >1;

Desired unmodified binder ratio ~ 1 (or greater).

(Too low a value for the unmodified binder shows poor elongational properties of the base binder, to which the modified binder will revert after sufficient oxidative aging.)

4) Calculate (DSRfn after PAV* 16 hr)/10^{-4}.

Desired ratio = 1 or less

Seven PG 70-22 SBS modified binders are summarized in Figure V-1. We note that modification generally results in a hardening rate that is less than that of the base binder, together with an improved ductility (thereby meeting those two goals), but that stiffness improvement (relative to the base binder) and initial stiffness (the absolute measure) generally fall short of the goal. Not shown in this figure are the base binder (ductility/calculated ductility) ratios (measure 3). This ratio varies from 0.8 to 2 for all of these base binders except one, for which the ratio is approximately 0.4.

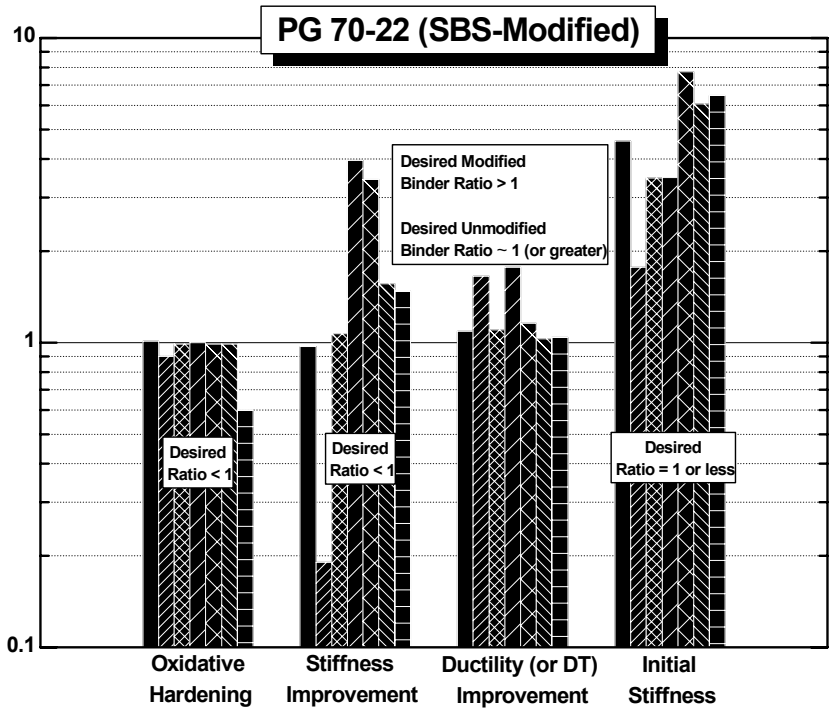

Figure V-1. The Four Screening Measures for Seven PG 70-22 SBS Modified Binders

Estimate Pavement Life

This method is a very approximate method, based only upon (presumed or measured) binder hardening rates in pavements and assumed pavement properties. The methods have not been validated by comparisons to actual pavement performance and thus, they can only serve as a strawman to be tested and improved upon.

Estimate Pavement Fatigue Life without Mixture Properties

This very approximate method should only be used to make rough estimates in the absence of data or other specific information about a given pavement mixture design and structure. The calculations are based upon the elongational flow hardening of binders due to oxidation and as indicated by the DSR function, follow these steps:

- Assume (or estimate) a pavement DSRfn hardening rate (average, high, low) based on the existing database on pavement hardening rates and estimated accessible air voids and climate. Measurements of binder hardening in Texas pavements have provided the following values (units are delta [ln(MPa/s)]/yr or equivalently, yr^{-1}):
  - For hardening rates in pavements that have good availability of oxygen (high air voids): high rate = 0.5/yr; medium rate = 0.3/yr; low rate = 0.2/yr.
  - For hardening rates in pavements that have both significant restriction of oxygen availability to the binder (accessible air voids ~ 2 percent or less) and a low inherent binder oxidation kinetics hardening rate: 0.1/yr. This would be an exceptionally low hardening rate in Texas.
  - For hardening rates in pavements that have low availability of oxygen (accessible air voids ~2 percent or less) and moderate binder hardening rate kinetics: 0.2/yr. This would normally be a quite low value of the

hardening rate in pavements and should not be used unless there is definitive evidence that such a rate is justified.

- The pavement service end value of the DSRfn is unknown. Therefore, using Equation V-6, calculate an approximate window of pavement life by using two values of the DSRfn at the pavement life's end, as a ratio to its initial value. Reasonable values for this ratio (based on data and calculations of this dissertation) are $DSRfn_{end,1}/DSRfn_o = 10$; $DSRfn_{end,2}/DSRfn_o = 1{,}000$. If the mixture is believed to have a very good response to binder hardening (fatigue life decline with binder oxidation is relatively low) and/or the traffic loading rate is low, then use a value of 1,000. However, if the mixture fatigue life is sensitive to binder oxidation and/or the loading rate is high, then a value of 10 is more appropriate. For $K_2 = 0.3$/yr, a ratio of 10 gives the pavement service life as 7.7 years while a ratio of 1,000 provides a service life of 23 years. (Note that it is the ratio of the DSR function that is important rather than the initial or final values alone, Equation V-6.)

$$t_{end} = \frac{1}{K_2} \ln \left[\frac{(DSRfn)_{end}}{(DSRfn)_o} \right] \qquad \text{(V-6)}$$

Based on the pavement aging model, kinetic data, and calculations, typical values of K_2 in Texas, for different binders, range from about 0.2 to 0.4 Δln (MPa/s)/yr (or, equivalently 0.2 to 0.4 yr^{-1} in terms of hardening ratios). The starting DSRfn is designated as $(DSRfn)_o$ and can be approximated by the PAV* 16 hr value of the DSRfn. The calculations are shown graphically in Figure V-2 for two initial DSRfn values and for several possible hardening rates. According to this fatigue calculation, the pavement service life is determined by the binder hardening rate in the pavement (K_2) and by how much hardening the binder can sustain (in terms of a DSRfn hardening ratio).

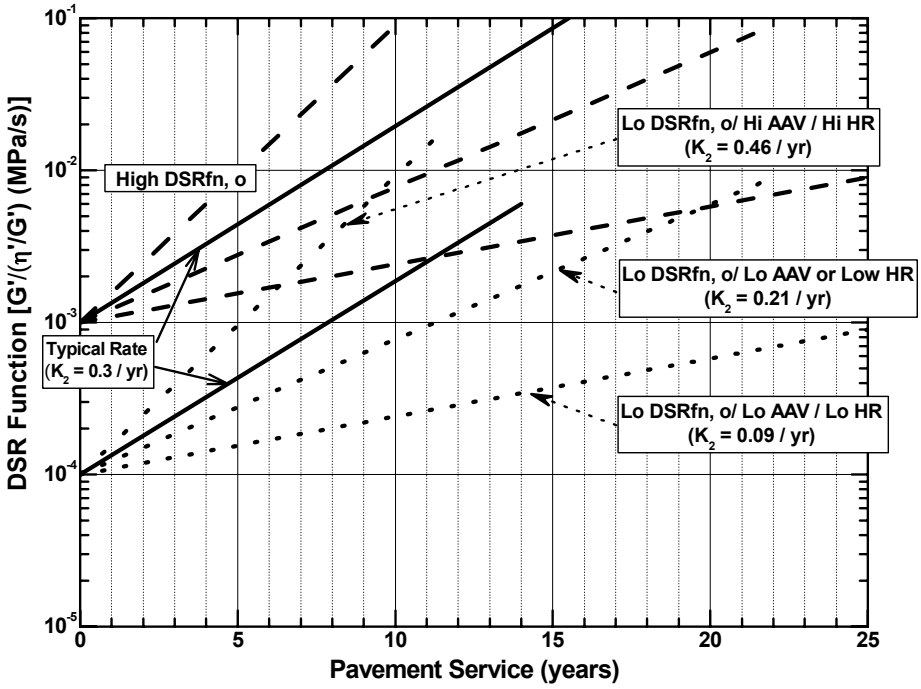

Figure V-2. Approximate Pavement Hardening Paths, Starting at Two Initial DSR Function Values and for Several Possible Hardening Rates (Values of K_2)

CHAPTER VI
CONCLUSIONS AND RECOMMENDATIONS

This research evaluated polymer modified asphalt durability through a number of determinations that included original binder property characterization, pavement-aged binder characterization (in both Texas and Minnesota), and both modified and unmodified binders. The data measurements were very extensive and tedious, but necessary to provide a comprehensive view of PMA durability in pavements.

The original binder measurements included rheological characterization (DSR, force-ductility, direct tension), composition characterization (Corbett analysis, size exclusion chromatography, FT-IR measurement of oxidation), and changes to these properties with oxidative aging (60 °C environmental room aging, pavement aging, accelerated aging in the PAV apparatus).

Pavement measurements included recovered binder properties (DSR, SEC, FT-IR) and their changes over time in the pavement and pavement total and accessible (interconnected air voids). Sixteen pavements in 11 Texas districts, plus four MnRoad (Minnesota) pavements (one unmodified, three unmodified binders) were evaluated. Many of the pavement cores were sawed into 0.5 in layers with the binder and air void properties determined for each layer. For some of the pavements, original binder was available and tested for its initial and aging properties. For the unmodified binder MnRoad site, binder was recovered from a pavement core and aged at three temperatures to obtain oxidative hardening kinetic data for use in developing a pavement oxidative hardening model.

Finally, from these laboratory and pavement performance data, important DSR and aging methods for predicting modifier effectiveness and durability were developed.

Conclusions

Changes to Binder Properties with Polymer Modification and Oxidative Aging

Corbett compositions of both modified and unmodified binders change with aging, as has been observed previously and reported in the literature.

There is a clear trend that polymer modification leads to an improvement in binder ductility, relative to the base binder, at low levels of oxidation. However, with increased oxidation, the ductility improvement dissipates.

Size exclusion chromatography of polymer-modified binders clearly shows a decrease in the size of the polymer peak maximum but an increase in polymeric material at smaller molecular weights due to oxidation.

The DSR function G'/(η'/G'), which relates to binder ductility for oxidatively aged unmodified binders, may either decrease or increase with polymer modification. Oxidative aging causes an increase in the DSR function so that modification, if it serves to start binder pavement service at a higher value of the DSR function, may work against its long-term durability.

Most of the modified binders show a DSR function hardening rate that is less than that for the modified binder, by as much as 40 percent. This result suggests that the polymer degradation that occurs due to oxidation may serve to moderate the hardening that occurs due to asphaltene formation and other composition changes that occur due to oxidation.

Mechanisms of PMA Loss of Ductility with Binder Oxidation

Oxidative aging of asphalt materials causes an embrittlement, and thus a loss of ductility, of both unmodified and modified binders.

SBS and SBR polymer modification typically results in ductility improvements to the base binder but oxidative aging degrades this improvement significantly over the

life of the pavement. Dynamic shear rheometer, ductility, and force-ductility measurements show that the primary cause of this degradation is base binder stiffening due to the oxidation. A secondary cause is polymer degradation (molecular size reduction), also from oxidation.

Softening a modified binder, either by raising the temperature or by blending with a softer asphaltic material, recovers the enhanced ductility performance of the modifier to a significant degree, but not fully. However, polymer degradation that may have occurred due to oxidation remains a factor contributing to reduced ductility performance.

A Model for Binder Oxidation Rates in Pavements

A simple 1-D, unsteady-state semi-infinite slab heat conduction model works surprisingly well for describing the temperature response of pavements to daily and annual thermal cycles.

This temperature response, coupled with binder reaction kinetics parameters and rheological data can be used to calculate the hardening of binders in pavements over time. The agreement to actual binder aging is surprisingly good.

The model and pavement core data suggest that normal air voids in pavements is sufficient to oxidize binders almost as though there is no diffusion resistance slowing the oxidation.

The model calculations show and the pavement data confirm binder oxidation can occur at very significant rates well below the surface of the pavement, contrary to a long and widely held belief to the contrary in the asphalt community.

Tight accessible air voids result in measurably and significantly slower rates of hardening of the binder. The slower rates can have a very significant beneficial impact on pavement durability.

Model calculations using known binder kinetic parameters for a variety of Texas binders show that even measuring hardening rates at 60 °C does not give accurate

relative comparisons of pavement hardening, due to the activation energy effect on hardening rates at different temperatures. Thus, the only method for comparing pavement hardening rates of different binders accurately is to determine the oxidation and hardening kinetic parameters at several temperatures and then to calculate pavement rates using a temperature history model.

A Protocol for Assessing PMA Durability in Pavements

Binder Durability Measures

Binder conditioning steps and measurements were developed to estimate the impact of polymer modifier on three base binder properties: 1) hardening rate (in terms of the DSR function) in 1 mm films at 90 °C and 20 atm air; 2) level of binder stiffness (in terms of the DSR function), and 3) elongation at break (either in terms of direct tension or ductility). A fourth measure addresses the absolute level of the modified binder stiffness (in terms of the DSR function): 4) DSR function stiffness relative to an arbitrary value of 0.0001 MPa/s.

Estimating Pavement Fatigue Life

This method is very approximate, based only upon (presumed or measured) binder hardening rates in pavements and assumed pavement properties. The method has not been validated by comparisons to actual pavement performance and thus, the protocol is a strawman, to be tested and improved upon.

Recommendations

Implement Methods for Maximizing Pavement Durability

The following methods for significantly improving pavement durability have been identified and should be implemented as soon as possible.

- Construct pavements with the lowest possible accessible (interconnected) air voids, consistent with other best construction and mix design practices. Target achieving less than 2 percent, the lower the better from an aging perspective. Decreasing the binder hardening rate in pavements by about 50 percent appears to be a reasonable goal.
- Use the pavement aging model for pavement design on a trial basis so that engineers become familiar with pavement aging rates in Texas.
- Use binders with a minimum DSR function at the PAV* 16 hr condition (consistent with the appropriate performance grade).
- Use polymer-modified asphalts that have a good base binder ductility-DSR function behavior at the PAV* 16 hr condition and for which modification improves the behavior.
- As a perpetual pavement strategy, use a porous friction course surface overlay of from 2 to 3 inches to reduce the oxidation rate of the top of the sub-layer by about 15 percent by reducing its maximum temperature. Remove and replace the PFC as needed. Further reductions in the oxidation rate by using a thicker overlay would be minimal and probably not cost-effective, based on the oxidation model calculations. The life-cycle cost-effectiveness of such an overlay should be determined.
- Assure that the base, subbase, and subgrade are firm and stable, to the extent feasible. The more rigid the pavement system (except when created by a stiffer binder), the better.

Other factors, not easily controlled or determined, also can lead to improved durability.

- Use binders that have inherently slow hardening rates in pavements. This objective requires detailed binder oxidation kinetic studies over at least a range of temperatures and ideally over a range of oxygen pressures as well.
- Use modifiers that provide the most reduction in the hardening rate. Detailed kinetic data on the modified binders are also required.

LITERATURE CITED

AASHTO, AASHTO 2002 Pavement Design Guide (NCHRP 1-37A Report), (2004). http://www.trb.org/mepdg/guide.htm, Accessed June 2007.

ASTM D 4124, Standard Test Methods for Separation of Asphalt into Four Fractions. 1994 Annual Book of ASTM Standards, 04.03, ASTM (1994).

ASTM D 6752, Standard Test Methods for Bulk Specific Gravity and Density of Compacted Bituminous Mixtures Using Automatic Vacuum Sealing Method. 2004 Annual Book of ASTM Standards, 04.03, ASTM (2004).

ASTM D 6857, Standard Test Methods for Maximum Specific Gravity and Density of Bituminous Paving Mixtures Using Automatic Vacuum Sealing Method. 2003 Annual Book of ASTM Standards, 04.03, ASTM (2003).

Bouldin, M.G., and J.H. Collins, "Influence of Binder Rheology on Rutting Resistance of Polymer Modified and Unmodified Hot Mix Asphalt," *Polymer Modified Asphalt Binders, ASTM STP 1108*, K.R. Wardlaw and S. Shuler, eds., American Society for Testing and Materials, Philadelphia, 50 (1992).

Burr, B.L., R.R. Davison, C.J. Glover, and J.A. Bullin, "Solvent Removal from Asphalt," *Trans. Res. Rec*., **1269**, 1 (1990).

Burr, B.L., R.R. Davison, C.J. Glover, and J.A. Bullin, "Softening of Asphalts in Dilute Solutions at Primary Distillation Conditions," *Trans. Res. Rec*., **1436**, 47 (1994).

Burr, B.L., R.R. Davison, H.B. Jemison, C.J. Glover, and J.A. Bullin, "Asphalt Hardening in Extraction Solvents," *Trans. Res. Rec*., **1323**, 70 (1991).

Burr, B.L., C.J. Glover, R.R. Davison, and J.A. Bullin, "New Apparatus and Procedure for the Extraction and Recovery of Asphalt Binder from Pavement Mixtures," *Trans. Res. Rec*., **1391**, 20 (1993).

Carslaw, H.S., and J.C. Jaeger, *Conduction of Heat in Solids*, 2nd edition, Oxford Science Publications, New York (1959).

Chaffin, J.M., R.R. Davison, C.J. Glover, and J.A. Bullin, "Viscosity Mixing Rules for Asphalt Recycling," *Trans. Res. Rec*., **1507** , 78 (1995).

Cipione, C.A., R.R. Davison, B.L. Burr, C.J. Glover, and J.A. Bullin, "Evaluation of Solvents for Extraction of Residual Asphalt from Aggregates," *Trans. Res. Rec*., **1323**, 47 (1991).

Clark, R.C., "Practical Results of Asphalt Hardening on Pavement Life," *J. AAPT*, **27**, 196 (1958).

Coons, R.F., and P.H. Wright, "An Investigation of the Hardening of Asphalt Recovered from Pavements of Various Ages," *J. AAPT*, **37**, 510 (1968).

Corbett, L.W., "Dumbbell Mix for Better Asphalt," *Hydrocarbon Processing*, **58**, 173 (1979).

Domke, C.H., R.R. Davison, and C.J. Glover, "Effect of Oxidation Pressure on Asphalt Hardening Susceptibility," *Trans. Res. Rec*., **1661**, 114 (1999).

Domke, C.H., R.R. Davison, and C.J. Glover, "Effect of Oxidation Pressure on Asphalt Oxidation Kinetics," *I&ECR*, **39**, 592 (2000).

Doyle, P.C., "Cracking Characteristics of Asphalt Cement," *Asphalt Paving Technology*, **27**, 581 (1958).

Glover, C.J., R.R. Davison, C.H. Domke, Y. Ruan, P. Juristyarini, D.B. Knorr, and S.H. Jung, "Development of New Method For Assessing Asphalt Binder Durability with Field Validation," Report FHWA/TX-03/0-1872-2, Texas Transportation Institute, College Station, TX (2005).

Goodrich, J.L., "Asphalt and Polymer Modified Asphalt Properties Related to the Performance of Asphalt Concrete Mixes," *Asphalt Paving Technology*, **57**, 116 (1988).

Halstead, W.J., "The Relation of Asphalt Ductility to Pavement Performance," *Asphalt Paving Technology*, **32**, 247 (1963).

Halstead, W.J., "Relation of Asphalt Chemistry to Physical Properties and Specifications," *Asphalt Paving Technology*, **54**, 91 (1985).

Jemison, H.B., B.L. Burr, R.R. Davison, J.A. Bullin, and C.J. Glover, "Application and Use of the ATR, FTIR Method to Asphalt Aging Studies," *Fuel Sci. & Tech. Int*., **10**, 795 (1992).

Kandahl, P.S., and M.E. Wenger, "Asphalt Properties in Relation to Pavement Performance," *Trans. Res. Rec*., **544**, 1 (1975).

Kandahl, P.S., "Low-Temperature Ductility in Relation to Pavement Performance," *Low-Temperature Properties of Bituminous Materials and Compacted Bituminous Paving Mixtures, ASTM STP 628,* C.R. Marek, Ed., American Society for Testing and Materials, Philadelphia, 95 (1977).

Lau, C.K., K.M. Lunsford, C.J. Glover, R.R. Davison, and J.A. Bullin, "Reaction Rates and Hardening Susceptibilities as Determined from POV Aging of Asphalts," *Trans. Res. Rec*., **1342,** 50 (1992).

Lee, D.Y., and R.J. Huang, "Weathering of Asphalts as Characterized by Infrared Multiple Internal Reflection Spectra," *Anal. Chem*., **46**, 2242 (1973).

Leicht, S.E., P. Juristyarini, R.R. Davison, and C.J. Glover, "An Investigation of Oxidative Curing on the Properties of High Cure Asphalt Rubber," *Pet. Sci. & Tech*., **19**(3-4), 317 (2001).

Lin, M. S., C. J. Glover, R. R. Davison, and J. A. Bullin, "The Effects of Asphaltenes on Asphalt Recycling and Aging," *Trans. Res. Rec*., **1507**, 86 (1995).

Lin, M. S, J. M. Chaffin, M. Liu, C. J. Glover, R. R. Davison, and J. A. Bullin, "The Effect of Asphalt Composition on the Formation of Asphaltenes and Their Contribution to Asphalt Viscosity," *Fuel Sci. & Tech. Int*., **14**, 139 (1996).

Liu, M., K.M. Lunsford, R.R. Davison, C.J. Glover, and J.A. Bullin, "The Kinetics of Carbonyl Formation in Asphalt," *AIChE J*., **42 (**1996).

Liu, M., J.M. Chaffin, R.R. Davison, C.J. Glover, and J.A. Bullin, "Reactivity of Asphalt Supercritical Fractions," *Ind. Eng. Chem. Res.*, **36** (6), 2177 (1997).

Liu, M., J.M. Chaffin, R.R. Davison, C.J. Glover, and J.A. Bullin, "Changes in Corbett Fraction Composition during Oxidation of Asphalt Fractions," *Trans. Res. Rec*., **1638**, 40 (1998a).

Liu, M., M.A. Ferry, R.R. Davison, C.J. Glover, and J.A. Bullin, "Oxygen Uptake as Correlated to Carbonyl Growth in Aged Asphalts and Asphalt Corbett Fractions," *I&ECR*, **37**, 4669 (1998b).

Lu X., and U. Isacsson, "Chemical and Rheological Evaluation of Aging Properties of SBS Polymer Modified Bitumens," *Fuel*, **77**, 961 (1997a).

Lu X., and U. Isacsson, "Rheological Characterization of Styrene-Butadiene-Styrene Copolymer Modified Asphalt," *Construction and Building Materials*, **11**(1), 1811 (1997b).

Lu X., and U. Isacsson, “Chemical and Rheological Characteristics of Styrene-Butadiene-Styrene Polymer-Modified Bitumens,” *Trans, Res. Rec.*, **1661**, 83 (1999).

Lu X., and U. Isacsson, “Artificial Aging of Polymer Modified Bitumens,” *Journal of Applied Polymer Science*, **76**, 1811 (2000).

Lu X., and U. Isacsson, “Modification of Road Bitumens with Thermoplastic Polymers,” *Polymer Testing*, **20**, 77 (2001).

Martin, K.L., R.R. Davison, C.J. Glover, and J.A. Bullin, "Asphalt Aging in Texas Roads and Test Sections," *Trans. Res. Rec.*, **1269**, 9 (1990).

MnDOT, 2002 Mn/Road Hot-Mix Asphalt Mainline Test Cell Condition Report, (2002). http://www.mnroad.dot.state.mn.us/research, Accessed June 2007.

Petersen, J.C., J.F. Branthaver, R.E. Robertson, P.M. Harnsberger, J.J. Duvall, and E.K. Ensley, "Effects of Physicochemical Factors on Asphalt Oxidation Kinetics," *Trans. Res. Rec.*, **1391**, 1 (1993).

Ruan, Y., R.R. Davison, and C.J. Glover, "An Investigation of Asphalt Durability: Relationships between Ductility and Rheological Properties for Unmodified Asphalts," *Pet. Sci. & Tech.*, **21**(1-2), 231 (2003a).

Ruan, Y., R.R. Davison, and C.J. Glover, “Oxidation and Viscosity Hardening of Polymer-Modified Asphalts,” *Energy & Fuel*, **17**, 991 (2003b).

Ruan, Y., R.R. Davison, and C.J. Glover, "The Effect of Long-Term Oxidation on the Rheological Properties of Polymer Modified Asphalts," *Fuel*, **82**(14), 1763 (2003c).

Shuler, T.S., J.H. Collins, and J.P. Kirkpatrick, “Polymer-Modified Asphalt Properties Related to Asphalt Concrete Performance”, *Asphalt Rheology: Relationship to Mixture, ASTM STP 941*, O.E. Briscoe, Ed., American Society for Testing and Materials, Philadelphia, 179 (1987).

Thenoux, G., C.A. Bell, and J.E. Wilson, “Evaluation of Asphalt Physical and Fractional Properties and Their Interrelationship,” TRB Annual Meeting, (1988).

U.S. Geological Survey, A Global Crustal Model. http://www.usgs.gov, Accessed June, 2007.

Vassiliev, N.Y., R.R. Davison, and C.J. Glover, “Development of a Stirred Airflow Test Procedure for Short-Term Aging of Asphaltic Materials,” *Bituminous Binders*, **1810**, 25 (2002).

Vellerga, B.A., and W.J. Halstead, “Effects of Field Aging on Fundamental Properties of Paving Asphalts,” *Highway Research Record*, **361**, 71 (1971).

Walubita, L.F., A. Epps Martin, S.H. Jung, C.J. Glover, E.S. Park, and A. Chowdhury, "Comparison of Fatigue Analysis Approaches for Two Hot Mix Asphalt Concrete (HMAC) Mixtures,” Report FHWA/TX-05/0-4468-2, Texas Transportation Institute, College Station, TX (2005).

Walubita, L.F., “Comparison of Fatigue Analysis Approaches for Predicting Fatigue Lives of Hot Mix Asphalt Concrete Mixtures (HMAC),” Ph.D. Dissertation, Texas A&M University, College Station, TX (2006).

Welborn, J.Y. "Physical Properties as Related to Asphalt Durability: State of the Art," *Transp. Res. Rec.*, **999**, 31 (1984).

APPENDICES

APPENDIX A
DATA TABLES FOR CHAPTER II

Table A-1. Corbett Analysis for Base Binders

Corbett Analysis		Asphaltenes (As)	Saturates (S)	Napthene Aromatics (NA)	Polar Aromatics (PA)	Compatibility Index (NA+PA)/(As+S)	C.I (PA)/(As+S)	C.II (PA)/(S)
Wright 64-22	Unaged	20.53	7.18	25.92	44.95	2.56	1.62	6.26
	SAFT	23.88	6.74	23.55	39.68	2.06	1.30	5.89
	P* 16 hr	27.44	8.18	26.89	31.50	1.64	0.88	3.85
	P* 32 hr	30.36	6.76	27.85	31.36	1.60	0.84	4.64
Alon 58-28	Unaged	16.64	7.63	21.83	52.34	3.06	2.16	6.86
	SAFT	19.22	7.60	21.78	51.36	2.73	1.91	6.76
	P* 16 hr	19.97	8.18	20.31	45.49	2.34	1.62	5.56
	P* 32 hr	20.70	7.30	12.15	56.11	2.44	2.00	7.69
64-22	Unaged	16.11	9.72	19.53	39.51	2.29	1.53	4.06
	SAFT	16.52	10.94	18.55	49.25	2.47	1.79	4.50
	P* 16 hr	28.91	10.76	18.89	40.50	1.50	1.02	3.76
	P* 32 hr	30.46	11.33	17.69	34.94	1.26	0.84	3.08
Koch 64-22	Unaged	20.45	7.35	21.40	48.39	2.51	1.74	6.58
	SAFT	23.64	5.12	26.66	44.29	2.47	1.54	8.65
	P* 16 hr	27.43	7.47	20.85	42.07	1.80	1.21	5.63
	P* 32 hr	28.88	5.49	21.27	40.19	1.79	1.17	7.32
Mn Road 58-28	Unaged	21.27	18.25	24.21	34.19	1.48	0.87	1.87
	SAFT	23.55	19.89	21.15	31.82	1.22	0.73	1.60
	P* 16 hr	27.84	20.11	22.11	28.16	1.05	0.59	1.40
	P* 32 hr	30.14	18.65	23.21	24.46	0.98	0.50	1.31
AC 120/150	Unaged	21.25	2.52	29.91	39.56	2.92	1.66	15.70
	SAFT	25.33	3.02	27.77	40.49	2.41	1.43	13.41
	P* 16 hr	28.85	2.99	28.71	33.57	1.96	1.05	11.23
	P* 32 hr	30.95	3.57	26.12	37.63	1.85	1.09	10.54
Lion Oil 64-22	Unaged	13.71	10.30	30.29	53.45	3.49	2.23	5.19
	SAFT	14.76	8.61	21.01	51.88	3.12	2.22	6.03
	P* 16 hr	15.21	7.75	18.72	51.66	3.07	2.25	6.67
	P* 32 hr	17.11	9.73	23.11	47.15	2.62	1.76	4.85
Valero-O 64-22	Unaged	17.46	10.62	17.84	50.06	2.42	1.78	4.71
	SAFT	19.89	10.01	21.09	44.97	2.21	1.50	4.49
	P* 16 hr	24.62	10.48	16.64	44.21	1.73	1.26	4.22
	P* 32 hr	25.99	11.16	14.85	46.81	1.66	1.26	4.19
64-22 (Base for SBR)	Unaged	21.47	4.76	20.87	50.11	2.71	1.91	10.53
	SAFT	22.66	5.42	18.26	48.26	2.37	1.72	8.90
	P* 16 hr	27.43	7.98	17.81	41.17	1.67	1.16	5.16
	P* 32 hr	29.26	6.88	13.26	46.19	1.64	1.28	6.71
Valero-C 64-22	Unaged	17.58	12.11	26.20	40.12	2.23	1.35	3.31
	SAFT	21.44	10.56	23.98	39.26	1.98	1.23	3.72
	P* 16 hr	25.12	11.21	20.44	37.11	1.58	1.02	3.31
	P* 32 hr	28.90	14.55	19.21	35.22	1.25	0.81	2.42
Valero-H 64-22	Unaged	10.97	14.21	22.18	48.21	2.80	1.91	3.39
	SAFT	13.55	13.88	20.14	46.33	2.42	1.69	3.34
	P* 16 hr	18.21	14.24	19.21	41.39	1.87	1.28	2.91
	P* 32 hr	24.86	13.16	17.44	40.87	1.53	1.07	3.11

Table A-2. Corbett Analysis for Base and Polymer Modified Binders

Wright		Asphaltenes (As)	Saturates (S)	Napthene Aromatics (NA)	Polar Aromatics (PA)	Compatibility Index (NA+PA)/(As+S)	C.I (PA)/(As+S)	C.II (PA)/(S)
64-22 (Base)	Unaged	20.53	7.18	25.92	44.95	2.56	1.62	6.26
	SAFT	23.88	6.74	23.55	39.68	2.06	1.30	5.89
	P* 16 hr	27.44	8.18	26.89	31.50	1.64	0.88	3.85
	P* 32 hr	30.36	6.76	27.85	31.36	1.60	0.84	4.64
70-22 (SBS)	Unaged	24.77	7.78	23.28	40.27	1.95	1.24	5.18
	SAFT	25.33	9.58	18.11	38.79	1.63	1.11	4.05
	P* 16 hr	26.92	6.98	20.39	45.11	1.93	1.33	6.46
	P* 32 hr	31.19	7.42	19.43	32.83	1.35	0.85	4.42
76-22 (SBS)	Unaged	24.62	12.04	17.01	46.17	1.72	1.26	3.83
	SAFT	26.31	10.94	16.53	40.27	1.52	1.08	3.68
	P* 16 hr	31.58	9.74	16.53	42.05	1.42	1.02	4.32
	P* 32 hr	32.78	10.35	17.07	38.94	1.30	0.90	3.76
Alon		**Asphaltenes** (As)	**Saturates** (S)	**Napthene Aromatics** (NA)	**Polar Aromatics** (PA)	**Compatibility Index** (NA+PA)/(As+S)	**C.I** (PA)/(As+S)	**C.II** (PA)/(S)
64-22 (Base)	Unaged	16.11	9.72	19.53	39.51	2.29	1.53	4.06
	SAFT	16.52	10.94	18.55	49.25	2.47	1.79	4.50
	P* 16 hr	28.91	10.76	18.89	40.50	1.50	1.02	3.76
	P* 32 hr	30.46	11.33	17.69	34.94	1.26	0.84	3.08
70-22 (SBS)	Unaged	19.45	6.24	23.04	50.62	2.87	1.97	8.11
	SAFT	22.73	5.68	20.99	50.36	2.51	1.77	8.87
	P* 16 hr	27.46	5.79	17.66	46.01	1.91	1.38	7.95
	P* 32 hr	29.76	5.9	19.11	40.35	1.67	1.13	6.84

Table A-3. Wright

Wright		η* (Poise) @ 60 ℃ 0.1 rad/s	η'/G' (s) @ 15 ℃ 0.005 rad/s	G' (MPa) @ 15 ℃ 0.005 rad/s	G'/(η'/G') (MPa/s) @ 15 ℃ 0.005 rad/s	Calculated Ductility (cm) -	Ductility (cm) @ 15 ℃ 1 cm/min	Carbonyl Area - -
64-22 (Base)	Unaged	3610	703.4	0.00610	0.0000087	38.80	over 100	0.47627
	SAFT	11678	433.5	0.02414	0.0000557	17.12	27.58	0.56370
	P* 16 hr	66555	258.3	0.12204	0.0004725	6.68	5.44	0.76678
	P* 32 hr	134970	210.0	0.20562	0.0009790	4.85	4.06	0.85269
	3 mo.	89753	233.1	0.17352	0.0007445	5.47	4.50	0.87547
	6 mo.	207760	183.9	0.29934	0.0016278	3.88	3.20	0.95226
	9 mo.	372700	151.9	0.41338	0.0027211	3.09	2.31	1.09676
	12 mo.	859450	113.1	0.66090	0.0058416	2.21	1.49	1.18976
70-22 (SBS)	Unaged	9656	460.1	0.01057	0.0000230	25.28	34.86	0.49826
	SAFT	26061	356.2	0.02823	0.0000792	14.66	17.79	0.57043
	P* 16 hr	108400	253.2	0.1161	0.0004585	6.77	7.36	0.81959
	P* 32 hr	219110	205.5	0.1963	0.0009554	4.90	5.36	0.99701
	3 mo.	157780	226.8	0.16176	0.0007134	5.58	6.05	-
	6 mo.	278670	189.6	0.27046	0.0014268	4.11	4.58	-
	9 mo.	453300	160.0	0.38032	0.0023776	3.28	3.51	-
	12 mo.	1059700	113.9	0.6454	0.0056678	2.24	2.03	-
76-22 (SBS-B) Atlanta Lab Mixture Binder	Unaged	22690	383.5	0.01833	0.0000478	18.31	33.09	0.50565
	SAFT	43049	325.5	0.03386	0.0001040	13.01	18.31	0.51839
	P* 16 hr	176030	236.3	0.12666	0.0005361	6.32	9.43	0.81649
	P* 32 hr	296920	201.8	0.2101	0.0010409	4.72	7.46	1.00520
	3 mo.	236010	222.6	0.19176	0.0008616	5.13	7.21	-
	6 mo.	471560	171.2	0.32794	0.0019155	3.61	4.86	-
	9 mo.	584410	145.5	0.43492	0.0029895	2.97	3.85	-
	12 mo.	1147970	106.2	0.62876	0.0059193	2.20	2.50	-
76-22 (Tire Rubber & SBS)	Unaged	18202	375.0	0.0294	0.0000784	14.73	16.97	0.49735
	SAFT	47545	288.0	0.05537	0.0001923	9.93	12.82	0.58386
	P* 16 hr	199220	202.1	0.1999	0.0009889	4.83	6.19	0.83582
	P* 32 hr	406310	164.6	0.30774	0.0018695	3.65	4.74	0.95377
	3 mo.	344250	174.2	0.32594	0.0018712	3.65	5.74	-
	6 mo.	604070	143.9	0.39758	0.0027633	3.07	3.88	-
	9 mo.	905690	120.5	0.53858	0.0044695	2.49	2.82	-
	12 mo.	1443800	98.3	0.74352	0.0075663	1.97	1.77	-
76-22 ('02) (SBS-A) Atlanta Field Core Binder	Unaged	17575	409.7	0.01523	0.0000372	20.46	52.22	0.51182
	SAFT	34039	341.6	0.02949	0.0000863	14.12	36.00	0.53631
	P* 16 hr	168180	226.7	0.14934	0.0006587	5.77	10.30	0.82944
	P* 32 hr	272170	193.6	0.23738	0.0012263	4.39	7.05	1.01206
	3 mo.	265900	204.9	0.21502	0.0010491	4.71	7.85	-
	6 mo.	444230	170.2	0.34242	0.0020123	3.53	5.21	-
	9 mo.	610700	147.9	0.45492	0.0030763	2.93	4.05	-
	12 mo.	1231400	110.5	0.65876	0.0059620	2.19	2.10	-

Table A-4. Alon

Alon		η* (Poise) @ 60 ℃ 0.1 rad/s	η'/G' (s) @ 15 ℃ 0.005 rad/s	G' (MPa) @ 15 ℃ 0.005 rad/s	G'/(η'/G') (MPa/s) @ 15 ℃ 0.005 rad/s	Calculated Ductility (cm) -	Ductility (cm) @ 15 ℃ 1 cm/min	Carbonyl Area -
58-28 (Base)	Unaged	1326	1913.6	0.00081	0.0000004	146.18	over 100	0.44795
	SAFT	2796	1167.2	0.00354	0.0000030	61.58	over 100	0.60094
	P* 16 hr	8491	633.9	0.01760	0.0000278	23.25	over 100	0.89021
	P* 32 hr	16632	460.6	0.04623	0.0001004	13.21	14.44	0.97199
	3 mo.	13693	507.0	0.03664	0.0000723	15.27	20.16	-
	6 mo.	32984	345.3	0.10274	0.0002975	8.19	6.28	-
	9 mo.	43999	306.8	0.14146	0.0004610	6.76	5.51	-
	12 mo.	96052	232.3	0.25408	0.0010939	4.62	3.23	-
70-28 (SBS)	Unaged	6993	493.5	0.00494	0.0000100	36.44	over 100	0.45982
	SAFT	9419	488.8	0.00801	0.0000164	29.33	78.69	0.50250
	P* 16 hr	26370	412.1	0.02817	0.0000684	15.65	28.06	0.80738
	P* 32 hr	41352	353.3	0.05658	0.0001601	10.76	15.35	0.95238
	3 mo.	44569	373.9	0.05284	0.0001413	11.37	19.82	-
	6 mo.	86130	287.2	0.11152	0.0003884	7.29	7.69	-
	9 mo.	216210	203.0	0.26918	0.0013263	4.24	4.79	-
	12 mo.	244870	192.8	0.33442	0.0017349	3.77	4.36	-
64-22 (Base)	Unaged	5573	1301.7	0.00774	0.0000059	45.83	over 100	0.52620
	SAFT	13099	705.0	0.03212	0.0000456	18.70	over 100	0.56704
	P* 16 hr	64466	293.0	0.26886	0.0009175	4.99	1.84	0.88047
	P* 32 hr	140370	199.9	0.47916	0.0023967	3.27	0.95	0.98816
	3 mo.	108350	212.9	0.45808	0.0021514	3.43	1.11	-
	6 mo.	302700	126.9	0.80784	0.0063669	2.13	0.57	-
	9 mo.	509250	99.3	1.13460	0.0114282	1.65	0.28	-
	12 mo.	800200	66.7	1.38200	0.0207132	1.27	0.15	-
70-22 (SBS)	Unaged	9366	655.5	0.00690	0.0000105	35.63	99.44	0.46569
	SAFT	14569	596.1	0.01328	0.0000223	25.63	57.76	0.53094
	P* 16 hr	49435	403.4	0.07144	0.0001771	10.29	16.97	0.78255
	P* 32 hr	76428	321.5	0.13468	0.0004189	7.05	9.42	0.97499
	3 mo.	75796	331.3	0.14390	0.0004343	6.94	9.10	-
	6 mo.	169610	235.0	0.28940	0.0012317	4.38	4.42	-
	9 mo.	277540	170.3	0.49460	0.0029040	3.01	2.02	-
	12 mo.	379940	150.0	0.57996	0.0038656	2.65	1.32	-
76-22 (Tire Rubber & SBS)	Unaged	12931	683.4	0.01283	0.0000188	27.63	59.55	0.55158
	SAFT	25217	571.8	0.02972	0.0000520	17.65	33.80	0.59339
	P* 16 hr	117980	271.7	0.18558	0.0006830	5.68	6.66	0.93313
	P* 32 hr	219880	222.2	0.39236	0.0017662	3.74	4.53	1.17849
	3 mo.	194990	229.6	0.39350	0.0017142	3.79	4.19	-
	6 mo.	487740	138.6	0.87162	0.0062895	2.14	0.79	-
	9 mo.	863260	96.4	1.13740	0.0117929	1.62	0.31	-
	12 mo.	1140700	79.6	1.38760	0.0174380	1.37	0.17	-

Table A-5. Koch

Koch		η* (Poise) @ 60 ℃ 0.1 rad/s	η'/G' (s) @ 15 ℃ 0.005 rad/s	G' (MPa) @ 15 ℃ 0.005 rad/s	G'/(η'/G') (MPa/s) @ 15 ℃ 0.005 rad/s	Calculated Ductility (cm) -	Ductility (cm) @ 15 ℃ 1 cm/min	Carbonyl Area -
64-22 (Base)	Unaged	5071	863.5	0.00864	0.0000100	36.44	over 100	-
	SAFT	8906	607.7	0.01906	0.0000314	22.04	over 100	-
	P* 16 hr	37761	339.5	0.11008	0.0003243	7.89	6.58	-
	P* 32 hr	83139	251.7	0.22736	0.0009033	5.03	4.73	-
	3 mo.	53830	295.9	0.16612	0.0005614	6.19	5.22	-
	6 mo.	145560	200.2	0.36246	0.0018102	3.70	2.81	-
	9 mo.	286700	163.2	0.49538	0.0030349	2.95	1.27	-
	12 mo.	378680	135.7	0.68042	0.0050146	2.36	0.65	-
70-22 (SBS)	Unaged	8852	636.9	0.01189	0.0000187	27.70	80.49	-
	SAFT	14726	529.6	0.02113	0.0000399	19.83	35.54	-
	P* 16 hr	60999	321.1	0.11150	0.0003472	7.65	8.45	-
	P* 32 hr	119330	244.1	0.23434	0.0009601	4.89	5.84	-
	3 mo.	79359	283.7	0.16454	0.0005799	6.11	6.44	-
	6 mo.	213780	186.6	0.37534	0.0020114	3.53	2.27	-
	9 mo.	379820	146.1	0.57364	0.0039255	2.63	1.23	-
	12 mo.	565160	122.7	0.80560	0.0065642	2.10	0.61	-
76-22 (SBS)	Unaged	23294	446.7	0.01833	0.0000410	19.59	61.62	-
	SAFT	30659	423.6	0.02448	0.0000578	16.85	40.17	-
	P* 16 hr	119880	297.0	0.11516	0.0003877	7.29	10.08	-
	P* 32 hr	184830	241.9	0.20784	0.0008591	5.14	6.36	-
	3 mo.	151860	261.0	0.19690	0.0007575	5.43	7.35	-
	6 mo.	329900	178.2	0.39050	0.0021917	3.40	2.57	-
	9 mo.	667800	133.7	0.65848	0.0049268	2.38	1.25	-
	12 mo.	778970	109.7	0.78692	0.0071702	2.02	0.62	-
70-28 (SBS)	Unaged	7553	430.7	0.00637	0.0000148	30.68	74.81	-
	SAFT	14561	408.7	0.00923	0.0000226	25.47	51.53	-
	P* 16 hr	45371	336.8	0.0313	0.0000929	13.67	16.77	-
	P* 32 hr	67104	308.2	0.04895	0.0001588	10.80	9.65	-
	3 mo.	51808	339.3	0.04098	0.0001208	12.18	10.84	-
	6 mo.	106820	265.7	0.10314	0.0003882	7.29	5.37	-
	9 mo.	187020	215.7	0.18814	0.0008722	5.10	4.22	-
	12 mo.	320120	180.9	0.30090	0.0016633	3.84	3.75	-
76-28 (SBS)	Unaged	27350	304.2	0.01025	0.0000337	21.36	63.27	-
	SAFT	40839	305.4	0.01199	0.0000393	19.97	52.25	-
	P* 16 hr	96028	282.9	0.03378	0.0001194	12.24	19.84	-
	P* 32 hr	133490	270.1	0.05459	0.0002021	9.71	10.89	-
	3 mo.	118980	279.8	0.04457	0.0001593	10.78	12.65	-
	6 mo.	194920	240.4	0.11106	0.0004620	6.75	6.18	-
	9 mo.	316460	194.5	0.22828	0.0011737	4.48	4.60	-
	12 mo.	445450	166.0	0.32844	0.0019784	3.56	3.82	-

Table A-6. MnRoad

MnRoad		η* (Poise) @ 60 ℃ 0.1 rad/s	η'/G' (s) @ 15 ℃ 0.005 rad/s	G' (MPa) @ 15 ℃ 0.005 rad/s	G'/(η'/G') (MPa/s) @ 15 ℃ 0.005 rad/s	Calculated Ductility (cm) -	Ductility (cm) @ 15 ℃ 1 cm/min	Carbonyl Area - -
58-28	**Unaged**	1659	1182.6	0.00155	0.0000013	89.19	over 100	-
(Base)	**SAFT**	3634	716.7	0.00569	0.0000079	40.34	over 100	-
(Koch)	**P* 16 hr**	16016	396.2	0.03702	0.0000934	13.64	14.05	-
	P* 32 hr	31261	319.0	0.06215	0.0001948	9.87	7.49	-
Cell #33	**3 mo.**	23683	358.9	0.05298	0.0001476	11.15	8.71	-
Field	**6 mo.**	74382	250.7	0.14124	0.0005633	6.19	4.79	-
Core	**9 mo.**	180780	196.5	0.24990	0.0012719	4.32	3.12	-
Binder	**12 mo.**	244940	168.2	0.38696	0.0023008	3.33	1.93	-
58-34	**Unaged**	2703	509.8	0.00219	0.0000043	52.89	over 100	-
(SBS)	**SAFT**	5856	428.6	0.00445	0.0000104	35.86	32.91	-
(Koch)	**P* 16 hr**	22662	346.4	0.01658	0.0000479	18.30	11.76	-
	P* 32 hr	36704	316.1	0.02859	0.0000904	13.83	8.70	-
Cell #34	**3 mo.**	29760	339.3	0.02389	0.0000704	15.44	10.05	-
Field	**6 mo.**	86186	262.8	0.07295	0.0002776	8.45	5.64	-
Core	**9 mo.**	169020	212.7	0.14686	0.0006904	5.66	4.02	-
Binder	**12 mo.**	201680	200.6	0.17732	0.0008841	5.07	3.38	-
58-40	**Unaged**	8381	288.3	0.00244	0.0000085	39.25	46.56	-
(SBS)	**SAFT**	10610	288.7	0.00328	0.0000113	34.48	22.82	-
(Koch)	**P* 16 hr**	39562	238.0	0.01382	0.0000581	16.81	6.79	-
	P* 32 hr	73286	219.4	0.02464	0.0001123	12.58	5.02	-
Cell #35	**3 mo.**	86683	217.9	0.03348	0.0001536	10.96	4.91	-
Field	**6 mo.**	200100	180.8	0.10510	0.0005812	6.10	3.18	-
Core	**9 mo.**	315890	155.8	0.18160	0.0011653	4.49	2.11	-
Binder	**12 mo.**	375830	142.5	0.21994	0.0017115	3.79	1.73	-
AC	**Unaged**	1580	1234.5	0.00149	0.0000012	92.55	over 100	-
120/150	**SAFT**	3805	698.6	0.00641	0.0000092	37.85	over 100	-
(Unmo.)	**P* 16 hr**	13643	426.4	0.03310	0.0000776	14.80	14.12	-
	P* 32 hr	30967	325.3	0.06861	0.0002109	9.53	6.75	-
Cell #1	**3 mo.**	23486	358.8	0.05894	0.0001643	10.64	8.12	-
Field	**6 mo.**	74654	248.9	0.16934	0.0006802	5.69	4.37	-
Core	**9 mo.**	144580	197.0	0.24578	0.0012477	4.36	2.89	-
Binder	**12 mo.**	256090	167.1	0.38642	0.0023122	3.32	1.78	-

Table A-7. Lion Oil

Lion Oil		η* (Poise) @ 60 ℃ 0.1 rad/s	η'/G' (s) @ 15 ℃ 0.005 rad/s	G' (MPa) @ 15 ℃ 0.005 rad/s	G'/(η'/G') (MPa/s) @ 15 ℃ 0.005 rad/s	Calculated Ductility (cm) -	Ductility (cm) @ 15 ℃ 1 cm/min	Carbonyl Area -
64-22 (Base)	Unaged	4019	1336.3	0.00526	0.0000039	54.92	over 100	-
	SAFT	6012	926.3	0.01151	0.0000124	33.13	over 100	-
	P* 16 hr	15688	535.7	0.04708	0.0000879	14.01	25.09	-
	P* 32 hr	25978	402.4	0.09401	0.0002336	9.11	10.14	-
	3 mo.	21930	457.2	0.07549	0.0001651	10.62	9.43	-
	6 mo.	40411	334.0	0.15506	0.0004643	6.74	5.13	-
	9 mo.	56844	287.6	0.21370	0.0007430	5.48	4.48	-
	12 mo.	73079	253.1	0.27968	0.0011050	4.60	3.56	-
70-22 (SBS)	Unaged	9956	668.2	0.01248	0.0000187	27.69	over 100	-
	SAFT	14635	575.3	0.01873	0.0000326	21.69	59.30	-
	P* 16 hr	60935	319.7	0.11152	0.0003488	7.64	13.54	-
	P* 32 hr	128970	241.8	0.22520	0.0009314	4.96	7.68	-
	3 mo.	98934	264.4	0.1896	0.0007171	5.56	7.69	-
	6 mo.	255110	174.8	0.43288	0.0024771	3.22	3.03	-
	9 mo.	532630	126.0	0.62180	0.0049333	2.38	2.28	-
	12 mo.	908360	101.9	0.91804	0.0090108	1.83	1.40	-
76-22 (SBS)	Unaged	26765	420.0	0.02167	0.0000516	17.71	over 100	-
	SAFT	48042	372.9	0.03153	0.0000846	14.25	83.15	-
	P* 16 hr	259510	223.3	0.16268	0.0007286	5.52	17.69	-
	P* 32 hr	479140	172.7	0.30812	0.0017845	3.72	9.67	-
	3 mo.	250810	208.9	0.23964	0.0011474	4.52	10.7	-
	6 mo.	578800	147.8	0.5135	0.0034746	2.78	3.53	-
	9 mo.	1044600	109.5	0.77582	0.0070851	2.03	2.38	-
	12 mo.	2042600	80.8	1.05900	0.0131014	1.55	1.41	-

Table A-8. Valero-Oklahoma

Valero-Oklahoma		η* (Poise) @ 60 ℃ 0.1 rad/s	η'/G' (s) @ 15 ℃ 0.005 rad/s	G' (MPa) @ 15 ℃ 0.005 rad/s	G'/(η'/G') (MPa/s) @ 15 ℃ 0.005 rad/s	Calculated Ductility (cm) -	Ductility (cm) @ 15 ℃ 1 cm/min	Carbonyl Area -
64-22 (Base)	Unaged	3502	1039.2	0.00508	0.0000049	49.96	over 100	-
	SAFT	6593	668.9	0.01534	0.0000229	25.30	73.77	-
	P* 16 hr	26485	362.8	0.08168	0.0002251	9.26	6.96	-
	P* 32 hr	46450	284.0	0.14436	0.0005084	6.47	4.92	-
	3 mo.	36368	311.7	0.10786	0.0003460	7.67	5.12	-
	6 mo.	82674	223.8	0.24626	0.0011003	4.61	3.30	-
	9 mo.	122210	195.5	0.34644	0.0017717	3.74	2.59	-
	12 mo.	184550	164.2	0.41918	0.0025526	3.18	2.15	-
70-22 (SBS)	Unaged	18913	455.6	0.02236	0.0000491	18.10	22.07	-
	SAFT	26253	399.5	0.03083	0.0000772	14.83	11.55	-
	P* 16 hr	137740	226.3	0.17534	0.0007749	5.38	6.22	-
	P* 32 hr	331860	174.9	0.30216	0.0017277	3.78	4.97	-
	3 mo.	222920	191.7	0.23958	0.0012499	4.36	4.83	-
	6 mo.	545020	140.1	0.46580	0.0033251	2.83	3.69	-
	9 mo.	826410	119.1	0.53344	0.0044795	2.48	2.78	-
	12 mo.	1186900	97.6	0.83238	0.0085260	1.87	1.88	-
76-22 (SBS)	Unaged	21782	353.4	0.02332	0.0000660	15.89	14.93	-
	SAFT	39971	301.3	0.03960	0.0001314	11.74	9.32	-
	P* 16 hr	590810	151.0	0.28332	0.0018765	3.64	4.93	-
	P* 32 hr	1346300	112.3	0.55976	0.0049865	2.37	3.97	-
	3 mo.	841710	121.0	0.45160	0.0037314	2.69	3.76	-
	6 mo.	2257000	86.3	0.72720	0.0084293	1.88	2.12	-
	9 mo.	4419400	64.6	1.00420	0.0155562	1.44	1.25	-
	12 mo.	6727800	55.6	1.11780	0.0201074	1.28	0.87	-
64-22 (Base)	Unaged	4147	868.3	0.00630	0.0000073	41.98	over 100	-
	SAFT	7837	606.2	0.01571	0.0000259	23.98	over 100	-
	P* 16 hr	30074	355.1	0.08312	0.0002341	9.10	7.06	-
	P* 32 hr	57959	283.0	0.14526	0.0005133	6.44	5.17	-
	3 mo.	53567	292.0	0.14496	0.0004964	6.54	5.26	-
	6 mo.	119360	215.8	0.26328	0.0012198	4.40	3.23	-
	9 mo.	192040	183.0	0.40060	0.0021895	3.40	2.07	-
	12 mo.	276710	159.0	0.46668	0.0029349	2.99	1.95	-
76-22 (SBR) Fort Worth (US281) Field Core Binder	Unaged	4737	627.0	0.00666	0.0000106	35.50	84.37	-
	SAFT	8811	512.8	0.01369	0.0000267	23.66	69.85	-
	P* 16 hr	65110	260.5	0.10768	0.0004133	7.09	25.58	-
	P* 32 hr	103980	224.4	0.17312	0.0007716	5.39	14.19	-
	3 mo.	69938	245.5	0.14800	0.0006028	6.00	22.05	-
	6 mo.	151730	199.8	0.24882	0.0012451	4.36	10.33	-
	9 mo.	207510	179.2	0.28446	0.0015874	3.92	2.78	-
	12 mo.	236660	166.7	0.28102	0.0016863	3.82	2.56	-

Table A-9. Valero-Corpus

Valero-Corpus		η* (Poise) @ 60 ℃ 0.1 rad/s	η'/G' (s) @ 15 ℃ 0.005 rad/s	G' (MPa) @ 15 ℃ 0.005 rad/s	G'/(η'/G') (MPa/s) @ 15 ℃ 0.005 rad/s	Calculated Ductility (cm) -	Ductility (cm) @ 15 ℃ 1 cm/min	Carbonyl Area -
64-22 (Base)	Unaged	5774	624.8	0.01090	0.0000175	28.53	over 100	-
	SAFT	12021	440.9	0.02491	0.0000565	17.01	30.35	-
	P* 16 hr	52352	277.5	0.10826	0.0003901	7.27	5.93	-
	P* 32 hr	102980	228.2	0.17714	0.0007762	5.37	4.48	-
	3 mo.	62539	263.9	0.12974	0.0004916	6.57	4.81	-
	6 mo.	136680	209.4	0.23638	0.0011291	4.56	3.52	-
	9 mo.	306310	160.8	0.43730	0.0027191	3.09	1.65	-
	12 mo.	432370	138.0	0.50982	0.0036945	2.70	0.85	-
70-22 (SBS)	Unaged	16428	418.5	0.01899	0.0000454	18.74	27.38	-
	SAFT	34494	343.1	0.03623	0.0001056	12.92	14.04	-
	P* 16 hr	149810	233.8	0.14228	0.0006084	5.98	6.16	-
	P* 32 hr	274530	195.4	0.23372	0.0011958	4.44	5.19	-
	3 mo.	184460	215.9	0.17892	0.0008288	5.22	5.77	-
	6 mo.	358640	172.9	0.29998	0.0017347	3.77	3.81	-
	9 mo.	632180	140.0	0.45644	0.0032604	2.86	1.53	-
	12 mo.	860880	121.1	0.60326	0.0049810	2.37	0.83	-
76-22 (SBS)	Unaged	21906	390.6	0.02247	0.0000575	16.88	24.12	-
	SAFT	39962	331.1	0.03789	0.0001144	12.47	14.37	-
	P* 16 hr	187010	224.0	0.14670	0.0006548	5.79	6.70	-
	P* 32 hr	323180	189.3	0.24196	0.0012784	4.31	5.33	-
	3 mo.	216530	213.8	0.18778	0.0008784	5.09	5.9	-
	6 mo.	436470	168.4	0.37852	0.0022481	3.36	4.22	-
	9 mo.	682560	139.6	0.44890	0.0032153	2.87	1.3	-
	12 mo.	1023300	117.1	0.66366	0.0056659	2.24	0.91	-

Table A-10. Valero-Houston

Valero-Houston		η* (Poise) @ 60 ℃ 0.1 rad/s	η'/G' (s) @ 15 ℃ 0.005 rad/s	G' (MPa) @ 15 ℃ 0.005 rad/s	G'/(η'/G') (MPa/s) @ 15 ℃ 0.005 rad/s	Calculated Ductility (cm) -	Ductility (cm) @ 15 ℃ 1 cm/min	Carbonyl Area - -
64-22 (Base)	Unaged	6361	595.4	0.01138	0.0000191	27.42	over 100	-
	SAFT	13447	427.9	0.02767	0.0000647	16.03	30.14	-
	P* 16 hr	64617	260.5	0.11424	0.0004385	6.91	5.28	-
	P* 32 hr	145230	204.6	0.23730	0.0011598	4.50	4.20	-
	3 mo.	84009	237.2	0.15626	0.0006587	5.77	4.7	-
	6 mo.	216030	177.3	0.33238	0.0018746	3.64	2.45	-
	9 mo.	436800	141.3	0.49680	0.0035150	2.76	1.48	-
	12 mo.	643490	122.1	0.64870	0.0053114	2.30	0.95	-
70-22 (SBS)	Unaged	18575	399.4	0.01992	0.0000499	17.97	29.63	-
	SAFT	34872	334.8	0.03425	0.0001023	13.10	14.24	-
	P* 16 hr	170900	223.6	0.14498	0.0006485	5.81	6.05	-
	P* 32 hr	328370	186.4	0.21954	0.0011779	4.47	5.06	-
	3 mo.	204180	214.5	0.18742	0.0008736	5.10	5.21	-
	6 mo.	422720	165.1	0.35178	0.0021311	3.44	2.95	-
	9 mo.	698710	137.4	0.54718	0.0039817	2.62	1.39	-
	12 mo.	1003100	116.6	0.69176	0.0059348	2.19	0.82	-
76-22 (SBS)	Unaged	29481	358.6	0.02403	0.0000670	15.79	28.29	-
	SAFT	54483	299.4	0.04244	0.0001418	11.35	13.79	-
	P* 16 hr	247160	211.2	0.15896	0.0007526	5.45	6.51	-
	P* 32 hr	434810	177.3	0.27084	0.0015272	3.99	5.51	-
	3 mo.	317400	197.5	0.23266	0.0011781	4.47	6.41	-
	6 mo.	551640	158.4	0.33626	0.0021227	3.45	4.33	-
	9 mo.	871240	133.3	0.44940	0.0033707	2.82	1.93	-
	12 mo.	1213300	112.6	0.68612	0.0060919	2.17	1.02	-

Table A-11. Ratio of the Modified Asphalt to Base Binder Properties

Supplier	PG Binder	Oxidative Hardening (Figure II-35)	Stiffness Improvement (Figure II-34)	Ductility (or DT) Improvement (Figure II-33)	Initial Stiffness (Figure II-36)
Wright	64-22 B	-	-	0.81	4.73
	70-22 S	1.01	0.97	1.09	4.59
	76-22 SB	0.91	1.13	1.49	5.36
	76-22 TRS	0.87	2.09	1.28	9.89
Alon	58-28 B	-	-	4.30	0.28
	70-28 S	0.66	2.46	1.79	0.68
	64-22 B	-	-	0.37	9.18
	70-22 S	0.90	0.19	1.65	1.77
	76-22 TRS	0.99	0.74	1.17	6.83
Koch	64-22 B	-	-	0.83	3.24
	70-22 S	0.99	1.07	1.10	3.47
	76-22 S	0.78	1.20	1.38	3.88
MnRoad	58-28 B	-	-	1.03	0.93
	58-34 S	0.86	0.51	0.64	0.48
	58-40 S	0.90	0.62	0.40	0.58
Lion Oil	64-22 B	-	-	1.79	0.88
	70-22 S	1.00	3.97	1.77	3.49
	76-22 S	0.91	8.29	3.20	7.29
Valero-Oklahoma	64-22 B	-	-	0.75	2.25
	70-22 S	0.99	3.44	1.16	7.75
	76-22 S	1.20	8.34	1.35	18.77
US281 (Valero-O)	64-22 BSR	-	-	0.78	2.34
	76-22 SR	0.80	1.77	3.61	4.13
Valero-Corpus	64-22 B	-	-	0.82	3.90
	70-22 S	0.99	1.56	1.03	6.08
	76-22 S	0.97	1.68	1.16	6.55
Valero-Houston	64-22 B	-	-	0.76	4.39
	70-22 S	0.60	1.48	1.04	6.49
	76-22 S	0.73	1.72	1.19	7.53

APPENDIX B
DATA TABLE FOR CHAPTER III

Table B-1. GEB (Valero-Oklahoma)

GEB (Valero-Oklahoma)		η* (Poise) @ 60 ℃ 0.1 rad/s	η'/G' (s) @ 15 ℃ 0.005 rad/s	G' (MPa) @ 15 ℃ 0.005 rad/s	G'/(η'/G') (MPa/s) @ 15 ℃ 0.005 rad/s	Calculated Ductility (cm) -	Ductility (cm) @ 15 ℃ 1 cm/min	Carbonyl Area -
64-22 (Base)	Unaged	2589	1001.8	0.00361	0.000004	57.15	over 100	0.50769
	SAFT	5470	635.5	0.01145	0.000018	28.13	40.88	0.54630
	P* 16 hr	28259	334.4	0.06768	0.000202	9.71	5.73	0.88856
	2 mo.	17957	393.6	0.04907	0.000125	12.01	7.07	0.81288
	4 mo.	30647	321.9	0.09346	0.000290	8.28	5.45	0.90813
	8 mo.	72555	234.1	0.16272	0.000695	5.64	4.17	1.04010
70-22 (SBS)	Unaged	4346	579.9	0.00707	0.000012	33.41	over 100	0.53199
	SAFT	10306	471.4	0.01784	0.000038	20.29	30.34	0.57652
	P* 16 hr	53614	310.7	0.08163	0.000263	8.65	10.33	0.81951
	2 mo.	37935	346.4	0.06177	0.000178	10.26	12.03	0.69658
	4 mo.	61105	300.2	0.10016	0.000334	7.79	10.49	0.82172
	8 mo.	122710	230.4	0.20574	0.000893	5.05	6.17	0.92871
76-22 (SBS)	Unaged	11523	441.5	0.01839	0.000042	19.46	28.91	0.65812
	SAFT	31484	344.0	0.04724	0.000137	11.51	13.7	0.73611
	P* 16 hr	119830	220.3	0.15112	0.000686	5.67	6.11	0.99397
	2 mo.	83365	246.2	0.13772	0.000559	6.21	7.57	0.92047
	4 mo.	159030	195.4	0.25784	0.001319	4.25	5.88	1.00326
	8 mo.	330960	159.3	0.43298	0.002718	3.10	4.39	1.13040
After Blending Aged PG 70-22 with Murphy Oil								
	P* 16 hr	12688	433.8	0.02248	0.000052	17.67	-	-
	2 mo.	9780	463.2	0.01849	0.000040	19.83	-	-
	4 mo.	11669	444.8	0.01970	0.000044	18.94	-	-
	8 mo.	10106	437.1	0.01858	0.000043	19.28	-	-
After Blending PG 64-22 (SAFT) and (PAV* 16 hr)								
	Blended PG 64-22	-	412.2	0.04120	0.000100	13.24	-	-
After Blending (Blended PG 64-22) and (PG 70-22 SAFT)								
	Blended Binder	-	441.6	0.02411	0.000055	17.27	-	-

APPENDIX C
DATA TABLES FOR CHAPTER IV

Table C-1. Polymer Modified Asphalts in Texas (a)

1st Core		Bulk S. G.		Maximum	Total Air Voids		Accessible A.V.		Binder
		SSD	Corelock	S. G.	SSD	Corelock	SSD	Corelock	Contents
Atlanta – RG (River Gravel)	**1st**	2.30	2.17	2.50	8.05	13.20	6.39	11.63	3.92
	2nd	2.31	2.24	2.49	7.47	10.37	5.52	8.47	4.57
	3rd	2.31	2.23	2.50	7.53	10.82	5.38	8.75	4.42
Atlanta – SS (Sandstone)	**1st**	2.29	2.02	2.43	5.99	17.12	5.32	16.53	3.67
	2nd	2.27	2.11	2.49	8.47	15.16	5.83	12.71	4.24
	3rd	2.26	2.11	2.47	8.72	14.80	5.90	12.17	4.41
	4th	2.23	2.11	2.45	9.12	14.10	6.28	11.42	4.9
Atlanta – Q (Quartzite)	**1st**	2.34	2.24	2.55	8.36	12.38	3.28	7.53	4.12
	2nd	2.37	2.34	2.53	6.40	7.50	4.16	5.29	4.35
	3rd	2.37	2.35	2.50	5.32	6.11	3.76	4.56	4.87
Odessa	**1st**	2.26	2.17	2.38	5.01	9.07	3.21	7.34	4.89
	2nd	2.28	2.27	2.40	5.03	5.33	1.29	1.61	6.34
	3rd	2.29	2.30	2.43	5.67	5.17	0.88	0.35	6.28
	4th	2.29	2.29	2.40	4.74	4.63	0.82	0.7	5.94
	5th	2.29	2.29	2.41	5.02	5.08	0.78	0.85	7.21
Waco	**1st**	2.31	2.29	2.49	7.28	8.22	5.13	6.10	4.89
	2nd	2.34	2.34	2.52	6.96	7.14	3.79	3.98	4.89
	3rd	2.35	2.35	2.53	7.28	7.35	3.18	3.26	5.05
	4th	2.35	2.34	2.43	3.53	3.60	3.32	3.68	5.15
	5th	2.34	2.34	2.45	4.57	4.60	3.72	3.76	5.14
	6th	2.39	2.39	2.46	3.17	3.07	1.02	0.91	5.64
Yoakum	**1st**	2.31	2.26	2.56	9.85	11.77	6.09	8.08	3.23
	2nd	2.32	2.25	2.57	9.55	12.26	6.18	8.98	3.55
	3rd	2.34	2.26	2.57	8.70	12.03	4.69	8.16	3.53
	4th	2.32	2.29	2.54	8.44	9.93	3.91	5.47	3.24
	5th	2.28	2.27	2.55	10.71	11.06	6.33	6.70	3.45

Table C-2. Polymer Modified Asphalts in Texas (b)

1st Core		Bulk S. G.		Maximum	Total Air Voids		Accessible A.V.		Binder
		SSD	Corelock	S. G.	SSD	Corelock	SSD	Corelock	Contents
Amarillo	1st	2.29	2.13	2.55	10.33	16.36	8.17	14.35	3.68
	2nd	2.31	2.23	2.43	5.09	8.21	6.74	9.81	4.01
	3rd	2.31	2.25	2.54	9.08	11.57	6.62	9.19	4.07
Pharr	1st	2.25	2.16	2.49	9.70	13.24	7.43	11.06	4.32
	2nd	2.27	2.20	2.42	6.20	9.14	5.59	8.55	4.51
	3rd	2.27	2.19	2.49	8.84	11.83	6.39	9.46	4.56
	4th	2.27	2.21	2.46	7.89	10.14	5.52	7.83	5.02
	5th	2.28	2.19	2.45	7.03	10.97	5.14	9.16	4.89
Lufkin	1st	2.33	2.19	2.55	8.56	14.15	6.26	11.98	3.61
	2nd	2.34	2.23	2.56	8.56	12.64	6.02	10.22	3.69
	3rd	2.34	2.22	2.54	7.71	12.47	5.52	10.40	3.72
	4th	2.38	2.18	2.54	6.21	14.15	4.71	12.78	3.47
F.W. SH183	1st	2.32	2.25	2.44	4.82	7.79	1.67	4.73	4.48
	2nd	2.32	2.31	2.42	3.99	4.60	1.40	2.03	4.59
	3rd	2.32	2.31	2.43	4.76	5.00	1.48	1.73	4.65
F.W. FM51	1st	2.33	2.31	2.55	8.29	9.43	3.70	4.90	4.06
	2nd	2.36	2.35	2.52	6.32	6.71	2.87	3.27	4.38
	3rd	2.40	2.39	2.50	4.03	4.36	1.58	1.93	4.53
	4th	2.41	2.39	2.51	3.97	4.79	1.06	1.91	4.34
F.W. US281	1st	2.28	2.20	2.48	8.07	11.08	8.25	11.25	3.99
	2nd	2.29	2.23	2.53	9.51	11.97	7.69	10.20	3.86

Table C-3. 48-9005 San Antonio Field Core in Texas

1st Core		Bulk S. G.		Maximum	Total Air Voids		Accessible A.V.		Binder
		SSD	Corelock	S. G.	SSD	Corelock	SSD	Corelock	Contents
San Antonio (Overlay)	1st	2.31	2.31	2.56	9.51	9.81	5.27	5.58	3.48
	2nd	2.33	2.32	2.53	7.99	8.41	4.60	5.03	4.07
	3rd	2.34	2.33	2.53	7.59	7.92	4.94	5.28	4.14
(OSL)	1st	2.32	2.32	2.53	8.31	8.18	4.3	4.17	4.67
	2nd	2.38	2.36	2.49	4.61	5.34	1.56	2.32	5.22
2nd Core		**Bulk S. G.**		**Maximum**	**Total Air Voids**		**Accessible A.V.**		**Binder**
		SSD	Corelock	S. G.	SSD	Corelock	SSD	Corelock	Contents
San Antonio (Overlay)	1st	2.33	2.33	2.55	8.58	8.82	5.74	5.98	-
	2nd	2.32	2.32	2.54	8.48	8.72	5.25	5.49	-
	3rd	2.32	2.29	2.51	7.67	8.69	4.71	5.76	-
(OSL)	1st	2.29	2.28	2.50	8.20	8.71	5.99	6.51	3.97
	2nd	2.31	2.28	2.44	5.35	6.84	4.23	5.74	4.54

Table C-4. 48-3835 Bryan Field Core in Texas

1st Core		Bulk S. G.		Maximum	Total Air Voids		Accessible A.V.		Binder
		SSD	Corelock	S. G.	SSD	Corelock	SSD	Corelock	Contents
Bryan (Overlay)	1st	2.34	2.25	2.56	8.65	12.44	4.28	8.26	3.52
	2nd	2.36	2.31	2.53	6.89	8.88	3.60	5.66	4.12
	3rd	2.33	2.31	2.54	8.04	8.92	4.82	5.73	4.17
(OSL)	1st	2.36	2.37	2.48	5.95	4.70	0.95	0.44	5.27
	2nd	2.33	2.36	2.54	8.32	7.10	2.31	1.01	4.97
	3rd	2.26	2.25	2.49	9.52	9.97	5.38	5.85	4.90
2nd Core		**Bulk S. G.**		**Maximum**	**Total Air Voids**		**Accessible A.V.**		**Binder**
		SSD	Corelock	S. G.	SSD	Corelock	SSD	Corelock	Contents
Bryan (Overlay)	1st	2.33	2.24	2.55	8.85	12.07	4.42	7.8	-
	2nd	2.36	2.32	2.54	7.01	8.70	3.52	5.26	-
	3rd	2.36	2.35	2.52	6.52	6.90	2.86	3.25	-
(OSL)	1st	2.33	2.33	2.45	5.87	6.07	1.99	1.90	4.53
	2nd	2.30	2.30	2.50	7.74	7.93	3.90	4.10	4.48
	3rd	2.30	2.25	2.46	6.26	8.62	5.16	7.55	4.05

Table C-5. Bryan US290 Field Core in Texas

1st Core		Bulk S. G.		Maximum	Total Air Voids		Accessible A.V.		Binder
		SSD	Corelock	S. G.	SSD	Corelock	SSD	Corelock	Contents
Bryan US290 (OSL)	1st	2.24	2.23	2.57	11.8	11.53	9.04	9.22	3.60
	2nd	2.27	2.28	2.51	9.69	9.41	6.6	6.31	3.76
	3rd	2.27	2.28	2.5	9.22	8.74	6.15	5.66	4.10
2nd Core		**Bulk S. G.**		**Maximum**	**Total Air Voids**		**Accessible A.V.**		**Binder**
		SSD	Corelock	S. G.	SSD	Corelock	SSD	Corelock	Contents
Bryan US290 (OSL)	1st	2.28	2.25	2.55	10.72	12.02	6.61	7.75	3.37
	2nd	2.28	2.25	2.53	10.06	11.38	5.83	7.21	3.60
	3rd	2.30	2.28	2.51	8.64	9.14	4.71	5.23	3.57

Table C-6. 48-1068 Paris Field Core in Texas

1st Core		Bulk S. G.		Maximum	Total Air Voids		Accessible A.V.		Binder
		SSD	Corelock	S. G.	SSD	Corelock	SSD	Corelock	Contents
Paris (Overlay)	1st	2.16	2.10	2.40	9.97	12.65	8.66	11.38	5.12
	2nd	2.20	2.13	2.45	10.45	13.07	6.75	9.48	5.55
	3rd	2.18	2.14	2.43	10.34	11.98	7.65	9.34	5.48
(OSL)	1st	2.22	2.21	2.49	10.77	11.27	6.41	6.94	3.66
	2nd	2.25	2.25	2.47	9.06	9.15	4.50	4.59	4.46
	3rd	2.27	2.28	2.50	8.95	8.54	4.02	3.58	4.62
	4th	2.29	2.30	2.47	7.14	7.01	2.85	2.71	3.91
2nd Core		**Bulk S. G.**		**Maximum**	**Total Air Voids**		**Accessible A.V.**		**Binder**
		SSD	Corelock	S. G.	SSD	Corelock	SSD	Corelock	Contents
Paris (Overlay)	1st	2.21	2.07	2.46	10.20	15.73	7.17	12.89	-
	2nd	2.23	2.10	2.49	10.41	15.8	7.14	12.73	-
	3rd	2.22	2.11	2.47	9.92	14.5	6.79	11.53	-
(OSL)	1st	2.22	2.20	2.49	10.77	11.74	6.83	7.84	3.73
	2nd	2.25	2.25	2.48	8.98	9.20	4.81	5.04	4.29
	3rd	2.26	2.27	2.46	7.86	7.54	4.47	4.14	4.59
	4th	2.27	2.27	2.47	7.86	8.10	3.26	3.50	4.52

Table C-7. MnRoad Field Core in Minnesota

1st Core		Bulk S. G.		Maximum	Total Air Voids		Accessible A.V.		Binder
		SSD	Corelock	S. G.	SSD	Corelock	SSD	Corelock	Contents
AC 120/150	1st	2.38	2.34	2.58	7.75	9.14	1.80	3.28	4.73
	2nd	2.41	2.43	2.57	6.23	5.35	0.82	0.20	5.18
	3rd	2.38	2.39	2.53	6.18	5.59	0.93	0.30	5.23
	4th	2.37	2.37	2.57	7.93	7.92	1.37	1.37	5.17
	5th	2.35	2.35	2.57	8.54	8.40	1.00	0.84	5.46
	6th	2.36	2.38	2.59	8.72	7.95	1.41	0.58	5.13
	7th	2.35	2.35	2.60	9.63	9.49	2.23	2.08	5.00
	8th	2.34	2.34	2.57	9.18	8.99	3.94	3.74	5.14
	9th	2.34	2.33	2.58	9.21	9.53	4.98	5.31	4.64
58-28	1st	2.38	2.34	2.57	7.54	9.03	4.10	5.65	4.99
	2nd	2.39	2.39	2.57	7.00	7.29	3.61	3.91	4.78
	3rd	2.4	2.39	2.53	5.21	5.47	3.68	3.94	4.94
	4th	2.36	2.35	2.56	7.73	8.32	4.18	4.80	5.31
	5th	2.40	2.38	2.55	6.02	6.89	3.24	4.15	4.89
	6th	2.40	2.40	2.59	7.31	7.36	3.55	3.60	5.07
	7th	2.39	2.36	2.61	8.66	9.57	3.97	4.93	4.91
58-34	1st	2.35	2.32	2.54	7.30	8.80	3.66	5.22	4.88
	2nd	2.38	2.37	2.52	5.54	5.68	3.38	3.52	5.18
	3rd	2.37	2.36	2.56	7.61	7.84	3.21	3.45	4.98
	4th	2.35	2.35	2.54	7.51	7.58	4.02	4.09	5.28
	5th	2.38	2.37	2.53	6.28	6.60	4.06	4.38	4.82
	6th	2.39	2.37	2.58	7.50	8.21	4.21	4.95	4.99
58-40	1st	2.36	2.31	2.61	9.47	11.27	5.48	7.36	3.51
	2nd	2.37	2.36	2.57	8.37	9.24	4.13	4.45	4.23
	3rd	2.37	2.35	2.59	8.37	9.24	2.53	3.45	4.19
	4th	2.37	2.38	2.54	6.71	6.40	2.95	2.62	4.54
	5th	2.36	2.36	2.57	8.09	8.19	4.22	4.32	3.95
	6th	2.38	2.37	2.57	7.55	7.61	4.09	4.15	4.14

Table C-8. Atlanta – RG Field Core

Atlanta – RG (River Gravel) Bind.: Wright 76-22 SBS-A Cons.: 2001 Thick.: 2 inch		**η*** (Poise) @ 60 ℃ 0.1 rad/s	**η'/G'** (s) @ 15 ℃ 0.005 rad/s	**G'** (MPa) @ 15 ℃ 0.005 rad/s	**G'/(η'/G')** (MPa/s) @ 15 ℃ 0.005 rad/s	**Calculated Ductility** (cm) -	**Carbonyl Area** - -
1st Core (11/2004)	**1st layer**	372050	174.8	0.42164	0.0024125	3.26	-
	2nd	191650	223.2	0.22156	0.0009927	4.82	-
	3rd	153530	230.3	0.19514	0.0008474	5.17	-
	1st to 3rd	219360	209.4	0.24056	0.0011487	4.52	-
Thin Film Aging in ER (60 ℃)	**0 month**	219360	209.4	0.24056	0.0011487	4.52	-
	2 mo.	487060	157.0	0.39080	0.0024890	3.22	-
	4 mo.	599330	144.0	0.52412	0.0036400	2.72	-
	6 mo.	733930	134.2	0.57496	0.0042839	2.53	-
	8 mo.	899160	121.1	0.62320	0.0051441	2.34	-
2nd Core (11/2005)	**1st to 3rd**	276490	190.3	0.36042	0.0018936	3.63	-
Original Binder (Wright 76-22 SBS-A)	**Unaged**	17575	409.7	0.01523	0.0000372	20.46	0.51182
	SAFT	34039	341.6	0.02949	0.0000863	14.12	0.53631
	P* 16 hr	168180	226.7	0.14934	0.0006587	5.77	0.82944
	P* 32 hr	272170	193.6	0.23738	0.0012263	4.39	1.01206
	3 mo.	265900	204.9	0.21502	0.0010491	4.71	-
	6 mo.	444230	170.2	0.34242	0.0020123	3.53	-
	9 mo.	610700	147.9	0.45492	0.0030763	2.93	-
	12 mo.	1231400	110.5	0.65876	0.0059620	2.19	-

Table C-9. Atlanta – SS Field Core

Atlanta – SS (Sandstone) Bind.: Wright 76-22 SBS-A Cons.: 2001 Thick.: 2.75 inch		**η*** (Poise) @ 60 ℃ 0.1 rad/s	**η'/G'** (s) @ 15 ℃ 0.005 rad/s	**G'** (MPa) @ 15 ℃ 0.005 rad/s	**G'/(η'/G')** (MPa/s) @ 15 ℃ 0.005 rad/s	**Calculated Ductility** (cm) -	**Carbonyl Area** - -
1st Core (11/2004)	**1st layer**	660610	135.3	0.74088	0.0054770	2.27	-
	2nd	497120	142.5	0.71078	0.0049871	2.37	-
	3rd	445380	150.7	0.62380	0.0041395	2.57	-
	4th	158100	237.9	0.22134	0.0009305	4.96	-
	1st to 4th	362880	164.3	0.47580	0.0028961	3.01	-
Thin Film Aging in ER (60 ℃)	**0 month**	362880	164.3	0.47580	0.0028961	3.01	-
	2 mo.	728640	122.4	0.77100	0.0062989	2.14	-
	4 mo.	951260	108.9	0.92840	0.0085228	1.87	-
	6 mo.	1147800	89.9	0.95888	0.0106675	1.70	-
	8 mo.	1421400	89.6	1.04340	0.0116492	1.63	-
2nd Core (11/2005)	**1st to 4th**	571330	131.5	0.74830	0.0056915	2.24	-
Original Binder (Wright 76-22 SBS-A)	**Unaged**	17575	409.7	0.01523	0.0000372	20.46	0.51182
	SAFT	34039	341.6	0.02949	0.0000863	14.12	0.53631
	P* 16 hr	168180	226.7	0.14934	0.0006587	5.77	0.82944
	P* 32 hr	272170	193.6	0.23738	0.0012263	4.39	1.01206
	3 mo.	265900	204.9	0.21502	0.0010491	4.71	-
	6 mo.	444230	170.2	0.34242	0.0020123	3.53	-
	9 mo.	610700	147.9	0.45492	0.0030763	2.93	-
	12 mo.	1231400	110.5	0.65876	0.0059620	2.19	-

Table C-10. Atlanta – Q Field Core

Atlanta – Q (Quartzite) Bind.: Wright 76-22 SBS-A Cons.: 2001 Thick.: 2.25 inch		**η*** (Poise) @ 60 ℃ 0.1 rad/s	**η'/G'** (s) @ 15 ℃ 0.005 rad/s	**G'** (MPa) @ 15 ℃ 0.005 rad/s	**G'/(η'/G')** (MPa/s) @ 15 ℃ 0.005 rad/s	**Calculated Ductility** (cm) -	**Carbonyl Area** - -
1st Core (11/2004)	**1st layer**	540900	147.5	0.52340	0.0035484	2.75	-
	2nd	268740	192.2	0.31624	0.0016452	3.86	-
	3rd	154760	229.3	0.18058	0.0007874	5.34	-
	1st to 3rd	251360	190.0	0.28232	0.0014859	4.04	-
Thin Film Aging in ER (60 ℃)	**0 month**	251360	190.0	0.28232	0.0014859	4.04	-
	2 mo.	610480	144.9	0.48212	0.0033268	2.83	-
	4 mo.	806610	129.5	0.57070	0.0044066	2.50	-
	6 mo.	998270	116.8	0.66948	0.0057300	2.23	-
	8 mo.	1175600	109.8	0.68174	0.0062105	2.15	-
2nd Core (11/2005)	**1st to 3rd**	395430	167.4	0.43942	0.0026248	3.14	-
Original Binder (Wright 76-22 SBS-A)	**Unaged**	17575	409.7	0.01523	0.0000372	20.46	0.51182
	SAFT	34039	341.6	0.02949	0.0000863	14.12	0.53631
	P* 16 hr	168180	226.7	0.14934	0.0006587	5.77	0.82944
	P* 32 hr	272170	193.6	0.23738	0.0012263	4.39	1.01206
	3 mo.	265900	204.9	0.21502	0.0010491	4.71	-
	6 mo.	444230	170.2	0.34242	0.0020123	3.53	-
	9 mo.	610700	147.9	0.45492	0.0030763	2.93	-
	12 mo.	1231400	110.5	0.65876	0.0059620	2.19	-

Table C-11. Odessa Field Core

Odessa Bind.: Alon 70-22 SBS ('02) Cons.: 2002 Thick.: 3 inch		**η*** (Poise) @ 60 ℃ 0.1 rad/s	**η'/G'** (s) @ 15 ℃ 0.005 rad/s	**G'** (MPa) @ 15 ℃ 0.005 rad/s	**G'/(η'/G')** (MPa/s) @ 15 ℃ 0.005 rad/s	**Calculated Ductility** (cm) -	**Carbonyl Area** - -
1st Core (12/2004)	**1st layer**	62505	338.4	0.16070	0.0004749	6.67	-
	2nd	21083	561.6	0.03624	0.0000645	16.05	-
	3rd	18274	609.6	0.03092	0.0000507	17.84	-
	4th	16780	641.8	0.02692	0.0000419	19.40	-
	5th	16678	600.4	0.03262	0.0000543	17.31	-
	1st to 5th	22032	550.8	0.04182	0.0000759	14.94	-
Thin Film Aging in ER (60 ℃)	**0 month**	22032	550.8	0.04182	0.0000759	14.94	-
	2 mo.	79913	286.6	0.23258	0.0008114	5.27	-
	4 mo.	132830	221.4	0.33414	0.0015090	4.01	-
	6 mo.	179240	186.9	0.48122	0.0025754	3.17	-
	8 mo.	214710	163.4	0.56996	0.0034878	2.77	-
2nd Core (04/2006)	**1st to 5th**	63263	309.7	0.16830	0.0005434	6.28	-

Table C-12. Waco Field Core

Waco Bind.: Alon 70-22 SBS ('02) Cons.: 2002 Thick.: 3.4 inch (OSL)		**η*** (Poise) @ 60 ℃ 0.1 rad/s	**η'/G'** (s) @ 15 ℃ 0.005 rad/s	**G'** (MPa) @ 15 ℃ 0.005 rad/s	**G'/(η'/G')** (MPa/s) @ 15 ℃ 0.005 rad/s	**Calculated Ductility** (cm) -	**Carbonyl Area** - -
1st Core (10/2005)	**1st layer**	25012	513.9	0.02378	0.0000463	18.58	-
	2nd	26036	515.5	0.02331	0.0000452	18.77	-
	3rd	23612	523.5	0.02035	0.0000389	20.06	-
	4th	23402	524.3	0.01966	0.0000375	20.38	-
	5th	23901	525.2	0.02074	0.0000395	19.92	-
	6th	19039	565.8	0.01828	0.0000323	21.76	-
	1st to 6th	22409	524.0	0.01968	0.0000376	20.36	-
Thin Film Aging in ER (60 ℃)	**0 month**	22409	524.0	0.01968	0.0000376	20.36	-
	2 mo.	45874	425.4	0.05042	0.0001185	12.28	-
	4 mo.	59341	378.5	0.07932	0.0002096	9.56	-
	6 mo.	74364	333.6	0.11254	0.0003374	7.75	-
	8 mo.	96336	293.5	0.15132	0.0005156	6.43	-
2nd Core (NA)	**1st to 6th**	-	-	-	-	-	-

Table C-13. Yoakum Field Core

Yoakum Bind.: Koch 70-22 SBS ('02) Cons.: 2001 Thick.: 2.5 inch		**η*** (Poise) @ 60 ℃ 0.1 rad/s	**η'/G'** (s) @ 15 ℃ 0.005 rad/s	**G'** (MPa) @ 15 ℃ 0.005 rad/s	**G'/(η'/G')** (MPa/s) @ 15 ℃ 0.005 rad/s	**Calculated Ductility** (cm) -	**Carbonyl Area** - -
1st Core (01/2005)	**1st layer**	227710	235.3	0.19166	0.0008144	5.26	-
	2nd	171730	253.7	0.14594	0.0005751	6.13	-
	3rd	138700	265.5	0.11838	0.0004460	6.86	-
	4th	107550	281.7	0.08363	0.0002969	8.20	-
	5th	129620	268.3	0.11612	0.0004328	6.95	-
	1st to 5th	201040	239.5	0.17606	0.0007352	5.50	-
Thin Film Aging in ER (60 ℃)	**0 month**	201040	239.5	0.17606	0.0007352	5.50	-
	2 mo.	391800	189.8	0.28628	0.0015081	4.01	-
	4 mo.	547160	163.5	0.41532	0.0025407	3.19	-
	6 mo.	702420	153.1	0.44804	0.0029264	3.00	-
	8 mo.	926860	133.0	0.52426	0.0039415	2.63	-
2nd Core (05/2006)	**1st to 5th**	227750	227.3	0.20212	0.0008894	5.06	-

Table C-14. Amarillo Field Core

Amarillo Bind.: Alon 70-28 SBS ('00) Cons.: 2000 Thick.: 1.75 inch		**η*** (Poise) @ 60 ℃ 0.1 rad/s	**η'/G'** (s) @ 15 ℃ 0.005 rad/s	**G'** (MPa) @ 15 ℃ 0.005 rad/s	**G'/(η'/G')** (MPa/s) @ 15 ℃ 0.005 rad/s	**Calculated Ductility** (cm) -	**Carbonyl Area** - -
1st Core (12/2004)	**1st layer**	511700	144.5	0.61794	0.0042766	2.54	-
	2nd	104420	256.7	0.13732	0.0005350	6.33	-
	3rd	130700	239.7	0.17752	0.0007405	5.48	-
	1st to 3rd	154590	222.6	0.22464	0.0010093	4.79	-
Thin Film Aging in ER (60 ℃)	**0 month**	154590	222.6	0.22464	0.0010093	4.79	-
	2 mo.	394260	160.4	0.37598	0.0023440	3.30	-
	4 mo.	570610	141.9	0.49622	0.0034961	2.77	-
	6 mo.	704200	124.3	0.60902	0.0048999	2.39	-
	8 mo.	927470	114.6	0.72448	0.0063204	2.14	-
2nd Core (06/2006)	**1st to 3rd**	264570	186.0	0.35880	0.0019295	3.60	-

Table C-15. Pharr Field Core

Pharr Bind.: Eagle 70-22 SBS Cons.: 2002 Thick.: 3.4 inch		**η*** (Poise) @ 60 ℃ 0.1 rad/s	**η'/G'** (s) @ 15 ℃ 0.005 rad/s	**G'** (MPa) @ 15 ℃ 0.005 rad/s	**G'/(η'/G')** (MPa/s) @ 15 ℃ 0.005 rad/s	**Calculated Ductility** (cm) -	**Carbonyl Area** -
1st Core (02/2005)	**1st layer**	548810	159.2	0.50080	0.0031460	2.90	-
	2nd	268820	206.4	0.27792	0.0013463	4.22	-
	3rd	238970	214.5	0.27016	0.0012596	4.34	-
	4th	444430	169.7	0.44690	0.0026337	3.14	-
	5th	502880	161.4	0.45952	0.0028480	3.03	-
	1st to 5th	331470	180.2	0.36268	0.0020125	3.53	-
Thin Film Aging in ER (60 ℃)	**0 month**	331470	180.2	0.36268	0.0020125	3.53	-
	2 mo.	570830	156.0	0.51324	0.0032902	2.85	-
	4 mo.	808350	135.3	0.54212	0.0040071	2.61	-
	6 mo.	847610	130.9	0.67542	0.0051601	2.33	-
	8 mo.	1078600	115.0	0.63570	0.0055264	2.26	-
2nd Core (04/2006)	**1st to 5th**	356840	178.8	0.38948	0.0021786	3.41	-

Table C-16. Lufkin Field Core

Lufkin Bind.: Marlin 70-22 SBS Cons.: 2003 Thick.: 2.2 inch		**η*** (Poise) @ 60 ℃ 0.1 rad/s	**η'/G'** (s) @ 15 ℃ 0.005 rad/s	**G'** (MPa) @ 15 ℃ 0.005 rad/s	**G'/(η'/G')** (MPa/s) @ 15 ℃ 0.005 rad/s	**Calculated Ductility** (cm) -	**Carbonyl Area** -
1st Core (02/2005)	**1st layer**	241840	213.3	0.22730	0.0010658	4.67	-
	2nd	112550	260.4	0.11816	0.0004537	6.80	-
	3rd	111310	265.4	0.12196	0.0004595	6.77	-
	4th	105620	266.3	0.11520	0.0004326	6.95	-
	1st to 4th	147560	254.0	0.13960	0.0005496	6.25	-
Thin Film Aging in ER (60 ℃)	**0 month**	147560	254.0	0.13960	0.0005496	6.25	-
	2 mo.	258220	204.0	0.18826	0.0009228	4.98	-
	4 mo.	338630	189.2	0.28984	0.0015319	3.98	-
	6 mo.	392830	176.9	0.31354	0.0017719	3.74	-
	8 mo.	516310	163.4	0.33618	0.0020580	3.50	-
2nd Core (06/2006)	**1st to 4th**	172830	228.8	0.20052	0.0008765	5.09	-

Table C-17. Fort Worth SH183 Field Core

F.W. SH183 Bind.: AC-10 SBR Cons.: 1985 Thick.: 1.75 inch		η* (Poise) @ 60 ℃ 0.1 rad/s	η'/G' (s) @ 15 ℃ 0.005 rad/s	G' (MPa) @ 15 ℃ 0.005 rad/s	G'/(η'/G') (MPa/s) @ 15 ℃ 0.005 rad/s	Calculated Ductility (cm) -	Carbonyl Area - -
1st Core (04/2005)	1st layer	118360	225.8	0.19760	0.0008752	5.10	-
	2nd	46878	308.7	0.09069	0.0002938	8.24	-
	3rd	33270	345.5	0.06873	0.0001990	9.78	-
	1st to 3rd	89335	247.0	0.14992	0.0006071	5.99	-
Thin Film Aging in ER (60 ℃)	0 month	89335	247.0	0.14992	0.0006071	5.99	-
	2 mo.	153270	198.8	0.23922	0.0012034	4.43	-
	4 mo.	184970	196.4	0.26686	0.0013591	4.20	-
	6 mo.	212730	186.5	0.26986	0.0014471	4.08	-
	8 mo.	244980	180.7	0.28250	0.0015632	3.95	-
2nd Core (05/2006)	1st to 3rd	93023	243.0	0.18162	0.0007473	5.46	-

Table C-18. Fort Worth FM51 Field Core

F.W. FM51 Bind.: AC-10 SBR Cons.: 1994 Thick.: 2 inch		η* (Poise) @ 60 ℃ 0.1 rad/s	η'/G' (s) @ 15 ℃ 0.005 rad/s	G' (MPa) @ 15 ℃ 0.005 rad/s	G'/(η'/G') (MPa/s) @ 15 ℃ 0.005 rad/s	Calculated Ductility (cm) -	Carbonyl Area - -
1st Core (04/2005)	1st layer	353160	153.5	0.44536	0.0029015	3.01	-
	2nd	125430	209.3	0.23368	0.0011166	4.58	-
	3rd	54459	278.4	0.09867	0.0003544	7.58	-
	4th	26051	353.9	0.05113	0.0001445	11.26	-
	1st to 4th	105010	217.8	0.20526	0.0009425	4.93	-
Thin Film Aging in ER (60 ℃)	0 month	105010	217.8	0.20526	0.0009425	4.93	-
	2 mo.	297500	160.8	0.33982	0.0021139	3.46	-
	4 mo.	363030	149.4	0.37248	0.0024925	3.22	-
	6 mo.	464740	134.4	0.52718	0.0039221	2.63	-
	8 mo.	558660	126.5	0.54214	0.0042855	2.53	-
2nd Core (05/2006)	1st to 4th	115240	214.8	0.22160	0.0010317	4.74	-

Table C-19. Fort Worth US281 Field Core

F.W. US281 Bind.: Valero-O 76-22 SBR Cons.: 2003 Thick.: 1 inch		**η*** (Poise) @ 60 ℃ 0.1 rad/s	**η'/G'** (s) @ 15 ℃ 0.005 rad/s	**G'** (MPa) @ 15 ℃ 0.005 rad/s	**G'/(η'/G')** (MPa/s) @ 15 ℃ 0.005 rad/s	**Calculated Ductility** (cm) -	**Carbonyl Area** - -
1st Core (04/2005)	**1st layer**	69242	277.8	0.16160	0.0005816	6.10	-
	2nd	42802	335.6	0.09993	0.0002978	8.19	-
	1st to 2nd	61441	287.8	0.14716	0.0005113	6.46	-
Thin Film Aging in ER (60 ℃)	**0 month**	61441	287.8	0.14716	0.0005113	6.46	-
	2 mo.	150970	205.8	0.27722	0.0013470	4.22	-
	4 mo.	206670	182.1	0.34902	0.0019169	3.61	-
	6 mo.	256280	168.9	0.41300	0.0024452	3.24	-
	8 mo.	374560	149.5	0.47168	0.0031545	2.90	-
2nd Core (05/2006)	**1st to 2nd**	82352	257.2	0.20022	0.0007785	5.37	-
Original Binder (Valero-O 76-22 SBR)	**Unaged**	4737	627.0	0.00666	0.0000106	35.50	-
	SAFT	8811	512.8	0.01369	0.0000267	23.66	-
	P* 16 hr	65110	260.5	0.10768	0.0004133	7.09	-
	P* 32 hr	103980	224.4	0.17312	0.0007716	5.39	-
	3 mo.	69938	245.5	0.14800	0.0006028	6.00	-
	6 mo.	151730	199.8	0.24882	0.0012451	4.36	-
	9 mo.	207510	179.2	0.28446	0.0015874	3.92	-
	12 mo.	236660	166.7	0.28102	0.0016863	3.82	-

Table C-20. 48-9005 San Antonio Field Core

San Antonio (Overlay) Bind.: Unknown/Unmodified Cons.: 1998 Thick.: 1.9 inch		**η*** (Poise) @ 60 ℃ 0.1 rad/s	**η_0*** (Poise) - -	**η'/G'** (s) @ 15 ℃ 0.005 rad/s	**G'** (MPa) @ 15 ℃ 0.005 rad/s	**G'/(η'/G')** (MPa/s) @ 15 ℃ 0.005 rad/s	**Calculated Ductility** (cm) -	**Carbonyl Area** - -
1st Core (07/2002)	**1st layer**	265740	338620	168.5	0.62144	0.0036874	2.71	-
	2nd	143390	186260	216.8	0.39164	0.0018062	3.70	-
	3rd	148240	182890	210.5	0.42090	0.0019998	3.54	-
	1st to 3rd	161050	200490	208.0	0.42374	0.0020376	3.51	-
Thin Film Aging in ER (60 ℃)	**0 month**	161050	200490	208.0	0.42374	0.0020376	3.51	-
	2 mo.	321220	390480	155.2	0.59984	0.0038651	2.65	-
	4 mo.	528320	698500	120.5	0.88128	0.0073159	2.00	-
	6 mo.	672420	981660	109.5	0.95144	0.0086888	1.86	-
	8 mo.	947660	1375100	96.7	1.06380	0.0110003	1.67	-
2nd Core (10/2005)	**1st to 3rd**	492370	612630	104.9	0.82920	0.0079082	1.93	-

(OSL) Bind.: Unknown/Unmodified Cons.: 1986 Thick.: 1.2 inch		**η*** (Poise) @ 60 ℃ 0.1 rad/s	**η_0*** (Poise) - -	**η'/G'** (s) @ 15 ℃ 0.005 rad/s	**G'** (MPa) @ 15 ℃ 0.005 rad/s	**G'/(η'/G')** (MPa/s) @ 15 ℃ 0.005 rad/s	**Calculated Ductility** (cm) -	**Carbonyl Area** - -
1st Core (07/2002)	**1st layer**	141890	149120	174.3	0.53232	0.0030536	2.94	-
	2nd	27050	28729	407.6	0.09795	0.0002403	9.00	-
	1st to 2nd	53406	57417	281.9	0.22066	0.0007828	5.35	-
2nd Core (10/2005)	**1st layer**	115460	123080	197.5	0.36406	0.0018438	3.67	-
	2nd	77943	86294	246.8	0.27714	0.0011229	4.57	-
	1st to 2nd	85043	89877	230.0	0.30188	0.0013125	4.26	-

Table C-21. 48-3835 Bryan Field Core

Bryan (Overlay) Bind.: Unknown/Unmodified Cons.: 2000 Thick.: 1.8 inch		**η*** (Poise) @ 60 ℃ 0.1 rad/s	**η_0*** (Poise) - -	**η'/G'** (s) @ 15 ℃ 0.005 rad/s	**G'** (MPa) @ 15 ℃ 0.005 rad/s	**G'/(η'/G')** (MPa/s) @ 15 ℃ 0.005 rad/s	**Calculated Ductility** (cm) -	**Carbonyl Area** - -
1st Core (07/2002)	**1st layer**	95993	105410	251.2	0.22226	0.0008847	5.07	-
	2nd	41001	46321	345.2	0.11424	0.0003310	7.82	-
	3rd	34206	37525	371.9	0.08141	0.0002189	9.38	-
	1st to 3rd	45760	50142	327.7	0.12832	0.0003916	7.26	-
Thin Film Aging in ER (60 ℃)	**0 month**	45760	50142	327.7	0.12832	0.0003916	7.26	-
	2 mo.	88122	100710	274.9	0.18692	0.0006800	5.69	-
	4 mo.	114530	136090	233.7	0.23852	0.0010207	4.76	-
	6 mo.	137260	168310	219.4	0.27408	0.0012494	4.36	-
	8 mo.	186070	220660	197.5	0.39266	0.0019879	3.55	-
2nd Core (10/2005)	**1st to 3rd**	56510	63330	310.1	0.15768	0.0005084	6.47	-

(OSL) Bind.: Unknown/Unmodified Cons.: 1991 Thick.: 1.7 inch		**η*** (Poise) @ 60 ℃ 0.1 rad/s	**η_0*** (Poise) - -	**η'/G'** (s) @ 15 ℃ 0.005 rad/s	**G'** (MPa) @ 15 ℃ 0.005 rad/s	**G'/(η'/G')** (MPa/s) @ 15 ℃ 0.005 rad/s	**Calculated Ductility** (cm) -	**Carbonyl Area** - -
1st Core (07/2002)	**1st layer**	25110	27625	460.5	0.09741	0.0002115	9.52	-
	2nd	28944	31254	442.2	0.12024	0.0002719	8.52	-
	3rd	62137	63577	279.7	0.32706	0.0011694	4.49	-
	1st to 3rd	35762	36751	382.9	0.15200	0.0003970	7.22	-
2nd Core (10/2005)	**1st layer**	53047	56584	294.6	0.25618	0.0008697	5.11	-
	2nd	164990	168850	148.1	0.73084	0.0049347	2.38	-
	3rd	178860	183150	134.5	0.85114	0.0063263	2.13	-
	1st to 3rd	119860	122030	185.2	0.62404	0.0033699	2.82	-

Table C-22. Bryan US290 Field Core

Bryan US290 (OSL) Bind.: Fina Cons.: 2002 Thick.: 1.7 inch		**η*** (Poise) @ 60 ℃ 0.1 rad/s	**η_0*** (Poise) - -	**η'/G'** (s) @ 15 ℃ 0.005 rad/s	**G'** (MPa) @ 15 ℃ 0.005 rad/s	**G'/(η'/G')** (MPa/s) @ 15 ℃ 0.005 rad/s	**Calculated Ductility** (cm) -	**Carbonyl Area** - -
1st Core (10/2005)	**1st layer**	49077	55106	319.9	0.09165	0.0002865	8.33	-
	2nd	47399	53923	315.7	0.08590	0.0002721	8.52	-
	3rd	34647	40192	348.0	0.06874	0.0001975	9.81	-
	1st to 3rd	38424	42339	334.3	0.07096	0.0002122	9.50	-
Thin Film Aging in ER (60 ℃)	**0 month**	38424	42339	334.3	0.07096	0.0002122	9.50	-
	2 mo.	59403	70838	297.0	0.09757	0.0003285	7.84	-
	4 mo.	74582	89707	275.9	0.12540	0.0004544	6.80	-
	6 mo.	99927	122350	256.0	0.15650	0.0006114	5.97	-
	8 mo.	137530	173130	230.8	0.19224	0.0008329	5.21	-
2nd Core (07/2006)	**1st layer**	51309	57765	293.9	0.08842	0.0003008	8.15	-
	2nd	45318	51177	311.0	0.08334	0.0002680	8.58	-
	3rd	40763	45134	322.1	0.07078	0.0002197	9.36	-
	1st to 3rd	46080	52837	302.4	0.08137	0.0002691	8.56	-

C-23. 48-1068 Paris Field Core

Paris (Overlay) Bind.: Unknown/Unmodified Cons.: 2000 Thick.: 2.2 inch		**η*** (Poise) @ 60 ℃ 0.1 rad/s	**η_0*** (Poise) - -	**η'/G'** (s) @ 15 ℃ 0.005 rad/s	**G'** (MPa) @ 15 ℃ 0.005 rad/s	**G'/(η'/G')** (MPa/s) @ 15 ℃ 0.005 rad/s	**Calculated Ductility** (cm) -	**Carbonyl Area** - -
1st Core (07/2002)	**1st layer**	52543	56733	311.8	0.22576	0.0007241	5.54	-
	2nd	31755	35076	396.2	0.12224	0.0003085	8.06	-
	3rd	30303	33103	401.8	0.11584	0.0002883	8.31	-
	1st to 3rd	36644	41530	366.5	0.15492	0.0004227	7.02	-
Thin Film Aging in ER (60 ℃)	**0 month**	36644	41530	366.5	0.15492	0.0004227	7.02	-
	2 mo.	58507	60919	283.2	0.21784	0.0007692	5.39	-
	4 mo.	73404	75791	254.2	0.26008	0.0010232	4.76	-
	6 mo.	81179	86174	244.4	0.32308	0.0013217	4.25	-
	8 mo.	95913	105340	224.2	0.38456	0.0017153	3.79	-
2nd Core (10/2005)	**1st to 3rd**	192110	194300	152.3	0.75412	0.0049524	2.38	-

(OSL) Bind.: Unknown/Unmodified Cons.: 1985 Thick.: 3.1 inch		**η*** (Poise) @ 60 ℃ 0.1 rad/s	**η_0*** (Poise) - -	**η'/G'** (s) @ 15 ℃ 0.005 rad/s	**G'** (MPa) @ 15 ℃ 0.005 rad/s	**G'/(η'/G')** (MPa/s) @ 15 ℃ 0.005 rad/s	**Calculated Ductility** (cm) -	**Carbonyl Area** - -
1st Core (07/2002)	**1st layer**	102700	115140	224.2	0.21526	0.0009603	4.89	-
	2nd	48520	50223	282.6	0.09270	0.0003281	7.85	-
	3rd	42187	45666	295.6	0.09180	0.0003106	8.04	-
	4th	37440	41459	309.9	0.07971	0.0002572	8.73	-
	1st to 4th	50568	54578	282.0	0.11452	0.0004061	7.14	-
2nd Core (10/2005)	**1st layer**	130090	145390	207.3	0.26984	0.0013018	4.28	-
	2nd	61026	67960	259.9	0.11644	0.0004480	6.84	-
	3rd	56607	62235	270.0	0.10174	0.0003768	7.38	-
	4th	52697	59244	280.9	0.09580	0.0003411	7.71	-
	1st to 4th	76825	84178	244.3	0.16836	0.0006892	5.66	-

Table C-24. MnRoad AC 120/150 Field Core

MnRoad Cell # 1 Bind.: AC 120/150 Cons.: 1992 Thick.: 5.9 inch		η* (Poise) @ 60 ℃ 0.1 rad/s	η'/G' (s) @ 15 ℃ 0.005 rad/s	G' (MPa) @ 15 ℃ 0.005 rad/s	G'/(η'/G') (MPa/s) @ 15 ℃ 0.005 rad/s	Calculated Ductility (cm) -	Carbonyl Area - -
1st Core (11/2004)	**1st layer**	27212	358.2	0.07353	0.0002053	9.64	-
	2nd	11615	497.0	0.02842	0.0000572	16.93	-
	3rd	5065	688.3	0.00983	0.0000143	31.16	-
	4th	4753	720.0	0.00867	0.0000120	33.58	-
	5th	6234	636.3	0.01253	0.0000197	27.05	-
	6th	9219	544.8	0.02093	0.0000384	20.16	-
	7th	12838	487.8	0.03132	0.0000642	16.09	-
	8th	16838	448.9	0.04327	0.0000964	13.45	-
	9th	25890	403.4	0.07329	0.0001817	10.18	-
	1st to 9th	11154	501.0	0.02721	0.0000543	17.31	-
Thin Film Aging in ER (60 ℃)	**0 month**	11154	501.0	0.02721	0.0000543	17.31	-
	2 mo.	41981	302.4	0.10240	0.0003386	7.74	-
	4 mo.	69916	254.0	0.14372	0.0005658	6.17	-
	6 mo.	107010	221.8	0.23292	0.0010503	4.70	-
	8 mo.	172480	188.9	0.31368	0.0016607	3.84	-
2nd Core (07/2006)	**1st to 9th**	14953	458.0	0.04105	0.0000896	13.89	-
Original Binder (AC 120/150)	**Unaged**	1580	1234.5	0.00149	0.0000012	92.55	-
	SAFT	3805	698.6	0.00641	0.0000092	37.85	-
	P* 16 hr	13643	426.4	0.03310	0.0000776	14.80	-
	P* 32 hr	30967	325.3	0.06861	0.0002109	9.53	-
	3 mo.	23486	358.8	0.05894	0.0001643	10.64	-
	6 mo.	74654	248.9	0.16934	0.0006802	5.69	-
	9 mo.	144580	197.0	0.24578	0.0012477	4.36	-
	12 mo.	256090	167.1	0.38642	0.0023122	3.32	-

Table C-25. MnRoad 58-28 Field Core

MnRoad Cell # 33 Bind.: Koch 58-28 Cons.: 1999 Thick.: 4.04 inch		**η*** (Poise) @ 60 ℃ 0.1 rad/s	**η'/G'** (s) @ 15 ℃ 0.005 rad/s	**G'** (MPa) @ 15 ℃ 0.005 rad/s	**G'/(η'/G')** (MPa/s) @ 15 ℃ 0.005 rad/s	**Calculated Ductility** (cm) -	**Carbonyl Area** - -
1st Core (11/2004)	**1st layer**	38943	328.7	0.10748	0.0003270	7.86	-
	2nd	18806	416.8	0.04864	0.0001167	12.37	-
	3rd	15981	448.0	0.04029	0.0000899	13.87	-
	4th	16352	450.2	0.04328	0.0000961	13.47	-
	5th	12398	497.4	0.03092	0.0000622	16.31	-
	6th	16155	452.3	0.04348	0.0000961	13.47	-
	7th	20450	416.0	0.05693	0.0001369	11.53	-
	1st to 7th	18920	418.9	0.04954	0.0001183	12.29	-
Thin Film Aging in ER (60 ℃)	**0 month**	18920	418.9	0.04954	0.0001183	12.29	-
	2 mo.	55317	276.2	0.14972	0.0005420	6.29	-
	4 mo.	93006	229.5	0.21726	0.0009468	4.92	-
	6 mo.	148180	202.4	0.27366	0.0013524	4.21	-
	8 mo.	226260	175.3	0.36948	0.0021082	3.46	-
2nd Core (07/2006)	**1st to 7th**	21417	401.9	0.05859	0.0001458	11.21	-
Original Binder (Koch 58-28)	**Unaged**	1659	1182.6	0.00155	0.0000013	89.19	-
	SAFT	3634	716.7	0.00569	0.0000079	40.34	-
	P* 16 hr	16016	396.2	0.03702	0.0000934	13.64	-
	P* 32 hr	31261	319.0	0.06215	0.0001948	9.87	-
	3 mo.	23683	358.9	0.05298	0.0001476	11.15	-
	6 mo.	74382	250.7	0.14124	0.0005633	6.19	-
	9 mo.	180780	196.5	0.24990	0.0012719	4.32	-
	12 mo.	244940	168.2	0.38696	0.0023008	3.33	-

Table C-26. MnRoad 58-34 Field Core

MnRoad Cell # 34 Bind.: Koch 58-34 SBS Cons.: 1999 Thick.: 3.92 inch		**η*** (Poise) @ 60 ℃ 0.1 rad/s	**η'/G'** (s) @ 15 ℃ 0.005 rad/s	**G'** (MPa) @ 15 ℃ 0.005 rad/s	**G'/(η'/G')** (MPa/s) @ 15 ℃ 0.005 rad/s	**Calculated Ductility** (cm) -	**Carbonyl Area** - -
Bulk (Loose) Mix		9329	463.5	0.00936	0.0000202	26.76	-
1st Core (11/2004)	**1st layer**	28948	370.0	0.03460	0.0000935	13.63	-
	2nd	15170	426.8	0.01817	0.0000426	19.27	-
	3rd	12151	449.0	0.01577	0.0000351	20.97	-
	4th	13247	455.7	0.01768	0.0000388	20.08	-
	5th	11660	474.9	0.01502	0.0000316	23.21	-
	6th	12471	464.6	0.01703	0.0000367	21.85	-
	1st to 6th	15050	440.9	0.01941	0.0000440	18.99	-
Thin Film Aging in ER (60 ℃)	**0 month**	15050	440.9	0.01941	0.0000440	18.99	-
	2 mo.	40061	323.3	0.05443	0.0001684	10.52	-
	4 mo.	69257	276.2	0.09509	0.0003443	7.68	-
	6 mo.	97253	246.4	0.12434	0.0005046	6.49	-
	8 mo.	149160	214.7	0.18360	0.0008551	5.15	-
2nd Core (07/2006)	**1st to 6th**	15215	426.3	0.02264	0.0000531	17.49	-
Original Binder (Koch 58-34 SBS)	**Unaged**	2703	509.8	0.00219	0.0000043	52.89	-
	SAFT	5856	428.6	0.00445	0.0000104	35.86	-
	P* 16 hr	22662	346.4	0.01658	0.0000479	18.30	-
	P* 32 hr	36704	316.1	0.02859	0.0000904	13.83	-
	3 mo.	29760	339.3	0.02389	0.0000704	15.44	-
	6 mo.	86186	262.8	0.07295	0.0002776	8.45	-
	9 mo.	169020	212.7	0.14686	0.0006904	5.66	-
	12 mo.	201680	200.6	0.17732	0.0008841	5.07	-

Table C-27. MnRoad 58-40 Field Core

MnRoad Cell # 35 Bind.: Koch 58-40 SBS Cons.: 1999 Thick.: 3.96 inch		**η*** (Poise) @ 60 ℃ 0.1 rad/s	**η'/G'** (s) @ 15 ℃ 0.005 rad/s	**G'** (MPa) @ 15 ℃ 0.005 rad/s	**G'/(η'/G')** (MPa/s) @ 15 ℃ 0.005 rad/s	**Calculated Ductility** (cm) -	**Carbonyl Area** - -
1st Core (11/2004)	**1st layer**	42740	250.9	0.06801	0.0002711	8.53	-
	2nd	14221	323.4	0.02503	0.0000774	14.81	-
	3rd	3703	472.2	0.00581	0.0000123	33.26	-
	4th	4855	455.8	0.00754	0.0000165	29.21	-
	5th	4280	474.5	0.00746	0.0000160	29.60	-
	6th	4461	472.1	0.00813	0.0000172	28.70	-
	1st to 6th	7490	379.7	0.01357	0.0000357	20.81	-
Thin Film Aging in ER (60 ℃)	**0 month**	7490	379.7	0.01357	0.0000357	20.81	-
	2 mo.	56243	226.8	0.07585	0.0003345	7.78	-
	4 mo.	89253	200.4	0.09918	0.0004949	6.55	-
	6 mo.	131020	187.8	0.13980	0.0007443	5.47	-
	8 mo.	195380	162.3	0.17812	0.0010977	4.61	-
2nd Core (07/2006)	**1st to 6th**	7798	380.2	0.01454	0.0000382	20.20	-
Original Binder (Koch 58-40 SBS)	**Unaged**	8381	288.3	0.00244	0.0000085	39.25	-
	SAFT	10610	288.7	0.00328	0.0000113	34.48	-
	P* 16 hr	39562	238.0	0.01382	0.0000581	16.81	-
	P* 32 hr	73286	219.4	0.02464	0.0001123	12.58	-
	3 mo.	86683	217.9	0.03348	0.0001536	10.96	-
	6 mo.	200100	180.8	0.10510	0.0005812	6.10	-
	9 mo.	315890	155.8	0.18160	0.0011653	4.49	-
	12 mo.	375830	142.5	0.21994	0.0017115	3.79	-

Table C-28. Temperature Effect (MnRoad AC 120/150)

MnRoad AC 120/150 (Cell # 1 Original Binder)		η'/G' (s) @ 15 ℃ 0.005 rad/s	G' (MPa) @ 15 ℃ 0.005 rad/s	G'/(η'/G') (MPa/s) @ 15 ℃ 0.005 rad/s	Calculated Ductility (cm) -	Carbonyl Area -
ER 6 month-aged Sample		248.9	0.16934	0.0006802	5.69	
60 ℃	**10 days**	236.2	0.17400	0.0007366	5.50	-
	20 da.	228.9	0.18800	0.0008215	5.24	-
	30 da.	225.8	0.19600	0.0008680	5.11	-
ER 6 month-aged Sample		248.9	0.16934	0.0006802	5.69	
75 ℃	**10 days**	188.5	0.28270	0.0014998	4.02	-
	20 da.	166.5	0.36616	0.0021998	3.40	-
	30 da.	140.4	0.52140	0.0037143	2.70	-
ER 6 month-aged Sample		248.9	0.16934	0.0006802	5.69	
95 ℃	**10 days**	118.3	0.59950	0.0050691	2.35	
	20 da.	61.3	1.10320	0.0179888	1.35	-
	30 da.	26.7	4.94500	0.1853906	0.48	-

Table C-29. DSR Function Hardening with Pavement Service Time (Texas PMA)

Site-Core	Date	DSR fn	Service time (years)	AAV
Atlanta Neat Binder SAFT		**0.0000863**		
Wright PG 76-22 SBS-A				
Atlanta	**Jun-01**		**0.00**	
Atlanta-RG	Nov-04	0.0011487	3.42	6
	Nov-05	0.0018936	4.42	
Atlanta-SS	Nov-04	0.0028961	3.42	6
	Nov-05	0.0056915	4.42	
Atlanta-Q	Nov-04	0.0014859	3.42	4
	Nov-05	0.0026248	4.42	
Amarillo	**Jun-00**		**0.00**	
Alon PG 70-28 SBS	Dec-04	0.0010093	4.50	7
	Jun-06	0.0019295	6.00	
Lufkin	**Jun-03**		**0.00**	
Marlin PG 70-22 SBS	Feb-05	0.0005496	1.67	6
	Jun-06	0.0008765	3.00	
Pharr	**Jun-02**		**0.00**	
Eagle PG 70-22 SBS	Feb-05	0.0020125	2.67	6.5
	Apr-06	0.0021786	3.84	
Yoakum	**Jun-01**		**0.00**	
Koch PG 70-22 SBS	Jan-05	0.0007352	3.59	5
	May-06	0.0008894	4.92	
Odessa	**Jun-02**		**0.00**	
Alon PG 70-22 SBS	Dec-04	0.0000759	2.50	1.5
	Apr-06	0.0005434	3.84	
Waco	**Jun-02**		**0.00**	
Alon PG 70-22 SBS	Oct-05	0.0000376	3.34	4
FW US281 Neat Binder SAFT		**0.0000267**		
Valero-O PG 76-22 SBR				
FW US281	**Jun-03**		**0.00**	
Valero-O PG 76-22 SBR	Apr-05	0.0005113	1.84	8
	May-06	0.0007785	2.92	
FW SH183	**Jun-85**		**0.00**	
AC-10 SBR	Apr-05	0.0006071	19.85	1.5
	May-06	0.0007473	20.93	
FW FM51	**Jun-94**		**0.00**	
AC-10 SBR	Apr-05	0.0009425	10.84	2
	May-06	0.0010317	11.92	

Table C-30. DSR Function Hardening with Pavement Service Time (Texas Unmodified)

Site-Core	Date	DSR fn	Service time (years)	AAV
San Antonio Overlay	**Jun-98**		**0.00**	
Unknown Unmodified Binder	Jul-02	0.0020376	4.08	5
	Oct-05	0.0079082	7.34	
Original Surface Layer (OL yr 12)	**Jun-86**		**0.00**	
Unknown Unmodified Binder	Jul-02	0.0007828	16.09	5
	Oct-05	0.0013125	19.35	
Bryan Overlay	**Jun-00**		**0.00**	
Unknown Unmodified Binder	Jul-02	0.0003916	2.08	4
	Oct-05	0.0005084	5.34	
Original Surface Layer (OL yr 9)	**Jun-91**		**0.00**	
Unknown Unmodified Binder	Jul-02	0.0003970	11.09	3
	Oct-05	0.0033699	14.35	
Bryan US290	**Jun-02**		**0.00**	
Fina	Oct-05	0.0002122	3.34	6
	Jul-06	0.0002691	4.08	
Paris Overlay	**Jun-00**		**0.00**	
Unknown Unmodified Binder	Jul-02	0.0004227	2.08	7
	Oct-05	0.0049524	5.34	
Original Surface Layer (OL yr 15)	**Jun-85**		**0.00**	
Unknown Unmodified Binder	Jul-02	0.0004061	17.09	4
	Oct-05	0.0006892	20.35	
TX 21				
Unknown Unmodified Binder	Jun-92	0.0001477		4
	Jun-96	0.0008900		8

Table C-31. DSR Function Hardening with Pavement Service Time (MnRoad)

Site-Core	Date	DSR fn	Service time (years)	AAV
AC 120/150 SAFT		**0.0000092**		
Unknown Unmodified Binder				
MnRoad Cell #1	**Jun-92**		**0.00**	
	Nov-04	0.0000543	12.43	1.5
	Jul-06	0.0000896	14.09	
PG 58-28 SAFT		**0.0000079**		
Koch				
MnRoad Cell #33	**Jun-99**		**0.00**	
	Nov-04	0.0001183	5.42	4
	Jul-06	0.0001458	7.09	
PG 58-34 SAFT		**0.0000104**		
Koch				
MnRoad Cell #34	**Jun-99**		**0.00**	
	Nov-04	0.000044	5.42	3.5
	Jul-06	0.0000531	7.09	
PG 58-40 SAFT		**0.0000113**		
Koch				
MnRoad Cell #35	**Jun-99**		**0.00**	
	Nov-04	0.0000357	5.42	3
	Jul-06	0.0000382	7.09	

VITA

Won Jun Woo was born on September 13, 1972 to Jong-Hwan Woo and Gi-Ja Jang in Seoul, the Republic of Korea. He received his Bachelor of Science in chemical engineering from Myongji University in Seoul in February 1999 and his Master of Science in chemical engineering from Myongji University in Seoul in February 2001. He graduated with his Ph.D. in chemical engineering from Texas A&M University, College Station, TX in August 2007. He can be reached through the following address:

Department of Chemical Engineering, c/o Dr. Charles J. Glover
Texas A&M University
3122 TAMU
College Station, TX, 77843-3122